Distribution et mobilité de l'arsenic dans les sols : effets de cycles redox successifs

Christopher Parsons

UNIVERSITÉ DE GRENOBLE

THÈSE

Pour obtenir le grade de

DOCTEUR DE L'UNIVERSITÉ DE GRENOBLE

Spécialité : **Géochimie de l'Environnement**

Arrêté ministériel : 7 août 2006

Présentée par

Christopher Parsons

Thèse dirigée par **Professeur Laurent Charlet** et
codirigée par **Dr. Gabriela Roman-Ross**

préparée au sein de **l'Institut des Sciences de la Terre**
dans **l'École Doctorale : Terre, Univers, Environnement**

Distribution et mobilité de l'arsenic dans les sols: Effets de cycles redox successifs

Thèse soutenue publiquement le **19 Octobre 2011**,
devant le jury composé de :

Prof. Laurent CHARLET Professeur à l'Université de Grenoble	Directeur
Dr. Gabriela ROMAN-ROSS Chercheur à AMPHOS 21, Barcelona	Co-Directrice
Prof. David POLYA Professeur à l'Université de Manchester	Rapporteur
Dr. Eric PILI Expert Senior au CEA, DAM-Île de France	Président
Dr. Benoit MADE Ingénieur, Direction Recherche et Développement, ANDRA	Membre invité

Synopsis

Redox sensitive contaminants in complex, three phase biologically mediated systems are susceptible to a myriad of biogeochemical interactions including protonation/de-protonation, sorption/desorption, complexation with organic matter, precipitation/dissolution and methylation/de-methylation as well as direct changes to oxidation state. This plethora of often simultaneous processes makes predicting mobility of contaminants in soils and aquifers, and hence effective resource management, very challenging. This thesis aims to elucidate the key biogeochemical processes and physical factors which control the mobility and distribution of redox sensitive contaminants including arsenic, chromium, uranium and mercury in frequently flooded soils. The work presented spans the colloidal to field scale and uses a combination of spectroscopic, analytical, geo-statistical and computational tools. Particular attention is paid to arsenic and the role of cyclic redox conditions which are prevalent in a number of contaminated environments.

Arsenic is an infamously toxic and carcinogenic metalloid which has received substantial attention from the international scientific community over the last two decades. This is principally due to the humanitarian disaster in southern Asia where tens of millions of people are affected by arsenic contaminated drinking water sourced from shallow alluvial aquifers. However, the threat posed by arsenic to human health is not limited to the sedimentary basins fed by the Himalaya. Sources of arsenic release to the environment are numerous and varied, with both anthropogenic and geogenic inputs a cause for concern. In Western Europe and North America the legacy of industrial activity and agricultural use of arsenic, compounded by natural geological input, has resulted in the contamination of many floodplain soils and wetlands. Contaminants are often concentrated in such sediments as their fine physical texture, and hence large surface area can retard the advective transport of arsenic in fluvial and groundwater systems. At the same time geothermal waters are often also loaded with As and may represent a threat to populations exposed through contaminated drinking water e.g. in the Atacama desert. Understanding the factors affecting arsenic mobility and toxicity in such systems is a challenge, demanding collaboration between traditionally separated academic fields. In addition to its current practical relevance, arsenic biogeochemistry is also of special academic interest due to the sensitivity of arsenic to solid and aqueous speciation changes within a range of Eh and pH conditions found in many near surface environments. The calcareous soils of the Saône floodplain in eastern France, close to the city of Macon, are known to host elevated concentrations of redox sensitive contaminants including arsenic and chromium. They are also subjected to regular redox oscillations due to seasonal flooding and form the focus of the experimental and field investigations presented in this thesis.

Summary Figure 1: The flooded alluvial plain of the Saône close to Macon during the winter.

During periods of flooding, pores in surface soils become saturated with water and diffusion of oxygen from the atmosphere to the soil is restricted. This forces soil bacterial communities to consume successively less efficient terminal electron acceptors and causes a progressive decrease in oxidation/reduction potential in the soil solution.

Summary Figure 2: How soil saturation causes changes to redox conditions in soils via limiting diffusion of oxygen from the surface to aerobic soil bacteria resulting in rapid oxygen depletion.

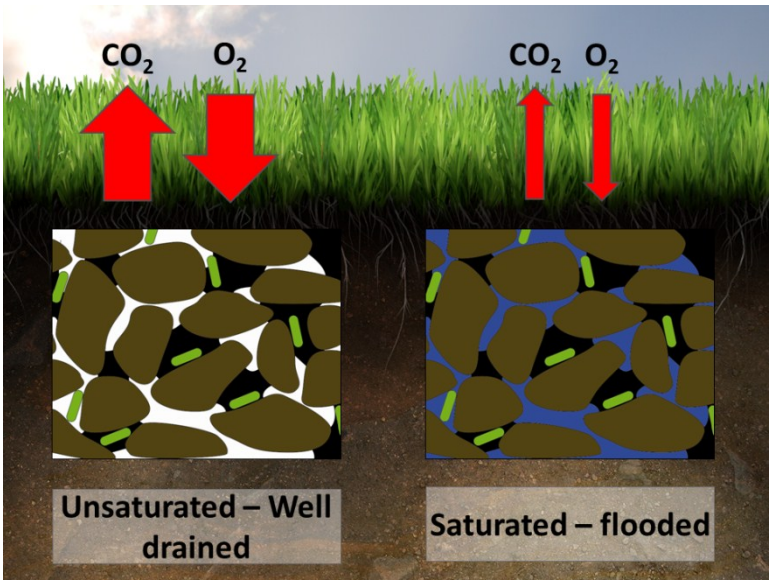

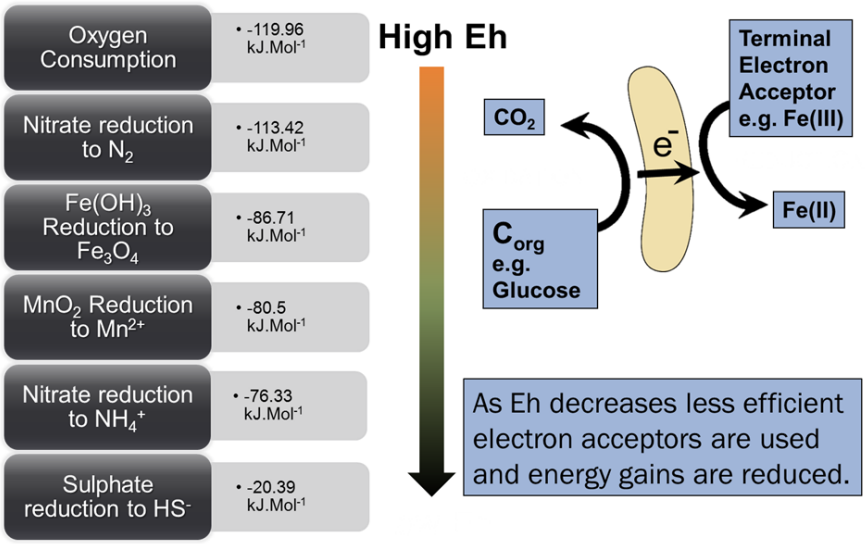

Summary Figure 3: The succession of terminal electron acceptors used by soil bacteria during oxidation of organic matter governed by energetic efficiency.

This microbially mediated redox shift causes changes in chemical equilibria and hence mineralogy, sorption processes and aqueous speciation, all of which impact arsenic mobility. A great deal of work has already been conducted over the last years to establish release mechanisms and sorbents of arsenic under reducing conditions. However, relatively limited attention has been paid to the cumulative effects of periodic redox cycling on soil mineralogy, the bacterial community, organic matter lability and ultimately, arsenic distribution and mobility. Neglecting cycling conditions represents an important gap in our understanding of a variety of both natural and anthropogenically influenced environments, including floodplains, rice paddies and shallow aquifers.

At the field scale, a critical evaluation of the analytical capability of field-portable X-ray fluorescence (FP-XRF) spectrometry for the standard-less, quantitative analysis of arsenic in soils was performed. It was found that due to recent improvements to hand held technology, instrumentation limitations were a secondary concern to sample preparation. Existing literature pertaining to the use of FP-XRF on soils has comprehensively investigated factors such as sample heterogeneity and particle size. However, results presented in this thesis suggest that the most important practical factor affecting precision and accuracy of FP-XRF analysis of trace arsenic concentrations in soils is the presence of soil pore water, even in comparatively dry soils. In order to maximise the accuracy of *in situ* analysis, a field-based sample preparation method was developed. This method allows the quantitative, multi-elemental analysis of soils and was validated by both lab based X-ray fluorescence and inductively coupled plasma mass spectrometry (ICP-MS) analysis.

Applying this sample preparation method, data obtained during field investigations were used to determine inter-elemental relationships in top soils, in addition to spatial and physical controls on arsenic distribution on the local field scale. It was found that one of the best predictors of arsenic concentrations was the particle size distribution within the finest soil fraction (less than 500 µm). Arsenic was associated most strongly with the finest clay / colloid fractions and strongly anti-correlated with very fine sands. Particle size distribution in the larger fractions (above 500 µm) appeared to have little effect on arsenic concentration.

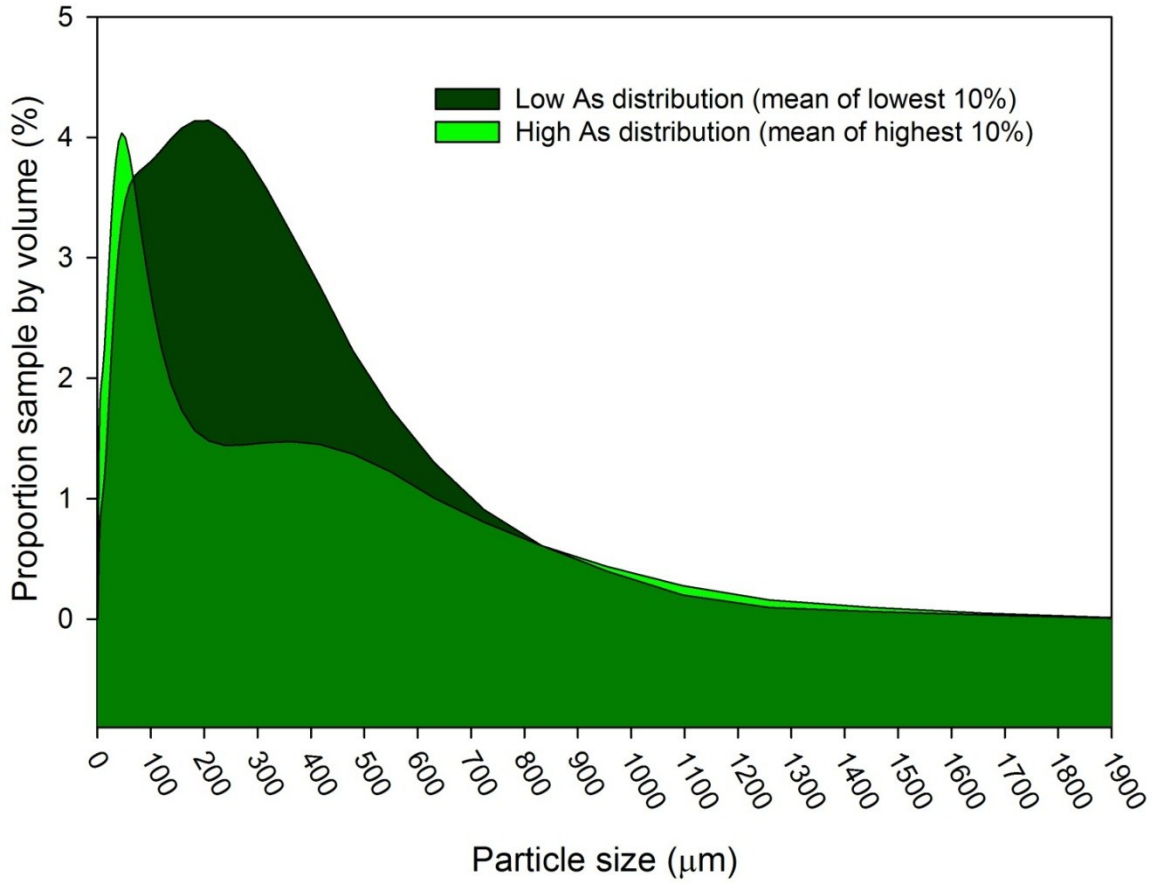

Summary Figure 4: Comparison of particle size distributions between average low arsenic and high arsenic soils illustrating the importance of the clay fraction to arsenic distribution.

Strong correlations were also found between total arsenic, iron and manganese concentrations. Weak correlations were found between arsenic concentrations and other indicators of soil hydrological conditions suggesting that hydraulic spatial redistribution of arsenic may be of limited importance within this area. The active carbonate and solid organic matter fractions were found to be poorly linked to arsenic concentration. This suggests that despite recent spectroscopic and modelling evidence demonstrating arsenic immobilization within the calcite structure, arsenic association with calcite may be of limited importance when metal oxides are also present in calcareous soils.

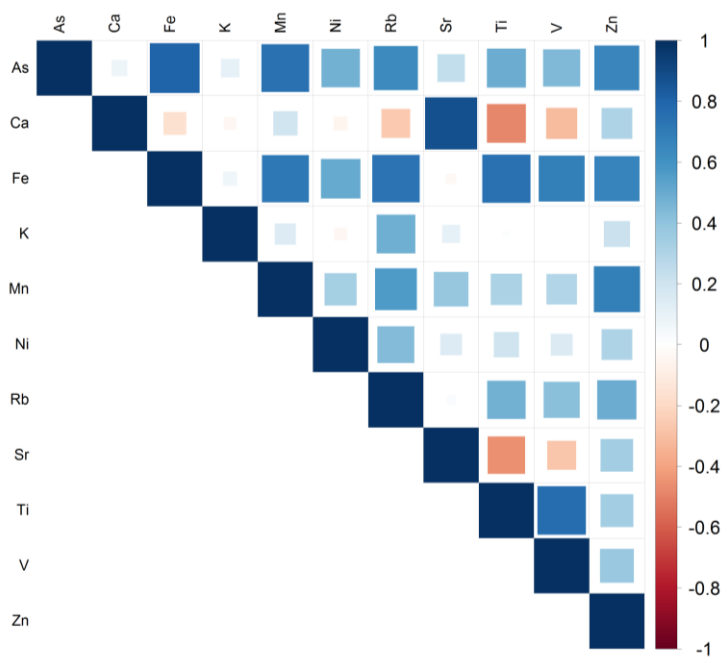

Summary Figure 5: Correlation matrix demonstrating inter-elemental relationships in soils on the Saône floodplain. Square size and colour corresponds to the correlation coefficient between elemental pairs (blue positively correlated, red negatively correlated).

At the batch scale, laboratory experiments were conducted using osmotic diffusion pore-water sampling devices to determine the extent of redox change experienced by temporally flooded soils on the Saône floodplain. Using this information a custom system of redox-stat, bio-reactors were designed to enable soil suspension experiments simulating cycles of oxidation and reduction experienced by the soils during seasonal flooding and draining.

These experiments allowed the mobility of arsenic to be monitored throughout consecutive reducing and oxidising events in addition to changes in aqueous chemistry, mineralogy, solid speciation and the composition and function of the natural bacterial community. These experiments revealed that even moderate total arsenic concentrations in soils can lead to high pore-water arsenic concentrations during periodic reducing events, and that contaminated floodplain soils can act as a significant secondary source of arsenic to surface water and increasingly exploited alluvial aquifers. An a priori unexpected result was that consecutive cycles of soil reduction and oxidation lead to the attenuation of arsenic release during subsequent reducing events.

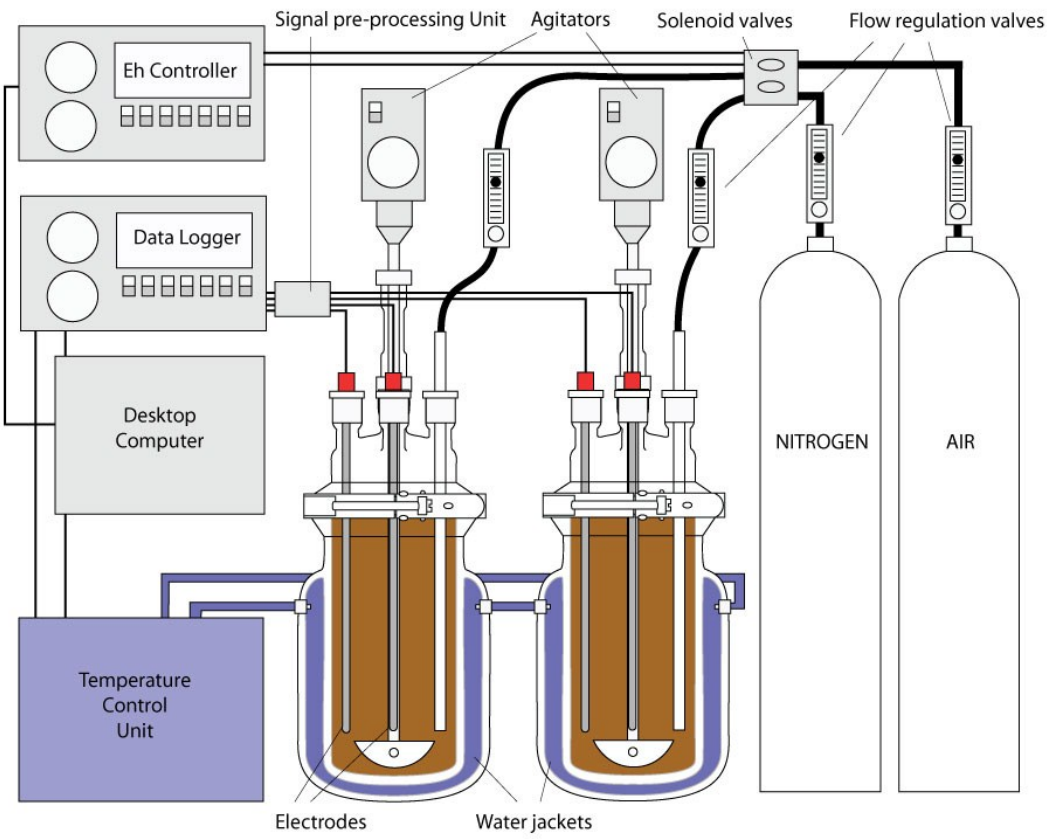

Summary Figure 6: The custom redox oscillation reactor setup used during experiments detailed in Chapters 5 and 6 whereby Eh in soil suspensions is controlled by sparging of air and nitrogen.

In complement to the information obtained from aqueous chemistry, spectroscopy and microbial ecology during these experiments, a thermodynamic and kinetic model simulating cycles of microbially driven oxidation and reduction in soils was implemented in PHREEQC. The model was used as both a prognostic and diagnostic tool to determine the processes controlling arsenic mobility during individual oxidising/reducing events and cumulatively across multiple cycles.

In this case, even under neutral to alkaline conditions close to the point of zero charge (pzc) of many metal oxides, it appears that poorly crystalline nano-iron-(hydr)oxide and ferric-arsenate minerals constitute the main immobilising phases for arsenic, despite accounting for less than 8% of the soil matrix. The data obtained, supported by the predictions of the model indicate that reductive dissolution of iron-(hydr)oxide and ferric-arsenate minerals by dissimilatory iron reducing bacteria (IRB) and their subsequent re-precipitation, were the primary controls on short and long term changes in arsenic mobility during redox cycling. The fundamental importance of the interplay between hydrolysis of particulate organic matter (POM) and heterotrophic metabolism in controlling dissolved organic carbon (DOC) concentrations within soil pore-water is demonstrated, which in turn acts as a primary factor controlling rates of iron reduction. The observed attenuation of arsenic during repetitive redox cycling is attributed to the combination of decreased microbially mediated iron reduction, due to depletion of biologically degradable organic carbon (BDOC) and an increasing ratio of co-precipitated/adsorbed arsenic with each consecutive redox cycle.

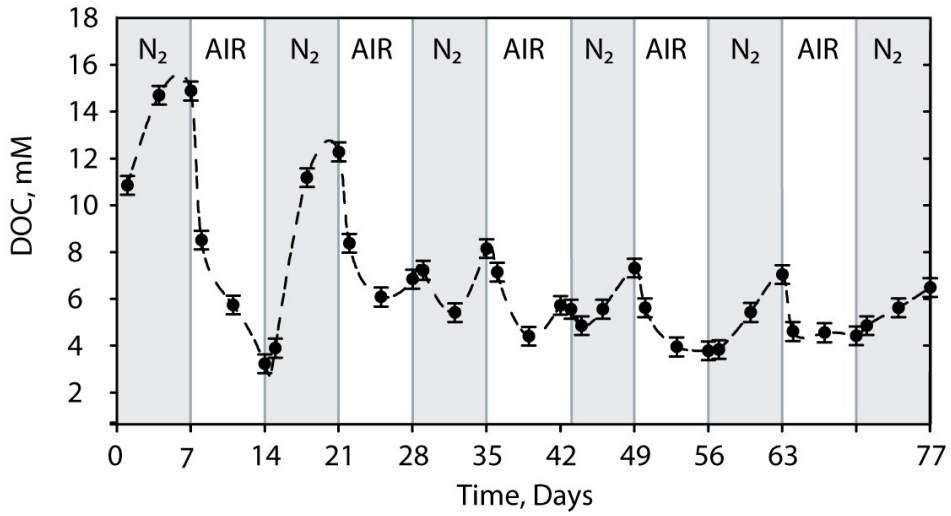

Summary Figure 7: Evolution of dissolved organic carbon concentrations in soil suspensions subjected to redox oscillating conditions.

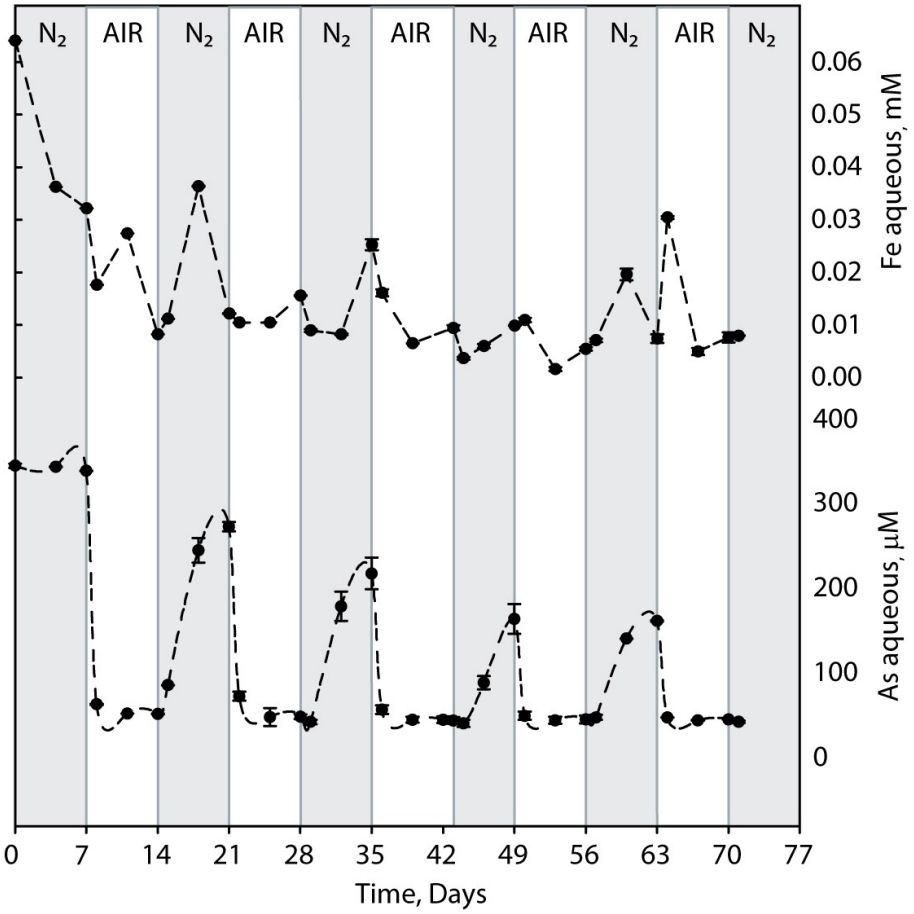

Summary Figure 8: Evolution of aqueous Fe and As concentrations with time in soil suspensions subjected to redox oscillations.

Redox oscillating conditions are also a concern to nuclear waste disposal organisations which are tasked with subsurface disposal of long lived low activity waste. Such waste is often association with secondary redox sensitive contaminants such as arsenic, chrome, selenium and mercury.

Current strategies involve near surface disposal of long-lived low-activity waste in clay-rich substrates which may be susceptible to redox changes due to groundwater rise and fall. Batch simulations of such cyclic redox changes were conducted on a suspension of Callovo-Oxfordian (COx) clay induced by gas sparging and addition of model humic substances, shown to be redox active components in such substrates. The effect of cycling on the mobility of added chromium, arsenic, mercury and uranium was investigated in the absence of microbial activity to isolate purely geochemical mechanisms. It was once again found that the transition between ferric and ferrous iron acted as the main buffer to redox change and had a primary influence on contaminant mobility. However cumulative trends in contaminant mobility were also present and indicate that repetitive cycling may attenuate aqueous chromium release during oxidising conditions.

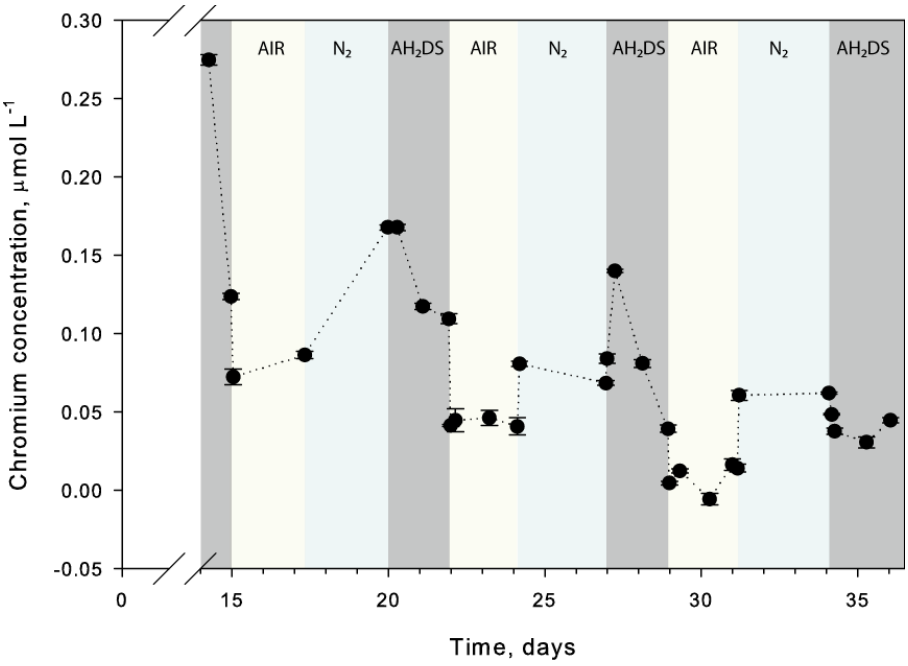

Summary Figure 9: The effect of experimental redox cycling on aqueous chromium concentration in a suspension of Callovo-oxfordian clay material. Note the changes to Chromium mobility both between oxidizing (white) and reducing (blue and grey) periods in addition to the cumulative reduction of aqueous concentrations due to mineralogical changes.

The results presented within this thesis highlight that although biogeochemical cycling of redox sensitive contaminants in dynamic natural systems is challengingly complex, by using a combination of techniques from traditionally separate academic disciplines, it is possible to strengthen our collective understanding of such systems.

Contents

Target publications and co-authors

Title: Quantitative use of FP-XRF for As analysis in Soils: Considerations for sample preparation and analytical validation

Authors: Chris Parsons, Eva Margui, Eric Pili, Geerke Floor and Gabriela Roman-Ross

Target journal: Journal of Hazardous Materials

Title: Physicochemical Controls on Arsenic Distribution on the Saône Floodplain

Authors: Chris Parsons, Eric Pili, Gabriela Roman-Ross and Laurent Charlet

Target journal: European Journal of Soil Science

Title: The Impact of Redox Cycling: Arsenic Attenuation in Contaminated Floodplain Soils

Authors: Chris Parsons, Raoul-Marie Couture, Enoma Omoregie, Fabrizio Bardelli, Jean-marc Greneche, Gabriela Roman-Ross and Laurent Charlet

Target journal: Environmental Science and Technology

Title: Redox cycling in clay rich barrier materials: Long term effects on contaminant mobility

Authors: Chris Parsons, Benoit Made and Laurent Charlet

Target journal: Chemosphere

Chapter 1: Review of redox processes affecting contaminant mobility

Abstract

Prevailing redox conditions have a profound effect on the mobility, toxicity and hence, the risk posed by many trace metals and metalloids in the environment (Borch et al., 2010). In soils and aquifers redox conditions are regulated by a complex combination of physical, chemical and biological processes which are ultimately driven by spatial partitioning of products from photo-chemical reactions driven by sunlight. The most obvious example of this is photosynthesis which produces highly reduced organic products and molecular oxygen. The molecular oxygen resulting from photosynthesis is released as a gas into the atmosphere whilst the reduced organic products form solids which ultimately are subject to sedimentation processes. This photosynthetic partitioning between oxidised gases and reduced solids in addition to long-term geological redox processes leads to a strong disequilibrium between the subsurface environment and the atmosphere thus creating a heterogeneous interface known as the critical zone. As solar irradiance on the earth surface varies cyclically due to the earth's spin (diurnal), solar orbit (annual), and other magnetic and orbital effects (e.g. Schwabe, Hale and Milankovitch cycles) so many redox processes affecting contaminant mobility are also subject to cyclic changes, linked to biological activity and cyclic climatic events. The effects of these cyclic redox conditions at different timescales in soils and sediments on contaminant mobility are numerous and complex.

The first chapter of this thesis summarizes the most critical factors which regulate redox conditions in the subsurface. An overview of some of the environments susceptible to temporal redox oscillations is given followed by a brief discussion of the main processes triggered by redox state change which may affect contaminant mobility and toxicity. The current state of knowledge of these processes in the natural environment in relation to four key redox sensitive inorganic contaminants; chromium, arsenic, mercury and uranium is then reviewed.

Processes affecting redox conditions in near surface soils and sediments

Oxygen transport from to the subsurface

The atmosphere has a mean oxygen concentration of approximately 20.95%. Processes controlling the transport and consumption of this oxygen in soils, sediments and aquifers act as primary controls on redox conditions. Oxygen can move through porous media via two key physical processes; advection and chemical diffusion (Fick's law).

Chemical Diffusion (Fick's Law)

Diffusion of oxygen from the surface into soils and sediments occurs via interconnected pore spaces. Partial pressure of oxygen in pore space decreases as a function of depth; this is often referred to as the soil redox gradient. This is due to the consumption of oxygen by aerobic bacteria, fungi and soil micro-fauna (e.g. protozoa, mites, springtails, nematodes, rotifers, and tardigrades) in addition to oxygen consumption by oxidation of chemically reduced species such as Fe^{2+}. The quality of the soil structure, particularly the presence of macro-pores and particle size distribution, directly affects the redox gradient by controlling the rate of oxygen diffusion with depth (Young and Crawford, 2004). In addition, soil structure creates local differences in

oxygen concentrations dependent on the interplay between diffusion rate within the soil microstructure and consumption rates by bacterial communities as illustrated in Figure 1.

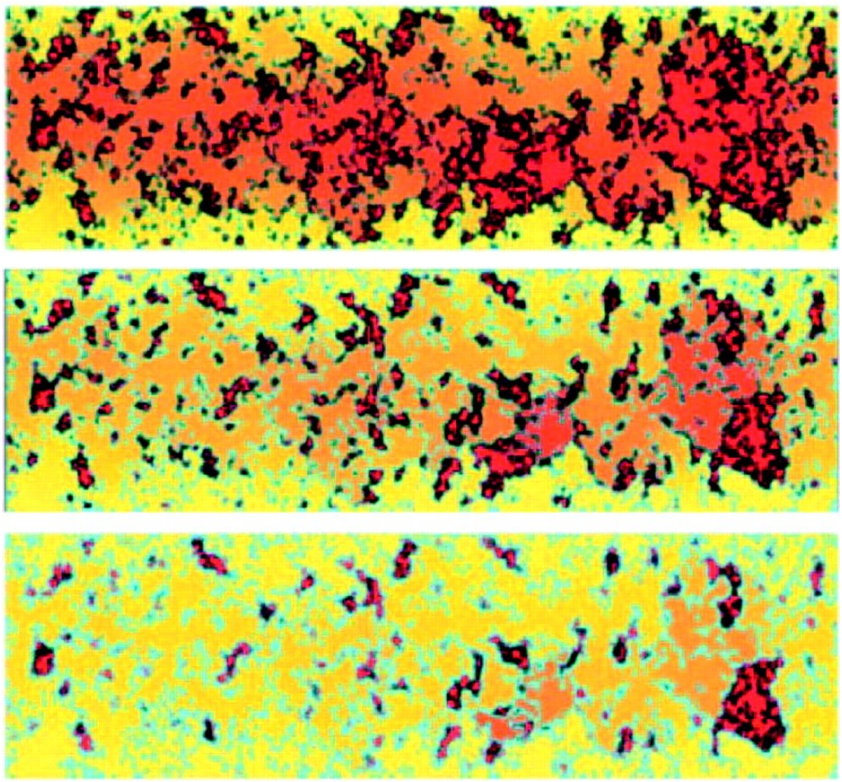

Figure 1: The predicted distribution of oxygen in structured soil modelled as a fractal and its dependence on microbial respiration rate. Each box represents a 2D layer of soil open to the atmosphere at the upper and lower boundary. The structure in each box is the same, whereas the potential respiration rate per unit volume decreases from a maximum (top) to a minimum (bottom). Red denotes low oxygen concentration, yellow denotes atmospheric concentration, and light blue is the soil matrix. The pore-scale spatial complexity and diversity of oxygen environments is obvious in all boxes, as is the spatial proximity of high and low oxygen concentration regimes. Even where potential microbial respiration is low, regions of low oxygen concentration prevail. From Young and Crawford (2004).

Soils with limited connectivity between pores or very low porosity are more likely to become sub-oxic and anoxic at a shallow depth than soils with high porosity and good pore connectivity. Rate of oxygen diffusion is also controlled by the composition of the fluid occupying the pore space. In air, oxygen diffusion occurs 10^4 times faster than in water (Ponnamperuma, 1972) therefore pore water greatly reduces the rate of oxygen diffusion. Thus seasonal changes in soil moisture can cause dramatic oscillations in oxygen concentration in soils and hence redox profiles. The depth extent of the vadose (or unsaturated) zone and redox gradient controlled by oxygen diffusion from the surface varies greatly between soils and sediments from between mm in saturated clay rich soils with high biological activity to hundreds of meters in highly porous loamy soils or in fractured rocks. Redox conditions within a soil profile however rarely conform to a simple gradient of oxic to reduced. Local soil and sediment structure has been shown to play an important role in regulating redox conditions (Pallud et al., 2010) with numerous studies showing dramatic micro-scale differences in redox conditions within the soil environment

caused by soil colloids, aggregates and otherwise poorly connected pore spaces where oxygen diffusion is limited. The recent synchrotron based µXRF and µXAS studies by Prietzel et al (2010) and Pallud et al (2010) focusing on sulphur and iron speciation within colloids and aggregates illustrate the prevalence of strong redox heterogeneity within soils even at the micro scale (Figure 2). Such micro-scale heterogeneity makes the task of predicting contaminant speciation challenging as average measured values used to feed thermodynamic and kinetic simulations rarely consider the wide range of local redox conditions possible.

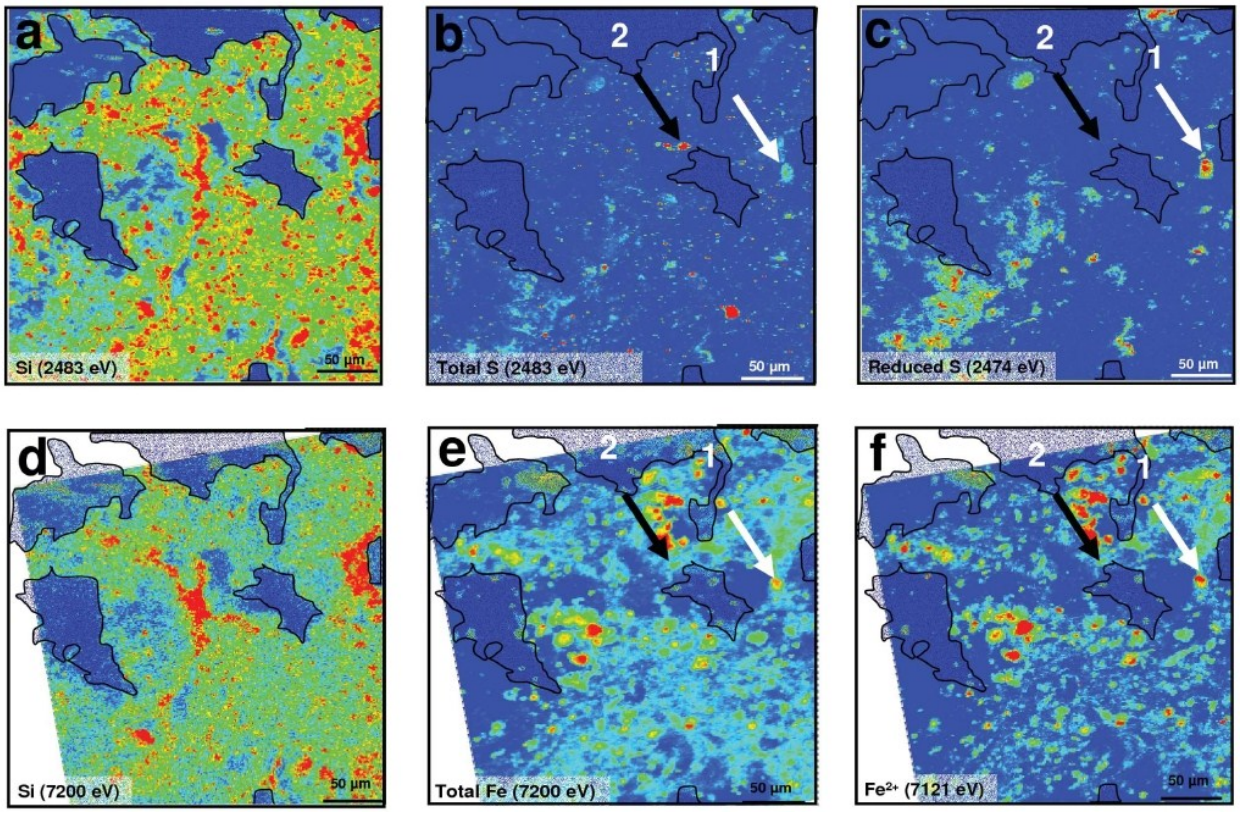

Figure 2: X-ray fluorescence maps of a dissected soil aggregate showing significant heterogeneity in structure, composition and speciation from Prietzel et al. (2010). (a) Map of total Si acquired with an X-ray energy of 2483 eV. (b) Map of total S acquired with an X-ray energy of 2483 eV. (c) Map of reduced S acquired with an X-ray energy of 2474 eV. (d) Map of total Si acquired at with an X-ray energy of 7200 eV. (e) Map of total Fe acquired with an X-ray energy of 7200 eV. (f) Map of elemental and divalent Fe acquired with an X-ray energy of 7121 eV. In maps (b)–(f), increasing concentrations of the elements or element species of interest are represented by a color change in the sequence blue–green–yellow–red.

Advection

Oxygen may also be transported from the surface to significant depth within pore water moving inside an aquifer (Figure 3). Rates of complex fluid movement through porous media can be orders of magnitude faster than diffusion dependent on the hydraulic conductivity of soils (a measure of the ease at which a fluid may travel through porous media based on porosity and interconnectivity of the soil pores usually expressed in cm/s) and the hydraulic gradient (a vector gradient dependent on the difference in hydraulic head at two measured locations). Aquifers with a high hydraulic conductivity and a high hydraulic gradient may transport fluids very rapidly both vertically and horizontally. This can lead to the presence of oxygen rich water at depth. In

addition, hydraulic gradient can vary dramatically between seasons depending on aquifer recharge; therefore some deep aquifers, which are not supplied with oxygen via diffusion from the surface, are also subject to oscillating redox conditions (Greskowiak et al., 2006).

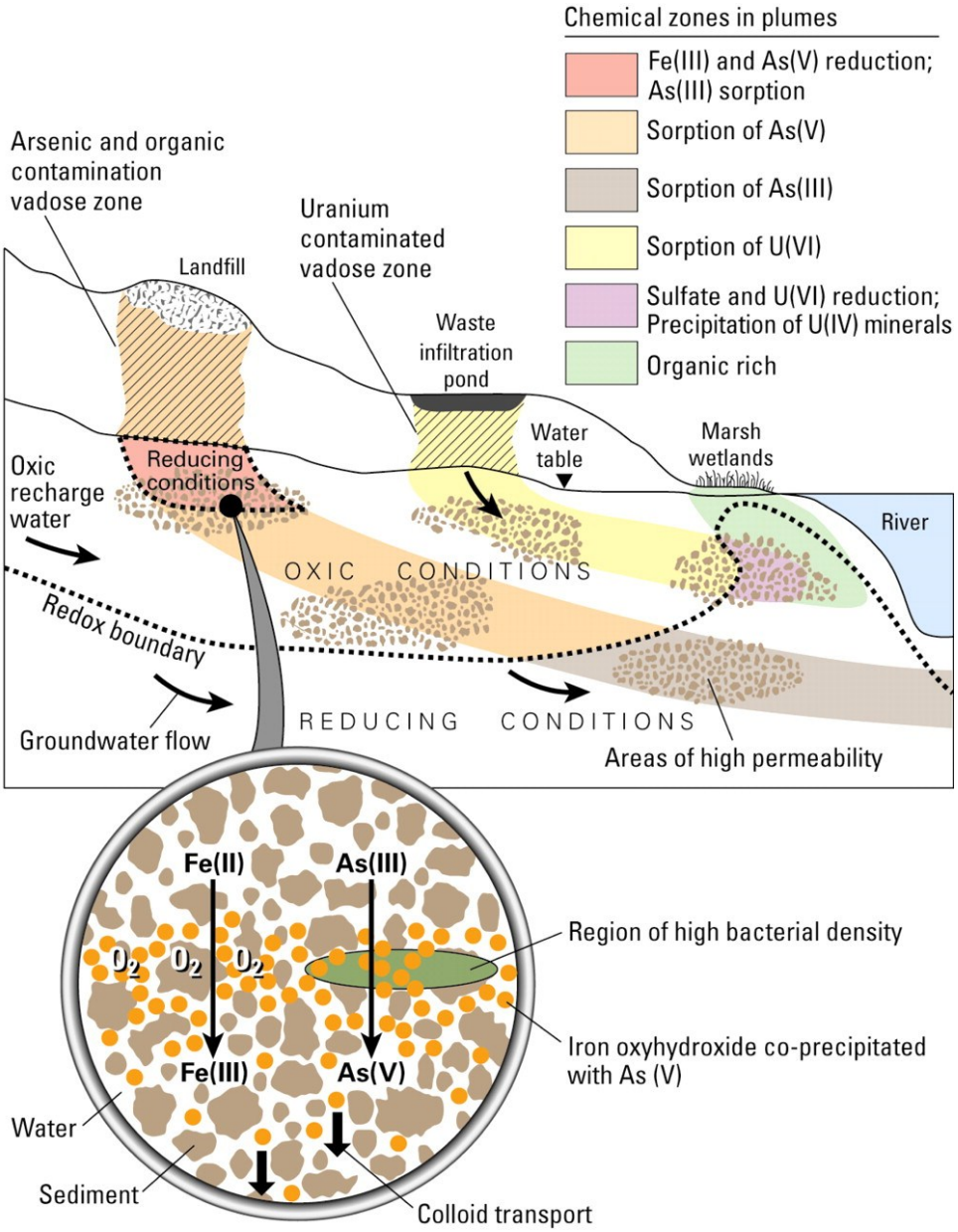

Figure 3: Schematic illustrating the effect of oxidative recharge by advection and the complex behaviour and transport of arsenic and uranium contaminants in changing sediment and redox environments from Davis et al. (2004).

Anaerobic metabolism of organic matter

Following oxygen concentration, the 2nd major control on redox conditions within the near subsurface is the microbial metabolism of organic matter linked to the reduction of various terminal electron acceptors (TEA). The extent of microbial and fungal activity in soil is not confined to the oxic region of the vadose zone. Many facultative and obligate anaerobic microorganisms are also able to use oxygen containing compounds such as nitrate, sulphate or iron oxides to metabolize organic matter, in some cases completely to CO_2 (Lovley and Phillips,

1986). The energetic efficiency of these TEAs, determines the order in which they are used by bacterial communities (Stumm and Morgan, 1996). As oxygen is the most efficient TEA available in the near subsurface Table 1) organisms cable of using it, (aerobes) are at a significant advantage compared to other bacteria when oxygen concentrations in the soil matrix are high and rapidly out compete others for space and nutrients. However, upon complete exhaustion of available oxygen, organisms must switch to alternative metabolic pathways or give way to other parts of the normally diverse bacterial community which are better adapted to prevailing conditions. Following oxygen consumption, as there is significantly more energy to be gained from the reduction of nitrate than sulphate, for example, (shown in Figure 4) bacterial communities will normally exhaust nitrate supply prior to the onset of sulphate reduction. Many of these reductive processes consume protons (shown in Table 2)and hence result in a net pH increase and Eh decrease as microbial communities descend this chain of TEAs.

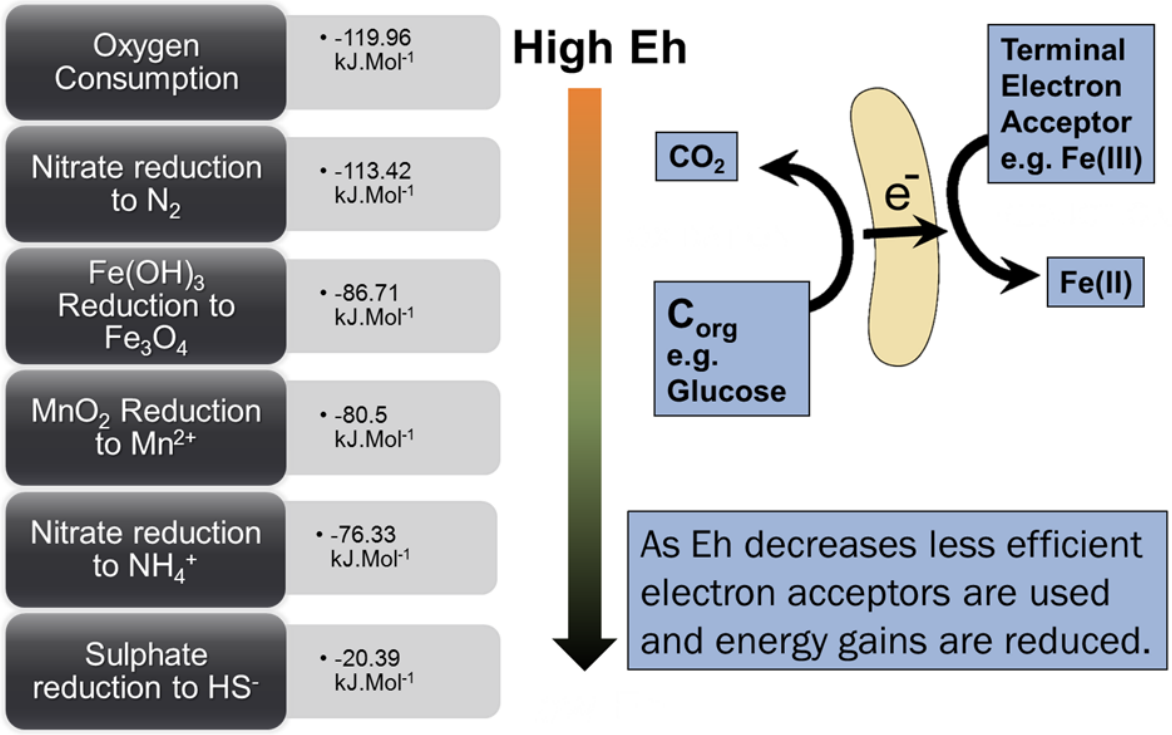

Figure 4: The reduction sequence in soils driven by microbial metabolism of organic matter using successively less efficient terminal electron acceptors. Energy (kJ per mol) values are the Gibbs free energy for the reduction of TEAs coupled to the oxidation of glucose at pH 7 and 25^{o}C normalised on a per electron basis.

One electron half-reaction for reduction of TEAs	ΣΔG° reactants (kJ/mol)	ΣΔG° products (kJ/mol)	ΔG_R^0 kJ/mol	Log K_R	Eh_{H0}, V	ΔG_R^7 kJ/mol (pH = 7)
$¼\ O_2 + H^+ + e^- \rightarrow ½\ H_2O$	0.00	-118.55	-118.55	20.77	1.23	-78.59
$^1/_5\ NO_3^- + {}^6/_5\ H^+ + e^- \rightarrow {}^1/_{10}\ N_2 + {}^3/_5\ H_2O$	-22.26	-142.26	-120.00	21.02	1.24	-72.05
$½\ MnO_2 + 2H^+ + e^- \rightarrow ½\ Mn^{2+} + H_2O$	-232.55	-351.15	-118.60	20.78	1.23	-38.69
$3Fe(OH)_3 + H^+ + e^- \rightarrow Fe_3O_4 + 5H_2O$	-2115.6	-2201	-85.30	14.94	0.88	-45.34
$^1/_8\ NO_3^- + {}^5/_4\ H^+ + e^- \rightarrow {}^1/_8\ NH_4^+ + {}^3/_8\ H_2O$	-13.91	-98.83	-84.91	14.88	0.88	-34.97
$^1/_8\ SO_4^{2-} + {}^9/_8\ H^+ + e^- \rightarrow {}^1/_8\ HS^- + ½\ H_2O$	-93.06	-117.04	-23.98	4.20	0.25	20.98
$^1/_8\ CO_2 + H^+ + e^- \rightarrow {}^1/_8\ CH_4 + ¼\ H_2O$	-49.30	-65.59	-16.29	2.85	0.17	23.67
$¼\ CO_2 + H^+ + e^- \rightarrow {}^1/_{24}\ C_6H_{12}O_6 + ¼\ H_2O$	-98.60	-97.19	1.41	-0.25	-0.01	41.36

Table 1: Reduction half reactions for common TEAs in soils and sediments at 25°C, calculated from ΔG_f^o values given in Lide (2009).

One electron reduction of common environmental TEAs coupled to glucose oxidation	ΣΔG° reactants (kJ/mol)	ΣΔG° products (kJ/mol)	ΔG_R^0 kJ/mol	Eh_H^0, V	ΔG_R^7 kJ/mol (pH = 7)
$^1/_{24}\ C_6H_{12}O_6 + ¼\ O_2 \rightarrow ¼\ CO_2 + ¼\ H_2O$	-37.917	-157.9	-119.96	1.24	-119.96
$^1/_{24}\ C_6H_{12}O_6 + {}^1/_5\ NO_3^- + {}^1/_5\ H^+ \rightarrow ¼\ CO_2 + {}^7/_{20}\ H_2O + {}^1/_{10}\ N_2$	-60.177	-181.6	-121.41	1.26	-113.42
$^1/_{24}\ C_6H_{12}O_6 + 3Fe(OH)_3 \rightarrow ¼\ CO_2 + {}^{19}/_4\ H_2O + Fe_3O_4$	-2153.52	-2240	-86.71	0.90	-86.71
$^1/_{24}\ C_6H_{12}O_6 + ½\ MnO_2 + H^+ \rightarrow ¼\ CO_2 + ¾\ H_2O + ½\ Mn^{2+}$	-270.47	-390.5	-120.01	1.24	-80.05
$^1/_{24}\ C_6H_{12}O_6 + {}^1/_8\ NO3- + ¼\ H^+ \rightarrow ¼\ CO_2 + {}^1/_8\ H_2O + {}^1/_8\ NH_4^+$	-51.829	-138.2	-86.32	0.89	-76.33
$^1/_{24}\ C_6H_{12}O_6 + {}^1/_8\ SO_4^{2-} + {}^1/_8\ H^+ \rightarrow ¼\ CO_2 + ¼\ H2O + {}^1/_8\ HS^-$	-130.98	-156.4	-25.38	0.26	-20.39

Table 2: Reduction of common environmental TEAs coupled to the oxidation of glucose at 25°C, calculated from $\Delta_f G^o$ values given in Lide (2009).

Substance/Species	Chemical Formula	$\Delta_f G^o$ at 25°C, kJ/mol	Reference
Oxygen	O_2	0	(Lide, 2009)
Water	H_2O	-237.1	(Lide, 2009)
Ammonia	NH_4^+	-79.3	(Lide, 2009)
Nitrate	NO_3-	-111.3	(Lide, 2009)
Nitrogen	N_2	0	(Lide, 2009)
Manganese dioxide	MnO_2	-465.1	(Lide, 2009)
Divalent Manganese	Mn^{2+}	-228.1	(Lide, 2009)
Divalent iron	Fe^{2+}	-78.9	(Lide, 2009)
Sulphate	SO_4^{2-}	-744.5	(Lide, 2009)
Hydrogen sulphide	HS^-	12.1	(Lide, 2009)
Carbon dioxide	CO_2	-394.4	(Lide, 2009)
Methane	CH_4	-50.5	(Lide, 2009)
Glucose	$C_6H_{12}O_6$	-910	(Schroeder, 1999)
Ferrihydrite	$Fe(OH)_3$	-705.2	(Majzlan et al., 2004)
Magnetite	Fe_3O_4	-1015.4	(Lide, 2009)

Table 3: Gibbs free energy of formation values used for calculations in Tables 1 and 2

Figure 5 shows the Eh conditions, at pH 6.5 to 7, whereby reduction of each of these TEAs becomes thermodynamically favourable, and is therefore predicted to occur. Also shown are some examples from the literature of the actual Eh conditions measured when microbial reduction of these TEAs is shown to occur.

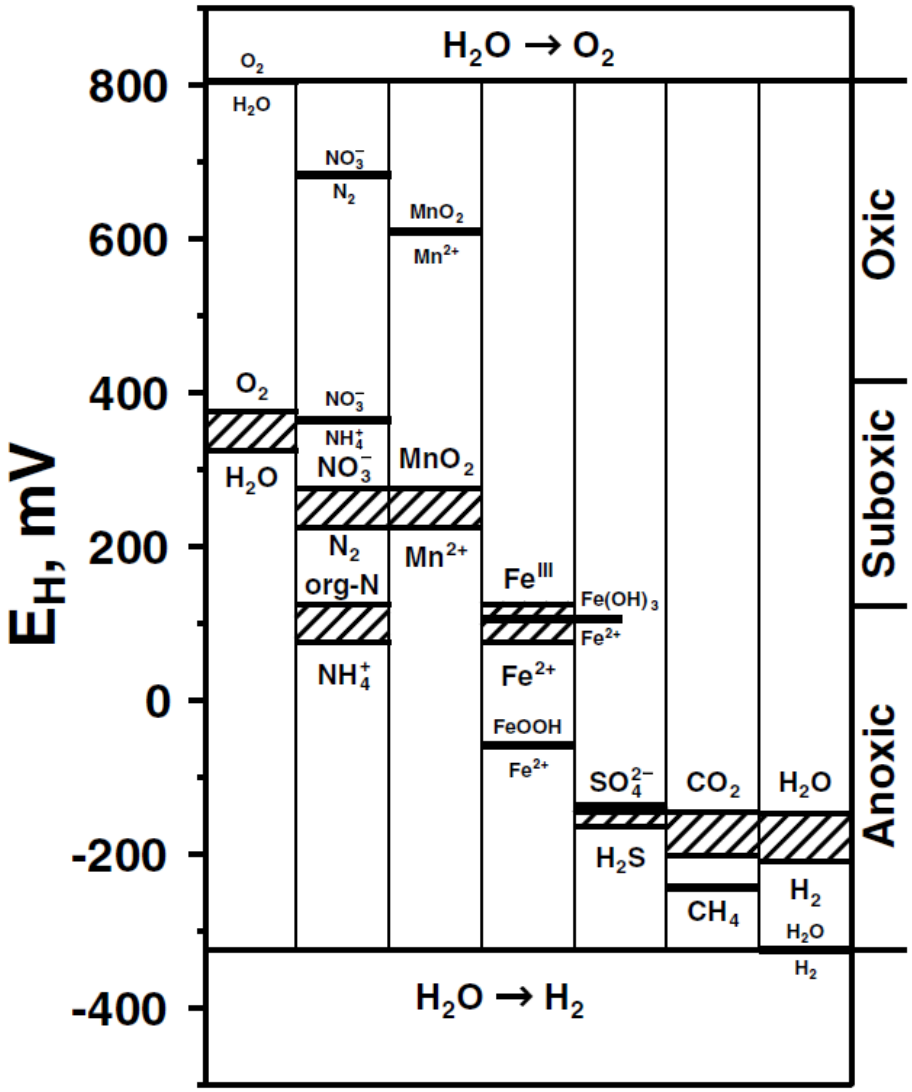

Figure 5: The reduction sequence in soils at pH 6.5 – 7 constructed using data from Patrick and Jugsujinda (1992); McBride (1994); and Sposito (2008). The Eh values where reduction of TEAs becomes thermodynamically favourable and is therefore predicted to occur are shown by black horizontal lines. Literature values for measured Eh during reduction of each of these TEAs are shown by shaded regions (from Essington (2004)).

Upon oxygen exhaustion in a soil or sediment matrix, further changes in redox conditions are usually determined by the availability of oxidisable organic carbon (or another suitable electron donor), the presence of an active anaerobic microbial community (and the nutrients they need to function) and the presence of a suitable TEA. In sediments rapid Eh drops have been measured due to the activity of facultative anaerobes (Nikolausz et al., 2008). Temporal variation in availability of labile organics, limiting nutrients or terminal electron acceptors can also lead to oscillating redox conditions.

Contaminant leachate plumes

The nature of contaminant leachate plumes from point sources such as landfills and industrial spills also directly influence redox conditions in sediments and pore water around the

contamination source. It is unlikely that the bulk potential of the leachate and the surrounding environment will be equal; therefore redox reactions between the leachate and the surrounding matrix are expected to occur often leading to a redox gradient as the plume moves through the host matrix. Frequently the fringes of leachate plumes are home to intense microbial activity as bacteria catalyse redox reactions profiting from the sharp disequilibrium as illustrated in Figure 3. In traditional municipal waste landfills the high proportion of organic waste often leads to highly reduced leachate plumes (Christensen et al., 1994) as bacteria oxidize organics coupled to reduction of terminal electron acceptors (see section .

Anaerobic metabolism of organic matter and Figure 3). These plumes become decreasingly reduced as they travel further from the leachate source and react with sediment and pore-water with typically higher redox potentials (Christensen et al., 1994). In contrast, leachate from industrial wastes containing for example, chromate, uranyl or chlorate ions conditions may be highly oxidizing and will become decreasingly oxidized as they move further into a comparatively reduced matrix. Determination therefore of leachate plume redox state and that of the surrounding sediment matrix is essential to determine possible redox interactions with the selected host sediment and to predict mobility of any given contaminant following releases to the environment.

Oxidation-Reduction Capacity of Sediment Matrix

As discussed in the previous section, depending on the stability of dominant Eh conditions within a sediment matrix, these conditions often result in the precipitation of minerals stable under these conditions and the equilibrium of redox sensitive aqueous species to these conditions. Intrusion of fluids which are in disequilibrium with matrix conditions will result in oxidation and reduction reactions between the intruding fluid and the matrix. Each matrix can be described as having an oxidation and reduction capacity dependent on redox active components in its structure.

Identification of redox active components within a soil or sediment matrix and evaluation of their capacity to buffer redox conditions through abiotic or microbially mediated reactions is crucial to determine the stability of redox conditions within the matrix. Common redox active matrix components include sulphide and oxide minerals and organic matter.

Environments commonly subject to temporal cycles of oxidation and reduction

Redox oscillating environments are diverse in nature and account for a significant proportion of the critical zone. Redox oscillations observed in nature vary both in amplitude (Eh conditions) and in length (time spent at Eh extremes). Short periodicity redox oscillating environments include those subject to diurnal Eh fluctuations, e.g. due to transport of oxygen into the rhizosphere by green-plants alternating between photosynthesis and respiration during the day and night respectively. Long periodicity redox oscillating environments include seasonally submerged soils on floodplains in temperate climates which experience redox oscillations which may last for several months. At the extreme end of the scale, coastline environments subject to flooding and draining due to changes in global sea level over thousands of years could be considered redox oscillating environments. However, for the purposes of this thesis the definition is constrained to environments subject to at least one full cycle of oxidation and reduction per year with a change of Eh substantial enough to cross stability boundaries of one or more major redox sensitive species (e.g. MnO_2/Mn^{2+} (log K_r = 20.8), NO_3^-/NH_4^+ (log K_r = 14.9), $HAsO_4^{2-}/H_3AsO_3$ (log K_r = 14.22), $FeOOH/Fe^{2+}$ (log K_r = 13.0) and SO_4^{2-}/HS^- (log K_r = 4.3)(James and Bartlett, 1999)). This definition encompasses a variety of environments which are characterised by constant adjustments of solid and aqueous phase speciation and microbial activity to new thermodynamic conditions. A short characterization of some of these environments is given below to highlight their prevalence in the critical zone.

Riparian floodplains

On floodplains seasonal climatic differences such as increased precipitation or snow melt high in the watershed often result in overbank or fluvial flooding. Depending upon the climate and topography within the watershed, this may result in the presence of a floodwater column over top soils for periods of days to months. This natural style of flooding is accompanied by input of fresh mineral sediment and solid organic matter. Such nutrient input stimulates microbial activity and higher soil fauna leading to rapid oxygen exhaustion during flooding and hence reducing conditions. Subsequently as floodwater drains back to the river the vadose zone is re-established and oxidising conditions prevail in top soils. However, the hydrological function of many rivers, particularly in the developed world are highly controlled in order to store water for recreation, domestic, industrial and agricultural use as well as to prevent damage to property and infrastructure caused by flooding. This anthropogenic flood prevention has a substantial impact on many natural processes and reduces sediment and hence nutrient deposition on floodplains.

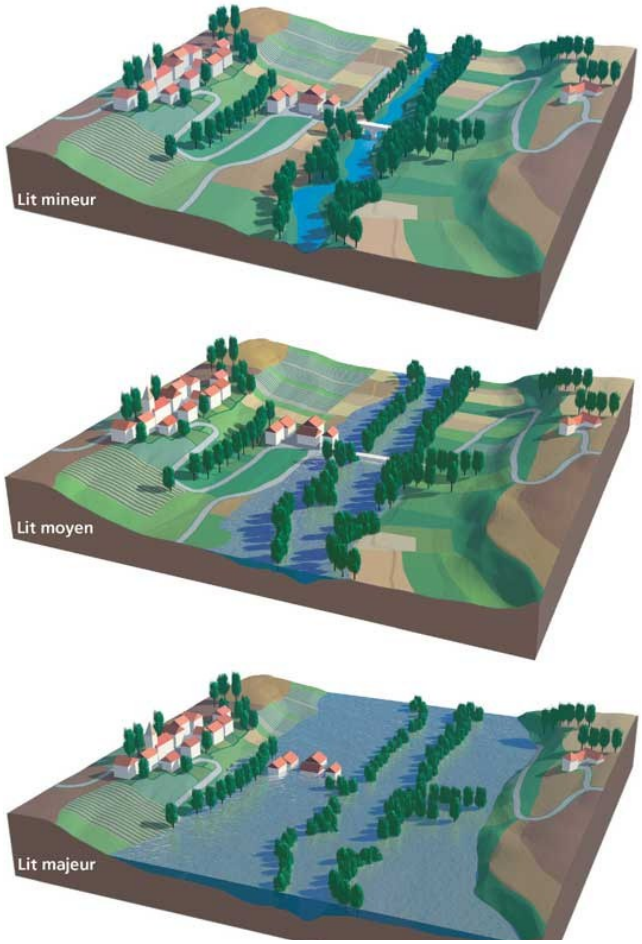

Figure 6: The progression of overbank/fluvial flooding. Reproduced from de Choudens, (2008). The terms Lit mineur, moyen and majeur correspond to river channel, lower and upper flood terraces.

Soils subjected to water table fluctuations

In some environments seasonal changes to aquifer recharge affect the level of the water table close to the surface even when physically separated from the nearest surface fluvial system. This can result in soils where the vadose zone extends to a depth of several meters at drier times of the year and where top soils are saturated and hence subject to reductive processes at wetter times of the year. This type of soil flooding caused by groundwater rise is known as phreatic flooding and soils at risk are often identified and mapped by government agencies due to the impact that such flooding may have on infrastructure and agriculture.

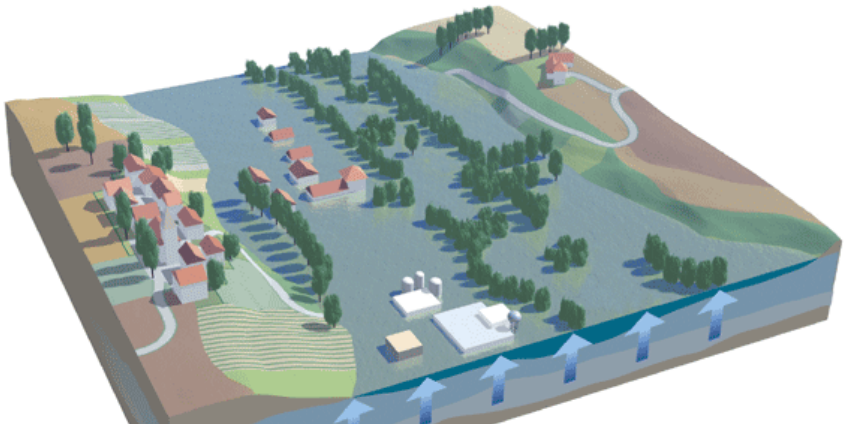

Figure 7: Illustration of the development of phreatic flooding. Reproduced from de Choudens, (2008).

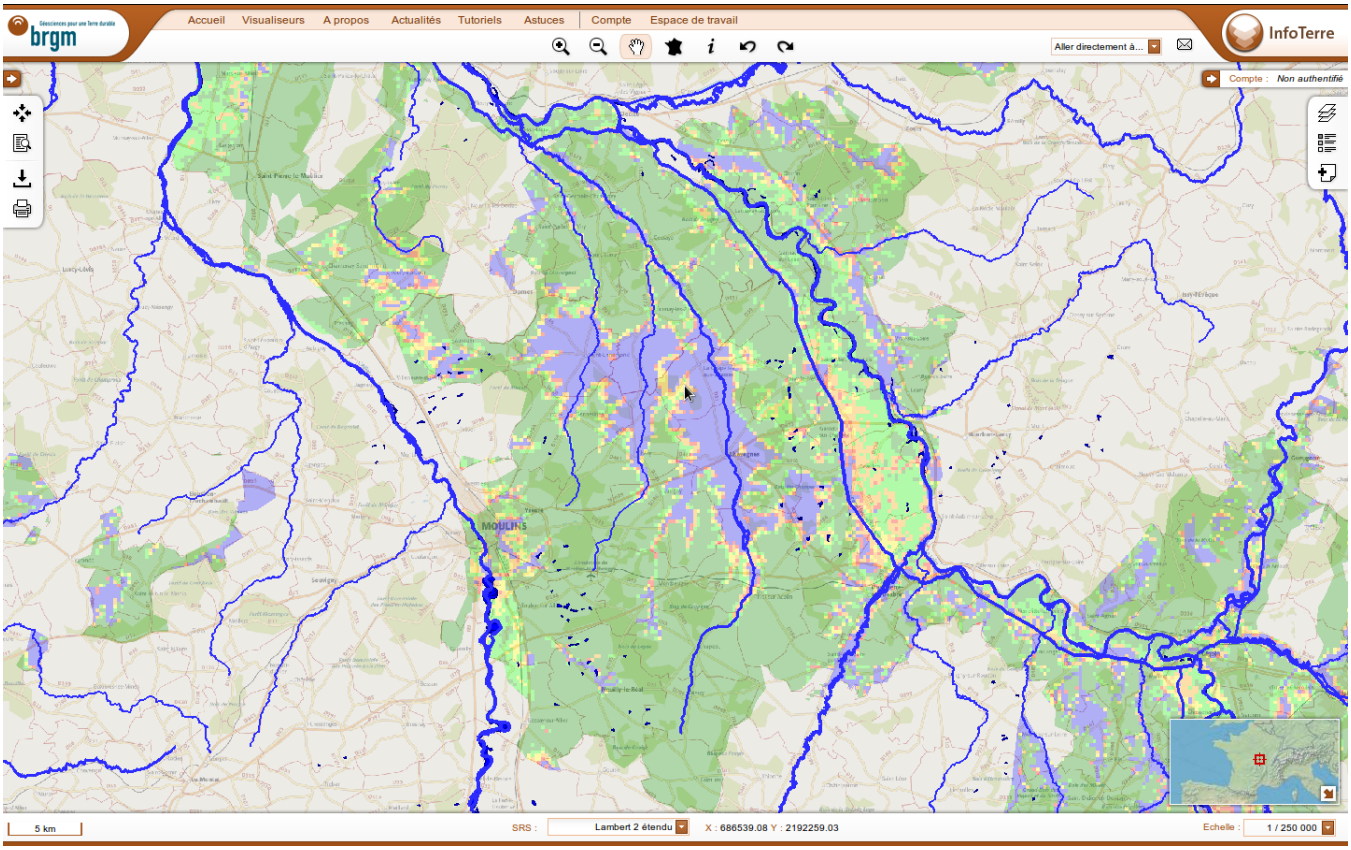

Figure 8: The BRGM InfoTERRE GIS (Geographic information system) tool (BRGM, 2010) can be used to visualize the risk of phreatic flooding in different areas of France. The risk of phreatic flooding to the area around the town of Moulins is shown (BRGM, 2006) with the fluvial system overlaid (Institut Geographique National de France, 2010) to illustrate the decoupling of the fluvial and phreatic hydrologic systems.

Rice fields

Although rice may be cultivated in the absence of flood water (Maclean et al., 2002) the most common practice is to flood fields periodically or continuously during the growing season which usually lasts for several months. Flooding helps protect the crop from vermin and reduces competition from less flood tolerant wild plants. Water depth must be carefully managed to avoid complete submersion of the rice plants for extended periods of time and may vary between a few cm to more than 1 m depending on the regional practices (Kirk, 2004). Flooding of rice fields may be accomplished via either limiting rain water runoff (the technique commonly employed in terraces e.g. Figure 9), by directing river water through artificial irrigation channels (e.g. the Ebro delta, Figure 10, or by pumping of groundwater (e.g. dry season rice in Bangladesh (Roberts et al., 2010) or Cambodia, Figure 11).

Figure 9: The Banaue Rice Terraces in the Philippines irrigated by rainwater runoff from the rainforests above. Photograph by Jon Rawlinson (2006) used under the creative commons license.

Figure 10: River fed rice field irrigation channel on the Ebro delta, Catalonia, Spain. Photograph by Alan Bell (2006) used under the creative commons license.

Figure 11: Flooding of rice fields by pumping shallow groundwater from tube wells in the Prey Krabah district of Takeo, Cambodia. Photograph by Dr. Donald Puckridge (2001) used under the creative commons license.

Top soil saturation and hence redox cycles in rice fields are often controlled by the irrigation practices of the farmer. A full reducing and oxidising cycle can vary between a few days and a full year depending upon whether fields are flooded periodically or continuously during the growing season.

Benthic sediments subject to bio-turbation by macro-fauna

Constant sediment turnover by benthic macro-fauna during burrow creation, grazing and burrow irrigation can result in temporal redox oscillations within the sediment. Deeper anoxic sediment is pushed upward into the sub-oxic surface and sub-oxic surface sediment is pushed down into the anoxic zone. Redox gradients are also experienced at tunnel edges as oxic water is flushed by organisms into burrows. As organisms move, burrows are created and filled resulting in complex three dimensional temporally varying redox conditions. As oxidised surface sediment is subject to greater biological activity and hence turnover than deeper sediment (Aller, 1994) estimate that this type of redox cycling results in sediment experiencing long anoxic periods (10-100x) and short oxic periods (x).

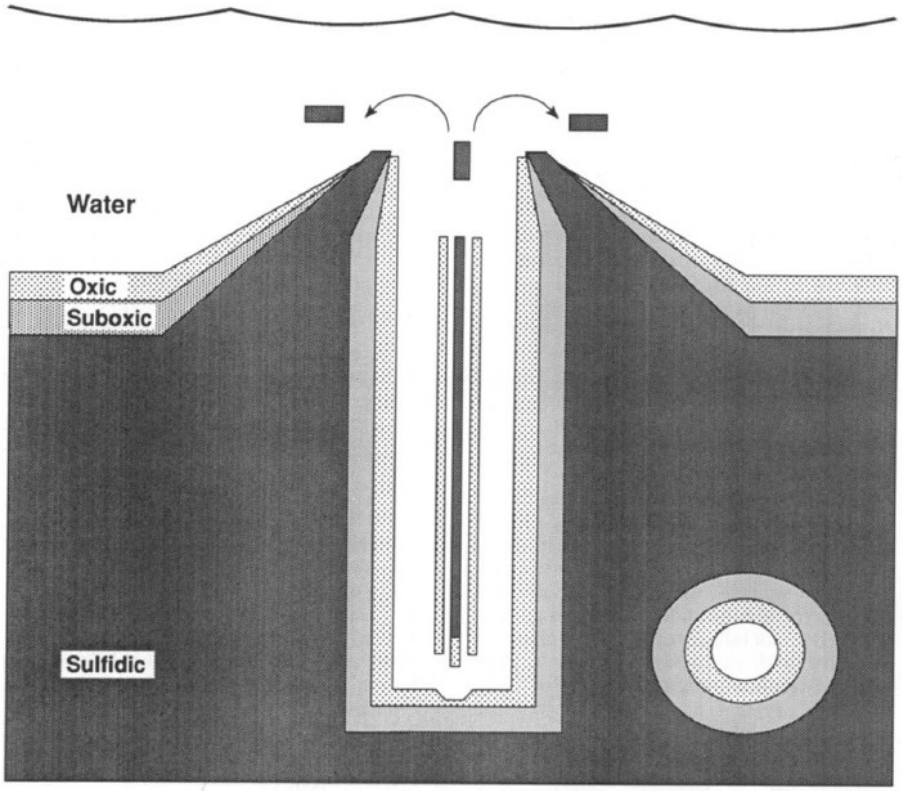

Figure 12: Schematic of temporally variable redox zonation caused by activity of benthic macro-fauna. Planar, radial, cylindrical and spherical redox geometries are all commonly observed in such environments. Reproduced from Aller (1994).

Soil subject to intense rainfall

Intense precipitation which provides water to a soil at a rate greater than percolation to deeper unsaturated sediments can result in complete soil saturation known as pluvial flooding (Kirk, 2004). This effect is often observed in tropical forest soils (Thompson et al., 2006) which are subject to annual rainfall as high as 1100 cm yr^{-1} (Giambelluca et al., 1986). Pluvial flooding is usually seasonal and therefore leads to cyclic oxidation and reduction in top-soils. In Hawaii for example soils are subjected to sustained saturation during the wet season between October and April and subsequently drain during the dry season from May until October. Pluvial flooding in this environment has been shown to be linked to Fe^{2+} concentrations in pore water indicative of iron oxide reduction. The cumulative redox cycling in this environment has been shown to have an important pedogenic effect resulting in transformation of short range ordered iron oxides to micro-crystalline goethite with successive cycling (Thompson et al., 2006).

Soil influenced by oxygenation within the rhizosphere

In some plants a type of highly porous tissue called aerenchyma forms in roots. Aerenchyma is particularly prevalent in plants which grow in saturated or periodically saturated soil (Armstrong, 1980). These large continuous cavities facilitate fast diffusion of gases between the root and the shoot. The presence of this tissue and hence fast gas exchange benefits the plant in a number of ways. The root tissues are supplied more rapidly with oxygen produced by green parts of the plant during photosynthesis and equally carbon dioxide produced by the root system during respiration diffuses upwards more quickly. Some of the oxygen within the root system diffuses out of root pores creating a thin oxygenated layer of soil around the roots (Armstrong, 1964). This oxic layer forms a redox barrier protecting the plant from high concentrations of reduced phytotoxins such as Fe^{2+}, Mn^{2+} and S^{2-} (Wheeler et al., 1985) as well as oxidising $NH^{4+}$to NO_3^- which is essential for plant nutrition (Bloom, 1996). The oxic zone also provides a habitat for aerobic bacteria around roots of aerenchymatous plants and leads to a highly diverse microbial community within the rhizosphere (Nikolausz et al., 2004).

Redox oscillations in the rhizosphere occur as green plants only photosynthesize and hence produce oxygen in the presence of sunlight. During darkness they continue to respire and consume oxygen and hence aerenchyma becomes depleted of oxygen during the night. As the diffusive input of oxygen to the rhizosphere decreases substantially during the night aerobic bacteria colonizing the rhizosphere rapidly exhaust residual oxygen. This combination of temporally variable photosynthesis, diffusion and respiration has been shown to result in strong diurnal redox cycling (Vorenhout et al., 2004; Nikolausz et al., 2008). In experiments conducted by Nikolausz et al (2008) Eh in the rhizosphere of the common rush plant (*Jumcus effuses*) oscillated between +300 and -320 mV within a 24 hour period dependent on light intensity. Oxidation in the rhizosphere has been shown to be limited to the zone immediately surrounding roots (approximately 0.4mm from the root surface (Revsbech et al., 1999)) and therefore generally leads to spatial heterogeneity of redox conditions. However, with sufficient root density such oscillations can significantly alter the bulk redox state of the soil.

Redox controls on contaminant mobility and toxicity

Distribution of redox sensitive inorganic contaminants within environmental media is governed by competition between organic complexation/decomposition, dissolution/precipitation, redox reactions, methylation/de-methylation and adsorption/desorption processes which are dependent on pH and Eh conditions (Borch et al., 2010). Determining pH and redox conditions in pore water and assessing the stability of the organic and mineralogical components of the soil matrix are critical to determining contaminant mobility and also toxicity.

Direct controls on oxidation state

The most direct redox control on contaminant toxicity and mobility is oxidation state change. Many different inorganic contaminants such as Mn, Cu, Co, Sb, Se, Tc, Pu and Np in addition to Cr, As, Hg and U discussed here may exist in different valence states, which affect their toxicity, bioavailability and mobility.

Whilst the dominant contaminant species and the proportion of secondary species stable in a natural matrix under given conditions may be determined thermodynamically from chemical composition, Eh, pH, temperature and pressure (expressed graphically in Pourbaix diagrams e.g.

Figure 31) and hence interactions between contaminant and matrix inferred, soils and sediments are rarely in thermodynamic equilibrium. This can be due to slow kinetic reaction rates or additionally due to rapid changes in redox potential due to complex biological catalysis of many processes responding to subtle environmental changes. In addition the thermodynamic calculations possible using programs such as PHREEQC (Parkhurst et al., 1999) or Geochemists workbench (Bethke and Yeakel, 2009) are reliant on the accuracy of constants contained within their thermodynamic databases which in some cases are well defined and in others are incomplete or poorly defined. The comparison conducted by Takeno in the Atlas of Eh-pH diagrams (Takeno, 2005) clearly demonstrates that even in a simple X-O-H system at room temperature there are often major inconsistencies between databases with respect to possible species and transitions. When extrapolated to natural systems with many different chemical components and changing conditions, thermodynamic calculations must be used with caution and an appreciation of their reliability in any particular system. Often to achieve the best possible understanding of speciation within a natural system, a combination of spectroscopic techniques such as XANES and EXAFS in addition to thermodynamic modelling is desirable (Voegelin et al., 2005; Kirpichtchikova et al., 2006).

One common trend with all redox reactions is the necessity for an electron transfer mechanism. These electron transfer mechanisms have been investigated experimentally and debated in the literature for decades and continue to be the subject of considerable research (Borch et al., 2010). In the simple case of aqueous reactions three electron transfer mechanisms have been described: inner sphere (Traube theory) which is not the rate limiting process, outer sphere (Marcus theory) and diffusion controlled which are both usually the rate limiting step in redox reactions. Outer sphere electron transfer is the most common mechanism in nature and therefore kinetics of redox reactions are determined by the rate of electron transfer and hence Markus theory.

The kinetics and thermodynamics of redox reactions are however far more complicated as many such reactions do not occur in aqueous solution. Surfaces such as bacterial membranes, minerals or organic matter can have a dramatic effect on redox reactions and often act as catalysts even if the surface itself does not participate directly in the redox reaction (Sposito, 2004). Redox reactions occurring at surfaces are often multi step reactions involving the surface complexation of the reductant or oxidant, formation of ternary complex involving the sorbed oxidant and the reductant, electron transfer and finally destabilization of the complex due to the formation of the reaction products (Sposito, 2004). It has been shown that during this process the surface simply acts as a physical facilitator of the reaction (Chakraborty et al., 2010) or in many cases structural components of the surface are involved in the reaction either as electron donors or acceptors (Wersin et al., 1994; Ilton et al., 2004).

Controls by surface sorption/desorption

Sorption and desorption of contaminants from mineral surfaces and solid organic matter are important controls on mobility in natural systems. While Eh variations may not directly influence the sorption capacity of a particular species to a particular surface these changes in Eh are accompanied by changes in pH which will affect the charge of the sorbent surface influencing sorption behaviour. Additionally Eh variations may influence the stability of different

aqueous species with different sorption behaviours. Various sorption processes e.g. chemisorption and physisorption, are shown in Figure 13.

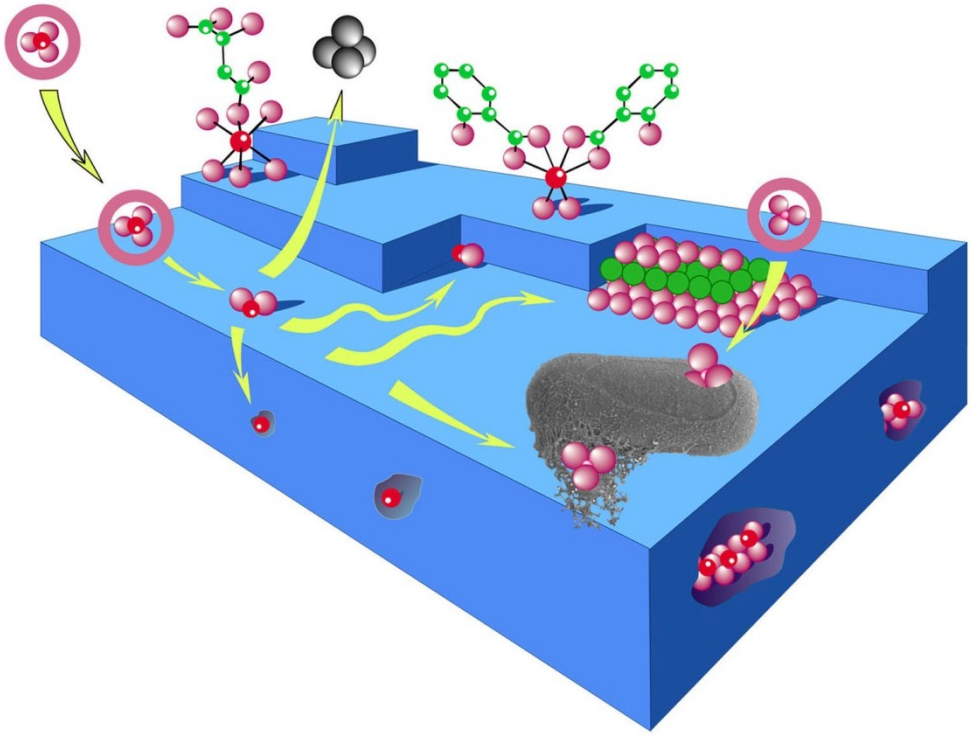

Figure 13: Summary of basic processes occurring at the mineral-water interface including: Physisorption, chemisorption, desorption, inclusion, occlusion, attachment, hetero nucleation, organo-mineral complexation and complexation to a bacterial film (From Manceau et al. (2002) modified from Charlet and Manceau (1992a).

Controls by solid precipitation/dissolution

Precipitation and dissolution of solid mineral phases also control contaminant mobility in the environment. Contaminant mobility may be reduced due to precipitation of major mineral phases by either inclusion (where a contaminant ion directly replaces an ion of similar charge and size within a mineral structure) or occlusion (whereby pockets of contaminant species are enclosed within a precipitating mineral) shown above in Figure 13. Additionally precipitation of discrete contaminant mineral phases (e.g. $Cr(OH)_3$ and Cr_2O_3) may also limit contaminant mobility in situations where high contaminant concentrations cause a super-saturation with respect to a particular mineral. As the saturation index for most minerals is highly dependent on Eh and pH conditions, overriding redox conditions in sediments also control contaminant mobility via precipitation and dissolution processes. In many case oxidation/reduction and dissolution/precipitation processes are linked when different oxidation states of an element have dramatically different solubilities. This is the case for both iron and uranium hence the oxidative dissolution of pyrite causing acid mine drainage or the biogenic precipitation of $U(IV)O_{2(s)}$ as a product of U(VI) reduction.

Minerals which often play an important role in contaminant mobility and are susceptible to dissolution/precipitation under environmental conditions include iron oxides, manganese oxides, iron oxy-hydroxides, metal carbonates and metal sulphides.

Iron and manganese oxides and oxyhydroxides have a strong affinity for many contaminants including As, Cr and U and as such can immobilize them either via surface sorption or incorporation. However iron and manganese oxides and oxyhydroxides are susceptible to reductive dissolution under anoxic conditions, a process which is often driven my facultative anaerobes such as Shewanella and Geobacter (Lovley et al., 1993) genera which can lead to the liberation of previously immobilized contaminants into pore water.

Under reducing conditions carbonates such as siderite ($FeCO_3$) and rhodocrosite ($MnCO_3$) or sulphides such as pyrite (FeS_2) may form which also act as sorbents for contaminants however rarely to the same extent as their oxidized equivalents. Upon a change to oxidizing conditions these minerals are also susceptible to oxidative dissolution which is again often catalysed by bacteria such as the Leptothrix genus bacteria.

Mercury

Mercury may exist in the environment in three different oxidation states 0 (Hg^0), +1 (Hg_2^{2+}) and +2 (Hg^{2+}) dependent on prevailing redox conditions (Andersson, 1979) either as a free ion, sorbed to mineral (Reimers and Krenkel, 1974) or organic surfaces (Drexel et al., 2002) or else as a mineral precipitate such as cinnabar (HgS). The simple Hg – H_2O system shown in Figure 14 where Hg^0 and $Hg(OH)_2$ dominate in almost all conditions, is however a poor reflection of the real speciation of Hg in the environment due to the tendency of Hg_2^{2+} and Hg^{2+} states to complex with many different organic and inorganic ligands in solution (including Cl^-, OH^-, S^{2-}, F^-, Br^-, I^-, SO_4^{2-}, NO_3^-). The thermodynamic dominance of Hg^{2+} over Hg_2^{2+} in the environment (Figure 14), in addition to its high solubility and reactivity have made the behaviour of Hg^{2+} in the environment the subject of significant and on-going research (Gabriel and Williamson, 2004). It has been shown that Hg_2^{2+} formed in the environment rapidly dissociates to Hg^{2+} and Hg^0.

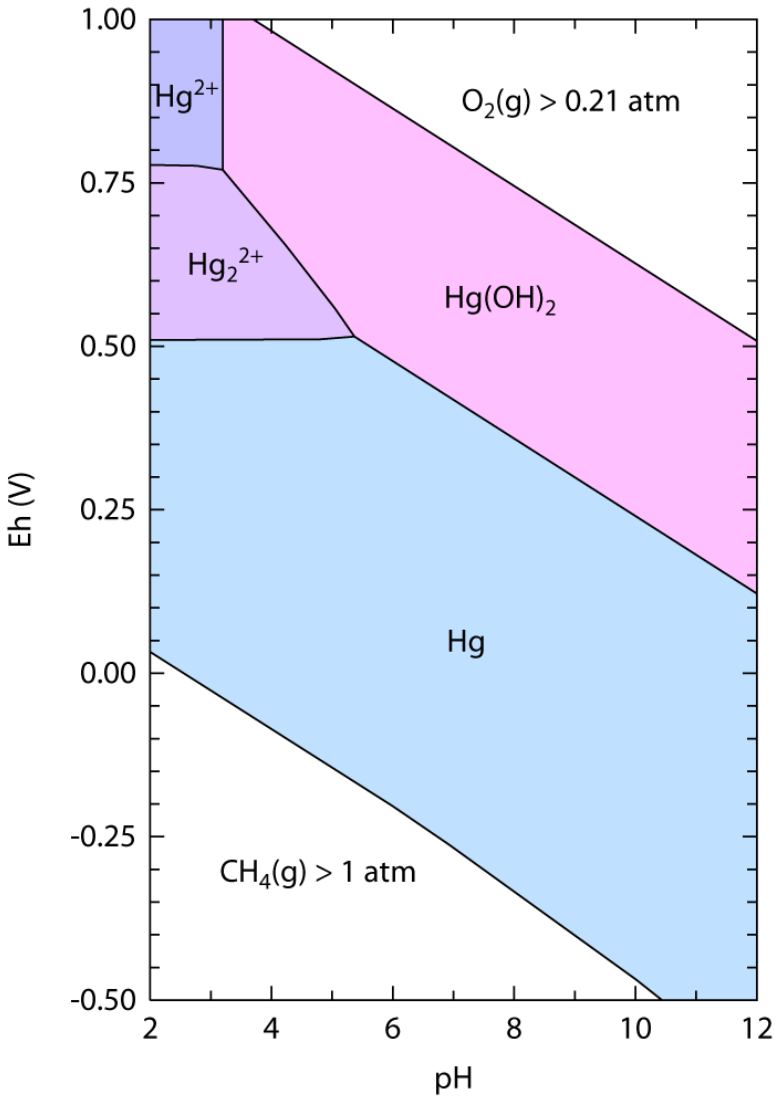

Figure 14: Pourbaix diagram of the Hg - H_2O – CO_2 system at 298.15K and 10^5 Pa from LLNL data.

The high toxicity of Hg, its propensity for accumulation in biological media in its methylated forms and its highly mobile nature across all three oxidation states make understanding its behaviour in the environment an important concern.

Sorption behaviour of Mercury in Soils and Sediments

It is considered that surface sorption is the dominant process controlling Hg mobility in soils and sediments, especially in oxic to sub-oxic conditions or in the absence of sulphide in anoxic conditions. While some mercury species may sorb to surfaces based on weak electrostatic attraction, it has been demonstrated that surface complexation is the stronger and most dominant mechanism under most environmental conditions as many aqueous mercury species, such as $Hg(OH)_2$ are neutrally charged. Surface complexation occurs primarily with OH^-, Cl^- and numerous organic anions with reduced sulphur functional groups (Schuster, 1991).

In addition to immobilization of free Hg species in solution and hence limiting transport of mercury within the subsurface, sorption to mineral surfaces or solid organic matter may promote or increase the potential for methylation and de-methylation of mercury species and hence limit or increase its toxicity dependent on the sorbent (Jackson, 1998). For this reason understanding sorption behaviour of Hg in soils and sediments is of dual importance.

Solution pH exerts a major control on Hg sorption in soils and sediments and as with most metals, Hg sorption generally increases with increasing pH due to de-protonation of surface sites allowing for increased metal sorption on negatively charged sites (Essington, 2004). This phenomenon is illustrated in Figure 15 using the example of sorption of Na^+ ions to the surface of Gibbsite.

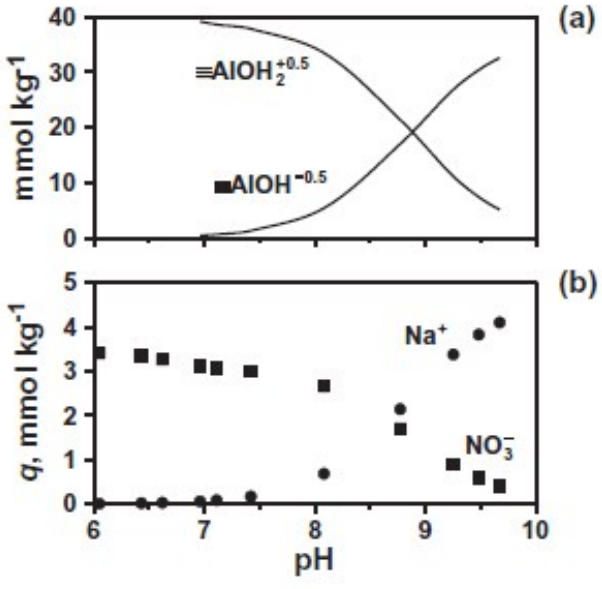

Figure 15: (a) The concentrations of positively and negatively charged surface sites on gibbsite and (b) the corresponding adsorption behaviour of Na^+ and NO_3^- as a function of solution pH (from Essington (2004)).

Acidification has been shown to cause rapid release of both inorganic and organic Hg species into solution even at pH values of as high as 5 (Driscoll et al., 1995; Amirbahman et al., 2002).

Measured sorption envelopes for Hg show however, that at neutral to high pH sorption of Hg to various mineral surfaces decreases (Sarkar et al., 1999) Figure 16. This is due to the hydroxylation of aqueous Hg species at high pH and hence the increasing dominance of the stable $Hg(OH)_{2(aq)}$ species leading to desorption from mineral surfaces (Schuster, 1991).

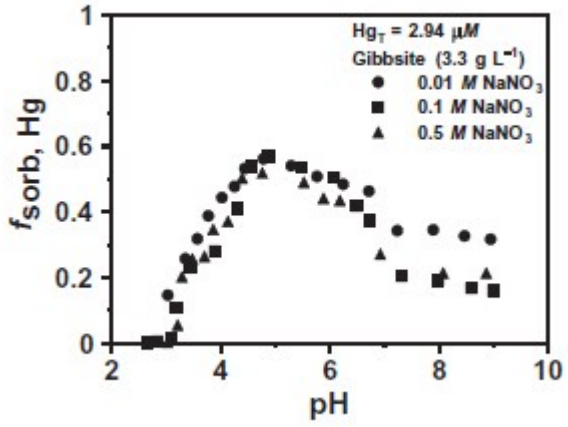

Figure 16: Adsorption of Hg(II), expressed as a fractional amount of the total Hg(II) concentration (f_{sorb}), by gibbsite as a function of pH and ionic strength (from Sarkar et al. (1999)).

Various minerals have been evaluated as sorbents of organic and inorganic Hg including metal oxides, hydroxides, oxy-hydroxides, metal sulphides and clays. Hg sorption on all minerals shows a strong pH dependence however certain minerals such as illite, gibbsite and iron oxides have been identified as more efficient sorbents than, for example, bentonite and kaolinite based upon the pH at which desorption occurs during acidification (Andersson, 1979). Kaolinite in particular has been identified as having a low sorption capacity for Hg whereas metal oxides have been shown to have high sorption capacities for Hg species.

Many authors report that organic matter in sediments acts as an important sorbent for Hg species and that especially in acidic conditions sorption to organic matter may be more important in controlling Hg mobility than sorption to mineral surfaces (Andersson, 1979; Schuster, 1991; Jackson, 1998). Some authors also indicate that sorption of Hg species to organic matter may become more important with increasing Cl^- concentrations (Reimers and Krenkel, 1974; Reddy and Aiken, 2001).

The influence of Cl^- concentrations in solution upon Hg sorption is not clear and studies have reported varying effects. Generally, increasing chloride concentration is thought to cause the formation of stable Hg Cl complexes (Figure 17) and a decrease in surface sorption of both methyl and inorganic mercury species is often recorded e.g. (Leckie, 1986; Jackson, 1998).

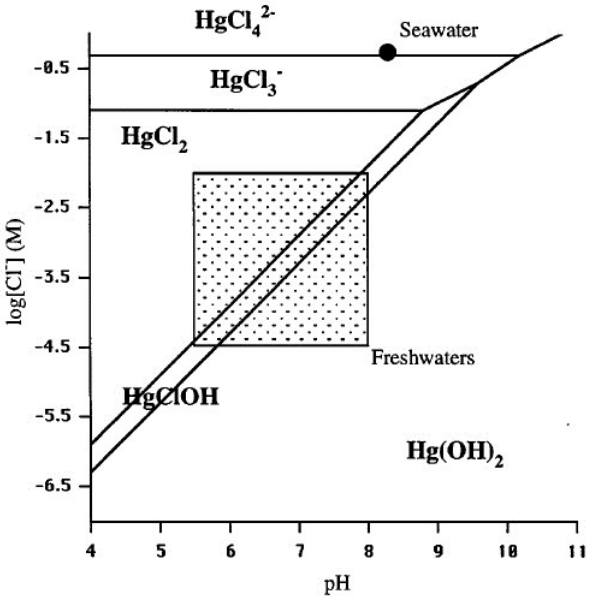

Figure 17: The effect of varying pH and chloride concentration on aqueous Hg speciation. From Morel et al. (1998).

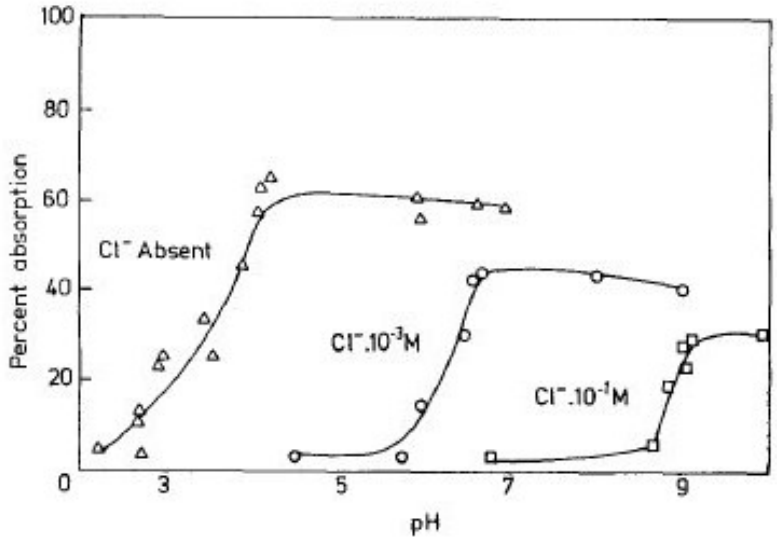

Figure 18: The adsorption of Hg(II) on silica as a function of solution pH and chloride concentration. For a given pH, increasing Cl concentration reduces Hg(II) uptake. From Leckie (1986).

This trend is supported by studies by Reimers & Krenkel (1974) who show the effects of different Cl concentrations on methyl-mercury and inorganic mercury species on various minerals over a range of pH conditions. They show that increasing chloride concentration decreases sorption of both organic and inorganic mercury on clays but that the severity of this effect is dependent on the clay mineralogy. Mercury species sorbed to illite were shown to be less affected than those sorbed to kaolinite (30% reduction in the sorption capacity of illite at 1000ppm chloride concentrations compared to 50% reduction in sorption capacity of kaolinite at just 100ppm chloride concentrations).

Conversely, Xu and Allard (1991) report that the presence of chloride may increase mercury sorption when pH is less than the point of zero charge (pzc) of the sorbent, possibly due to the formation of $HgCl_3^-$ species in solution. This result has implications for clay surfaces covered in iron oxide coatings which typically have high pzc e.g. hematite at pH 8.5 -8.8 (Eggleston and Jordan, 1998).

The role of dissolved organic carbon (DOC) on Hg adsorption and methylation is a subject of intense current research however in the majority of cases increasing DOC inhibits surface sorption due to the formation of stable, soluble Hg-organic complexes (Ravichandran, 2004). It has long been suggested that such strong Hg-organic complexes are the result of Hg binding to thiol like functional groups and recently this suggestion has been confirmed via spectroscopic techniques (Xia et al., 1999; Drexel et al., 2002). Other authors suggest that DOC may limit sorption of aqueous Hg species by competing for surface sorption sites (Drexel et al., 2002).

Under some circumstances however, the presence of DOC has been shown to increase surface sorption of aqueous Hg species due to strong affinity between the organic anion and the sorbent (Xu and Allard, 1991).

Oxidation and Reduction of Mercury in Soils and Sediments

Reduction of Hg^{2+} to Hg^0 and re-oxidation of Hg^0 to Hg^{2+} are important and well documented processes regulating mercury mobility and toxicity in soils and sediments. Reduction and oxidation have been shown to occur both abiotically and biotically (Schluter, 2000). Hg^0 is considerably more volatile than ionic mercury species and hence reduction to Hg^0 can lead to significant increases in mobility via transport in the gas phase. Abiotically, in addition to photochemical reduction of $Hg(OH)_2$ by sunlight (Munthe and McElroy, 1992), Fe^{2+}, fulvic and humic acids (Allard and Arsenie, 1991) have also all been shown to reduce Hg^{2+} to Hg^0 in the environment. Mechanisms of abiotic reduction of Hg^{2+} vary considerably, however Hg^{2+} is a readily available electron acceptor in reducing conditions, (Allard and Arsenie, 1991) have shown that abiotic reduction by fulvic acid proceeds only after complexation with Hg^{2+} and is followed by dissociation after reduction.

Microbial reduction of Hg^{2+} to Hg^0 is a detoxification mechanism by soil micro-organisms is a well-known process and one which is often exhibited by soil communities usually by the presence of the mercury reductase enzyme encoded by the merA gene (Barkay et al., 2003). The addition of mercury in the subsurface has been shown to modify the composition of microbial communities favouring those parts of the community with mercury resistance and the ability to reduce Hg^{2+} to Hg^0 (Harris-Hellal et al., 2009). Some organisms have also been shown to be able to oxidize reduced methyl mercury species as an energy gaining process (Billen et al., 1974). Comparing the relative importance of abiotic and biotic reduction processes in the laboratory is challenging as the common process used to sterilize soils and sediments, autoclaving, may potentially degrade humic and fulvic acids, which as previously discussed are key abiotic reductants of Hg^{2+} (Schluter, 2000). It has however been shown that a relatively high threshold concentration of Hg^{2+} is necessary within soils and sediments in order to induce microbial reduction to Hg^0 (Faassen, 1973). This threshold value is poorly defined as availability of Hg^{2+} for microbial reduction varies considerably between sediments due to factors such as mineralogy and complexation, however (Faassen, 1973) indicates that at least several hundred ppm of total

Hg are required in an unreactive matrix, for instance large grained quartz sand in the absence of significant complexing ligands, to induce biotic reduction. In addition to this threshold value a lag period is observed during microbial reduction upon addition of Hg^{2+} to sediment linked to the growth period required for Hg^{2+} reducing organisms. For this reason it is thought that in highly contaminated soils and sediments with all the necessary nutrients to support an active microbial community biotic reduction is likely to be the dominant process but where concentrations are lower, there is lack of a suitable microbial community or in the presence of large amounts of reactive organic matter, abiotic processes are likely to dominate (Schluter, 2000).

To some extent however microbial activity supports abiotic mercury reduction as reactive organic reductants of Hg^{2+} are often products of other microbial metabolic processes. Equally iron reducing bacteria such as Geobacter species are ubiquitous in the subsurface and may provide Fe^{2+} for abiotic reduction of Hg^{2+} as product of other energy gaining processes.

Due to the high binding strength of Hg^{2+} to organic matter re-oxidation of Hg^{0} often occurs at redox potentials significantly lower than those predicted purely thermodynamically by the relevant half reactions (Jernelov, A, 1969).

Precipitation and dissolution processes affecting Mercury mobility in Soils and Sediments

Despite the fact that mercury has a strong affinity for hydroxide and chloride ions, and that these anions are very commonly present in high concentrations in pore water, the solubility products of mercury di-chloride and mercury di-hydroxide are very high and therefore Hg activity in solution is too low in low temperature natural systems to cause precipitation of such minerals (Schuster, 1991). HgS or cinnabar does however have a very low solubility (0.002 ng g^{-1}) (Schuster, 1991)and is stable under reducing conditions making it the only Hg mineral found to occur, or thermodynamically predicted to occur, in contaminated soils and sediments, despite the existence of a large variety of high temperature mercury containing minerals within ore bodies.

Whilst HgS in simple systems is extremely stable under reducing conditions, numerous factors have been shown to increase its solubility. The simplest factor which has been shown to cause the dissolution of both α-HgS and β-HgS is addition of O_2 (Holley et al., 2007). Factors affecting the rates of oxidative dissolution of both forms of HgS are poorly understood with disparate dissolution rates reported in the literature (Barnett et al., 2001; Holley et al., 2007). The presence of natural dissolved organic carbon has also been shown to increase solubility of HgS and to inhibit its precipitation (Ravichandran et al., 1998, 1999) the same effects have been observed upon addition of humic and fulvic acids due to competition between their negatively charged functional groups and the sulphide ion for complexation with the Hg^{2+} ion under reducing conditions (Reddy and Aiken, 2001). Until recently HgS oxidative dissolution was considered to be a purely abiotic process however studies by (Jew, A. D. et al., 2007)convincingly demonstrate that microbial oxidation of both α-HgS and β-HgS may, increase dissolution rates by up to 25 orders of magnitude compared to abiotic dissolution. Their work suggests that this process is enzymatic but is still poorly understood. Until now such microbial driven dissolution of HgS has only been recorded under oxidizing conditions and so far only by natural biofilm

consortiums of bacteria however this finding drastically changes understanding of HgS stability in oxic systems.

Redox controls on Mercury toxicity

Mercury is highly toxic in all oxidation states however when evaluating risk, speciation and exposure pathway is of greater importance than oxidation state (Borch et al., 2010). With regards to toxicity, three mercury forms are often discussed inorganic mercury salts, organic mercury compounds and metallic mercury.

Organic mercury compounds are generally the most toxic and due to their solubility in lipids accumulate within the food chain to often dangerous levels, for instance in carnivorous fish such as tuna or swordfish. These compounds easily cross the blood brain barrier and result in neurological damage (Clarkson, 1993).

Metallic mercury (Hg^0), is significantly less toxic than many methyl-mercury species if ingested due to very low sorption (<0.01%) (Langford and Ferner, 1999), however, it is highly volatile and is very bio-accessible via inhalation in its vaporized form. Upon sorption within either the lungs or gastro-intestinal tract metallic mercury accumulates within the body and causes damage to the central nervous system.

Inorganic mercury salts, for instance sulphides or oxides, are less toxic than methyl mercury species and less accessible bio-accessible than metallic mercury. However the toxicity of inorganic salts exceeds that of elemental mercury when ingested and depends greatly on their oxidation state, as monovalent mercury salts are typically less soluble and so less easily adsorbed in the gastro-intestinal tract than divalent mercury salts (Friberg and Nordberg, 1973).

Uranium

Uranium may exist in oxidation states of +3, +4, +5 and +6 (e.g. $U^{3+}_{(aq)}$, $UOH^{3+}_{(aq)}$, $UO_2^{+}{}_{(aq)}$, $UO_2^{2+}{}_{(aq)}$). However the +4 and +6 valence states are the most stable under environmental conditions. The hexavalent form exists under oxic and sub-oxic conditions and is typically more mobile and toxic than its normally insoluble quadrivalent form. Aqueous uranium chemistry is complex, as subtle changes in pH, ionic strength or solution composition can cause profound changes in uranium speciation due to the large variety of possible complexing ligands and oligomeric species.

In its hexavalent form uranium exists as a uranyl ion (UO_2^{2+}) whereby two axial oxygen atoms are strongly bound to the central uranium atom, these oxygen atoms are largely unreactive and sorption behaviour is usually controlled by complexing ligands. At low pH the monomeric uranyl ion is surrounded by 4 equatorial water molecules (Burgess, 1978) however as pH increases the ion undergoes hydrolysis as the equatorial waters are replaced with hydroxide groups. At higher pH uranyl ions tend to form large oligomeric species such as $(UO_2)_3(OH)_7^-$. The uranyl ion is known to form complexes with a variety of anions including carbonate, nitrate, sulphate and many organic molecules such as acetate which may result in both negatively and positively charged ions (e.g. $(UO_2)_3(OH)_5^+$ and $UO_2(CO_3)_2^{2-}$) over a wide pH range.

In its quadrivalent form uranium exists most commonly in nature in the mixed valence triuranium octoxide (U_3O_8) with an average U valence state of +5.33 and to a lesser extent in the

uranium dioxide mineral uraninite (UO_2). Both of these phases are stable and highly insoluble in water making them therefore far less mobile than uranyl ions in the environment. The reduced solubility when compared to uranyl compounds also makes these phases significantly less toxic.

Toxicity of Aqueous Uranium Species

In addition to health impacts related to its radioactivity uranium is well known as a nephrotoxin, neurotoxin, carcinogen and a developmental toxicant. However the toxic and radioactive effects of uranium are only prevalent if it is internalized. Although internalization is most common via inhalation of dust particles and dermal penetration due to weaponization, ingestion via contaminated drinking water, food products or soil (amongst children) is also a relevant human exposure pathway when considering uranium inputs to the environment via waste contaminant leachate plumes or accumulation due to fertilizer usage.

Toxicity of ingested uranium is largely dependent on its solubility as this determines uptake in the gastro-intestinal tract. Although only a small percentage of ingested uranium is absorbed (Harduin et al., 1994), mostly in the small intestine(Smith, 2001) highly soluble species such as uranyl-carbonates are estimated to be absorbed 10 times more effectively (5% gut uptake factor) than insoluble minerals such as UO_2 or U_3O_8 (0.2% gut uptake factor) and hence are considered far more hazardous to human health (International Atomic Energy Agency., 1989).

Sorption behaviour of Uranium in Soils and Sediments

Predicting sorption behaviour of uranium species in soils theoretically is challenging due to the plethora of monomeric and oligomeric species possible due to the tendency of the uranyl ion to complex with a variety of organic and inorganic ligands. U(VI) complexes may exist with a positive, negative or neutral surface charge over a wide range of pH and therefore precise knowledge of solution chemistry, including Eh, pH, ionic strength, uranium concentration and the presence of complexing ligands is essential to predict aqueous uranium speciation and mineral surface interactions.

Numerous minerals present in soils and sediments have been shown to be good sorbents of aqueous U(VI) species including iron oxides (Waite et al., 1994), manganese oxides (Brennecka et al., 2011) , aluminium oxides (Froideval et al., 2006) and phyllosilicate minerals (Chisholm-Brause et al., 2001). More recently various researchers are reporting the importance of organic soil components as sorbents of aqueous U(VI) species in the natural environment (Zhou and Gu, 2005; Dong et al., 2006).

However despite many studies evaluating the affinity of sorbents in soils for U(VI) species and the identification of many soil components with high sorption capacity (Qafoku and Icenhower, 2008), there are conflicting opinions in the current literature regarding the relative importance of various soil components as U(VI) sorbents in natural aquifer sediments and soils. Whilst some authors argue that sorption capacity of U(VI) species in soils and sediments is dominated by certain complexes on particular minerals, for instance $(FeO)_2UO_2CO_3^{2-}$ (see Figure 23) on ferrihydrite (Barnett et al., 2002) other studies indicate that affinity of U(VI) to any particular sorbent is dominated to a lesser extent by solution composition and mineralogy and to a greater extent by the reactive surface area of a sorbent (Pabalan et al., 1998). Proponents of the first view cite statistically significant results of surface complexation modelling applied to several

different heterogeneous natural systems which assume the only reactive component to be ferrihydrate. However advocates of the second view indicate that while distribution coefficients (K_d values) for U(VI) species are very different for different minerals, that when these coefficients are normalized to specific surface area (referred to K_a by Payne et al., (n.d.) values for all minerals appear to be very similar (Figure 19 Payne et al. (n.d.).

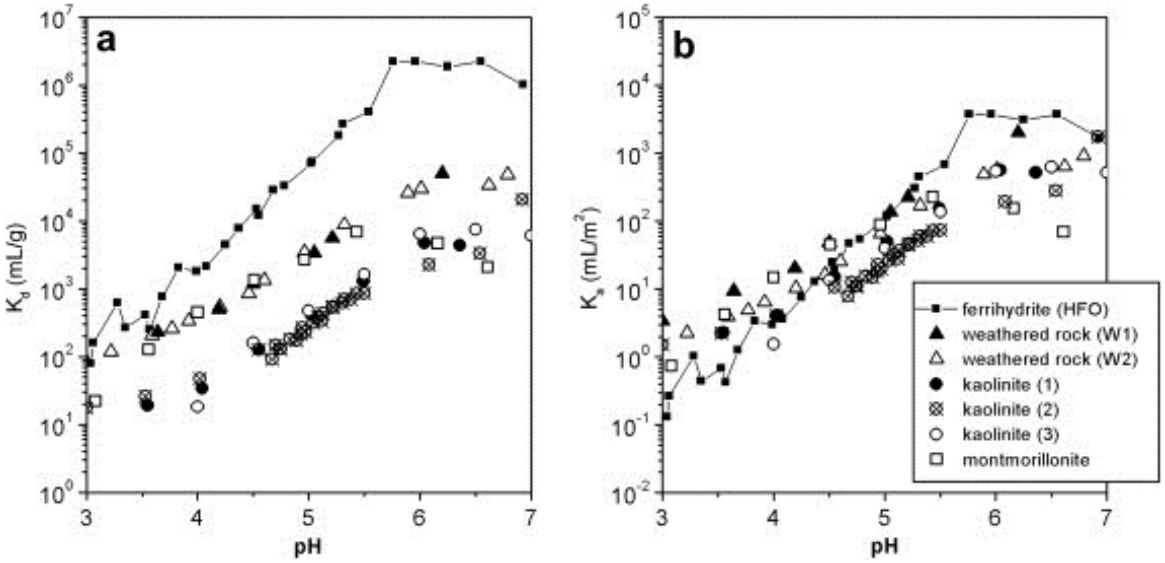

Figure 19: The sorption edge for uranium(VI) uptake by different minerals across the pH range from 3 to 7 expressed as: (a) distribution coefficients (K_d), and, (b) surface area-normalized distribution coefficients (K_a). Note the much smaller spread of experimental data in the computed K_a compared to the range of K_d for these minerals. From Payne et al. (n.d.).

The success of surface complexation models implementing ferrihydrite as the only active component may therefore simply be due to the dominance of ferrihydrite due to its high specific surface area (600m^2/g (Waite et al., 1994) and references therein) compared to other soil components e.g. Quartz (0.03 m^2/g) and Kaolinite (8.4 – 11.8 m^2/g) (Payne et al., n.d.).

As sorption of U(VI) species to clay surfaces is often of relevance with regard to nuclear waste disposal, a short summary of U(VI)/clay surface interactions is given below to demonstrate the differences between clays and sorption characteristics in differing solutions. In the natural environment, however, a heterogeneous mineralogy is highly probable and therefore data describing uranium sorption behaviour in mixed natural samples may provide more accurate predictions of mobility under given conditions.

Sorption behaviour of aqueous U(VI) species on clays has been shown to be controlled by two processes; exchange of the uranyl ion with cations in the clay interlayer at low ionic strength and low pH and surface complexation with hydroxylated edge sites at high ionic strength and high pH. (Hyun et al., 2001)

Spectroscopic investigations conducted by (Chisholm-Brause et al., 2001) indicate that even quite dramatic changes to solution composition cause only subtle changes to the nature of sorption complexes formed by U(VI) on Montmorillonite between pH 3 and 7. They suggest that solution composition has minimal influence on U(VI) mobility in comparison to primary factors controlling the abundance and nature of U(VI) sorption complexes in clays such as surface

coverage, sorption site abundance and reactivity. In this study the authors identify uranyl inner sphere, outer sphere and exchange complexes Montmorillonite. Of the complexes identified the inner sphere variety appeared to be the most prevalent and persistent over a range of surface coverages and solution conditions.

Experiments investigating the role of pH, surface coverage and complexing ligands were also conducted by (Bachmaf et al., 2008)over a pH range of 3 to 8. Whilst in this study only the abundance of the surface complexes and not their nature was investigated the authors concur with (Chisholm-Brause et al., 2001) that surface coverage is a primary factor controlling adsorption with greater sorption occurring at low surface coverages. However, in contrast to Chrisholm-Brause et al, Bachmaf et al show that competition between SO_4^{2-} ions and UO_2^{2+} for surface sites and formation of uranyl-sulphate-complexes at low pH (Figure 20) can lead to a reduction of U(VI) sorption to bentonite at low pH. They also show that the presence of carbonate decreased U(VI) adsorption above pH 7 due to the formation of negatively charged uranyl-carbonate-complexes (Figure 21) and that the presence of phosphate greatly increased U(VI) adsorption.

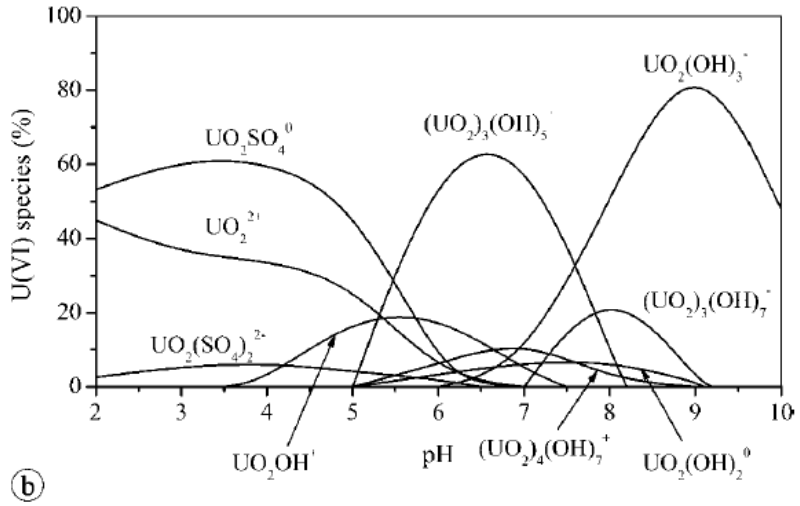

Figure 20: U(VI) speciation in 0.01 M NaCl + 0.005M Na_2SO_4, [U] = 5×10^{-5} M generated using PHREEQC and the WATEQ4F thermodynamic database (from Bachmaf et al. (2008)). The presence of uranyl-sulphate-complexes at low pH and their absence at neutral to high pH is shown.

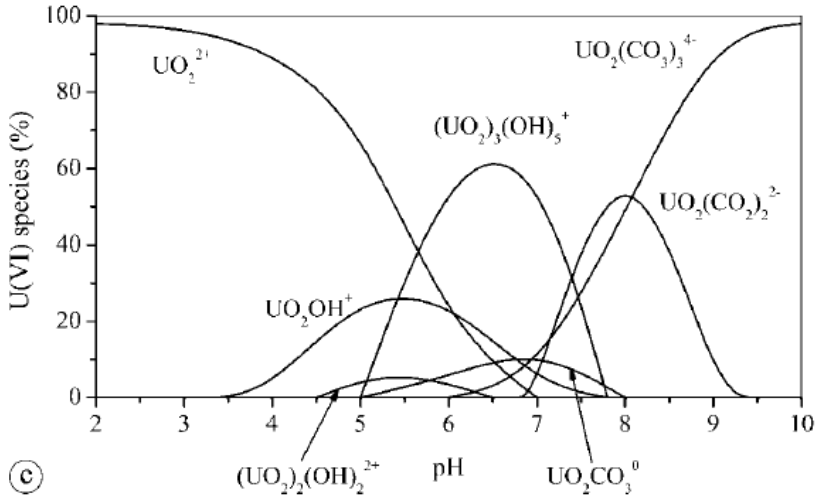

Figure 21: U(VI) speciation in 0.01M NaCl + 0.003M $NaHCO_3$, [U] = 5×10^{-5} M generated using PHREEQC and the WATEQ4F thermodynamic database (from Bachmaf et al. (2008)). . The formation of strongly anionic uranyl-carbonate-complexes at high pH is shown.

In a later study Bachmaf and Merkel (2010) continued their investigations of U(VI) adsorption on clays to include the influence of higher pH, sodium concentration and clay type (smectite type clays compared to kaolinite type clays). They found significant differences between the sorption envelopes for smectite type clays and kaolinite type clays as is shown in Figure 22 illustrating the reduced adsorption of U(VI) complexes by smectite type clays at pH values greater than 7 indicating that surface complexation is the dominant sorption process at this pH. The difference in sorption capacity for U(VI) between the two clay types is attributed to the greater number of aluminol surface sites on kaolinite type clays than smectite type clays, the latter of which exhibit more silanol sites which have a lesser activity towards U(VI) complexes. The authors also demonstrate that sodium concentration in solution can affect sorption of U(VI) complexes and that the influence of sodium concentration on U(VI) adsorption to clays is dependent on clay type. The authors found that sorption of U(VI) species to smectite type clays (shown in Figure 22) were more affected by sodium concentration than kaolinite type clays. This difference is attributed by the authors to competition between uranyl and sodium ions.

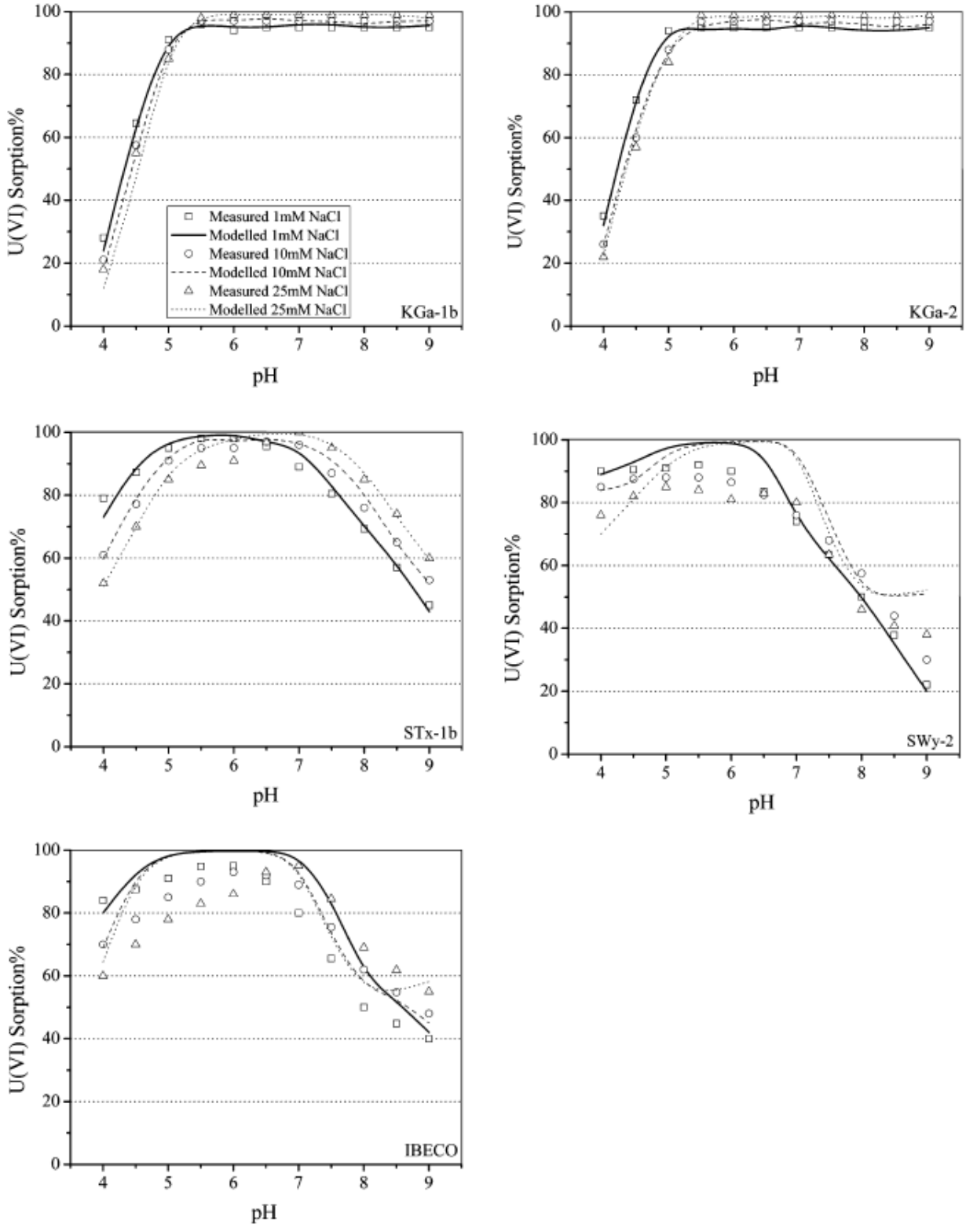

Figure 22: Comparison of uranium sorption data on kaolinite (KGa-1b), kaolinite (KGa-2), montmorillonite (STx-1b), montmorillonite (SWy-2), and natural bentonite (IBECO) at different sodium concentrations and pH (from Bachmaf and Merkel (2010)).

The sorption envelopes shown in Figure 22 relating to kaolinite type clays vary quite significantly at high pH from typical sorption envelopes demonstrated with natural substrates such as those shown in Figure 23 (Barnett et al., 2002)

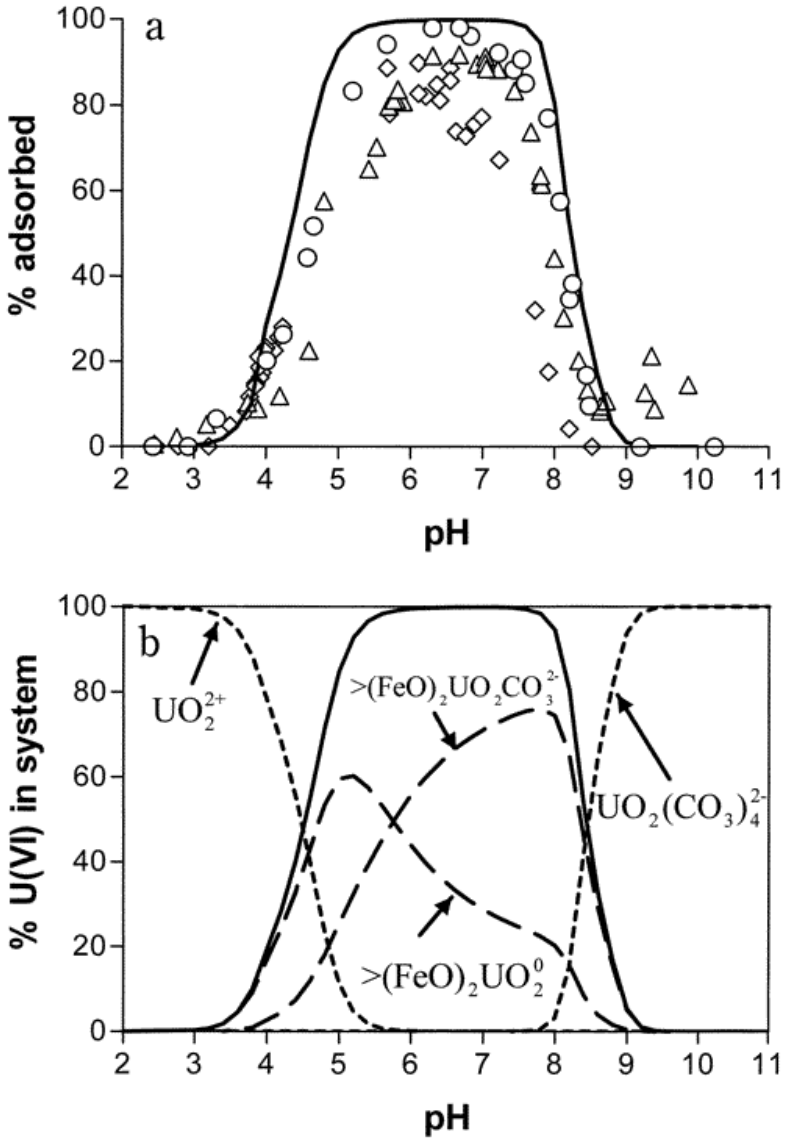

Figure 23: Adsorption of 1 mg/L U(VI) to subsurface materials from the Oak Ridge (circles), Hanford (diamond), and Savannah River (triangle) department of energy locations at *I* = 0.1 M in equilibrium with atmospheric CO_2(g). (b) Modelled U(VI) speciation: dissolved species (short dashes), adsorbed species (long dashes), and total adsorbed concentration (solid line). From Barnett et al. (2002).

Whilst sorption envelopes such as those shown in Figure 23 are typical of those encountered in the literature from laboratory studies involving heterogeneous natural media caution should be used when applying these sorption envelopes to alkali natural subsurface systems. This is due to the impact of carbonate on U(VI) sorption. Many sorption envelopes for U(VI) species such as the ones shown in Figure 23 were measured in solutions at constant $CO_{2(g)}$ partial pressure (i.e. in equilibrium with atmospheric CO_2 concentrations) and not at constant carbonate concentrations. As total carbonate concentrations in solutions in equilibrium with atmospheric $CO_{2(g)}$ are significantly higher than typical carbonate concentrations measured in groundwater, it is possible that the rapid desorption edge seen at between pH 8 and 9 is merely an effect of the predominance of highly mobile $UO_2(CO_3)_4^{2-}$ and that in closed systems with lower carbonate

concentrations the desorption edge would occur at a far higher pH. The results of surface complexation modelling performed by Barnett et al appear to indicate that this is the case.

Oxidation and Reduction of Uranium in Soils and Sediments

Uranium is a highly redox active element and redox transformations within the subsurface environment impose a primary control over uranium mobility as quadrivalent U is significantly less mobile than hexavalent uranium. The energetic stability boundary between U(IV) and U(VI) occurs at sub-oxic to anoxic conditions dependent on pH, within the range of Eh values commonly encountered in the near subsurface (shown in Figure 24). A variety of redox reactions causing either the reduction of U(VI) or the oxidation of U(IV) have been identified within the subsurface, both abiotic (Wersin et al., 1994)and microbially mediated (Lovley et al., 1993). Many of these reactions are multi step/coupled reactions and pass via an unstable U(V) valence state or via mixed valence solids (Wersin et al., 1994; Renshaw et al., 2005).

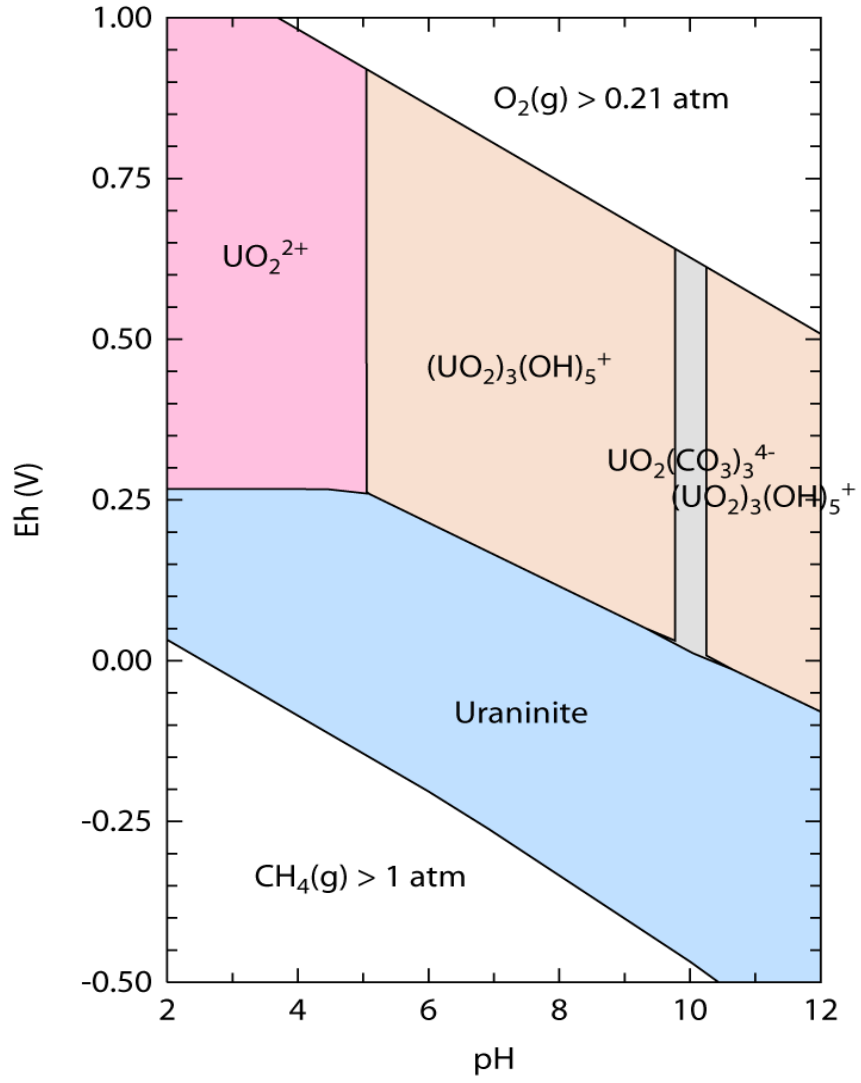

Figure 24: Pourbaix diagram of the U, H_2O CO_2 system at 298.15K and 10^5 Pa from LLNL data.

Potentially important reductants of U(VI) in the subsurface include aqueous and structural Fe(II), sulphides and organic matter (Liger et al., 1999). Rates of abiotic reduction of U(VI) by most

forms of natural organic matter had been thought to be extremely slow at temperatures commonly found in the environment (<45°C) (Disnar and Sureau, 1990) and therefore organic matter was only considered to be a relevant reductant for U(VI) in the presence of a microbial community capable of coupling the reduction of U(VI) to the oxidation of organic matter as part of a metabolic process (Lovley et al., 1993; Liger et al., 1999). Recent research suggests however that highly redox active forms of organic matter such as soil humic substances with quinone moieties are capable of fast reduction of U(VI) in aqueous solution (Wang et al., 2011) although reaction rate is strongly dependent on pH and complexing ligands (shown in Figure 25)

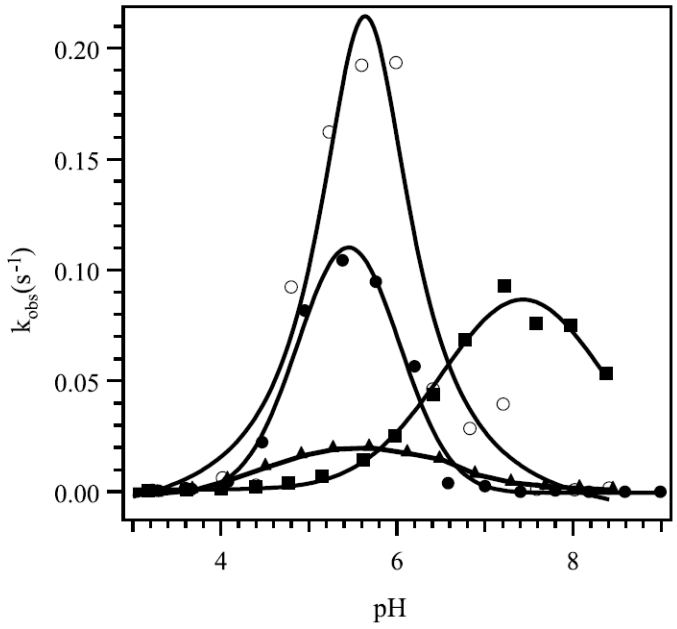

Figure 25: Observed pseudo-1st-order rate constants of U(VI) reduction by AH_2DS^{2-} as a function of pH in four systems (open circle – OH–, filled circle – carbonate, filled triangle – desferriferrioxamine B, filled square – EDTA). The solid lines are fitted trend lines with arbitrary functions. From Wang et al. (2011)

Reduction of aqueous U(VI) by Fe(II) has been shown to be thermodynamically feasible at low to neutral pH although this homogeneous reduction has only been demonstrated to occur freely at low pH (Liger et al., 1999). The presence of a wide variety of minerals has been shown to catalyse the reaction between Fe(II) and U(VI) by surface sorption of Fe(II) including; montmorillonite (Chakraborty et al., 2010) and haematite (Liger et al., 1999). These studies consistently indicate that Fe(II) has a stronger reduction potential when adsorbed to mineral surfaces than in solution resulting in abiotic reduction of U(VI) by Fe(II) under conditions where reduction would not occur in solution including at neutral pH. Other studies also show that surface sorbed Fe(II) is often persistent in reduced systems even at neutral to high pH due to the comparatively fast sorption of Fe(II) to stable mineral surfaces compared to the precipitation of ferrous carbonates, sulphides or phosphates which may be expected to form (Charlet et al., 1998). This indicates that Fe(II) is therefore an available reductant for oxidized U species over a wide range of conditions.

Other studies show that Fe(II) contained within a mineral's structure is also able to act as an electron donor to surface sorbed U(VI) species (Wersin et al., 1994). Minerals shown to be directly capable of U(VI) reduction at their surfaces include biotite (Ilton et al., 2004), galena, pyrite (Wersin et al., 1994) magnetite (Behrends and Vancappellen, 2005; Scott et al., 2005), corundum (Regenspurg et al., 2009) and vivianite (Veeramani et al., 2011). In some cases the presence of bicarbonate was shown to facilitate surface reduction of U(VI) on Fe(II) bearing minerals due to the formation of surface Fe(II)-carbonate phases (Regenspurg et al., 2009).

A number of different groups of organisms have also been shown to be cable of coupling extracellular reduction of U(VI) to oxidation of organic matter including Fe(III) reducing and sulphate reducing organisms such as Geobacter and Desulfovibrio species (Payne et al., 2002; Lloyd et al., 2003) . Both of the aforementioned groups of organisms use c-type cytochromes for electron transfer which results in the precipitation of U(VI) in the periplasm and outside the cell. The exact mechanisms for microbial U(VI) reduction are a subject of on-going research however recent XAS investigations by (Renshaw et al., 2005) indicate that reduction of U(VI) coupled to oxidation of acetate and fumarate mediated by Geobacter species is a multi-step process of one electron reduction by the microbe resulting in an unstable U(V) phase which rapidly disproportionates to give a mix of U(IV) and U(VI) species.

Although U(IV) minerals such as uraninite are stable under low temperature reducing conditions (Janeczek and Ewing, 1992) in the absence of suitable oxidants and are thought to be a desirable form of uranium in the subsurface due to their limited mobility, oxidation of U(IV) may occur upon availability of oxidants such as oxygen or nitrate (Moon et al., 2007). It has been shown that there is a strong kinetic control on the oxidative dissolution of U(IV) minerals dependent on the specific surface area amongst other factors (Grandstaff, 1976). This would indicate that bio-reduced uranium precipitates are far more susceptible to re-oxidation than other forms of uraninite due to their comparatively large surface area. Whilst some U(VI) reduction processes result in the formation of surface sorbed U(IV) species (Chakraborty et al., 2010) others result in formation of U(IV) precipitates with varying degrees of stability (Renshaw et al., 2005). This variety of U(IV) precipitates results in varying re-oxidation kinetics, some studies record the slow oxidation and hence slow mobilization of U(IV) (Szecsody et al., 1998) whilst other studies demonstrate extremely fast re-oxidation (Zhou and Gu, 2005).

Zhou and Gu (2005) have shown that rapid re-oxidation of biogenic $UO_{2(s)}$ does not occur when exposed to oxygen unless bi-carbonate is also present however, oxidation of biogenic U(IV) by bi-carbonate in the absence of oxygen does not occur (Figure 26).

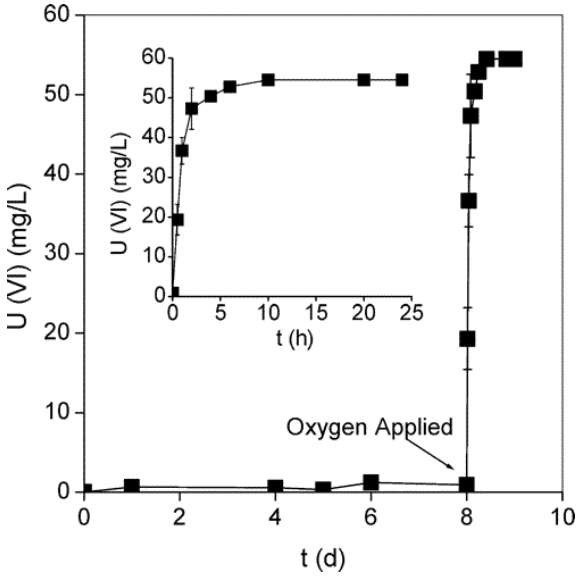

Figure 26: Re-oxidation and mobilization of bio-reduced U(IV) using 1 M $NaHCO_3$ under anaerobic and oxic conditions. From Zhou and Gu (2005).

It has also been shown that even under strict anaerobic conditions U(IV) products of bio-reduction maybe remobilized through addition of organic ligands and complexing agents such as EDTA or citrate (Luo and Gu, 2011). Although the total percentage of uranium leached in this way appears to be low (~0.1%) the fear is that immobilized U(IV) previously considered to be stable under anaerobic conditions may be slowly leached from sediment along with Al and Fe by organic ligands which form strong complexes with uranium (Luo and Gu, 2011).

Precipitation and dissolution processes affecting Uranium mobility in Soils and Sediments

Due to the striking differences in solubility and hence the tendency to form mineral phases of U(VI) and U(IV), precipitation and dissolution processes affecting uranium are often linked to changes in redox conditions or as the result of physically or biologically catalysed redox reactions.

As discussed in the previous section oxidative dissolution of biogenic U(IV) minerals may occur in the subsurface upon addition of a suitable oxidant, such as oxygen or nitrate, however rates of re-oxidation vary considerably dependent on the stability of the U(IV) phase.

Extracellular precipitation of uraninite by bio-reduction of U(VI) has been shown to occur coupled to oxidation of organic matter (Burgos et al., 2008) in addition to abiotic precipitation of U(IV) minerals following surface catalysed U(VI) reduction (Behrends and Vancappellen, 2005).

Despite the predominance of U(IV) and mixed valence minerals in nature, where high concentrations of U(VI) species occur under oxic conditions the super-saturation with respect to pure U(VI) phases such as schoepite $(UO_2)_4O(OH)_6.6H_2O$ or rutherfordine, $UO_2CO_{3(s)}$ (Carroll et al., 1992) is also possible. Laboratory studies have shown however that precipitation of such phases may be kinetically limited at low levels of super-saturation (Giammar and Hering, 2001). (Giammar and Hering, 2001) also show that low levels of super saturation may be maintained due to metastable surface sorption.

A potentially more important immobilization process for uranyl ions than precipitation of pure U(VI) minerals is the immobilization of U(VI) species with iron oxide minerals or calcite during their precipitation (Reeder et al., 2001; Duff et al., 2002; Kerisit et al., 2011).

Chromium

Chromium may exist in oxidation states ranging from +6 (e.g. CrO_4^{2-}) to -2 (e.g. $Na_2[Cr(CO)_5]$). In the environment the most stable and commonly occurring oxidation states are Cr(III) (e.g. Chromium hydroxide, $Cr(OH)_3$) and Cr(VI) (e.g. CrO_4^{2-}).

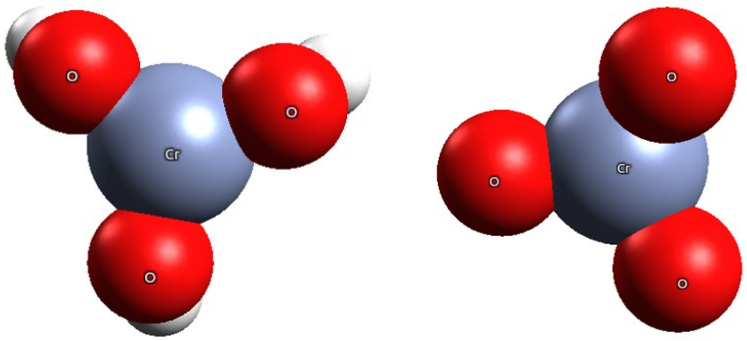

Figure 27: Chromium hydroxide (left) and chromate (right).

Dependent on prevailing pH and Eh conditions inorganic aqueous Cr may be stable as monoatomic cations (Cr^{2+}, Cr^{3+}), hydroxides (e.g. Cr(III): $CrOH^{2+}$, $Cr(OH)_2^+$, $Cr(OH)_3$ $Cr(OH)_4^-$) or oxyanions (e.g. Cr(VI): H_2CrO_4, $HCrO_4^-$, CrO_4^{2-} or Cr(V): CrO_4^{3-})(Rai et al., 1989; Richard and Bourg, 1991)(Richard and Bourg, 1991)(Richard and Bourg, 1991)(Richard and Bourg, 1991)(Richard and Bourg, 1991)(Richard and Bourg, 1991). In addition to this variety of inorganic aqueous Cr species, many different aqueous organic Cr complexes exist in nature (Luo et al., 2010) and in some cases can account for a large proportion of total Cr (Ahern et al., 1985; Icopini and Long, 2002). Whilst overriding Eh and pH conditions directly affect aqueous Cr speciation (including oxidation state, protonation state and chemical coordination), sorption behaviour of individual species to mineral surfaces, hence mobility is also directly affected by these conditions. The interplay between sorption/desorption, complexation/decomposition and oxidation/reduction of aqueous Cr in natural systems is summarized in Figure 28 and the stability fields of dominant species are shown in Figure 29.

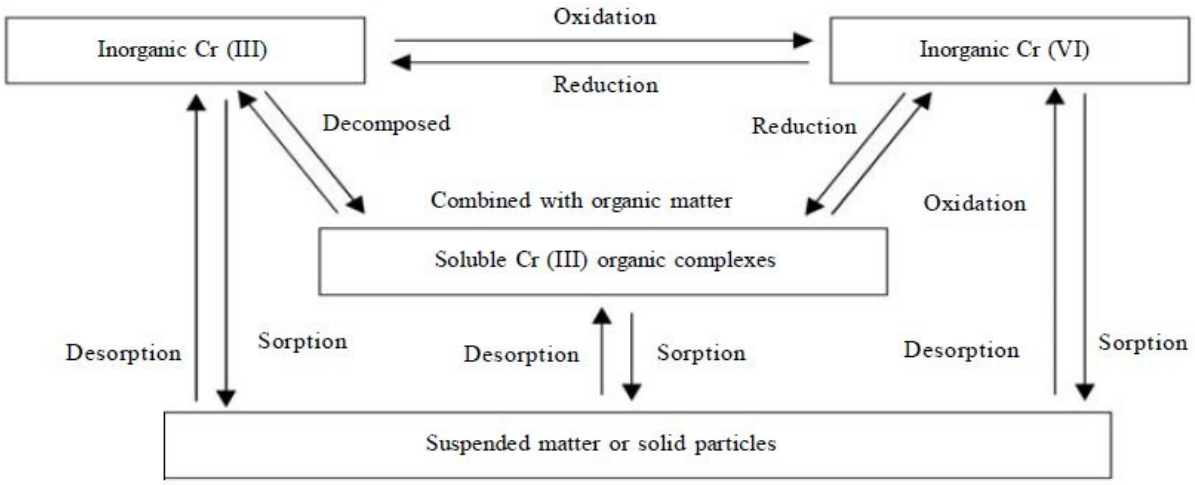

Figure 28: Processes affecting aqueous Chromium species (modified from Luo et al. (2010)).

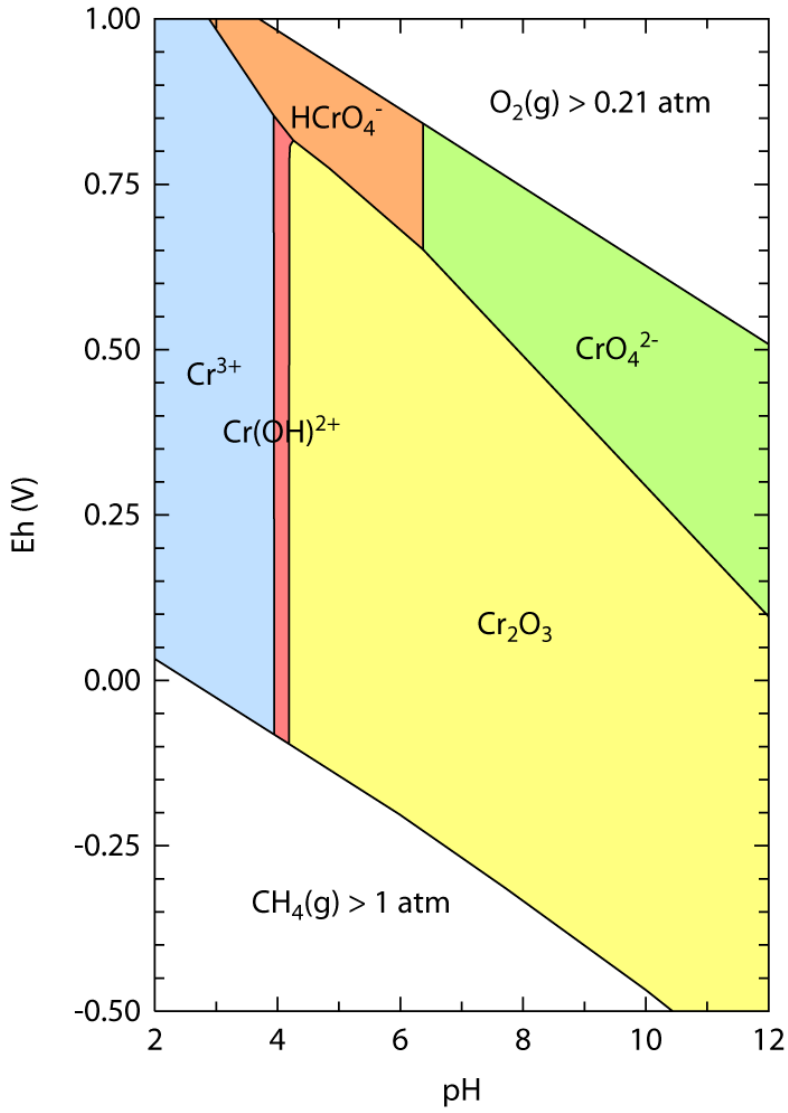

Figure 29: Pourbaix diagram of the Cr-H_2O-CO_2 system at 298.15K and 10^5 Pa from LLNL data.

Sorption behaviour of Chromium in soils and sediments

Sorption behaviour of Chromium is highly dependent on oxidation state. $Cr^{3+}_{(aq)}$ exhibits typical cationic sorption behaviour with greater sorption to mineral surfaces occurring at higher pH when mineral surfaces are more negatively charged (see Figure 15) (Griffin et al., 1977). Greater sorption of Cr^{3+} is therefore expected to mineral surfaces which have a low point of zero charge (PZC) and high surface area such as clay minerals. Specific sorption of $Cr^{3+}_{(aq)}$ to soil minerals including Fe and Mn oxides (Zachara et al., 1987), clay minerals (Griffin et al., 1977) and quartz is rapid although competition for surface sorption occurs between $Cr^{3+}_{(aq)}$ and other inorganic cations (Richard and Bourg, 1991).

Chromate ions ($HCrO_4^-$, CrO_4^{2-}) exhibit typical anionic sorption behaviour with greater sorption to mineral surfaces occurring at lower pH when mineral surfaces are more positively charged (Griffin et al., 1977; Mustafa et al., 2001). Greater sorption of chromate is therefore expected to mineral surfaces which have a high point of zero charge such as iron oxides. In contrast to $Cr^{3+}_{(aq)}$ adsorption, chromate adsorption consists of surface complexation with hydroxyl surface sites (Mustafa et al., 2001). Spectroscopic investigation via extended X-ray absorption fine structure spectroscopy (EXAFS) has revealed that chromate can form inner sphere mononuclear mono-dentate, mononuclear bi-dentate or binuclear bi-dentate surface complexes at iron oxide surfaces (Fendorf et al., 1997). Adsorption is decreased by the presence of competing anions such as Cl^-, NO_3^-, SO_4^{2-}, HPO_4^{2-}, HCO_3 (Richard and Bourg, 1991).

Oxidation and Reduction of Chromium in soils and sediments

Oxidation of Cr(III) has been found to occur in the presence of dissolved oxygen (Schroeder and Lee, 1975) however, this oxidation is unlikely to occur in soils and sediments as it is a slow process when compared to concurrent sorption or precipitation reactions under environmental conditions. Oxidation of Cr(III) occurs far more rapidly coupled to the reduction of Mn(IV) as $MnO_{2\ (S)}$ to Mn(II) as $Mn^{2+}_{(aq)}$ following adsorption of Cr(III) to the MnO_2 surface (Bartlett and James, 1979; Eary and Rai, 1987). It is this process which is thought to be responsible for the majority of Cr(III) oxidation in the environment as no other inorganic oxidants have been found commonly in the environment capable of rapid Cr(III) oxidation (Rai et al., 1989).

Reduction of Cr(VI) has been shown to occur in the presence of numerous reduced species including aqueous ferrous iron, dissolved sulphides (Schroeder and Lee, 1975) and redox reactive organic species such as humic and fulvic acids (Wittbrodt and Palmer, 1997). Additionally numerous species of Cr(VI) resistant bacteria have shown to be capable of the reduction of chromate in solution (Chen and Hao, 1998) as a detoxification mechanism. Whilst biological reduction of Cr(VI) was initially assumed to lead to the precipitation of amorphous $Cr(OH)_3$ recent investigations suggest that a variety of stable soluble and insoluble organo-Cr(III) complexes are also produced (Puzon et al., 2005) which may account for the prevalence in the environment of Cr(III) in solution even under conditions where Cr(VI) should dominate (Icopini and Long, 2002; Puzon et al., 2008)(Puzon et al., 2008)(Puzon et al., 2008)(Puzon et al., 2008)(Puzon et al., 2008)(Puzon et al., 2008).

Precipitation and dissolution processes affecting Chromium mobility in soils and sediments

In addition to previously mentioned iron and manganese oxides, discrete Chromium mineral phases play an important role in controlling Cr mobility in the environment. Natural Cr(VI) minerals are rarely found in nature due to their high solubility and their high Eh stability range (Richard and Bourg, 1991). Far more prevalent are Cr(III) precipitates which are stable in moderately oxidizing and reducing environments often found in soils and sediments. Although the most thermodynamically stable phase over a large Eh-pH field in the Cr-H_2O-CO_2 system is eskolaite (Figure 29) or in natural systems chromite, these phases are rarely found in significant quantities in natural environments due to the rapid precipitation of $Cr(OH)_3$ or Fe(III) Cr(III) hydroxide ($(Fe_{1-x},Cr_x)OH_3$ in solid solution) under similar conditions (Charlet & Manceau 1992). The direct precipitation of chromite ($FeCr_2O_4$) is equally not expected at the low temperatures found in most environmental settings (Hem, 1977).

Redox controls on Chromium toxicity

Inorganic Cr(VI) has received a disproportionate amount of research attention compared to inorganic Cr(III) due to its greater toxicity to bacteria, animals and plants and greater mobility in soils and aquifers. Aqueous Cr(VI) species are well known carcinogens and allergens whereas trace concentrations of Cr(III) of 50-200µg day^{-1}, are considered to be an essential nutrient for metabolism in animals and plants due to its role in glucose metabolism and nucleic acid synthesis (Richard and Bourg, 1991; Dayan and Paine, 2001).

Uptake of Cr(III) compounds by the body is generally very low by dermal, oral and inhalation routes which contrasts with the high adsorption of Cr(VI) by the same pathways.

Although Cr(V) is not readily stable under environmental conditions numerous articles suggest that it does exist as an intermediate during reduction of Cr(VI) in the environment (Chen and Hao, 1998) and in the body (Klein, 1996). Due to the reported similarity in response of Cr(V) and Cr(VI) to popular colorimetric analyses (Eckert et al., 1991), previously reported Cr(VI) concentrations from natural waters may in fact be a mixture of Cr(VI) and Cr(V). It is thought that the reduction of Cr(VI) via Cr(V) to Cr(III) within the body is the cause of much of chromium's genotoxicity potentially due to the formation of OH' radicals by Fenton like reactions (Shi and Dalal, 1989).

Arsenic

Arsenic is a metalloid which can exist in oxidation states ranging from -3 (e.g. AsH_3) to +5 (e.g. $HAsO_4^{2-}$) (-III, -1, 1, 2, 3 and 5) however in the environment it is most stable and commonly found in either it's trivalent (As(III) e.g. H_3AsO_3) or pentavalent (As(V) e.g. $HAsO_4^{2-}$) form (shown in Figure 30) (Smedley and Kinniburgh, 2002). However, under highly reduced conditions in soils and sediments low concentrations of inorganic or methylated arsines (AsH_3 , $MeAsH_2$, Me_2AsH and TMA) may be formed (Cheng and Focht, 1979; Mestrot et al., 2011).

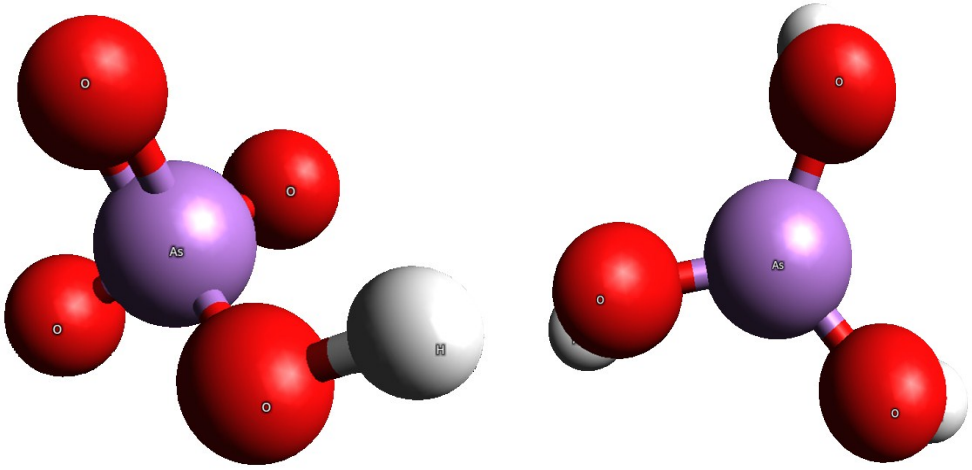

Figure 30: Arsenate (left) arsenite (right).

Under most conditions inorganic arsenic forms neutrally or negatively charged oxyanions; as As(V) under oxic conditions and high pH ($H_3AsO_4°$, $H_2AsO_4^-$, $HAsO_4^{2-}$ and AsO_4^{3-}) and as As(III) under reducing conditions and low pH ($H_3AsO_3°$, $H_2AsO_3^-$, $HAsO_3^{2-}$ and AsO_3^{3-}) (Figure 31). Arsenic, unlike chromium and uranium, never exists as monoatomic cations in solution therefore its sorption behaviour and mobility is very different to the majority of metal contaminants (e.g. Pb^{2+} Cu^{2+}). The stability fields of each of these species are shown in Figure 31. In addition to oxidation and protonation state variation between inorganic arsenic oxyanions, many methylated arsenic species and arseno-organic complexes are commonly found in the environment (e.g. monomethlyarsonic acid (MMA^V), dimethylarsinic acid (DMA^V) and trimethylarsine oxide $TMAO^V$).(Smith et al., 1998)

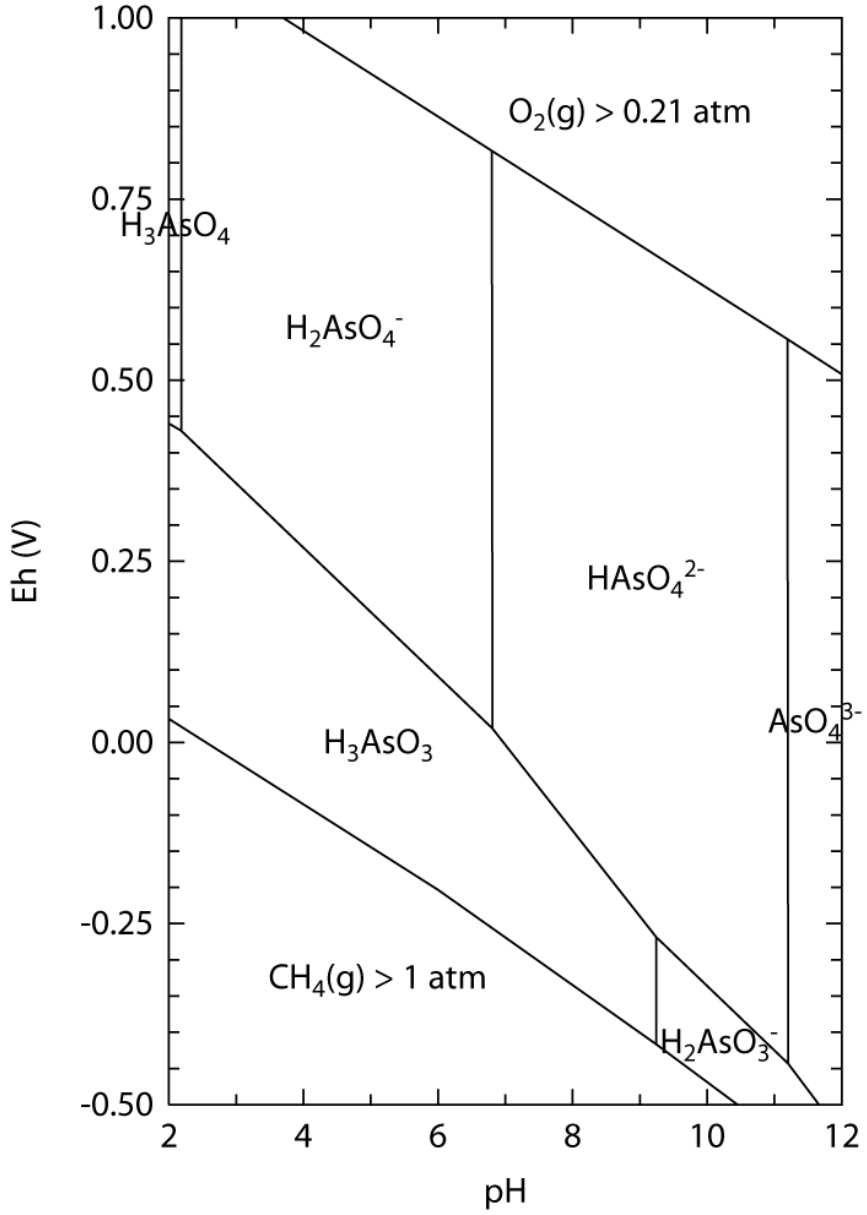

Figure 31: Pourbaix diagram of the As, H_2O CO_2 system at 298.15K and 10^5 Pa from LLNL data.

Whilst overriding Eh and pH conditions directly affect aqueous As speciation (including oxidation state, protonation state and chemical coordination), sorption behaviour of individual species to mineral surfaces, hence mobility is also directly affected by these conditions. The interplay between sorption / desorption, complexation / decomposition, methylation / de-methylation, precipitation/dissolution and oxidation/reduction of As in natural systems is summarized in Figure 32.

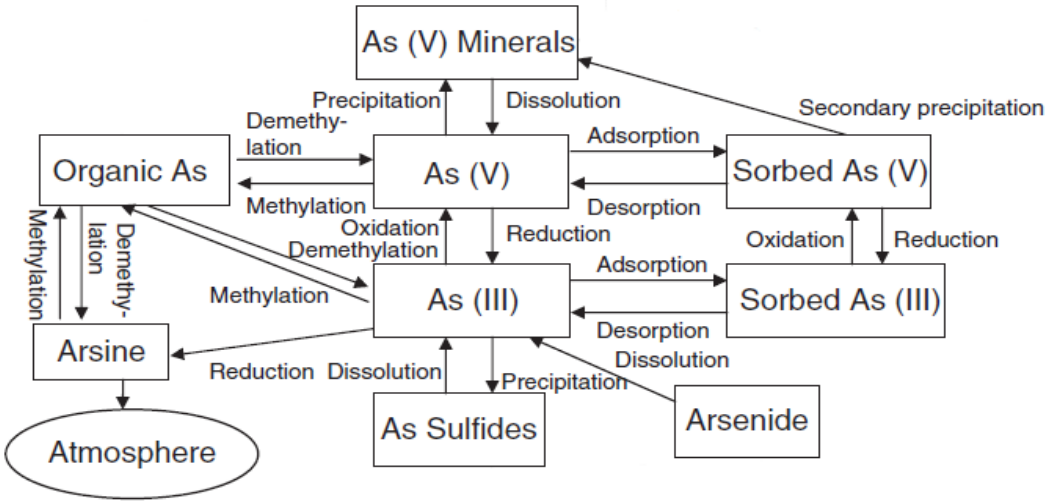

Figure 32: Schematic summary of Arsenic Biogeochemistry. (Modified from Zhang and Selim (2008)).

Sorption behaviour of Arsenic in soils and sediments

Sorption behaviour of arsenic in soils and sediments is complex and strongly dependent on Eh and pH conditions. Changes in pH influence both protonation state of arsenic oxyanions and the surface charge of potential sorbents. A key difference between arsenite and arsenate oxyanions is their charge under environmental conditions. Whilst arsenite remains neutrally charged across a pH range encompassing most natural environments (pK_a1 = 9.2) arsenate is negatively charged from pH 2.3 upwards, loosing additional protons at pH 6.8 and 11.6 (Goldberg and Johnston, 2001). It is largely the interaction between the pK_a of arsenic ions and the PZC of matrix minerals which determines the adsorption envelope (Figure 33 Figure 34). Generally at low pH arsenate adsorption is greater than that of arsenite but at higher pH where most common minerals obtain a negative surface charge arsenite adsorption is greater.(Raven et al., 1998; Jain and Loeppert, 2000; Zhu et al., 2011). Often a sorption maximum for arsenite is observed close to the pK_a1 at pH 9.2 (see Figure 33, Goldberg (2002)). Aerobic high pH conditions (i.e. pH greater than the PZC for iron oxide minerals, at approximately 8.5) have been shown to increase arsenic mobility and often lead to significant arsenic release as arsenate is desorbed from the surface of iron oxides (Robertson, 1989; Smedley et al., 2002).

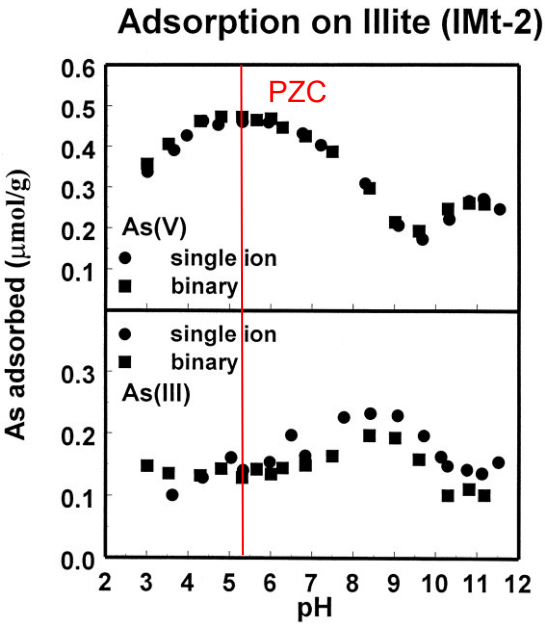

Figure 33: Adsorption of arsenate and arsenite on illite as a function of pH. Modified from Goldberg (2002).

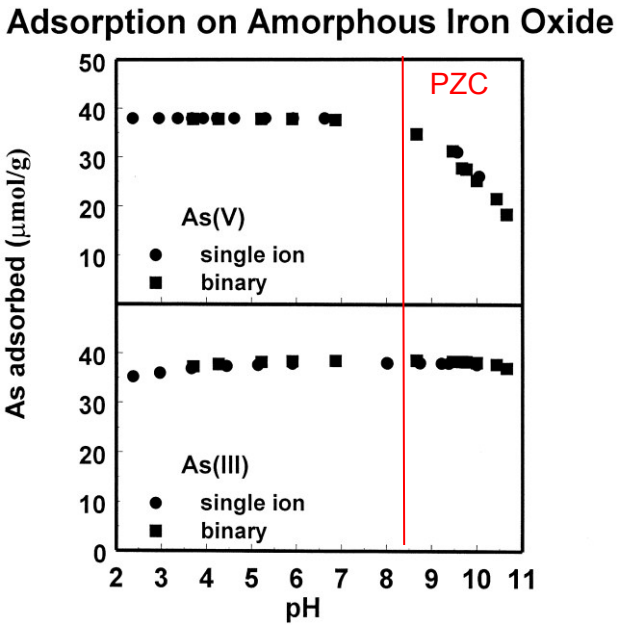

Figure 34: Adsorption of arsenate and arsenite on amorphous iron oxide as a function of pH. Modified from Goldberg (2002).

Numerous studies show the strong positive correlation between total iron concentration in soils and sediments total arsenic concentrations e.g. (Hossain et al., 2008). Potentially the most important sorbents of both arsenite and arsenate in soils and aquifers are metal oxides and oxyhydroxides due to their large sorption capacity for a range of negatively and neutrally charged oxyanions and high surface area (Vitre et al., 1991; Sullivan and Aller, 1996; Smedley and Kinniburgh, 2002). Many other minerals and soil materials have also been implicated as sorbents of arsenic in natural environments including metal carbonates (Alexandratos et al., 2007; Guo et al., 2011), sulphides (Farquhar et al., 2002; Wolthers et al., 2005), clays (Goldberg, 2002) and organo-clay complexes (Saada et al., 2003). Sorption capacities for some of these iron containing minerals compiled by (Charlet et al., 2011) are shown in Table 4.

Table 4: Kd of As(V) and As(III) onto Fe(II)-Fe(III)-bearing phases derived from sorption edge experiments (pH 7 and 7.5) [a] derived from constant capacity modelling of adsorption edge experiments. From Charlet et al. (2011)

Mineral	**Solid g/L**	**K_d (L/g) pH 7 As(V)**	**K_d (L/g) pH 7 As(III)**	**Reference**
Hydrous Ferric Oxide	0.03	49.3	85.72	(Dixit and Hering, 2003)
Goethite	0.05	8.05	14.46	(Dixit and Hering, 2003)
Mackinawite	0.044	9	2	(Wolthers et al. 2005c)
Siderite	2.5	3.36	0.28	(Jonsson and Sherman, 2008)
Magnetite	3.1/0.5	8.89	0.08/1.85	(Jonsson and Sherman, 2008)
Fougerite	4.5	-	0.12	(Jonsson and Sherman, 2008)
Vivianite	2.5	0.18	-	(Thinnappan et al., 2008)
Biotite [a]	4.25	3.4	0.97	(Chakraborty et al., 2007)
Muscovite [a]	4.1	0.36	0.36	(Chakraborty et al., 2007)

Sorption of arsenate and arsenite to iron and aluminium oxides and oxyhydroxides has been extensively studied (Fendorf et al., 1997; Goldberg, 2002; Dixit and Hering, 2003). It has been shown that both arsenate and arsenite can form inner sphere complexes via exchange for hydroxyl groups in the coordination spheres of structural metal atoms (Fendorf et al., 1997; Manning et al., 1998) but that arsenite may also form outer sphere complexes (Goldberg and Johnston, 2001). It has also been shown via spectroscopic investigation (extended X ray absorption fine structure spectroscopy (EXAFS)) that arsenate may form mononuclear mono-dentate, mononuclear bi-dentate or binuclear bi-dentate surface complexes (Fendorf et al., 1997).

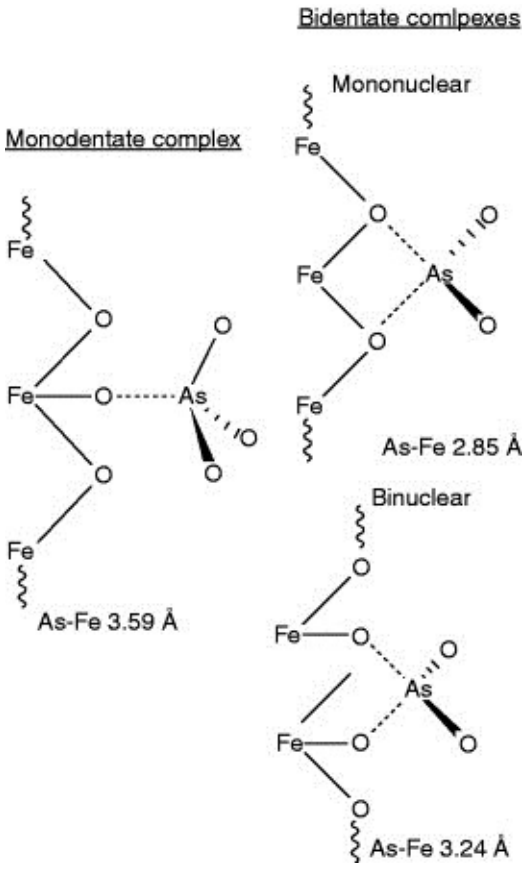

Figure 35: Schematic illustration of the surface structure of As(V) on goethite based on the local coordination environment determined with EXAFS spectroscopy. From Fendorf et al. (1997)

Clay minerals generally have a low adsorption capacity for anionic arsenic species in comparison to other minerals with comparable surface area due to their negatively charged surfaces (Goldberg, 2002). However, the edge $AlOH_2^+$ functional groups of layered silicates have been proposed as sites for arsenic anion adsorption and it is this mechanism which is thought to explain the generally strong arsenic sorption exhibited by clay minerals with high surface areas.(Manning and Goldberg, 1996).

Whilst it is iron oxides which are considered to be the most important sorbents of aqueous arsenic within oxic environments, in anoxic environments iron oxides are subject to reductive dissolution mediated by facultative anaerobes including geobacter and shewanella species (Lovley et al., 1993). Arsenic is often released under such reducing conditions (McGeehan and Naylor, 1994; Islam et al., 2004; Ackermann et al., 2008) as Fe(II) and As(III) species predominate. However, it is thought that the adsorption of released arsenic species to Fe(II) and mixed Fe(II) Fe(III) (green rust) minerals, which are often the product of microbial reductive dissolution of ferric oxides (Ona-Nguema et al., 2010), may impose important controls on mobility of aqueous arsenic species, particularly in environments which enter reducing conditions for limited periods of time (Tufano and Fendorf, 2008; Charlet et al., 2011).

In addition to strong pH and Eh controls on the sorption of arsenic to mineral surfaces the presence of competing ligands, especially phosphate, within the solution also has a strong influence on arsenic sorption (Jain and Loeppert, 2000; Zhu et al., 2011). The effects of numerous other potential competitive ligands have been investigated including sulphate, carbonate and selenate. Carbonate was found to have a very mild competitive effect with

arsenate and arsenite compared to phosphate (Radu et al., 2005). Zhu et also found that most competing anions resulted in greater arsenate and particularly arsenite release at low pH whereas the competitive effect of phosphate was enhanced at high pH.

Recent investigations on the effects of dissolved organic matter on arsenic mobility indicate the presence of dissolved organic matter can cause release of adsorbed arsenic (Bauer and Blodau, 2006; Wang and Mulligan, 2006a; Zhu et al., 2011). This effect is thought to be due to a combination of competition for sorption sites, the formation of highly soluble arseno-organic complexes and redox reactions between reactive organic species and arsenic.

Oxidation and Reduction of Arsenic in soils and sediments

As(III) as arsenite may be readily oxidized to As(V) as arsenate via a number of mechanisms. Although arsenite is not thermodynamically stable in the presence of dissolved oxygen it is frequently found in natural oxidized environments due to the slow kinetics of arsenite oxidation (Scott and Morgan, 1995). Mn(IV) as δ-MnO_2 and γ-MnOOH have been shown to oxidize free aqueous and surface sorbed arsenite extremely rapidly following a surface sorption complex in a similar way to oxidation of Cr(III) (Scott and Morgan, 1995; Chiu and Hering, 2000; Parikh et al., 2010). This process is illustrated in Figure 36. Spectroscopic investigations of this mechanism have also shown the surface precipitation of a Mn(II) arsenate phase (Tournassat et al., 2002).

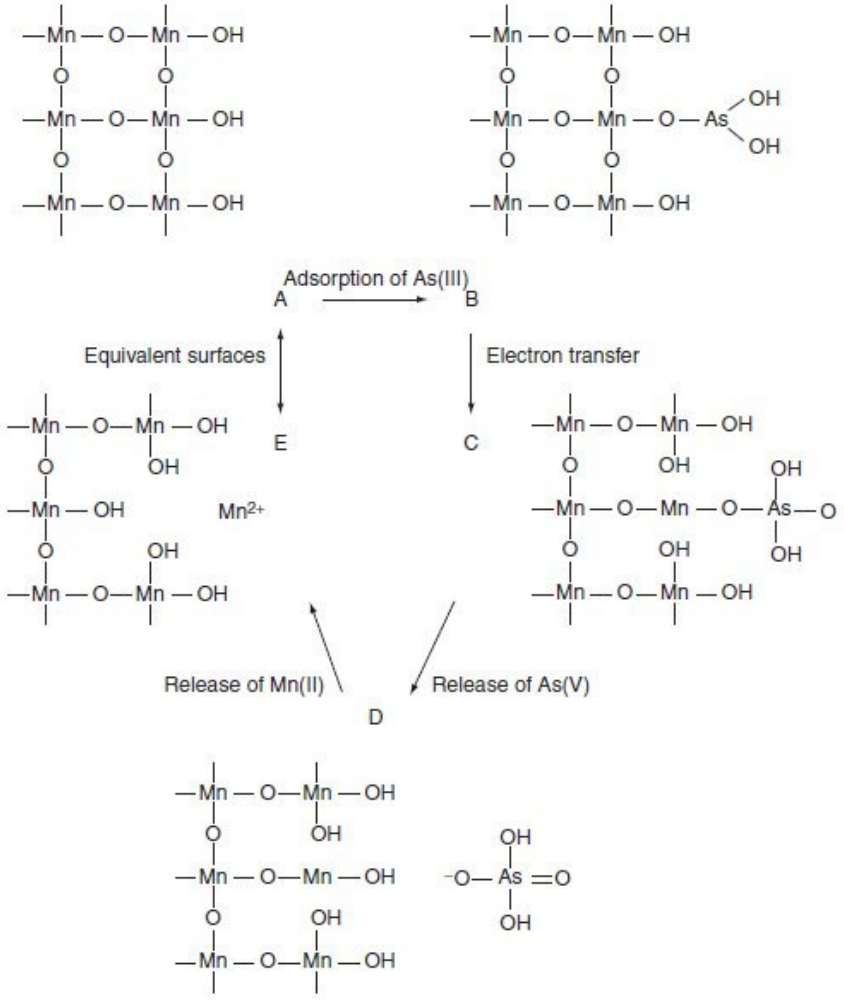

Figure 36: Oxidative sorption of arsenite to manganese oxide resulting in the release of arsenate and Mn(II). From Scott and Morgan (1995).

Despite the thermodynamic prediction of arsenite oxidation following adsorption to iron oxide surfaces this has been found to be limited, slow and highly dependent on pH conditions (Sun and Doner, 1998).

In addition to chemical oxidation mechanisms many micro-organisms have been shown to oxidize As(III), both as an energy

generating process and as a detoxification mechanism and are considered to be ubiquitous in the subsurface (Santini et al., 2000; Macur et al., 2004).

Reduction of arsenate to arsenite also readily occurs in nature both as a chemically and biologically mediated process (Fendorf et al., 2010). Biologically, bacteria, fungi and algae have been shown to reduce arsenate either as a detoxification mechanism whereby arsenate is reduced to arsenite and then expelled from the cell, or as an energy gaining process where arsenate is used as a terminal electron acceptor coupled to the oxidation of organic matter or sulphide (Oremland and Stolz, 2003; Hoeft et al., 2004). Few reduced inorganic and organic species have been implicated in arsenic reduction however there is evidence for reduction of arsenate by sulphides and humic acids (Rochette et al., 2000; Palmer and von Wandruszka, 2010).

Precipitation and dissolution processes affecting Arsenic mobility in soils and sediments

As arsenic is usually present in trace concentrations in the environment the activity of arsenic in solution is usually not sufficient to cause precipitation of discrete arsenic minerals except in highly contaminated environments (Zhang and Selim, 2008). Arsenic mobility is more often controlled by co-precipitation, inclusion and occlusion in other major phases such as iron oxides and hence by the dissolution and precipitation of such phases (Violante et al., 2006).

Arsenate minerals known shown to precipitate in highly contaminated soils and sediments include scorodite (Foster et al., 1998; Kocourková et al., 2011), amorphous ferric arsenate (Jia et al., 2006; Paktunc and Bruggeman, 2010) and angelellite (Gómez-Parrales et al., 2011). Under conditions where arsenite is dominant the precipitation of $CaHAsO_3$ is thought to act as a possible control on arsenic mobility (Roman-Ross et al., 2006). These As(III) and As(V) minerals often precipitate as surface coatings on other major minerals.

Anionic substitution during precipitation of minerals such as jarosite, schwertmannite, gypsum and calcite has also been demonstrated as a mechanism for arsenic immobilization (Foster et al., 1998; Regenspurg and Peiffer, 2005; Fernandez-Martinez et al., 2006; Roman-Ross et al., 2006)

Redox controls on Arsenic toxicity

All species of arsenic exhibit toxicity to some degree and no human dietary requirement for arsenic has been established. Therefore arsenic is considered to be a non-threshold element by most regulatory agencies including the World Health Organisation, The European Commission and the United States Environmental Protection Agency. arsenic toxicity is highly dependent on speciation and particularly on oxidation state (Hughes, 2002). Inorganic arsenic species are highly toxic and are generally considered to be considerably more toxic than organic species (Zhang and Selim, 2008). However toxicity between methylated species varies considerably dependent on degree of methylation (MMA, DMA) and arsenic oxidation state (MMA^{V}, MMA^{III}) and some methylated species may be more toxic than inorganic species (see Table 5).

Table 5: Acute arsenic toxicity in laboratory animals (from data in Hughes, 2002)

Chemical Species	Animal Species	Route	LD_{50} (mg As/kg)	Reference
Arsenite	Mouse (m)	im	8	(Bencko et al., 1978)
Arsenite	Hamster (m)	ip	8	(Petrick et al., 2000)
Arsenate	Mouse (m)	im	22	(Bencko et al., 1978)
MMA^{III}	Hamster (m)	ip	2	(Petrick et al., 2000)
MMA^{V}	Mouse (m)	Oral	916	(Kaise et al., 1989)
DMA^{V}	Mouse (m)	Oral	648	(Kaise et al., 1989)
$TMAO^{V}$	Mouse (m)	Oral	5500	(Kaise et al., 1989)

From LD_{50} values given in Table 5 we see that arsenate is approximately 3 times more toxic than arsenite and that MMA^{V} and DMA^{V} are 30-40 times less toxic than arsenate. However it should also be noted that MMA^{III} has been shown to be approximately 4 times more toxic than arsenite (Petrick et al., 2000).

Arsenic is widely known as a carcinogen and has been classified as a group 1 carcinogen to humans by the World Health Organisation International Agency for Research on Cancer (WHO IARC, 2004). Mechanisms of arsenic toxicity vary between oxidation states and species although it is thought that arsenate may replace phosphate in many biochemical reactions due to its similar structure and properties (Dixon, 1996). Arsenate has been shown to uncouple ATP formation vital for energy transfer (Hughes, 2002). Arsenite is known to interfere with the function of many enzymes by reacting with thiols or sulhydryls within their structure (Hughes, 2002).

Chapter 2: Arsenic inputs to the exogenic biogeochemical cycle and distribution in the pedosphere

Abstract

Arsenic is ubiquitous in soils, sediments and natural waters. However, its distribution across different types of environmental media and spatially on continental, regional and even micro-scales is highly heterogeneous (Reimann et al., 2009; Smedley and Kinniburgh, 2002; Ackermann et al., 2010; Salminen et al., 2005). Examples of this spatial heterogeneity at different scales are shown in Figures 37 and 38. Table 6 clearly shows that variation of arsenic concentrations in different types of environmental media can span several orders of magnitude. Strong spatial heterogeneity within contaminated soils and shallow aquifer materials can make procurement of safe drinking water and appropriate land use challenging (Winkel et al., 2008). The current observed variation of arsenic concentrations in natural media is due to the combined effect of both natural and anthropogenic processes and controls, which constitute the global biogeochemical cycle of arsenic.

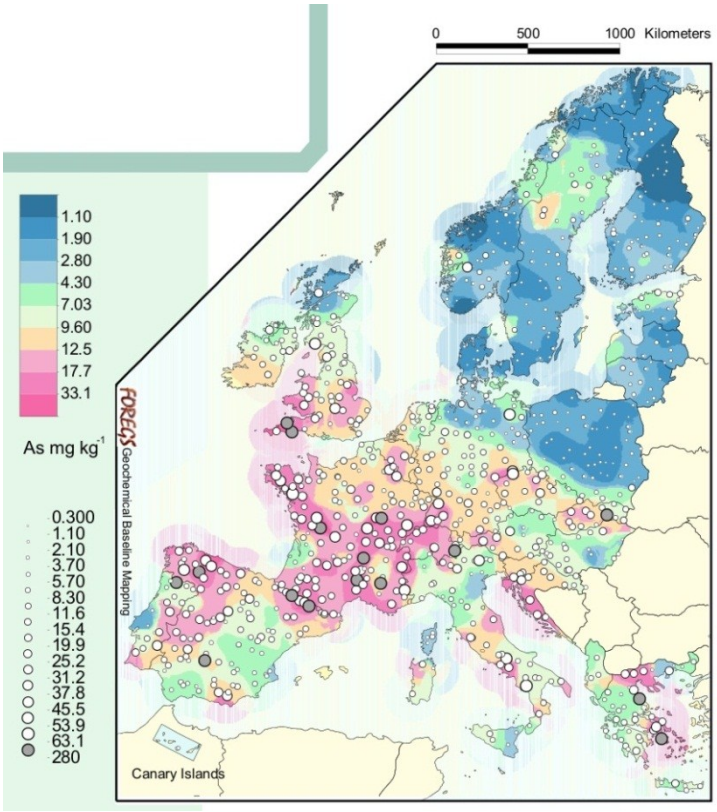

Figure 37: Heterogeneous arsenic distribution in top-soils on the European scale. Modified from Salminen et al., (2005).

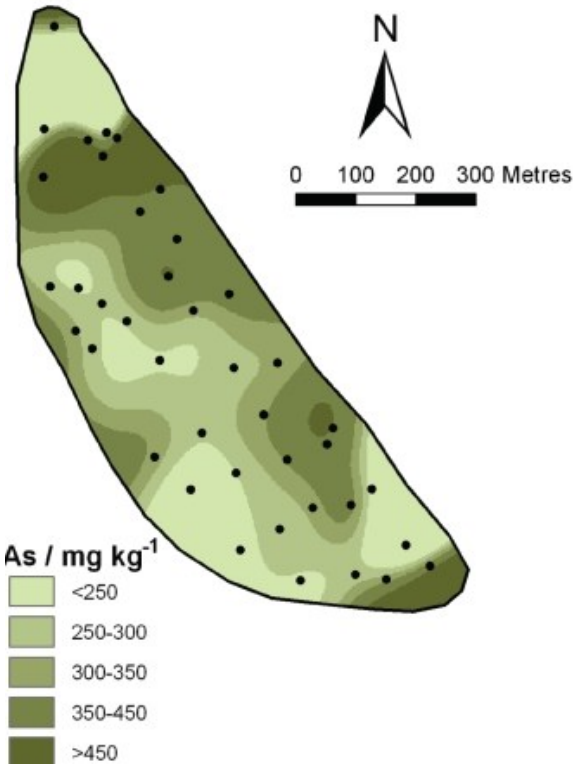

Figure 38: Heterogeneous arsenic distribution in floodplain soils on the local scale in eastern Germany. Modified from Ackermann et al., (2010)

This chapter aims firstly to review the most important sources of arsenic to the exogenic cycle and to evaluate the relative significance of anthropogenic and geogenic arsenic inputs to soils. Subsequently the current understanding of processes known to fractionate arsenic in soils and

hence influence its distribution in and liberation from the pedosphere are reviewed. The effects of current anthropogenic activities which may affect arsenic distribution and concentrations in soils in the future are briefly discussed including soil acidification, flooding, climate change and the use of agricultural amendments.

Table 6: Variation of arsenic concentrations within different environmental media. Compiled from data in Smedley and Kinniburgh (2002).

Media	**Units**	**Highest concentration occurrence**	**Lowest concentration occurrence**
Igneous rocks	mg kg^{-1}	113 in basic rocks	0.03 in ultrabasic rocks
Metamorphic rocks	mg kg^{-1}	143 in phyllite/slate	<0.1 in schist/gneiss
Sedimentary rocks	mg kg^{-1}	35,000 in coals	0.3 in coals
Unconsolidated sediments	mg kg^{-1}	170 in glacial till	0.5 in lake sediments
Soils	mg kg^{-1}	8000 close to sulphide deposits	0.1 in various soils
Rain water	ug L^{-1}	16 in USA (impacted by copper smelter)	<0.005 USA costal (mid atlantic)
River water	ug L^{-1}	21,800 in Northern Chile	<0.02 in Norway
Lake water	ug L^{-1}	1000 in USA (geothemally influenced)	0.06 in Sweden
Sediment pore water	ug L^{-1}	100,000 in Canada (tailings impound)	1.3 baseline in Swedish estuary
Groundwater	ug L^{-1}	50,000 in geothermal water	<0.5 UK baseline
Sea water	ug L^{-1}	3.7 in Spanish coastal water	0.5 in Spanish coastal water
The Atmosphere	ug m^{-3}	1 close to industrial plants	10^{-5} Unpolluted baseline

Arsenic input to the exogenic cycle:

Arsenic input to the environment from the lithosphere may occur via either natural geological or anthropogenic processes (Figure 39). Determining the relative environmental significance of these two types of input globally is challenging as quantitative natural and anthropogenic arsenic fluxes to the atmosphere, hydrosphere and pedosphere are unknown for some pathways (i.e. chemical weathering of arsenic bearing rocks). Additionally for some pathways (e.g. volcanic emissions) estimates vary substantially between published sources (Lantzy and Mackenzie, 1979; Matschullat, 2000; Chilvers and Peterson, 1987). These large variations can usually be attributed to differing methodology but do indicate a high degree of uncertainty within the literature. A number of well constrained national and local studies do exist e.g. (Wang and Mulligan, 2006b; Drahota et al., 2006; Couture et al., 2008) and these studies are often able to determine a dominant arsenic source such as smelter emission (Couture et al., 2010) or weathering of arseno-pyrite bearing rocks (Drahota et al., 2006). However, local particularities mean that these studies do not adequately represent arsenic inputs at global scales and negate the possibility of extrapolation. The most highly referenced quantitative review of global anthropogenic trace element emissions to soil, aquatic systems and the atmosphere was conducted by Nriagu and Pacyna (1988),(cited 1448 times as of July 2011). Nriagu and Pacyna (1988) and others indicate that approximately 60% of arsenic in the environment is anthropogenic in origin and that anthropogenic arsenic input to soils is between 2.84 and 9.4 $\times 10^7$ kg a^{-1} (Chilvers and Peterson, 1987; Nriagu and Pacyna, 1988). Furthermore, Senesil et al. (1999) show that the biogeochemical cycles of many trace metals and metalloids including arsenic have been drastically altered by anthropogenic technological development. Considering estimates provided by several global cycling studies (Table 7) it appears that anthropogenic inputs of arsenic to the environment (soil, water and air) are considerably higher than geogenic inputs. This conclusion has been drawn by numerous authors e.g. (Bhattacharya et al., 2002) Nevertheless, quantitative estimates of arsenic input to soils and river systems due to weathering of primary and secondary lithology have been neglected in previous attempts to quantify the arsenic biogeochemical cycle and therefore such conclusions can only be considered speculative. Evidence from large scale arsenic distribution studies in soil and water (Salminen et al., 2005; Amini et al., 2008) indicate that bedrock geology affects a major control over arsenic distribution. If weathering and erosion did not cause large inputs of arsenic to the exogenic environment it is reasonable to assume that arsenic distribution would be dominated by known anthropogenic arsenic sources and areas of volcanic activity. This is not the case (Salminen et al., 2005), therefore, flux of arsenic from lithosphere to pedosphere and hydrosphere by weathering is almost certainly very high, and the lack of quantitative data severely limits our understanding of the global cycle of arsenic and our ability to compare anthropogenic and geogenic inputs. Despite this limitation, from the estimates of arsenic fluxes that are currently available it is clear that anthropogenic arsenic input does also play a significant role in the biogeochemical cycle of arsenic. Equally, large scale geochemical mapping demonstrates that the distribution of arsenic in the hydrosphere and pedosphere is strongly affected, at least locally by anthropogenic emissions.

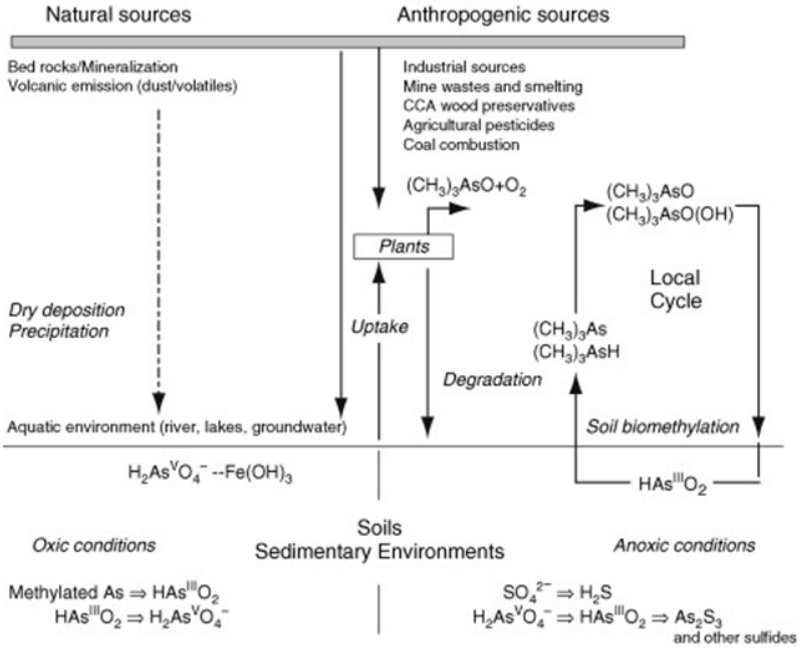

Figure 39: Conceptual model for the terrestrial biogeochemical cycling of arsenic. Reproduced from Jacks and Bhattacharya (1998).

Table 7: Summary of major As sources inputs to the environment (air, water and soils) estimated by previous studies.

As Input type	**Study 1** (Nriagu and Pacyna, 1988) **(10^3 kg yr^{-1})**	**Study 2** (Chilvers and Peterson, 1987) **(10^3 kg yr^{-1})**	**Study 3** (Lantzy and Mackenzie, 1979) **(10^3 kg yr^{-1}) atmospheric input only**
Volcanic emissions	Not estimated	17,150	280
Low temperature volatilization	Not estimated	26,200	16,000
Natural weathering and erosion processes	Not estimated	Not estimated	Not estimated
Non-ferrous metal production	22,500 - 49,580	110,195	Not estimated
Coal combustion	7130 - 40,530	41,340	Not estimated

Geogenic Input

The natural flux of arsenic from the geosphere to the environment is thought to be dominated by two key processes, volcanism and the weathering and erosion of arsenic bearing rocks.

Volcanic emission (280 – 17,150 x 10^3 kg yr^{-1})

Volcanism is considered by some authors to be the primary geological process exporting arsenic to the environment (Matschullat, 2000). However, published quantitative estimates of arsenic emissions during eruptions and degassing vary considerably from 0.3×10^6 kg a^{-1} (Lantzy and Mackenzie, 1979) to 1.715×10^7 kg a^{-1} (Chilvers and Peterson, 1987) and arsenic input due to weathering, necessary for comparison, is very poorly defined. The differences between reported volcanic emission estimates are attributable partly to methodology and partly to the author's choice of critical constants. Some studies use arsenic concentrations from volcanic ash from a single well studied volcano to determine total particulate arsenic emission (Chilvers and Peterson, 1987) whereas others use average arsenic concentrations in only one type of volcanic rock deemed to represent an average value for all volcanoes (Lantzy and Mackenzie, 1979). Both of these approaches are clearly limited in their accuracy as even between well monitored volcanoes considerable differences in arsenic emission are present, for instance arsenic emissions from Mount Saint Helens total approximately 8.9×10^6 kg a^{-1} compared to 0.04×10^6 kg a^{-1} from Poas (Pacyna, 1986). Therefore whilst such extrapolations currently offer some degree of quantitative estimation and indicate the importance of volcanism as an arsenic source, reported global estimations of arsenic emission by volcanism are poorly constrained and should be treated with caution. A more comprehensive study of volcanic emissions incorporating a more widespread sampling campaign, involving collaboration between many volcanic observatories is required to account for the variation between different types of volcanoes.

Erosional and weathering processes (?)

Arsenic is the 20th most abundant element in the crust with an average concentration of 1.8 mg kg^{-1} (Lide, 2009) however significant variation in arsenic concentration exists even in primary rocks dependent on mineralogy. Arsenic is a strongly chalcophile metalloid, as such it rarely forms a structural component in silicates and is more commonly associated with sulphides and oxides.

Although arsenic minerals themselves (e.g. Orpiment (As_2S_3), Realgar (AsS)) are relatively rare in the environment, occurring mostly in highly mineralised areas, many common minerals also host significant quantities of arsenic and occur in a much more varied range of environments, these include reduced sulphides (Pyrite, Marcasite, Galena etc.) (Wolthers et al., 2005) and ferric iron minerals including Fe oxides, Fe hydroxides and Fe oxyhydroxides (Ona-Nguema et al., 2005)

The variation seen in primary rocks can be further enhanced by erosion and weathering processes, leading to the broadest range of arsenic concentrations in sedimentary rocks and soils (Smedley and Kinniburgh, 2002). Concentrations of As in sands and sandstones tend to be the lowest due primarily to the lack of arsenic in their constituent minerals (typically quartz and feldspars) whereas more argillaceous rocks tend to contain much higher As concentrations owing to a higher proportion of sulphides, oxides and organic matter.

Both sulphides and oxides (the two main groups of minerals which tend to host arsenic) can be rapidly dissolved within the range of conditions experienced in the near surface environment which may result in liberation of arsenic into pore and surface water.

Liberation mechanism 1: Oxidative dissolution of metal sulphides

Sulphides are rapidly oxidised when exposed to the earth's surface where they come into contact with oxygenated water. This oxidative dissolution can release arsenic either incorporated as an impurity within another sulphide mineral (e.g. Pyrite, the most common mineral in metal sulphide ores despite iron rarely being the target metal for extraction by the mining industry) or when arsenic itself forms part of the mineral structure (e.g. Arsenopyrite). The geochemical reactions for the oxidative dissolution of Pyrite and Arsenopyrite are well understood and are shown in equations 1 to 5. Such reactions also generate acidity and it is this breakdown of sulphides which is responsible for acid mine drainage, when the exposure is due to mining, or acid rock drainage, when sulphide exposure is natural i.e. due to a land slip such as Mam Tor (Vear and Curtis, 1981). Arsenic liberated in this way is then transported to other environmental reservoirs such as the waters listed in Table 1 where mass redistribution of arsenic can occur carried within the terrestrial water cycle.

Equation 1 $2FeS_2 + 7O_2 + 2H_2O \rightarrow 2Fe^{2+} + 4SO_4^{2-} + 4H^+$ (Gray, 1997)

Equation 2 $4Fe^{2+} + O_2 + 4H^+ \rightarrow 4Fe^{3+} + 2H_2O$ (Konhauser, 2007)

Equation 3 $Fe^{3+} + 3H_2O \rightarrow Fe(OH)_3 + 3H^+$ (Konhauser, 2007)

Equation 4 $FeS_2 + 14Fe^{3+} + 8H_2O \rightarrow 15Fe^{2+} + 2SO_4^{2-} + 16H^+$ (Edwards et al., 2000)

Equations 1 to 4: Sulphide oxidation e.g. pyrite which can contain up to 10 w% arsenic. (Blowes et al., 2003; Plant et al., 2003).

Equation 5 $4FeAsS + 13O_2 + 6H_2O \rightarrow 4Fe^{2+} + 4AsO_4^{3-} + 4SO_4^{2-} + 12H^+$

Equation 5: Oxidation of Arsenopyrite, a Fe and As sulphide mineral (Plant et al., 2003).

Similar oxidation reactions apply to a variety of other metal sulphide minerals including Bornite (Cu_5FeS_4), Chalcocite (Cu_2S), Chalcopyrite ($CuFeS_2$), Covellite (CuS), Galena (PbS), Millerite (NiS), Molybdenite (MoS_2), Trollite (FeS) and Sphalerite ((Zn,Fe)S) (Gray, 1997). It is import to note that the redox changes shown in the above reactions do not occur synchronously but are the net result of a series of electron transfer reactions which are well understood (Konhauser, 2007).

The slowest reaction and thus the rate limiting step in the abiotic chemical oxidation of pyrite has been shown to be the oxidation of Fe(II) to Fe(III) (Equation 2) (Singer and Stumm, 1970). Certain species of bacteria and archaea increase the rate of this reaction using it as an energy generating process. This catalysis has been shown (in the case of *Thiobacillus Ferrooxidans*) to increase the rate of Fe(II) oxidation to Fe(III) by 5 or 6 orders of magnitude (Lacey and Lawson, 1970).

Liberation mechanism 2: Reductive dissolution of metal oxides

Arsenic bearing metal oxides and hydroxides, most importantly of iron and manganese are also easily broken down under environmental conditions leading to the release of arsenic either from within the structure of the mineral or sorbed to its surface. This dissolution is most commonly bacterially mediated under reducing conditions coupled to the oxidation of organic matter (Islam et al., 2004). A wide variety of facultative and obligate anaerobes are able to gain energy for growth and reproduction from this process which is summarised in equation 6. Although many different bacteria have been shown to be capable of the dissimilatory reductive dissolution of ferric oxides and hydroxides, *Geobacter* (Cutting et al., 2009) and *Shewanella* (Arnold et al., 1990) are amongst the most well studied. These organisms have been shown to be extremely versatile using a variety of oxidised metals as electron acceptors and employing a range of electron transfer mechanisms (Lloyd et al., 2003; Reguera et al., 2005). Iron oxides also dissolve and release arsenic contained within them under oxic and acidic conditions where $Fe^{2+}_{(aq)}$ is more thermodynamically favourable (Majzlan et al., 2004).

Reductive dissolution of goethite mediated by bacteria oxidising organic matter (Arnold et al., 1988).

Equation 6 $24\ FeOOH_{(S)} + C_6H_{12}O_{6(S)} + 42H^+_{(aq)} \dashrightarrow 24Fe^{2+}_{(aq)} + 6\ HCO_3^-{}_{(aq)} + 24\ H_2O_{(aq)}$

Whether arsenic is liberated from the solid phase by reductive or oxidative dissolution, following transport via the terrestrial water cycle, a significant proportion of mobilised arsenic is subsequently trapped in the pedosphere via sorption and co-precipitation processes. The average residence time of arsenic within the pedosphere is considered to be on the order of 1000-3000 years in moderate climates (Bowen, 1979). Based on this timeframe arsenic additions made to soil systems now and during previous decades may pose a risk to health for a considerable time into the future.

Quantifying the processes of erosion, weathering, transport, immobilisation, and remobilisation with respect to arsenic is extremely challenging and most studies which quantify the biogeochemical cycle of arsenic do not attempt it. The rates therefore of arsenic input to, and output from, the pedosphere, are currently unknown. This represents a severe short coming in our understanding of the biogeochemical cycle of arsenic as demonstrated by Reimann et al., (2009) and more quantitative work to determine rates of immobilisation and liberation of arsenic in soils under varying conditions is required.

Although it is true that erosional zones in many watersheds may not contain, and hence export, significant quantities of arsenic, lithological variations in arsenic concentration form a major control on geogenic arsenic input to terrestrial basins and hence arsenic's distribution in natural waters, sediments and soils. This conclusion is supported by most predictive models for arsenic concentrations in groundwater, which rely heavily on geological information (Amini et al., 2008; Lado et al., 2008; Winkel et al., 2008). Equally considerable differences between arsenic concentrations exist in river water and groundwater dependant on the lithology of the watershed even before considering the impact on anthropogenic inputs. Whilst uncontaminated oceanic rain water contains approximately 19 ng/L of arsenic (Andreae, 1980)

river water may vary from 127 ng/L in unpolluted watersheds with karst lithology (Seyler and Martin, 1991) to 21,800 μg/L from arid unpolluted watersheds hosting volcanic sediment (Cáceres et al., 1992)

Groundwater is similarly influenced by environmental context including aquifer lithology and redox conditions this is demonstrated by the range of groundwater environments that exhibit high concentrations of arsenic. Firstly, the well-known high-arsenic groundwater areas in South and South-east Asia (West Bengal (India), Bangladesh, Cambodia and Vietnam) are typically low-lying, floodplains with little topographic variation, of rivers which originate in the Himalayas. The arsenic contaminated groundwaters in this region are almost exclusively found in young (Holocene) aquifers. The second type of large-scale 'natural' arsenic groundwater tends to be found in inland or closed basins in arid or semi-arid areas, also containing geologically young sediments and where groundwater flow is sluggish. The third group of arsenic-rich groundwaters are geothermal. Here high arsenic concentrations are the result of water-rock interactions at depth.

In type one areas where arsenic-rich groundwater occurs, weathering of Himalayan-derived sediment during erosion and transport leads to downstream deposition of arsenic. The primary sources of arsenic within the Himalayas are thought to be eroding coal seams and rocks containing sulphide minerals (Fendorf et al., 2010). During erosion of these minerals, As(III) occurring in sulphide minerals is oxidised to As(V) and subsequently adsorbed to precipitated iron(hydr)oxides. On the floodplains sedimentation is rapid and organic material is buried more rapidly than it can be oxidised by aerobic bacteria at the surface. Therefore at depth organic material is available in abundance which acts as an electron donor for bacterial metabolism. Due to the abundance of organic carbon, the high activity of micro-organisms and limited extent of oxygen diffusion from the surface, reducing conditions are established in the shallow aquifers (Islam et al., 2004). These conditions lead to microbial dissolution of Fe oxides resulting in the co-liberation of arsenic into the aqueous phase, i.e. in groundwater. Furthermore, as expected from the redox sequence (Stumm and Morgan, 1996) the more labile As(III) typically dominates over As(V) in reducing environments and therefore the reduction to As(III) probably also contributes to the release of arsenic to the groundwater (Smedley and Kinniburgh, 2002). Some bacteria have also been shown to be capable of direct reduction of arsenate under reducing conditions (e.g. *Sulfurospirillum barnesii* (Zobrist et al., 2000)). Some sorption studies suggest however that arsenite and arsenate are both strongly adsorbed by iron oxyhydroxides and that the oxidation state change from As(V) to As(III) may be of minor importance with regards to mobility compared to the reductive dissolution of iron oxyhydroxides (Dixit and Hering, 2003). Due to the uplift of the Himalayas, sediment accumulation in the deltas of South and Southeast Asia has occurred rapidly, resulting in the deposition of thick sequences of Holocene sediment. The aquifers are therefore composed of young, fresh sediments that contain fine grained minerals with larger surface to volume ratios than older, well-crystallised sediments which have undergone significant Ostwald ripening. The high surface to volume ratio observed in young Holocene sediments results in a higher capacity for arsenic adsorption when compared to older more crystalline sediments with similar composition. Furthermore, in Southeast Asia, delta initiation and progradation occurred simultaneously with the Holocene Climate Optimum, resulting in the burial of organic matter at a high rate. Key characteristics of arsenic-affected

areas in this region are thus the presence of natural (bio)degradable organic carbon, rapidly buried, young (Holocene) sediments and low hydraulic gradients in flat and low-lying areas.

In the second groundwater environment, arsenic release is controlled by pH changes. High pH (>8.5) conditions can develop usually as a result of the combined effects of silicate and carbonate weathering and high evaporation rates. This pH change leads either to the desorption of adsorbed arsenic (especially As(V) species) from mineral oxides, especially Fe oxides, or it prevents them from being adsorbed. Probably the largest region of high-arsenic groundwaters formed in arid oxidising environments is the Chaco-Pampean Plain of central Argentina covering around $1x10^6$ km^2 (Smedley and Kinniburgh, 2002). Groundwater arsenic concentrations up to 11500 mg L^{-1} were recorded by Nicolli et al. (1989). The high-arsenic groundwaters are derived from Quaternary deposits of loess (mainly silt) with intermixed volcanic ash (Nicolli et al., 1989); (Smedley et al., 2002)). In this environment arsenic is dominantly present as As(V). Metal oxides in the sediments (especially Fe and Mn oxides and hydroxides) are thought to be the main source of dissolved arsenic, caused by desorption under high-pH conditions (Smedley and Kinniburgh, 2002). although the direct dissolution of volcanic glass has also been cited as a potential source (Nicolli et al., 1989).

In the third (geothermal) group, the amount and nature of dissolved species in these fluids is determined by local geology and the thermal gradient but most often involves volcanic rocks and/or sulphide-bearing minerals. For example, in the volcanic areas of southern Italy, high arsenic concentrations have been related to the deep-rising fluids of the active geothermal systems (Aiuppa et al., 2003). Nevertheless, the relationship between high arsenic concentrations and geothermal waters is not a simple one. Arsenic concentrations are high in the thermal waters of Kamchatka, New Zealand, Japan, Alaska, California, and Wyoming, where black shales are common, but they are low in thermal waters from Hawaii and Iceland where most of the rocks are geologically young basalts (Nordstrom, 2002). The highest arsenic concentrations (20-200 mg/kg) in rocks are typically found in organic-rich and sulphide-rich shales, sedimentary ironstones, phosphatic rocks, and some coals (Smedley and Kinniburgh, 2002). Aquifers with carbonaceous shales and without obvious thermal gradients, such as in Taiwan, also can lead to high dissolved arsenic concentrations (Nordstrom, 2002).

While some mass balance studies consider the release due to the weathering and erosion of rocks and soils to be negligible compared to volcanic and anthropogenic inputs (Paces and Pacesova, 2001) it has been shown that in areas containing large sulphide deposits, that this natural export of arsenic can be significant (Navas and Machin, 2002; Smedley et al., 2002), accounting for up to 99.7% of total arsenic input to soils in some cases, even in areas where arsenic is applied to the soil directly in agrochemicals (Drahota et al., 2006). Although it is true that erosional zones in many watersheds may not contain, and hence export, significant quantities of arsenic to the environment (Seyler and Martin, 1991), lithological variations in arsenic concentration, form a major control on geogenic arsenic input to terrestrial basins and hence arsenic's distribution in natural waters, sediments and soils.

In summary the role and relative importance of geogenic processes on arsenic content in soils and surface waters is highly variable. Each environmental system must be considered

individually due to lithological heterogeneity in erosional zones, variations in hydrologic regime, the presence or absence of volcanic influence and differences between soil and sediment types.

Anthropogenic input

Anthropogenic inputs of arsenic to the environment are diverse, however, they can generally be divided into two groups: Input where arsenic release is an undesirable bi-product of human activity, as is the case for mining effluents, smelters and coal combustion, and input where arsenic release is due to its intentional use i.e. pesticides, soil sterilisation and addition to metal alloys. Intentional inputs of arsenic to the pedosphere have been slowly decreasing for the last 60 years due to increased awareness of the risks posed by arsenic and its long residence time in soils. However, as coal combustion, copper smelting and other industrial activities increase globally, unintentional arsenic emissions have risen considerably in the last 3 decades.

Arsenic inputs to the environment as bi-products of industrial processes (group one inputs)

Group one (bi-product) inputs of arsenic to the environment account for the majority of anthropogenic arsenic export. This is principally due to coal combustion for power production and non-ferrous metal production (Chilvers and Peterson, 1987; Matschullat, 2000; Han et al., 2003).

Coal combustion (~63,317 x 10^3 kg yr^{-1})

Arsenic concentration in coal varies considerably, from less than 0.3mg/kg to 35,000 mg/kg (Table 1). Most commonly, arsenic concentrations in coal are close to 10 mg/kg (Bragg et al., 1997; Finkelman et al., 1999) however in coal affected by epigenetic mineralization such as in the Guizhou province in China can host considerably higher concentrations (Bragg et al., 1997; Zhao et al., 2008). During combustion this arsenic is either volatilised (Germani and Zoller, 1988) or released in fly ash which is eventually deposited contaminating soils and waterways. Chilvers and Peterson (1987) estimated global coal combustion to be 3696 x 10^6 tonnes per year, emitting 6240 tonnes of arsenic to the atmosphere and 35,100 tonnes to the pedosphere. These figures are often cited in more recent literature (Matschullat, 2000; Henke, 2009) despite the substantial global increase in coal use since 1987 due predominantly to increased use by the People's Republic of China. The world coal institute estimate that 5845 x 10^6 tonnes of hard coal was produced in 2008 (World Coal Institute, 2010), an increase of 58% over 1987 usage. Even excluding the additional 951 x 10^6 tonnes of lignite production in 2008, if emission estimates are scaled up from 1987 to 2008 usage, 9859 tonnes of arsenic were released to the atmosphere and 55,458 tonnes of arsenic were added to the pedosphere via coal combustion.

Non-ferrous smelting (~155,103 x 10^3 kg yr^{-1})

Many economically viable ores of non-ferrous metals such as copper, zinc, lead and nickel exist as sulphide deposits. The target minerals in such deposits include Bornite (Cu_5FeS_4), Chalcocite (Cu_2S), Chalcopyrite ($CuFeS_2$), Covellite (CuS), Galena (PbS), Millerite (NiS), Molybdenite (MoS_2), Trollite (FeS) and Sphalerite ((Zn,Fe)S) (Gray, 1997). As discussed previously when considering geogenic inputs by chemical weathering and erosion, arsenic is often present in sulphide deposits in high concentrations as an accessory mineral or as structural mineral components (e.g. orpiment As_2S_3). The smelting process used to obtain many non-ferrous metals from ore minerals results in volatilization of some of arsenic present in the ore in addition to substantial

particulate emission as flue dust. Flue dust varies in composition considerably depending on the type of smelter, the quality of the ore and the target metal. Analysis of flue dust from copper smelters shows that the dust is highly concentrated with respect to arsenic containing 0.3 and 29.4% As (Twidwell and Mehta, 1985). Copper smelters result in the highest anthropogenic arsenic emission globally. Gaseous and particulate emission factors are estimated to be 1.5kg of arsenic per tonne of Cu produced (Chilvers and Peterson, 1987). When particulate and gaseous emissions are combined with arsenic released in contaminated waste water and sludge the resulting global flux of arsenic to the environment from copper smelters was estimated to be 87,545 tonnes per year in 1982 which represented approximately 80% of arsenic released from all non-ferrous metal smelting and refining processes at that time (Chilvers and Peterson, 1987). Since 1982 global copper production has, like coal combustion, increased substantially. Current data indicates that 14.5×10^6 tonnes of copper was produced globally in 2009 (Edelstein, 2011) of this 12.46×10^6 tonnes was produced via smelting of primary materials, an increase of 55% over 1982 estimates. Assuming that emission factors have not decreased since 1987, emissions to the atmosphere, pedosphere and hydrosphere totalled 135,497 tonnes in 2009 from copper smelting accounting for 85% of all arsenic emitted from non-ferrous smelting. Estimates of non-ferrous smelting arsenic emission are detailed in Table 8. Increases in arsenic emission are demonstrated for copper and lead whereas decreases are shown for zinc. This is due to the diminishing use of energy intensive pyrometallurgical refining processes (the imperial smelting process) which emits more arsenic than electrolytic processing. In 198 18% of all zinc was produced by the imperial smelting process. In 2002 this figure had reduced to 8% (Australasian Institute of Mining and Metallurgy.;Queensland., 2002).

Table 8: Estimated arsenic emissions to the environment from non-ferrous smelting in 1982 and 2009. Red numbers indicate an increase in arsenic emission since 1982, green numbers indicate a decrease in arsenic emission since 1982.

Process	Global production (1982), tonnes per year	Global production (2009), tonnes per year	Atmospheric As emission factor, kg_{As} $tonne^{-1}$	Estimated arsenic input directly to the hydrosphere and pedosphere, tonnes per year 1982/2009	Total arsenic emission to the environment, tonnes per year 1982/2009
Copper smelting of primary materials	8.05×10^6	12.46×10^6 (Edelstein, 2011)	1.5	75,465/ 116,807	87,545/ 135,497
Copper refining of primary materials	9.55×10^6	12.30×10^6 (Edelstein, 2011)	0	10,810/ 13,996	10,810/ 13,996
Lead smelting of primary materials	3.58×10^6	3.96×10^6 (Guberman, 2011)	0.4	3580/ 3960	5010/ 5544
Zinc smelting of primary materials using the imperial smelting process	1.20×10^6	0.89×10^6 (Tolcin, 2011)	0.65	6050/ 4487	6830/ 5066

Wood combustion (~463 x 10^3 kg yr^{-1})

In many parts of the world wood is the primary fuel for domestic heating and cooking. During the combustion process arsenic is released via both volatilization and in particulate matter. Arsenic emission factors due to combustion of plant material are low due to the low total arsenic concentrations found in most plant tissue. Despite this, due to the large scale of global wood fuel combustion, which was estimated 1.85 x 10^9 m^3yr^{-1} (approximately 925 x 10^6 tonnes of wood) in 2009 (FAO, 2011) total arsenic emissions constitute approximately 463 tonnes per year, a considerable arsenic input to the atmosphere and pedosphere. This emission represents a 9% increase over 1981 estimates (Chilvers and Peterson, 1987).

Destruction of woodland and pasture (~3632 x 10^3 kg yr^{-1})

The widespread "slash and burn" approach used to clear forest and pasture land, primarily for subsistence agriculture, releases significant quantities of arsenic to the atmosphere and pedosphere via the same chemical pathways as combustion of wood as a domestic fuel. Land clearance via burning is estimated to account for combustion of approximately 7249 x 10^6 tonnes of dry plant material annually (Levine, 1991). Despite the relatively small arsenic emission factor attributed to combustion of plant material, the large scale of biomass burning results in a total arsenic annual arsenic emission of approximately 3632 tonnes per year.

Irrigation with contaminated groundwater (?)

An additional type of group one input is the case of arsenic added to soils via irrigation with arsenic-rich containing groundwater. Irrigating soils with arsenic rich water causes arsenic to accumulate in topsoil primarily adsorbed to iron (hydr)oxide minerals (Neumann et al., 2011), although in some cases this may be partially mitigated by removal during natural flooding (Roberts et al., 2010). This mechanism of top soil contamination has only recently been critically investigated and therefore global estimates of fluxes from ground water to top soils via irrigation are still currently unavailable.

Direct use of arsenic in industry and agriculture (group two inputs)

Group 2 inputs of arsenic to the environment are considerably less than group 1 inputs and are primarily due to the use of various arsenic compounds in pesticides, herbicides, fungicides and wood preservatives. The toxicity of high concentrations of arsenic to most forms of life ensures its effectiveness in such applications but has resulted in accumulation of arsenic in many agricultural soils (Merry et al., 1983; Embrick et al., 2005; Jorgensen et al., 2005). Arsenic is also released into the environment due to its use in production of alloys, glass and electronics (GaAs semiconductors) which are eventually disposed of in landfills (Loebenstein, 1994).

The sum of group two (direct use) inputs can be estimated quite accurately based on the annual quantity of arsenic extracted by mining companies for industrial use as there is very little recycling of arsenic during its anthropogenic flow and residence time in anthropogenic flow is short (<1 to 30 years) (Loebenstein, 1994).

In 2009 global production of pure arsenic (As_2O_3 weight or equivalent) was estimated to be 54,400 × 10^3 kg a^{-1} (Brooks, 2010). Matschullat (2000) reports that approximately 50% of extracted arsenic is used in pesticides and insecticides and 30% in CCA (chromated copper arsenate) wood preservatives, the remaining 20% is split between various industries including electronics, glass production, animal feed addition and alloy production. However, this is in disagreement with Loebenstein (1994) who indicates that wood preservation accounts for the largest input of arsenic to the environment (in the United States) arguing that the use of both inorganic and organic arsenic in pesticides has drastically reduced since its peak in the 1950's. This discrepancy may be due to differences between the use of arsenic in the United States and the

rest of the world (i.e. the continued use of arsenic containing fertilizers in other countries) or due to the lack of current high quality global arsenic use data. Despite disparities between published sources on recent arsenic usage, it is clear that agricultural pesticides and wood treatment processes have dominated recent arsenic usage (Table 9). It is expected that arsenic usage in both of these applications will decrease considerably within the next decade following various legislative restrictions imposed by various countries including the U.S.A., Canada the European Union and Australia (Liikanen, 2003; APVMA, 2005; Edwards, 2006; Brooks, 2010). Indeed the decreasing trend in arsenic production is already evident in 2009 arsenic production data (Brooks, 2010).

Table 9: Comparison of direct arsenic usage estimates between published studies.

Arsenic use	**Study 1 U.S.** (Greenwood, 1989)**, tonnes per year**	**Study 2 U.S.** (Loebenstein, 1994)**, tonnes per year**	**Study 3, Global,** (Chilvers and Peterson, 1987)**, tonnes per year**	**Study 4, Global,** (Matschullat, 2000)**, tonnes per year**
Pesticides and desiccants	26,000 (65%)	4200 (20.49%)	20,000 (42%)	15,226.5 (50%)
Wood preservatives	7200 (18%)	14,400 (70.23%)	16,000 (33%)	9135.9 (30%)
Feed additives	-	-	4762 (10%)	-
Glass production	3800 (10%)	800 (3.9%)	2381 (5%)	-
Alloys and electronics	1100 (3%)	800 (3.9%)	2381 (5%)	-
Other	1500 (4%)	300 (1.46%)	2381 (5%)	-
Total	39,600	20,500	48,000	30,453

Agriculture (15,227 – 20,000 x 10^3 kg yr^{-1})

Arsenic compounds have been used in agriculture for hundreds of years as pesticides, including rodenticides, herbicides, insecticides and fungicides. Compounds used include arsenic trioxide, metal arsenates (Pb, Ca, Cu and Na), metal arsenites (Na, K and Cu) and more recently methylated arsenic acids (Murphy and Aucott, 1998; Cai et al., 2002). Lead arsenate was the most extensively used arsenic based insecticide which was applied heavily to protect fruit crops in the west from various moths and beetles between 1892 and the late 1950s (Murphy and Aucott, 1998). With use the target pests developed increasing resistance to the pesticide and hence increasing quantities of lead arsenate were applied in response. Health concerns and the availability of more effective synthetic organic pesticides such as DDT led farmers to reduce use of lead arsenates during the 1950s (Murphy and Aucott, 1998). Less toxic organic arsenicals including mono and disodium methyl arsenates (MSMA and DSMA) calcium acid methyl arsenate (CAMA) and sodium cacodylate (sodium dimethylarsenate) were also used starting in the 1950s (DSMA) and 1960s (MSMA, CAMA, cacodylic acid). Although less toxic than inorganic variants the use of organic (As_V) arsenicals has been questioned due to the potential for transformation of these compounds to more toxic inorganic forms in soils (Datta et al., 2006). The US-EPA has now withdrawn the registration status of organic arsenicals for use as pesticides (Edwards, 2006) and their use will be phased out completely by

2013 (Keigwin, 2009). Therefore current and future agricultural input of arsenic to the pedosphere in pesticides is substantially lower than the values estimated by Chilvers and Peterson (1987) and Nriagu and Pacyna (1988). Despite the current limited use of arsenic pesticides in the west their large scale historical usage has led to soils highly contaminated with arsenic and associated metals, particularly on land previously used for fruit production (Merry et al., 1983; Embrick et al., 2005). Additionally despite strong regulatory responses in the west it is likely that arsenic based pesticides will continue to be used in developing countries for some years to come.

Wood Preservation (9136 – 14,400 x 10^3 kg yr^{-1})

Due to its effectiveness as a pesticide, arsenic has also been used since 1933 in the wood preservation industry. The combined application of dichromic acid, copper and arsenic acid (CCA) results in timber which is highly resistant to fungal, bacterial and insect degradation. Although the pressure impregnation process used during CCA treatment of wood is designed to minimize leaching by chemically binding arsenic and copper to cellulose and lignin within the wood, high concentrations of arsenic have been recorded in soils in close proximity to CCA treated wood (Chirenje et al., 2003) and in rainwater runoff from pressure treated structures (Khan, Solo-Gabriele, et al., 2006). Due to the effectiveness of the CCA process its use has become widespread since its development in 1933. As can be seen in

Table 9 global estimates of total arsenic use in the CCA process vary considerably between studies, countries and year. However over the last 2 decades CCA treatment has accounted for between 18% and 70% of total arsenic consumption (the wide range is due to diminishing agricultural use affecting total arsenic consumption and increasing adoption of the CCA process). Recently several government regulatory bodies including the European Commission and the US-EPA have acted upon concerns over the safety of CCA treated wood and have restricted the residential use of CCA treated wood. Other authorities however, including the New Zealand Environmental Risk Management Authority (ERMA), have concluded that such restrictions are unnecessary citing over estimations of the exposure risk posed by CCA wood by other studies (Read, 2003). Based on this ERMA continue to recommend the use of CCA treated wood in all settings (Read, 2003).

Although arsenic is the most mobile of the three components used in the CCA pressure treatment process and leaching appears to be a cause for concern (Khan, Jambeck, et al., 2006), potentially the greatest emission of arsenic to the environment resulting from the CCA treatment process is the industrial and domestic burning of treated timber (Aggett and Aspell, 1980; Chilvers and Peterson, 1987; Wasson et al., 2005). During burning arsenic is released both as volatile species and concentrated in fine particulates (Wasson et al., 2005). At present many people are unaware of the risks of burning CCA treated wood and due to its large scale residential usage in fencing, decks, porches etc. wood is often disposed of in uncontrolled garden fires or in wood burning stoves which can lead to severe health impacts (Peters et al., 1984).

Natural distribution and transport of Arsenic in soil

Once arsenic is introduced to the pedosphere, whether by atmospheric deposition, direct addition of agrochemicals (pesticides) or by hydrological transport (e.g. in river or groundwater), its distribution, transport and eventual removal is subsequently controlled by its speciation, the soil hydrological regime, the microbial community and the mineralogical and organic nature of the soils matrix. It is considered that soils, despite removal due to hydrological transport and methylation/volatilization, are currently accumulating arsenic (Nriagu and Pacyna, 1988; Senesil et al., 1999)

Arsenic may move through the soil matrix and hence be redistributed geographically either by diffusion, which is a comparatively slow process or by hydrological transport (advection) which depending on the hydraulic conductivity of the soil and the hydraulic gradient may be much faster. For hydrological transport to take place arsenic must either be in aqueous form or in particles small enough to be transported with flow through the soils pore network (i.e. nano-particles or colloids). An understanding of controls on partitioning between solid phase and aqueous phase (pore-water) arsenic is therefore crucial to understanding its mobility.

Speciation

Arsenic can exist in oxidation states ranging from -3 to +5 (-III, -1, 1, 2, 3 and 5) however it most commonly exists in either its trivalent (As(III)) or pentavalent (As(V)) form in soils, dependent primarily on soil redox potential. In addition to oxidation state variation, arsenic in soil forms both inorganic and organic molecules with varying protonation states across a range of pH and Eh conditions. This wide variety of arsenic compounds with varying stability, size and charge can interact in very different ways with the rest of the soil matrix. When considering arsenic distribution and mobility, speciation is important as the charge and size of arsenic species are important factors in determining the probability of arsenic sorption onto mineral surfaces and complexation with organic matter and hence the partitioning between solid and aqueous phases.

Whilst the dominant arsenic species and the proportion of secondary species stable in soil pore water under given conditions may be determined thermodynamically from chemical composition, Eh, pH, temperature and pressure (expressed graphically in a Pourbaix diagram Figure 40) and hence the known interactions between arsenic and the soil matrix inferred (i.e. hydrogen arsenate Figure 41 with a charge of -2 can be expected to adsorb to positively charged mineral surfaces) soils are rarely in thermodynamic equilibrium. This can be due to slow kinetic rates of speciation changes or additionally due to rapid changes soil redox potential due to complex biological catalysis of many processes responding to subtle environmental changes. In addition the thermodynamic calculations possible using programs such as PHREEQC (Parkhurst et al., 1999) or Geochemical workbench(Bethke and Yeakel, 2009) are reliant on the accuracy of constants contained within their thermodynamic databases which are sometimes incomplete or poorly defined for some systems. The comparison conducted by Takeno (2005) clearly demonstrates that even in a simple X-O-H system at room temperature there are often major inconsistencies between databases with respect to possible species and transitions.

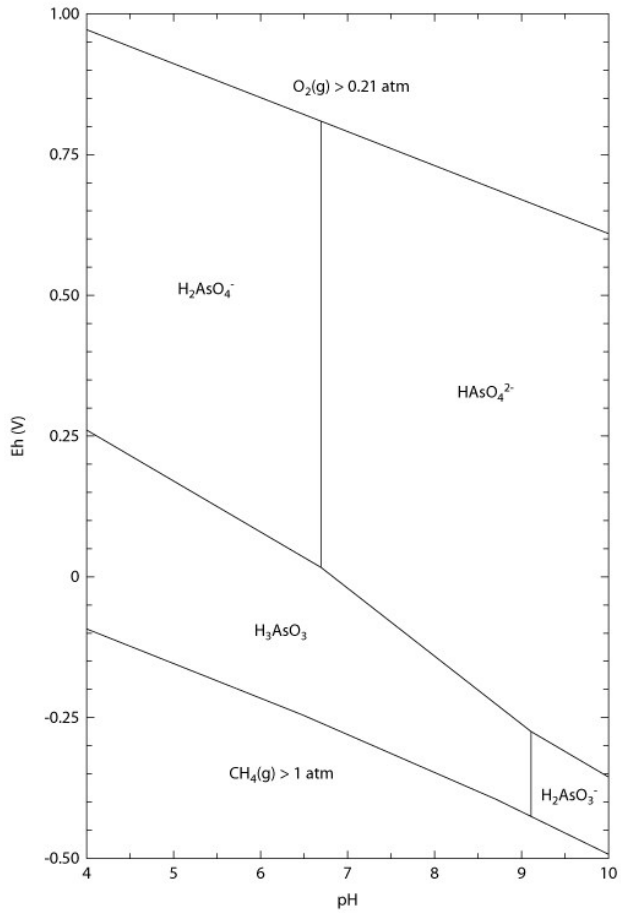

Figure 40: Eh-pH diagram of the system As-O-H. As = 10^{-10}, 298.15K, 10^5 Pa. Constructed using the minteq v4 thermodynamic database (Parkhurst et al., 1999).

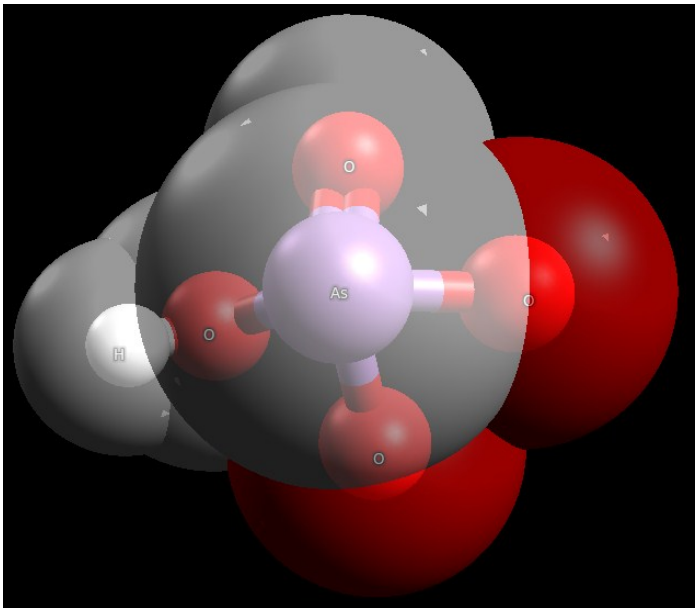

Figure 41: Hydrogen arsenate ($HAsO_4^{2-}$) with partial charge indicated by colour (white = neutral, red = negative). Constructed using Avogadro software.

Kinetic and thermodynamic modelling of soil systems can help to understand arsenic speciation and behaviour in some systems, however, as reaction rates vary between soil systems and are very often microbially mediated the creation of accurate kinetic and thermodynamic models is also very challenging especially in redox oscillating environments such as floodplains.

Direct measurement of some arsenic species is possible by using advanced spectroscopic (synchrotron based e.g. X-ray adsorption spectroscopy (XAS)) or analytical (e.g. high performance liquid chromatography inductively coupled plasma mass spectroscopy (HPLC-ICP-MS)) techniques, although only a limited number of species are routinely measurable and such techniques are costly and complicated, they can offer the best insight into the real state of arsenic in a soil system at any given point in time.

Despite the numerous complications in determining accurate arsenic speciation in soils, the combination of spectroscopic and analytical techniques and simplified thermodynamic and kinetic modelling does allow estimation of arsenic speciation and understanding on a practically useful level of many soil/arsenic interactions, particularly when other redox couples such as sulphate/sulphide and ferric/ferrous iron are also monitored.

Hydrological controls

A soils hydrological regime may effect both the partitioning of arsenic between the solid and aqueous phases and the rate of physical arsenic transport within the aqueous phase.

Pore-water saturation directly affects O_2 concentration within soils as diffusion of oxygen occurs 10^4 times faster in air than in water (Ponnamperuma, 1972). If labile organics are present within the soil matrix the bacterial community will use oxygen during their metabolism – in some cases completely to CO_2 to liberate energy for growth and reproduction. When the bacterial consumption of oxygen exceeds oxygen diffusion into the soil (which is usually the case when pores are saturated with water) the soil will become oxygen depleted causing a drop in Eh. The bacterial community will then be forced to use successively less efficient electron acceptors (Nitrate, Mn(IV), Fe(III), Sulphate) to oxidise organic matter which in turn will cause further Eh drops. This microbial activity and associated changes in Eh can also directly (and indirectly) influence pH, dNOM, CO_2 concentration, mineral stability and hence contaminant mobility, including arsenic.

In saturated soils, water moving through interconnected pores can also carry aqueous arsenic species with the direction of flow. The speed of this water movement is dependent on the hydraulic gradient within the soil and also the soils specific hydraulic conductivity. In this way arsenic may be transported laterally or vertically within soils until such a time that it encounters a suitable mineral surface to which it may bind or until chemical conditions within the soil cause co-precipitation of arsenic within other minerals or precipitation of pure arsenic mineral phases.

In flooded soils, strong reducing conditions dominate, and soluble arsenic increases (Selim et al. 2001). Therefore, flooding of arsenic-rich soils causes flushing; the flood-water flushes out the accumulated arsenic, washing it into surface or groundwaters, or into other soils (Roberts et al., 2010). This process can lead to redistribution of arsenic within soils due to leaching of arsenic from some areas and concentration of arsenic in other areas with a different chemical and mineralogical composition.

Soil Matrix controls

Soil usually consists of a mix of minerals, solid organics, pore-water, gas micro-organisms and plant roots. In addition to the chemical speciation of arsenic, the physical structure and chemical composition of soil can strongly influence arsenic retention and hence distribution.

Physically, particle size and morphology play an important role in arsenic distribution. Soils containing a high proportion of fine particles (e.g. clay rich soils) have a significantly higher surface area and hence reactivity, than soils with a larger particle size; even ignoring the effect of mineralogy changes between particle size classes. Particle morphology is also an important factor controlling arsenic mobility, as grains with pores and pits in their surfaces have been shown to host micro-environments which take longer to equilibrate with pore water conditions than smooth un-pitted grains (Millward and Liu, 2003).

Therefore arsenic is more likely to be immobilised from pore water by fine grained soils and immobilisation and remobilisation of arsenic from soils is likely to occur more slowly in soils containing grains (or aggregates) with surface pores and pits. Particle size distribution also effects hydraulic conductivity as coarse soils are more likely to have larger pores with a higher degree of interconnectivity.

Chemical and mineralogical composition also play important roles in arsenic distribution. Many different minerals can adsorb arsenic to their surfaces either as arsenate, arsenite or organo-arsenic complexes. The most effective natural sorbents of arsenic found in soils include metal oxides and hydroxides (e.g. Goethite - FeOOH, Birnesite - MnO_2), metal carbonates (e.g. Siderite - $FeCO_3$ or Rhodocrosite - $MnCO_3$) and iron sulphides. Therefore iron and manganese concentrations in soils can be good indicators of arsenic concentration. Mechanistically this is due to "trapping" of aqueous arsenic from pore-water, transported from other areas. Other arsenic sorbents in soils include clay minerals (where arsenic typically binds to $AlOH^{2+}$ "edge" sites rather than plate surfaces) and, under strongly alkaline soil conditions calcite.

Soils which contain large proportions of quartz or feldspar (typically sand size particles) tend to contain less arsenic due to their low surface reactivity and also the typical size and hence surface area of these minerals.

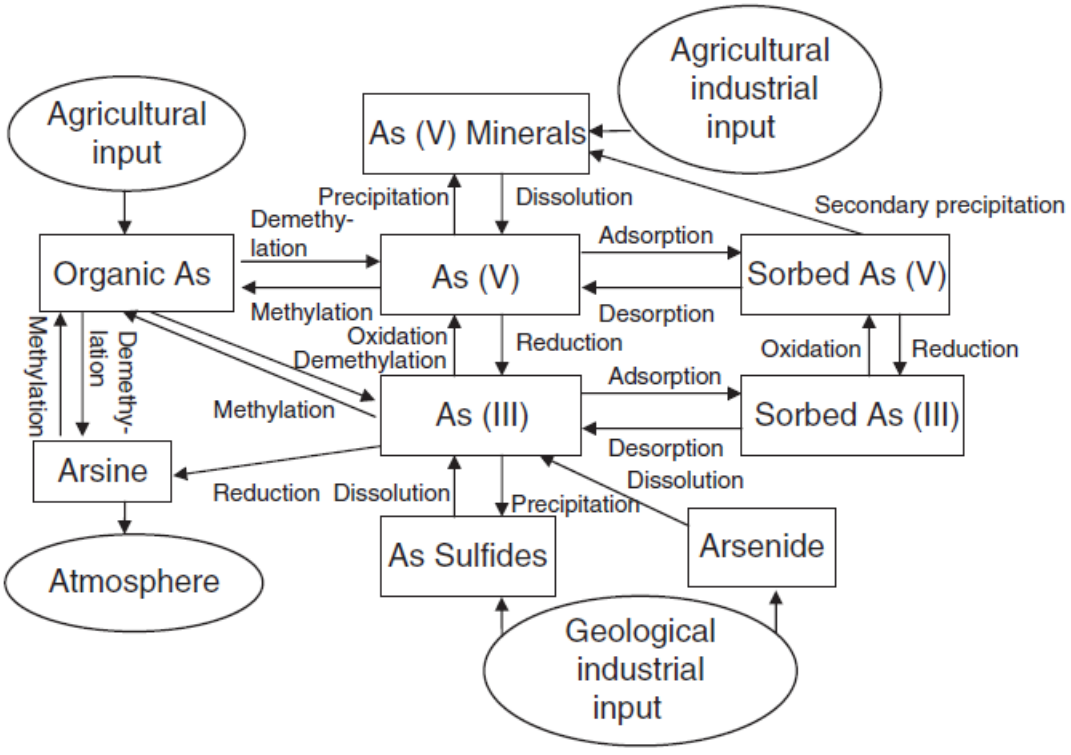

Figure 42: Global cycle of arsenic including key speciation changes. Reproduced from Zhang and Selim (2008)

Other chemical composition controls include ionic strength of the pore water and concentration of compounds which compete with arsenic for positively charged mineral surface sites. The most common ligands competing with arsenic for sorption sites in soils are dissolved organics (Wang and Mulligan, 2006a), phosphates (Livesey and Huang, 1981; Violante and Pigna, 2002) and carbonates (Appelo et al., 2002). In soils with higher concentrations of these competing ligands, positively charged sorption sites on mineral surfaces and more likely to be limiting and arsenic is more likely to be forced into pore-water by competitive sorption.

Anthropogenic influence on release of arsenic from soils

Release of arsenic from the soil solid phase to pore-water, increasing its mobility and its probability of entering the human food chain (in drinking water or crops) can occur for a number of reasons, however, these are dominated by desorption and dissolution processes.

Desorption from mineral surfaces can occur due to oxidation state change of the surface bound arsenic (Eh dominated), protonation state change of the surface bound arsenic (pH dominated), a change of ionic strength in the pore-water or changes in concentrations of other compounds competing for sorption sites.

Dissolution of arsenic immobilizing minerals can occur due to pH changes (FeOOH to $Fe(OH)^{2+}$)(pH dominated) or Eh changes (e.g. oxidative dissolution of iron sulphides or reductive dissolution of reductive dissolution of iron oxides).

Practically these changes in soil chemistry can be caused or influenced by a variety of human activities.

Soil acidification

Some human activities directly affect soil pH. Soil acidification (in the form of excessive nitrogen addition or via acid mine drainage) or soil liming (application of $CaCO_3$ to counter soil acidification and raise pH) can affect arsenic mobility as pH is a major controlling factor in many arsenic release processes. A rise or fall in pH could increase or decrease the mobility of arsenic dependent on mineralogy and original pH. Solution pH controls two fundamental factors: mineral surface potential and arsenic speciation, which in turn impacts arsenic adsorption on mineral surfaces (Zhang and Selim, 2008). For example, the soil clay fraction is negatively charged at neutral-alkaline pH and hence does not act as a sorbent for arsenic, however at lower pH and in the presence of $AlOH^{2+}$ edges, clays become suitable sites for adsorption. Desorption of arsenic from clay minerals is also significantly influenced by the aging process (Sadiq, 1997; Lin and Puls, 2000; Goldberg, 2002). In this example an increase in pH from acidic to circumneutral could result in the release of arsenate sorbed to $AlOH^{2+}$ edge sites. Alternatively if arsenic is bound within FeOOH minerals or sorbed strongly to their surfaces a drop in pH could cause the dissolution of FeOOH to $Fe(OH)^{2+}$ and the release of arsenic into solution.

Soil redox-conditions and flooding

Soil Eh may also be substantially altered due to human activities. For example, ploughing of soil leads to an immediate increase in soil porosity (Nicou, 1986). Conversely intensive agriculture with heavy machinery can lead to destruction of soil porosity through soil compaction (Hamza and Anderson, 2005). Changes to soil porosity restricts or enhances diffusive pathways for CO_2 output and O_2 input in soils and results in more reducing or more oxidising top-soil conditions (Lipiec and Hatano, 2003).

Climate change also has potentially drastic implications for soil chemistry and hence contaminant mobility. Whilst current climate predictions indicate increased evapotranspiration and greater precipitation globally, equatorial regions are predicted to become drier while temperate regions (including most of Europe) will become wetter and subject to more frequent and more intense precipitation (EEA-EC-JRC and UN-WHO,

2008). Predicted changes in precipitation volume, frequency and intensity are also likely to cause major changes to a soils hydraulic regime and hence to soil chemistry. In addition to changing soil hydraulic conditions due to increasing pluvial input, natural fluvial flooding of top-soils is also expected to increase, particularly in winter and spring (EEA-EC-JRC and UN-WHO, 2008). Controlled flooding of previously un-flooded soils in attempts to divert excess fluvial input away from highly populated or economically important areas is likely. If soils which have remained historically oxic and have been gradually accumulating arsenic due to atmospheric deposition of industrial contamination become flooded, the onset of reducing conditions could cause major release events similar to those observed by Burton et al., (2008) in Australia due to the adoption of wetland reclamation initiatives.

Increasing temperature

Since pre-industrial times Europe has experienced temperature increases averaging 1.2^{o}C, 0.2^{o}C higher than global averages (EEA-EC-JRC and UN-WHO, 2008). This trend is of increasing temperatures is predicted to continue in the near future. Temperature has also been shown to affect the rate of arsenic releases as microbial metabolism and chemical kinetics are accelerated at higher temperatures. Several studies have observed seasonal trends in dissolved arsenic concentrations in rivers (McLaren and Kim, 1995; La Force et al., 2000; Masson et al., 2007). High levels of dissolved arsenic are typically seen in the spring and summer months, where temperatures are high and dissolved oxygen levels are low. Dilution of the arsenic inputs during the higher flows of the winter months cannot entirely explain the patterns observed (Aggett and O'Brien, 1985; Masson et al., 2007). Two recent studies have investigated the possible effects of temperature on arsenic release (Joubert et al., 2007; Weber et al., 2010). They both found that increased temperatures (from 4 to 37^{o}C and 5 to 23 ^{o}C) were linked to increased microbial activity and the release of arsenic.

Agricultural amendments

Agricultural amendments of various types can also cause an increase in arsenic mobility. In addition to liming which directly affects pH, treatment of soils with phosphate containing fertilizers or the addition of organic matter can increase competing ligands in pore water and result in arsenic release due to competitive sorption. Organic amendments such as manure may also stimulate microbial activity inducing Eh decrease and potential reductive dissolution of metal hydroxides.

Chapter 3: Quantitative use of FP-XRF for trace analysis of As in Soils: Considerations for sample preparation and analytical validation

Abstract

Recent technological improvements to batteries, excitation sources, detectors and microprocessors have led to the adoption of field portable energy dispersive X-ray fluorescence (FP-ED-XRF or pXRF) by numerous governmental agencies, environmental consultancies and research institutions as a fast, cost effective analytical technique for *in-situ* multi-elemental analysis in soils. Many FP-XRF units, such as the Niton XLt series, include analysis modes specifically designed for analysis of trace elements in soils and sediments. These devices allow almost point and shoot ease of use, and can offer results comparable to those of laboratory based instruments. Nevertheless, FP-XRF analysis is sensitive to spectral interferences as well as sometimes important physical and chemical matrix effects. In this study we demonstrate, through the analysis of As in a floodplain soil in eastern France with a X-ray tube based FP-XRF analyser, the extent to which sample treatment and instrumental conditions can affect the precision and accuracy of quantitative results at trace concentrations and propose practical strategies which can be implemented to minimise sources of error and maximise data precision and accuracy. The results show that the effect of soil pore water has been underestimated in previous studies and that even, in relatively dry soils, can dramatically affect analytical performance. We also highlight the importance of adapting validation methods to the composition of the measured soil in order to ensure accurate correction of field values.

Introduction

XRF spectrometry is based upon the principal that inner orbital electrons maybe excited and ejected from their orbital by an incident photon with energy greater than their binding energy. Upon ejection an electron from an outer orbital will drop to the vacant position in the inner orbital and in doing so release a photon of characteristic energy, determined by the orbital transition (e.g. L to K / Kα) and atomic number (Figures 43 & 44). The number of photons generated at a given energy may be used to determine the concentration of a particular element in the sample (Jenkins, 1995).

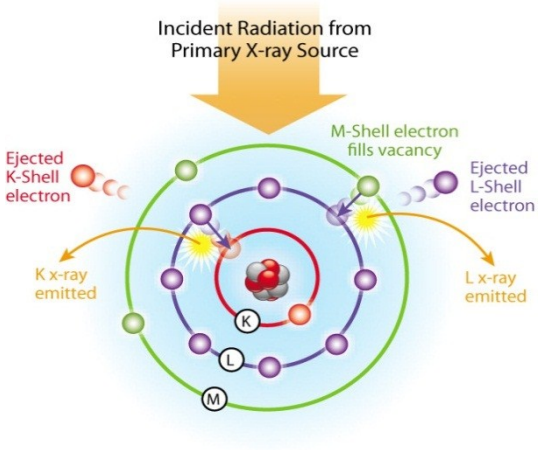

Figure 43: Illustration of the mechanism of X-ray fluorescence. Reproduced from Thermo Scientific (2011)

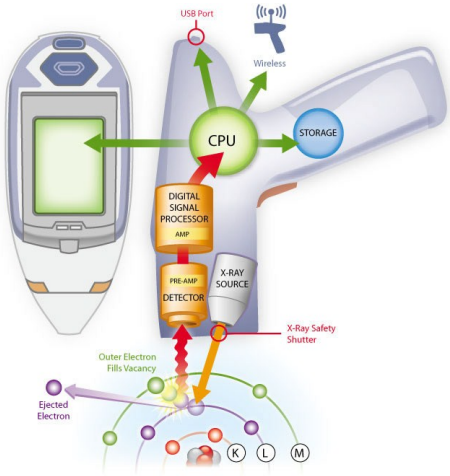

Figure 44: Illustration of the functional parts of a FP-XRF spectrometer. Reproduced from Thermo Scientific (2011)

Laboratory based energy dispersive (ED) and wavelength dispersive (WD) XRF spectrometry has for several decades been an accepted and widely used method for multi-elemental analysis in fields such as geochemistry, forensic science and archaeology (Gill, 1997; Langford, 2005; Shackley, 2011).

XRF spectrometry has several key advantages when compared to other commonly used laboratory techniques such as inductively coupled plasma mass spectrometry (ICP-MS) or atomic absorption spectroscopy (AAS) including: the limited preparation of solid samples, possibility of simultaneous multi-elemental analysis, sample preservation (XRF analysis is non-destructive), decreased total analysis time and a decrease in the production of hazardous wastes. FP-XRF retains many of these advantages while additionally reducing analysis time and laboratory costs by completing analysis in-situ as well as representing significantly reduced initial and running costs compared to ICP systems. Rapid in-situ analysis also allows for elemental mapping in order to determine samples of interest for further laboratory based analysis.

Although the first generation of commercial FP-XRF devices appeared as early as the 1940s (Abbott, 1948) improvements in technology including the miniaturisation and increased efficiency of detectors and microprocessors coupled with the availability of efficient radio isotope excitation sources (e.g. Cd^{109}, Am^{241}, Co^{57} and Fe^{55}) facilitated the widespread adoption of these devices as viable field analytical tools in the 1990s. Since that time FP-XRF usage has been steadily growing. This growth can be attributed to a number of factors including: reducing equipment cost, increasing detector sensitivity, broadening elemental range, increasing ease of use and most significantly, the advent of commercially available miniature X-ray tube excitation sources in 2002 (Mercuro, 2010) which negated the need to carry radioactive sources. Whilst FP-XRF devices are often seen as qualitative screening tools, numerous studies have demonstrated their semi-quantitative and quantitative ex-situ use in soils and sediments for a range of different elements(Bernick et al., 1995; Kilbride et al., 2006; Jang, 2010).

In this study we demonstrate the quantitative *in-situ* analysis of trace As concentrations in soils on the floodplain of the Saône in eastern France and highlight factors which affect, and ways to maximise, the quality (precision and accuracy) of final results compared to quality criteria outlined by the US-EPA (US-EPA, 1998). We attempt to quantify the main sources of error during sample preparation, measurement and validation of results which should be considered prior to FP-XRF analysis, and propose practical methods to ensure high quality, quantitative *in-situ* data.

We investigate and discuss the effect of (1) sample parameters including water content, particle size, chemical composition and bulk sample size, (2) instrumental parameters including internal and external filter use, calibration methods and analysis time (3) validation using ICP-MS, interferences and matrix effects on the quality of final results.

Methods

FP-XRF instrumentation:

A NITON® XLt™, 700 Series™ FP-XRF environmental analyser (Thermo-scientific Europe, Munich, Germany) equipped with a miniature 1.0 W X-ray tube 40 kV / 50 µA excitation source, an Ag anode target and a high performance peltier cooled solid state Si-PiN X-ray detector with a resolution of approximately 220 eV at the Mn Kα (Thermo Scientific, 2011) was used for data acquisition during this study. Photon counts from the detector are amplified, digitised and processed internally by a multi-channel analyser and concentrations are displayed in ppm on the integrated touch screen. This instrument is capable of analysing elements in the z range of 19 (K) to 92 (U) by using K and L shell emission lines and is equipped

with 2 modes which use primary/source filters named only filter 1 and filter 2 to increase sensitivity to particular analytes. These filters can be enabled via the on-screen menu. Selection of either of these filters also automatically adjusts the voltage of the X-ray tube. Filter mode 1 corresponds to a molybdenum source filter and an X-ray tube voltage of 40 kV which is used for quantification of elements with $z \geq 25$. Filter mode 2 corresponds to a copper source filter and an X-ray tube voltage of 25 kV which is used for quantification of lighter elements ($19 \leq z < 25$). The unit features a variety of modes designed for lead based paint, alloys, thin samples e.g. dust wipes, bulk samples e.g. soils as well as user definable modes. The "bulk standard soil" mode was used throughout this study. This mode assumes that the sample is sufficiently thick and dense that the critical saturation mass is exceeded and therefore that any increase in sample thickness would not lead to an increase in measured photons at the detector. Quantification of analyte concentration is achieved based on the ratio of characteristic fluorescence to the intensity of the Compton (inelastic) scattering peak. This quantification method is preferred when a heavy analyte is present at sub % concentrations in a light matrix but is sensitive to differences in the mass attenuation coefficient between the measured and calibration samples (Jenkins, 1995). Using this mode no user calibration is required as Niton pre-calibrates all units using a selection of standard soil samples, however for the highest data quality site specific standards may be used to perform an empirical calibration prior to a survey.

Field site and soil sampling:

A total of 10 soils were analysed in-situ and then sampled from within a 60 km^2 area between the towns of Pont-de-Vaux and Saint-Didier-Sur-Chalaronne on the east side of the floodplain of the Saône in eastern France. Sediments on the alluvial plain of the Saône are known to host elevated concentrations of arsenic (up to 37 mg kg^{-1} measured during this study) although the origin of this contamination is undetermined (Comite Syndical de l'EPTB, 2007). Following in-situ XRF analysis, soils were sampled using acid washed (5% HNO_3) plastic tools and transferred to double sealed low density polyethylene (LDPE) bags for transport. Samples were stored in cool dark conditions prior to laboratory analysis.

Soil properties:

Prior to laboratory based XRF and ICP-MS analysis, soils were characterised by a combination of granulometric, X-ray diffraction (XRD), total organic carbon (TOC) and total carbonate (TCO_3) analyses.

Soil granulometry was determined by a combination of dry sieving (> 1< 2mm fraction) and laser diffraction (< 1mm fraction). Laser diffraction analyses were performed with a Malvern Mastersizer 2000 particle size analyser (Malvern Instruments, France) across a measurement range of 0.01 to 1500 µm. Lyophilised soils were suspended in water, and subjected to an ultra-sonification step prior to analysis to ensure correct sample dispersion and analysis of elemental particles only rather than aggregates. Distributions were calculated as sample percentage by volume falling into 100 equivalent spherical diameter class sizes. Granulometric analysis revealed that the sampled soils were dominated by clay to medium sand sized particles (< 500 µm fraction), although significant variation in particle size distribution (PSD) within this fraction was present between samples.

Mineralogy of the < 2mm fraction of a representative soil sample was determined by powder XRD analysis using a Bruker D5000 (Bruker Corporation, AXS, France) with a $CuK_{\alpha}1$ source over a range of 2°2θ – 80°2θ with a step size of 0.05°2θ and a counting time of 1 second. The instrument is equipped with a Göbel mirror and the spectra were acquired using Soller slits on both the X-ray tube and the detector. Diffraction patterns reveal the presence of Quartz (SiO_2), Calcite ($CaCO_3$), Illite $K(Al,Fe)_2(Si,Al)_4O_{10}OH_2$ and Chlorite $(Fe,Mg,Al)_6(Si, Al)_4O_{10}(OH)_8$ suggesting a typical light soil matrix.

Measurement methods by FP-XRF:

Three Niton recommended soil measurement methods, in and ex-situ, were compared to ICP-MS analysis for precision and accuracy; (1) in-situ measurement with minimal preparation, (2) ex-situ measurement with minimal preparation in LDPE bags and (3) ex-situ analysis with thorough sample preparation in polyethylene terephthalate (Mylar®) covered XRF analysis cups. A summary of these methods is provided in Table 10. The FP-XRF detector was re-calibrated after every 5 samples or 2 hours using internal standards for all preparation methods, detector resolution remained between 200 and 220 eV at the Mn Kα line throughout analysis.

Table 10: Summary of investigated preparation and analysis methods.

Method	Count time (Filter 1/Filter 2)	Preparation	Supplementary Equipment used during analysis
In-situ – field preparation	100/1-20	Homogenization of 2250cm^3 soil volume, sieving (< 2mm), and compaction.	Niton soil testing guard accessory
Ex-situ – LDPE bags	100/20	Homogenization of 2250cm^3 soil volume, sieving (< 2mm) and analysis ex-situ in 50 µm thick LDPE bags.	Niton soil testing guard accessory and LDPE bags.
Ex-situ - in XRF cups	100/20	Homogenization of 2250cm^3 soil volume, sieving (< 2mm), lyophilisation, grinding to < 63 µm, compaction and surface preparation in Mylar® covered XRF cup.	Niton Environmental Test Platform, open cell cups, 6 µm Mylar® film.

In-situ soil preparation and measurement:

For in-situ analysis, soils were prepared in the field with a method modified from US-EPA 6200 (Sackett and Bedford, 1998). At each sample location a 15 by 15 cm square of soil was homogenized to a depth of 10cm using acid washed plastic tools in accordance with established soil sampling guidelines (U.S. EPA Environmental Response Team, 2000). This soil was dry sieved to remove all particles with a size greater than 2mm and hardened aggregates were broken using an agate pestle and mortar. The soil dried substantially during the sieving process (air temperature of > 35^{o}C with low humidity) and aggregate crushing process. The < 2mm soil fraction was then replaced in the 15 by 15 cm sampling square, compacted and analysed twice for a period of 100 seconds using filter mode 1 and 20 seconds for filter mode 2. The 'soil testing guard'(STG) accessory provided by Niton was used for all analysis to protect the XRF window and ensure that the obligatory proximity button remained depressed for the duration of analysis. The position and orientation of the FP-XRF was changed between the 2 measurements in an attempt to lessen the effect of inaccuracies due to large particle size combined with a small analysis area ~2cm^2 which are inherent to in-situ analysis with a field portable device. All samples were analysed within a period of 5 days during August 2009 during which there were no significant changes in soil conditions.

Ex-situ measurement in LDPE sampling bags:

Ex-situ in-bag analysis was conducted on field sampled soils in the laboratory through 50 µm LDPE sampling bags (Fischer scientific, France). A soil thickness of at least 3cm was maintained during analysis and use of

the STG was necessary to ensure pressure on the proximity button. Bagged soils were analysed three times for a period of 100 seconds using filter mode 1 and 20 seconds using filter mode 2.

Ex situ thorough preparation and analysis using powder sample cups:

Ex-situ analysis was also conducted on prepared field sampled soils. Soils were first homogenized and sub-sampled (100g) by quartering (Raab et al., 1991). Sub-sampled soils were lyophilised and ground in an agate ball mill to a particle size of < 63µm. At least 5 grams of ground and lyophilised soil was used to fill plastic XRF cups (Figure 45) which were then sealed with 6 µm Mylar® film and analysed using the NETP (a shielded holder used to support the instrument and sample during laboratory based analysis). Samples were analysed three times for a period of 100 seconds using filter mode 1 and 20 seconds using filter mode 2.

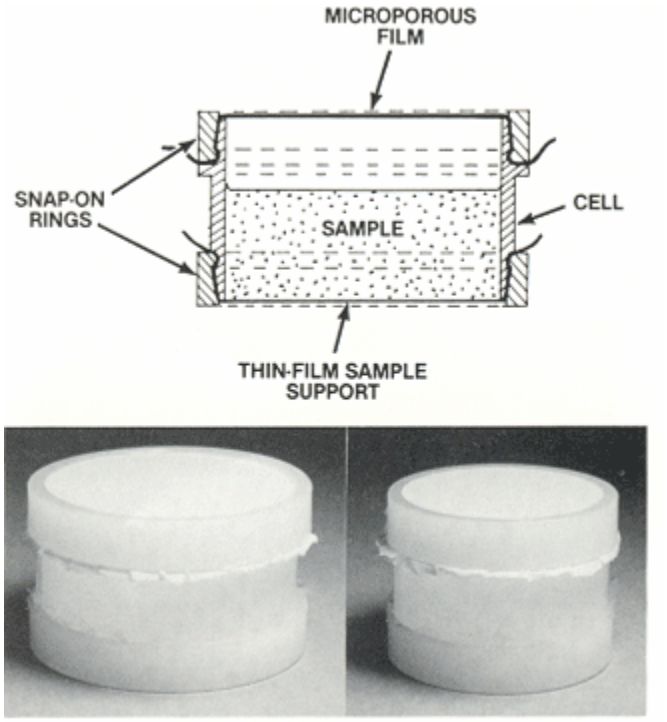

Figure 45: Diagram and photos of open cell XRF cups used for Ex-situ analysis. Re-produced from Solazzi, (1984).

Effect of soil moisture:

Two types of water may be present in soils; interstitial water which occurs in the pore spaces between soil structural components and water trapped during formation of constituent minerals (fluid inclusions). Constitutive water of nominally hydrous minerals is considered to be constant for the purposes of this study and its effects ignored. Interstitial water is however highly variable in soils, both spatially and temporally and has been identified as a cause of error during FP-XRF analysis (Kalnicky et al., 1992; Kalnicky and Singhvi, 2001). The replacement of air with water in pore-spaces increases photoelectric absorption in addition to Rayleigh and Compton scattering. These effects are summarised by mass attenuation coefficients which are slightly higher for water than air. In addition to this, an increase in pore saturation will increase the density of the sample significantly (pure water is approximately 840 times denser than air at 25^{o}C (Lide, 2009)) and so increase these 3 effects. The ultimate effect of these processes is a raise in baseline values and a lowering in emission peaks leading to an overall loss of accuracy, higher limits of detection and reduction in apparent concentration.

To quantify the total effect of soil moisture on concentrations recorded by FP-XRF cups 18.2 mΩ water was added to one representative soil (lyophilised and ground) at 0, 1, 5, 10, 20, 30 and 50 wt%. Each cup was measured 5 times for 300 seconds with each filter mode.

Effect of analysis time

To establish the effect of analysis time on precision and accuracy one XRF cup sample was measured 5 times for 50, 75, 100, 150, 175, 200, 250, 300 and 500 seconds using only filter mode 1.

Effect of sample size/Critical penetration depth in soils

Although previous studies suggest that X-ray penetration from FP-XRF units is limited to approximately 2mm (Kalnicky and Singhvi, 2001) Niton recommends that at least 5 grams of sample be used to fill cups during ex-situ analysis to ensure that critical sample mass is exceeded, an assumption required for quantification. This equates to a depth of between 4 and 6 mm in 32mm diameter sample cups assuming a soil bulk density of between 1.1 and 1.6 g/cm^3 (Hillel, 1980). Therefore, either the Niton recommendation of 5 grams is highly conservative or X-ray penetration maybe greater than 2mm in soils for some elements. To determine the critical penetration depth in soils empirically, a range of cups were prepared with varying dry soil mass. Four cups filled with different quantities of the same lyophilised and ground soil (0.61, 1.01, 2.8 and 5 grams, equivalent to depths of 0.7, 1.1, 3.2 and 5.7 mm assuming a bulk soil density of 1.1 g/cm^3) were analysed 8 times each for a period of 300 seconds over the full analysis range of the unit.

Cross-validation procedure

Total microwave digestion (1: HNO_3 + HF + H_2O_2, 2: H_3BO_3 + HF) was performed on all lyophilised and ground soils following a modification of US-EPA method 3052 (U.S. EPA, 1996). This method was used to ensure that all mineral soil components were digested including silicate phases which are included in XRF analysis but commonly ignored during acid digestion of soil samples for ICP analysis (Kilbride et al., 2006).

A quadrupole-based ICP-MS system (Agilent 7500c, Agilent Technologies, Tokyo, Japan) equipped with an octapole collision-reaction cell was used as the reference technique for As determination in the soils. The measurements were performed using a mixed helium (0.5 ml/min) and hydrogen (3.0 ml/min) pressurized collision cell with an octopole potential of -14 V and a quadrupole potential of -13 V. The ICP-MS was optimized daily using a tuning solution for highest sensitivity and lowest CeO/Ce ratios (~1%). The plasma was operated at 1500 W with 15 mL min^{-1} plasma gas and 1.0 mL min^{-1} aerosol carrier gas. Matrix-matched standards were used for quantification purposes. Ethanol (3%, Sigma-Aldrich) was added to standards and sample aliquots to increase the As sensitivity, decrease interferences and buffer the effect of carbon present in the samples. Rhodium (~15 µg/L in nitric acid, Sigma-Aldrich) was added as internal standard. Data acquisition was performed in peak-hopping mode with 3 points per peak, 1s dwell time and 4 replicates.

Results & Discussion

Effect of Instrumental parameters:

Comparison of measurement modes:

Quantification of elements $z \geq 25$ (Mn and above) is achieved in filter mode 1 using a Mo source filter and an X-ray tube voltage of 40 kV. This mode is most effective within the Kα emission energy ranges of Mn to Sr ($25 < z < 38$) and Ag to Sb ($47 < z < 51$) as analytes with emission lines between 15 and 20 KeV may be obscured by the presence of strong scattering peaks from the filter (Figure 46). Above this range

Bremsstrahlung/continuum scatter may obscure fluorescence peaks (Figure 46). This effective analysis range is ideal for quantification of arsenic.

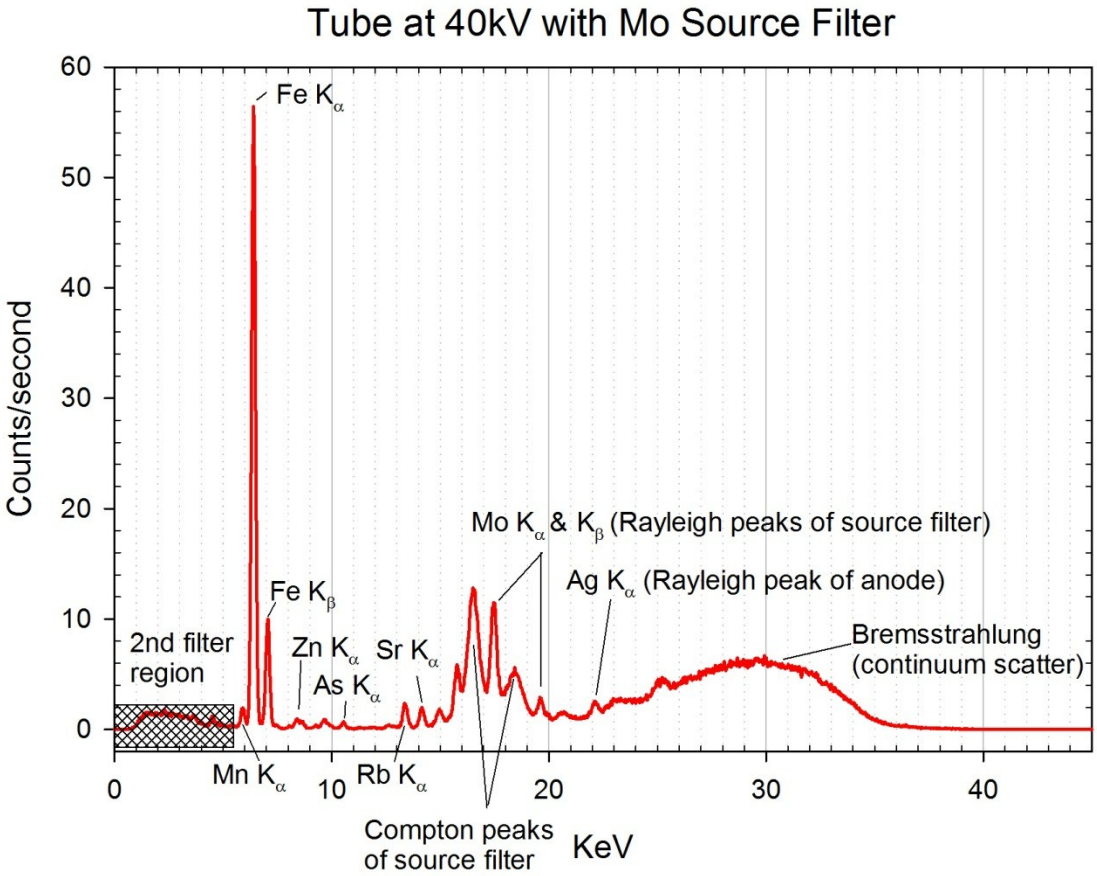

Figure 46: Example soil XRF spectra obtained using filter mode 1 highlighting quantification range, Rayleigh, Compton and Continuum scatter peaks.

Quantification of lighter elements ($19 \leq z < 25$) is achieved in filter mode 2 using a Cu source filter and an X-ray tube voltage of 20 kV (Figure 47). Elements lighter than potassium cannot be quantified due to the absorption of characteristic X-rays by air between the sample and detector and elements heavier than Chromium are better quantified in filter mode 1.

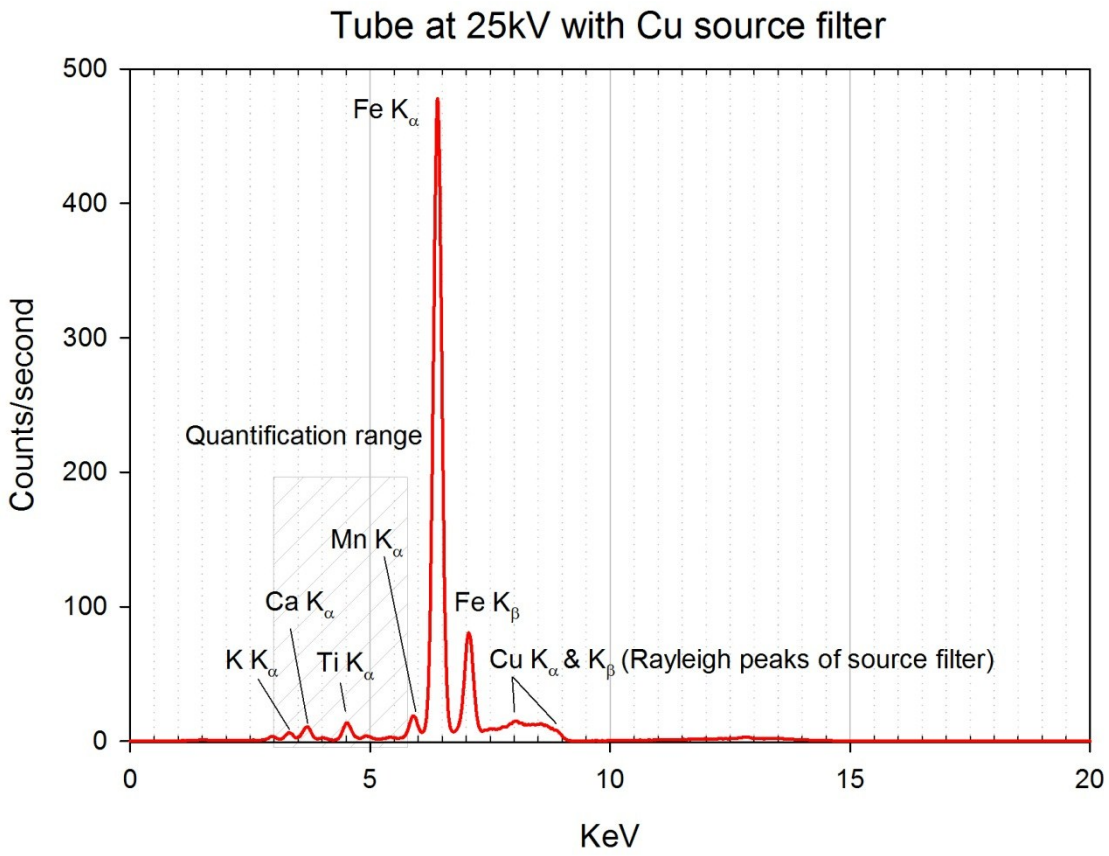

Figure 47: Example soil XRF spectra obtained using filter mode 2 highlighting quantification range and Rayleigh scatter peaks.

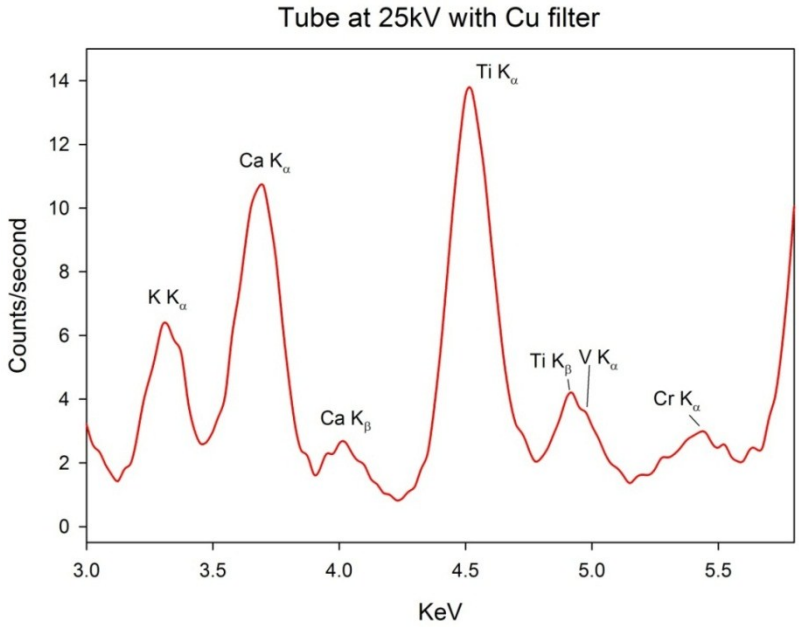

Figure 48: Region of the X-ray fluorescence spectrum recorded with filter mode 2 which is used for quantification.

Effect of external filters:

Several different external filters may be present during FP-XRF analysis. Between the source and the sample there is always a Polyimide (Kapton®) window which protects the source and detector. This window is in place during factory calibration of the Niton XLt series and therefore any attenuating properties are already considered during quantification of sample concentrations. However, the use of additional filters such as the Kapton® window on the STG, the Mylar® film used on XRF cups and the measurement of soils through LDPE bags may act to attenuate and scatter incident and emitted radiation.

Fortunately as the X-ray properties of Kapton®, Mylar® and LDPE are well known (Henke et al., 1993) and the filters are of known thickness, corrections for absorbance can be easily applied to measured data assuming that the analyte is above the limit of quantification despite attenuation (e.g. Equations 1 and 2 for Mylar® (Dick et al., 1977)).

Equation 7 $I_{corr} = I_m \exp(k_{mylar} x)$, where I_{corr} is the corrected intensity, I_m is the measured intensity x is the film thickness and k_{mylar} is the absorption coefficient of Mylar® film at a particular wavelength, given by:

Equation 8 $k_{mylar} = 13.5\lambda^{2.80}$, where λ is the wavelength of the analyte emission line.

Alternatively automated web-based and traditional software tools are available to perform calculations of X-ray transmission through various filter materials over a wide range of photon energies (Henke et al., 2011; Webb, 2011).

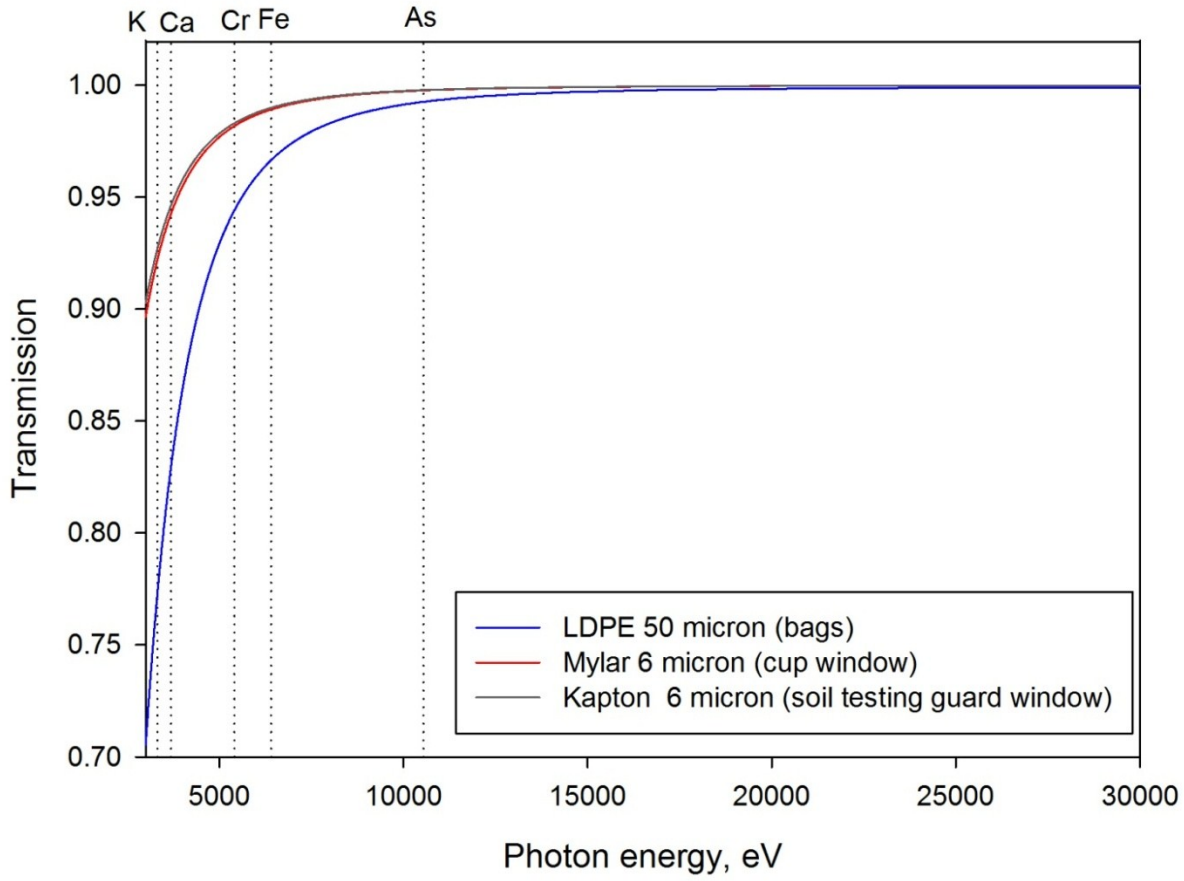

Figure 49: X-ray transmission through external filter materials (LDPE, Mylar and Kapton®). Calculated using web-based software by (Henke et al., 2011). Vertical guides correspond to K alpha emission lines for the labelled elements.

As can be seen in Figure 49 and Table 11, absorbance of X-rays with lower energies is greater than for higher energy X-rays. Therefore, lighter elements such as K and Ca are more susceptible to attenuation by analysis in Mylar® covered XRF cups or LDPE bags. It is clear however that the thin Kapton® and Mylar® windows used in XRF cups and the Niton Soil Testing Guard allow significantly more transmission of low energy X-rays than 50 micron LDPE bags. For arsenic, attenuation of K alpha emitted radiation is less that 1% for all filters and therefore analysis in bags, cups or with the soil guard may be appropriate without further correction. However, for potassium up to 27% of K alpha emitted radiation maybe attenuated by the use of LDPE bags and therefore either external filters should be avoided or measured values should be corrected.

Table 11: Percentage X-ray transmission through external filter materials at K alpha emission energies for various elements.

Element	K alpha emission (eV)	LDPE: 50 micron	Mylar®: 6 micron	Kapton®: 6 micron
K	3314	73.07%	90.63%	91.20%
Ca	3691	83.14%	94.32%	94.69%
Cr	5414	94.47%	98.20%	98.32%
Fe	6404	96.65%	98.91%	98.99%
As	10544	99.26%	99.77%	99.78%

Analysis time

Increasing analysis time should lead to lower limits of detection (LOD) and an exponential decrease in relative standard deviation (RSD) between replicates as:

Equation 9: $$RSD = \left(\frac{1}{\sqrt{Number\ of\ counts}}\right) \times 100$$ (Beckhoff, 2006)

During a field sampling and analysis campaign precision and analysis time are often equally important. As %RSD diminishes exponentially with analysis time (Equation 9) extended periods of analysis may not result in significant improvements in precision as other factors such as sample homogeneity may become limiting. Our experimental data (Figure 50) shows that optimal analysis time was strongly dependant on the element investigated and the concentration present, this is logical as the number of measured counts depends both of concentration and the fluorescent yield of the target analyte. For zinc at approximately 100 mg/kg no significant improvement in precision was observed even after 50 seconds of analysis, for arsenic at low concentrations (< 30 mg/kg) no significant improvements in precision were observed when analysing for periods of longer than 100 seconds while for manganese at 500 mg/kg no improvements in precision were observed after 300 seconds. Previous research suggests that a suitable analysis time to optimise precision is 120 seconds (Kilbride et al., 2006). However, our experimental results show that different analytes achieved quality thresholds at different count times, consistent with varying fluorescent yield and concentration. Therefore we conclude that it is essential to conduct preliminary tests on a range of site specific samples to determine appropriate analysis time especially if the objective of the survey is to meet quality criteria (for example US-EPA Q1, Q2 or Q3 levels). In this example Q3 level or "definitive" precision (<10% RSD) was achieved consistently for Fe and Zn after just 50 seconds and for Mn after 150 seconds. Arsenic quantification did not achieve Q3 level precision even after analysis for 500 seconds, however Q2 "quantitative screening" precision (< 20% RSD) was achieved for periods of analysis of 100 seconds or greater (Figure 50).

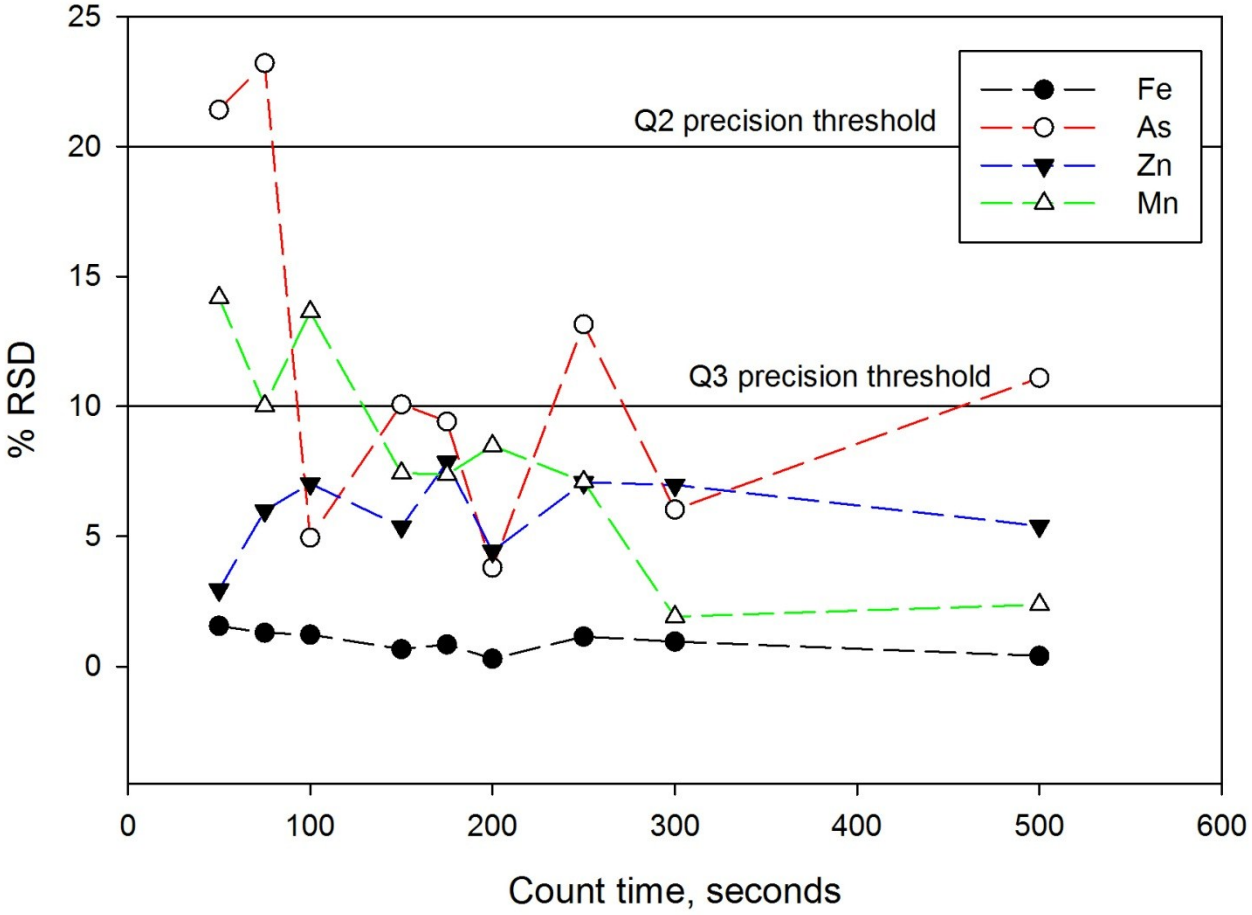

Figure 50: Count time compared to %RSD for Fe, As, Zn and Mn (5 replicates at each count time), illustrating US-EPA quality criteria (Q2 < 20% RSD, Q3 < 10% RSD).

Sample parameters:

Water content:

Previous work suggests that soil moisture does not have a significant impact on the accuracy of FP-XRF analysis until a threshold value of 20% moisture content is reached and that errors resulting from soil moisture below this threshold are minor (Kalnicky et al., 1992). This 20% threshold has been approved and reproduced in many official protocols since its original publication e.g. Sackett and Bedford (1998). However, during this study 20% soil moisture resulted in a decrease in recorded concentration of up to 42.7% (Mn) compared to the same dry sample (Figure 51) which is evidently not a minor error.

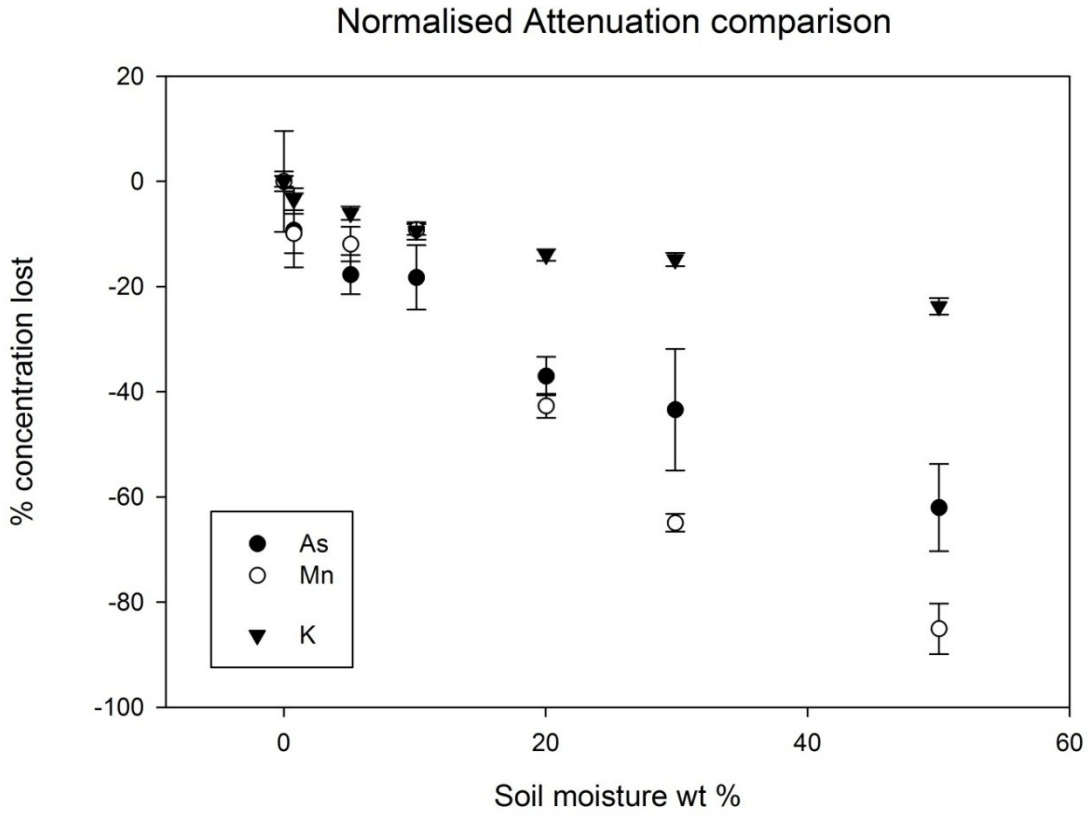

Figure 51: Normalised attenuation of measured concentrations of various elements due to the presence of soil moisture.

Increasing water content resulted in an exponential decrease in recorded concentrations for all elements investigated up to a maximum of 50wt% water. Whilst the water content of most soils is significantly less than 50wt% this serves as a useful theoretical maximum for high porosity aggregated clay rich soils in saturated conditions (Appelo, 2005). The exponential decrease of recorded concentrations follows closely the Beer-Lambert law (Equation 3) which governs the transmission of electromagnetic radiation (e.g. X-rays) through a material:

$$I = I_0 e^{-\alpha x}$$

Equation 10: Beer-Lambert law.

where I is the intensity of the transmitted radiation, I_0 is the incident intensity, alpha is the linear attenuation coefficient of the material and x is the path length.

I_0 (source intensity) remained equal during soil moisture experiments but I (peak height and recorded concentration) changed as a result of pores filling with a denser material with a higher attenuation coefficient. Path length, x, can be substituted with soil moisture wt % as increasing water content will cause a greater proportion of the path length in the soil matrix to be saturated. An excellent fit with an equation of the form of equation 4 was found between recorded concentrations for all elements and water content. Values for factors a and b are tabulated in Table 12.

$$y = ae^{-bx}$$

Equation 11: 2 parameter exponential decay function used to fit concentration/soil moisture data.

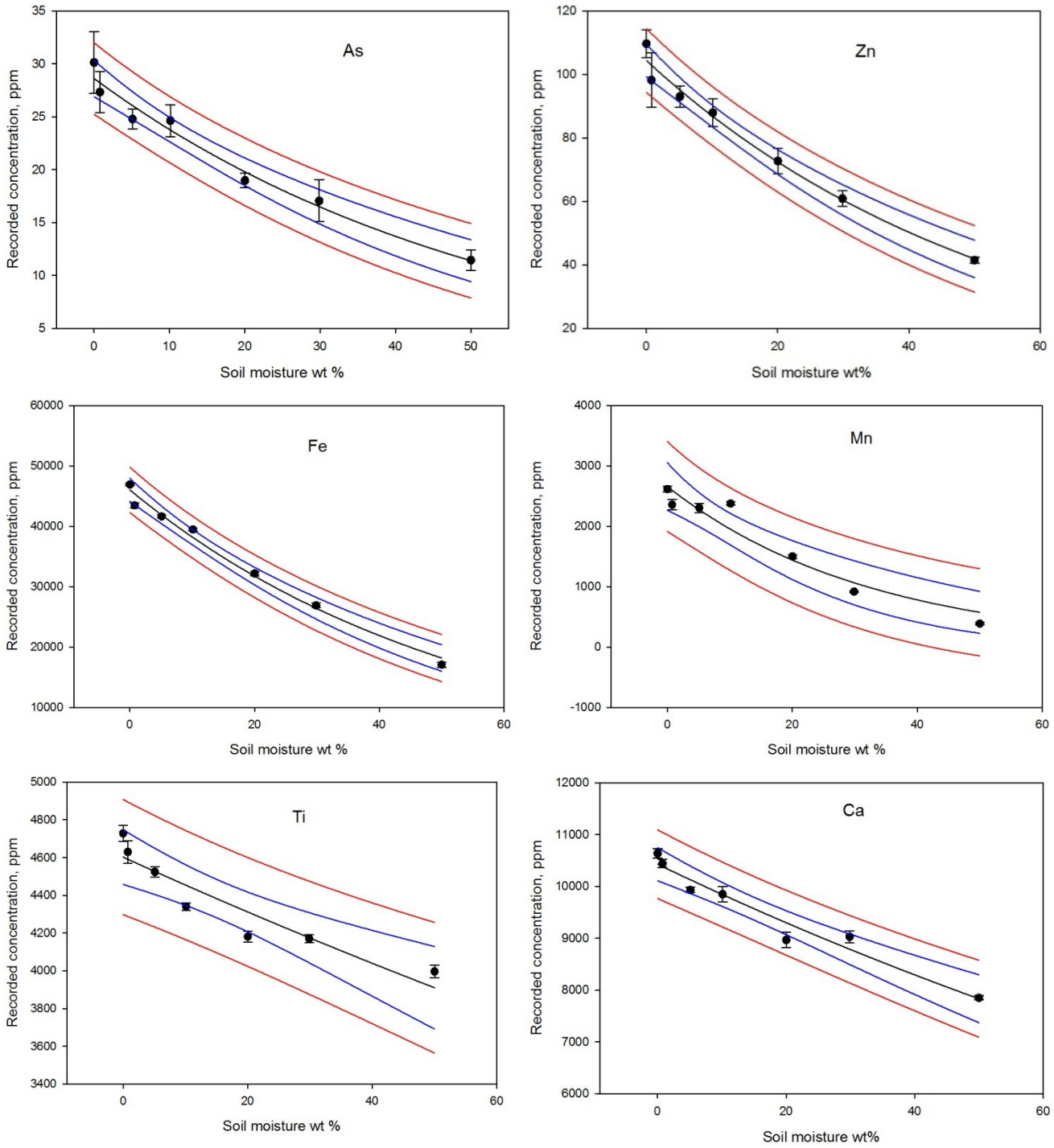

Figure 52: Elemental concentrations recorded by FP-XRF analysis with increasing soils moisture. Black lines are the fitted exponential decay functions, blue lines are the 95% confidence bands on the regression and red lines are the 95% prediction bands of the regression.

Table 12: Values used to fit 2 parameter exponential decay functions to concentration/soil moisture data for As, Zn, Fe, Mn, Ti, Ca and K.

Element (z)	Recorded concentration, ppm 0% soil moisture	'*a*' value from exponential decay fitting	'*b*' value from exponential decay fitting	r^2
As (33)	30.13	28.61	0.0184	0.975
Zn (30)	109.71	104	0.0183	0.992
Fe (26)	46932.32	46480	0.0194	0.992
Mn (25)	2618.93	2659	0.0306	0.968
Ti (22)	4728.74	4595	0.0032	0.875
Ca (20)	10637.75	10418	0.0057	0.957
K (19)	14814.92	14377	0.0049	0.958

It is reasonable to assume that low z elements with correspondingly low electron binding energies will be more severely affected by the presence of soil moisture than high z elements with higher electron binding energies. This is as the differences between mass attenuation coefficients for water and air are higher for low energy X-rays (Hubbell and Seltzer, 2009) (Figure 53). These differences are accentuated by the difference in density between water and air as demonstrated by their linear attenuation coefficients (Figure 54). The difference between linear attenuation coefficients for water and air, accounting for density differences at temperature and pressure expected in top soils, is shown in Figure 55. This represents the practical difference at different energy levels by replacing air pore space with water.

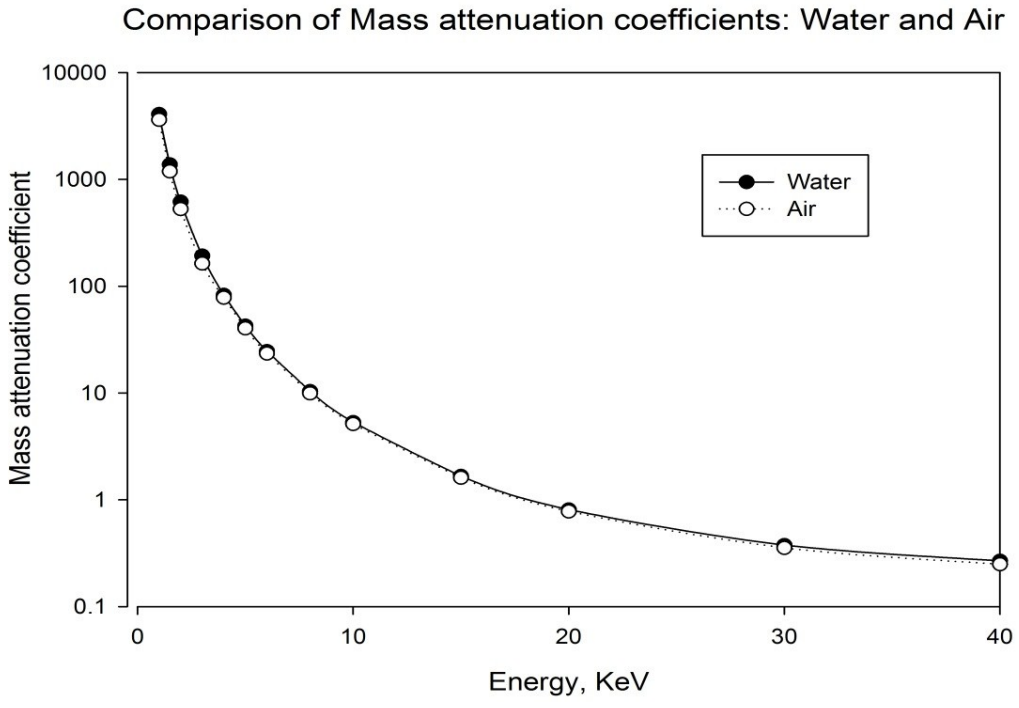

Figure 53: Mass attenuation coefficients for water and air across the energy range used in FP-XRF analysis. Data from Hubbell and Seltzer (2009)

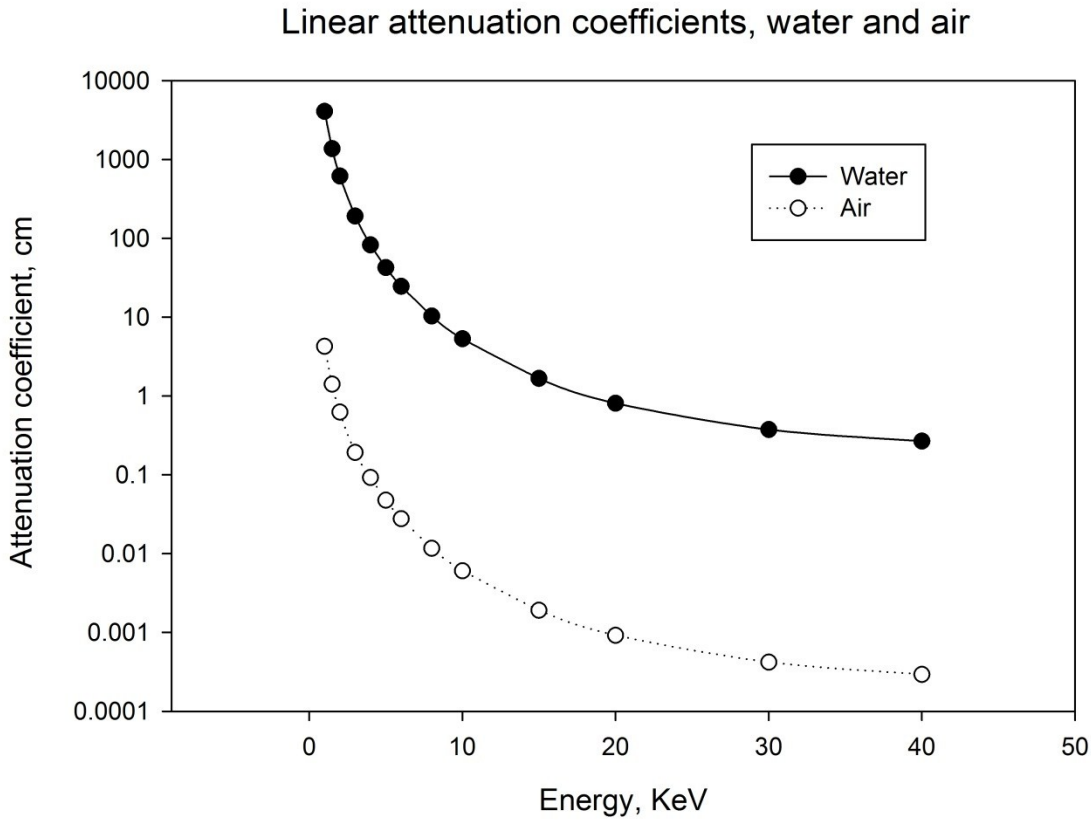

Figure 54: Linear attenuation coefficients for pure water and air across the energy range used in FP-XRF analysis

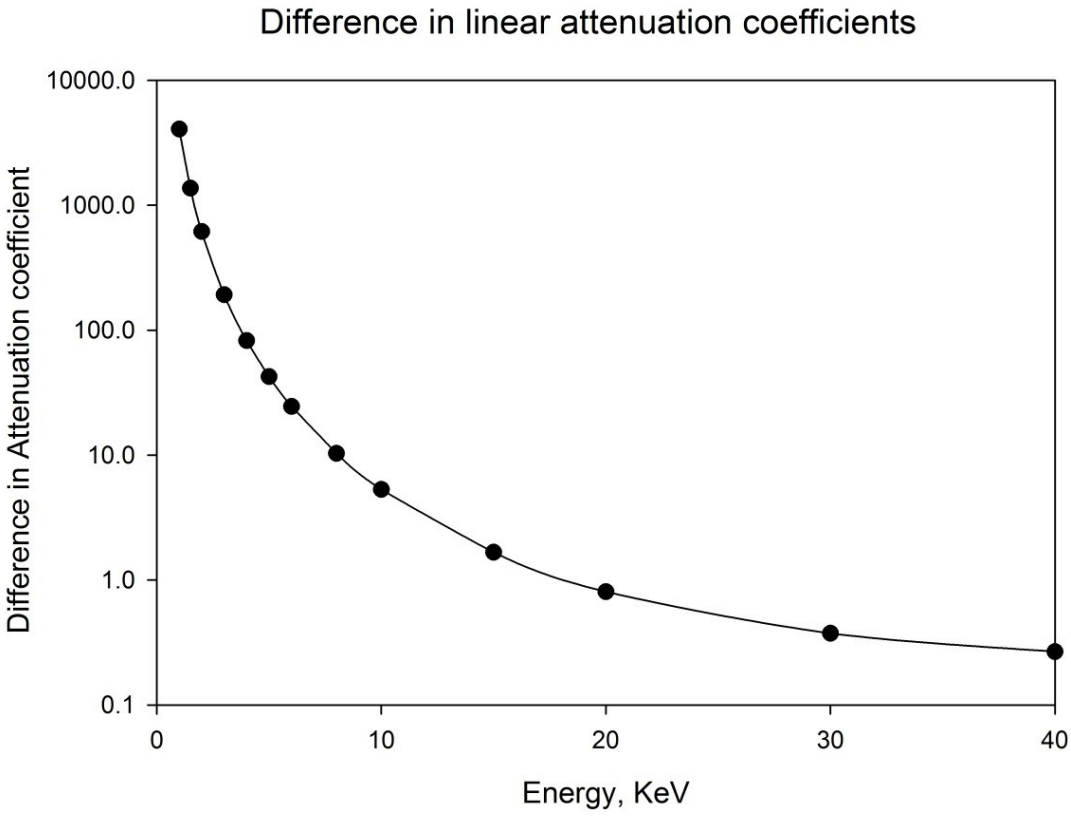

Figure 55: Difference between linear attenuation coefficients (adjusting for density differences) for water and air across the energy range used in FP-XRF analysis.

Therefore fluorescence from light elements will be absorbed and scattered to a greater extent in water than fluorescence from heavy elements. Whilst this trend is observed relatively well experimentally for elements of $z \geq 25$ (e.g. increasing soil moisture affects measured Mn concentrations to a greater extent than As concentrations) the same effect is not observed for elements with $z < 25$ (e.g. increasing soil moisture does not affect K concentrations to a greater extent than Mn or As concentrations) (Figure 51).

In addition, contrary to theoretical expectations, experimental results indicate that elements with z < 25 are significantly less affected by soil moisture than higher z elements.

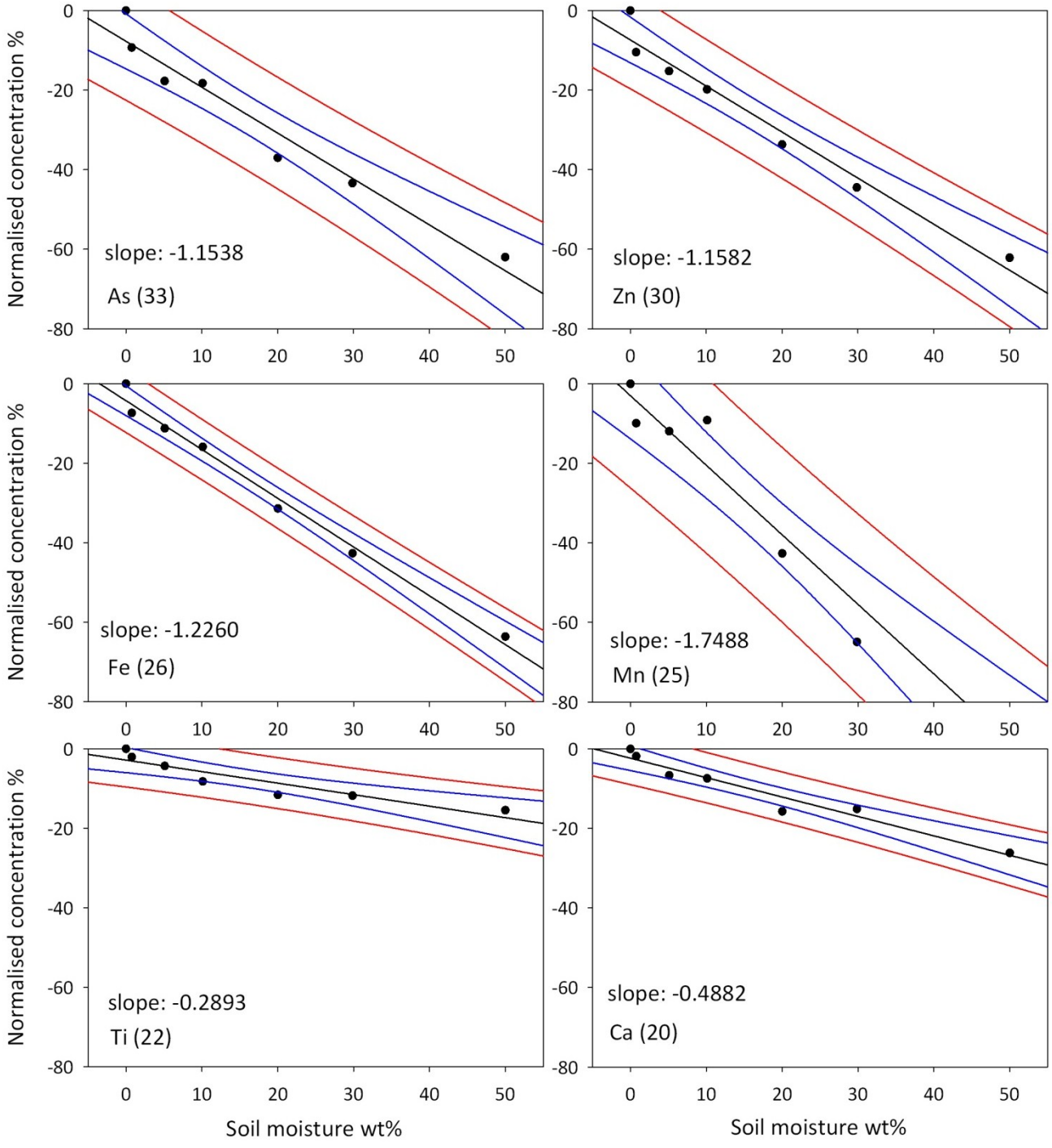

Figure 56: Normalised attenuation of measured concentrations of As, Zn, Fe, Mn, Ti and Ca due to the presence of soil moisture demonstrating the effect of atomic number on the effect of soil moisture and the disparity between elements with z ≥ 25 (As, Zn, Fe and Mn) and z < 25 (Ti and Ca).

This effect can be explained due to the mode of quantification of the Niton XLt 700 for light elements. Quantification of light element concentration is performed based on spectra obtained using filter mode 2, use of this filter causes a 2nd Compton normalization calculation to be performed. As the matrix correction applied to elements of z < 25 is based upon the Compton scattering peak from a source with a different output spectrum to filter mode 1 the influence of the sample matrix may be corrected more or less

effectively. In the case of this soil matrix it appears that matrix correction calculations based on the Compton scattering peak reduce the influence of water in the sample matrix more effectively using filter mode 2 than filter mode 1 and therefore lighter elements appear to be less affected by soil moisture (Figure 56). However, in both analysis modes, water content constitutes an important source of error during in-situ measurement with between 0.3 and 1.7% of measured analyte concentration lost per 1% increase in soil moisture.

Correction of for soil moisture effects is possible, either on a sample to sample or an entire survey basis. Where soil moisture varies significantly between samples correction must be applied on a sample to sample basis, which requires the laboratory analysis of samples with a similar matrix to determine appropriate correction factors for each element and measurement of exact soil moisture in each sample in the field. Correction for soil moisture based purely on statistical comparisons with a validation method may be appropriate in some cases where soil moisture is uniform across the sampling area, however careful attention should be paid to ensure that this is the case (i.e. statistical comparison between field measured soil moisture values and residuals of elemental concentrations from the FP-XRF/ICP-MS regression as discussed further below).

***Particle size**:*

Although the effect of particle size was not directly investigated in this study it remains an important factor when considering data quality during XRF analysis. There are two main reasons for this, the first is due to sample heterogeneity, the second; surface effects. As the FP-XRF analysis window is relatively small (approximately $2cm^2$) it is important that the average composition of the sample is well represented within this area. In the case of sample with large grain size (for instance gravel) it is possible that all of the analysis area is dominated by a single grain which may not be representative of the overall composition of the sample. A well homogenized sample with small particle size better represents average sample composition within this small visible area.

As grain size distribution was dominated by the very fine (< 500 µm) fraction for all investigated samples it is expected that the influence of particle size on data quality was limited compared to other factors. Kilbride et al. (2006) show that particle size distribution within the < 2mm soil fraction had no effect on the quantification of Cu, Fe, Pb and Zn in soils during analysis using dual source and X-ray tube source pXRF. However other studies indicate that particle sizes > 60 µm can have an appreciable influence on the quality of XRF data (Beckhoff, 2006). This inconsistency between literature sources indicates that the importance of particle size may differ substantially between different soils dependent on the micro scale distribution of analytes and the critical penetration depth compared to particle size for a particular matrix and analyte (Beckhoff, 2006). Therefore particle size should be considered an important factor when planning field preparation protocols for soils with a large particle size distribution. For soils with large grain size, in field grinding may be the most effective way to improve data quality by reducing surface and heterogeneity effects.

Chemical composition:

Chemical composition of the soil also has a significant effect on the accuracy of FP-XRF analysis; this can be due to interferences between emission lines of different elements and due to the density of the soil matrix. As the resolution of the detector in field portable instruments is lower than laboratory based instruments, field portable instruments are susceptible to a wider range of interferences. Common interferences in soils include Pb (L alpha emission at 10.55KeV) and As (K alpha emission at 10.54KeV) and V (K beta emission at 5.43KeV) and Cr (K alpha emission at 5.41KeV). It is important that possible interferences such as these be

investigated for analytes of interest and in some cases errors may be so large that even qualitative analysis by FP-XRF is inappropriate.

The density of the soil matrix is also an important factor to consider as measurement of high Z elements (i.e. contaminants such as Pb, As or U) in a low Z matrix may be effected by scattering and attenuation. Light element matrices result in high degree of inelastic (Compton) scattering which may obscure emission peaks. Correction of the Compton scattering peak is possible and in the case of the Niton Xlt 700 this is performed on board without user input. However accurate Compton normalisation requires knowledge of the full composition of the sample matrix. When the matrix is composed of low z elements such as clays and silicate minerals (high in Al and Si) accurate internal estimation of the sample matrix is not possible as light elements are not typically measurable without vacuum or helium purging techniques due to the strong absorption of low energy emission lines in air between the sample and detector (see Table 13). Although in newer FP-XRF designs with larger, more sensitive silicon drift detectors and geometry optimized to minimize the distance between sample and detector do allow for analysis of lighter elements ($z \geq 12$). In the case of the Niton XLt 700 a correction for a standard soil matrix is applied based on the height of the Compton scattering peak. In some cases this correction may function well, allowing for good quantitative use of field data, however if the soil matrix used during factory calibration by Niton does not match the soil matrix measured well (as is the case with the addition of water to soils in this study) then significant errors in displayed concentrations may be present.

Table 13: Transmission of K alpha fluorescence emitted from Mg, Al and Si through air at 1 atm.

Element (z)	Energy (eV)	Transmission 1 cm air path %	Transmission 5 cm air path %
Mg (12)	1,254	9.57	0.0008
Al (13)	1,487	23.19	0.0671
Si (14)	1,740	39.10	0.9137

Bulk sample size:

Constant critical penetration depth values or sample mass values previously reported in literature pertaining to portable XRF (pXRF) analysis (e.g. 2mm, Kalnicky and Singhvi, 2001) are theoretically invalid as critical penetration depth is a variable dependant on analysis geometry, sample density and total mass attenuation coefficients of primary and characteristic radiation in the sample (Potts et al., 1997). Total mass attenuation coefficients have been shown to vary by up to 1 order of magnitude between soils dependent on composition within the energy ranges used during pXRF analysis (~3.5 – 40 KeV)(Mudahar et al., 1991). Sandy soils tend to exhibit lower total mass attenuation coefficients than clay rich soils. Additionally the total mass attenuation coefficient within any particular soil has been shown to vary by up to 1 order of magnitude dependent on photon energy and hence the analyte (Mudahar et al., 1991). These differences combined with density differences between soil matrices (1.1 – 1.6 g/cm^3 range for most soils (Hillel, 1980)) can result in large variations in critical penetration depth. Investigations on similar media such as silicate rocks indicate that critical penetration depth may vary between 30µm and 12mm dependent on the analyte (K and Ce in Rhyolite) and also show considerable differences in critical penetration depth as a function of mineralogy (Potts et al., 1997).

To test whether the current recommended minimum dry sample mass to be used in Niton XRF cups is sufficient for clay rich soils, a series of cups were prepared using different quantities of the same sample. Samples were measured 8 times each using the Molybdenum internal filter with the source tube at 40 kV for a period of 300 seconds. The results of these measurements are plotted for As, Zn, Fe and Mn in Figure 57. The error bars show the standard deviation between the 8 repeated measurements.

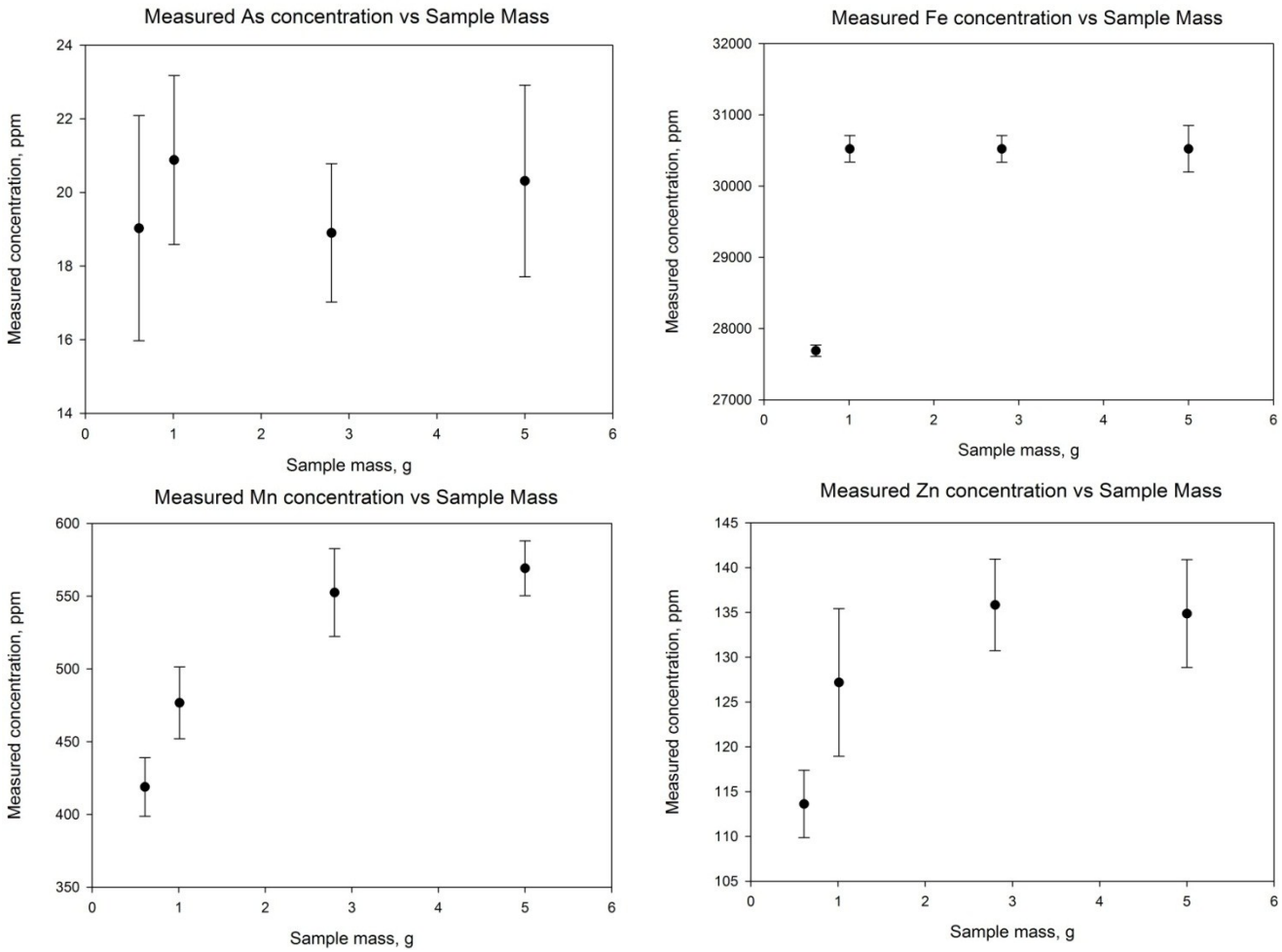

Figure 57: Mass of sample used in Mylar® covered XRF cups compared to mean recorded concentration.

Analysis of low mass samples resulted in a significant decrease in recorded analyte concentration for all elements (except for As where low precision potentially masked this effect) indicating that the critical penetration depth for all analytes was greater than the depth of the smallest sample. As expected the extent of the effect of low mass samples on recorded concentration varied considerably by analyte with As and Fe in this case less effected than Zn and Mn. As low Z elements emit lower energy emission lines upon excitation critical penetration depths applicable to their analysis are generally less than for high Z elements. For all analytes investigated within this soil (Mn, Fe, Zn and As) an increase in sample mass from 2.8 to 5 grams in XRF cups (Figure 45) did not result in significant increases to measured concentrations. Therefore, in this soil matrix, quantitative analysis of elements with $z < 33$ maybe acceptable with as little as 2.8 grams of sample. However, for analysis of heavier elements, in a soil matrix with a lower total mass attenuation coefficient considerably more sample would be required. To avoid the risk of critical penetration depth exceeding sample depth, particularly when analysing for heavy elements in sandy soils sample masses of up to 15 grams (equivalent to depths of 12 to 17mm) may be necessary. Despite this, when analysing for low Z elements in a heavier soil matrix such as clay, minimum sample masses of less than 5 grams may be acceptable after careful consideration of analyte, sample density and attenuation properties of the soil matrix.

Cross-validation procedure:

Many approved methods for FP-XRF analysis, for example US-EPA 6200 (Sackett and Bedford, 1998), require the validation of FP-XRF accuracy by analysis of 5-10% of samples using an alternative laboratory technique such as ICP-MS or OES analysis. In previous studies of the accuracy and precision of XRF analysis,

XRF results have been directly compared to aqua-regia hot-plate extractions (Kilbride et al., 2006). XRF analysis targets all atoms within the critical penetration depth, regardless of mineral structure, therefore, in order to ensure comparability between laboratory ICP-OES/MS analyses and FP-XRF data only complete digestion protocols should be used. Aqua-regia hot-plate dissolution prior to ICP-OES/MS analyses has been shown in some cases to result in significantly less recovery of arsenic and other elements than microwave extraction protocols incorporating hydrofluoric acid to break down silicate phases (Chen and Ma, 2001). While digestion by aqua-regia may be useful to determine the environmentally available fraction of a particular element in soil, it is not directly comparable to the total analyte concentration measured during XRF analysis. Therefore total microwave acid digestion or alkaline fusion digestion methods suitable for organic rich and silicate containing media with proven recoveries approaching 100% (e.g. Vandecasteele et al., 1993; U.S. EPA, 1996) should be used in preference to ensure maximum comparability between FP-XRF and ICP validation data. Additionally ICP-MS analysis is also susceptible to various matrix effects and interferences which should be considered prior and quantified prior to the use of ICP-MS results to validate FP-XRF accuracy.

Procedural blanks

The procedural blanks correspond to 0.4 ppm of arsenic which was subtracted from all other analyses.

ICP-MS matrix effects

ICP-MS analysis often uses internal standardization to correct for non-spectral interferences (signal suppression or signal enhancement caused by the sample matrix), instrument instability and signal drift (Vanhaecke et al., 1992). It is important to choose an internal standard with a mass close to the analyte of interest (Vanhaecke et al., 1992). In soils, the selection of an internal standard is not always straightforward because a lot of elements are present in the soil matrix. In this study ^{103}Rh (rhodium) was used as internal standard. The importance of using an internal standard can be illustrated comparing the results with and without internal standardization. Although matrix-matched standards were used, the difference in the two approaches is in between 25 and 40%. The use of three reference materials shows that using ^{103}Rh adequate concentrations are obtained; while without internal standard the As content is underestimated. Nevertheless, as ^{103}Rh and ^{75}As respond slightly different to matrix effects ensuring maximum matrix matching between samples and calibration solutions is essential.

ICP-MS Interferences

Several polyatomic interferences can occur on $^{75}As^{+}$, including Ar-based and H-based polyatomic ions, double charged ions and oxide ions. The most reported interference is $^{35}Cl^{40}Ar^{+}$. Several mathematical equations exist to correct for this interference (Kershisnik et al., 1992; de Boer, 1999; Polya et al., 2003; Colon et al., 2009). Despite relatively high Cl concentrations in the soil due to evapo-concentration (~ 5 mM in interstitial water determined by IC analysis), Cl-containing reagents have been avoided in the sample preparation and a pressurized collision-reaction cell has been used in the measurements, therefore we expect to have a low abundance of $ArCl^{+}$. Nevertheless, the effect of this potential interference has been investigated using the excess counts on 77 (counts on m/z 77 corrected for Se using m/z 78) and isotopic abundances (Colon et al., 2009). The difference is < 2% in all cases, which is within the error margin of the ICP-MS measurements. When investigating soils or sediments from estuarine environments or marine environments, Cl concentrations maybe significantly higher and $ArCl^{+}$ interferences may become important. The interference of GeH is increased due to the use of hydrogen in the collision-reaction cell. However, Ge is rarely present above trace level concentrations in soils (median soil concentration values of < 2 mg/kg Scribner et al., 2006). The effect using excess counts on 77 and the isotopic abundance is < 3%. In addition the double charged ions Sm^{++} and Nd^{++} overlap with $^{75}As^{+}$. The formation of double charged ions within the

plasma is ~1.5 % (monitored as $^{140}Ce/^{70}Ce^{++}$ during tuning). The contribution of Sm^{++} has been investigated using the excess counts on 77 and the isotopic abundance and is <0.2 %. While this error is acceptable pour the purposes of validating FP-XRF results, in soils containing high total concentrations of Nd the effects of Nd^{++} ions maybe significant. The presence of NiO^{+} and CoO^{+} cannot be investigated using excess counts on 77. However, Co concentrations in the soils are low (below the limit of detection via XRF analysis) and NiO^{+} at m/z 75 is only present in very small amounts (only 0.026% of NiO occurs at m/z 75).

Correlation and linear regression analysis

Comparison of results from FP-XRF and ICP-MS analysis requires at least basic statistical investigation, most commonly in the form of correlation and linear regression analysis. In the case of US-EPA quality criteria for FP-XRF data (US-EPA, 1998 -Table 14) to be considered quantitative (Q2 quality criteria) linear regression analysis between FP-XRF and the validation method must result in a coefficient of determination (r^2) greater than 0.7. To achieve definitive (Q3 quality criteria) r^2 must be greater than 0.85.

Table 14: Definitions of U.S. EPA validation quality criteria: definitive, quantitative screening and qualitative screening.

Data quality level	**Statistical requirement**
Definitive Q3	r^2 = 0.85–1. Relative standard deviation (RSD) ≤ 10%. Inferential statistics (test for gradient of line = 1 and *y*-intercept = 0) must indicate the two data sets are statistically similar (at the 5% level), i.e. relationship $y = x$ accepted.
Quantitative screening Q2	r^2 = 0.70–1. Relative standard deviation (RSD) < 20%. Inferential statistics indicate the two data sets are statistically different, i.e. relationship $y = mx$ or $y = mx + c$ accepted.
Qualitative screening Q1	r^2 = less than 0.70 Relative standard deviation (RSD) > 20% Inferential statistics indicate two data sets are statistically different.

Linear regression analysis was performed to compare ICP-MS analysis for arsenic to FP-XRF results using the 3 investigated in and ex-situ methods. It was found that excellent linearity (r^2 values of greater than 0.85) was achievable for arsenic by all three methods (Figures 58, 59 and 60) although important statistical differences were present between the 4 sets of measurements (see Table 15).

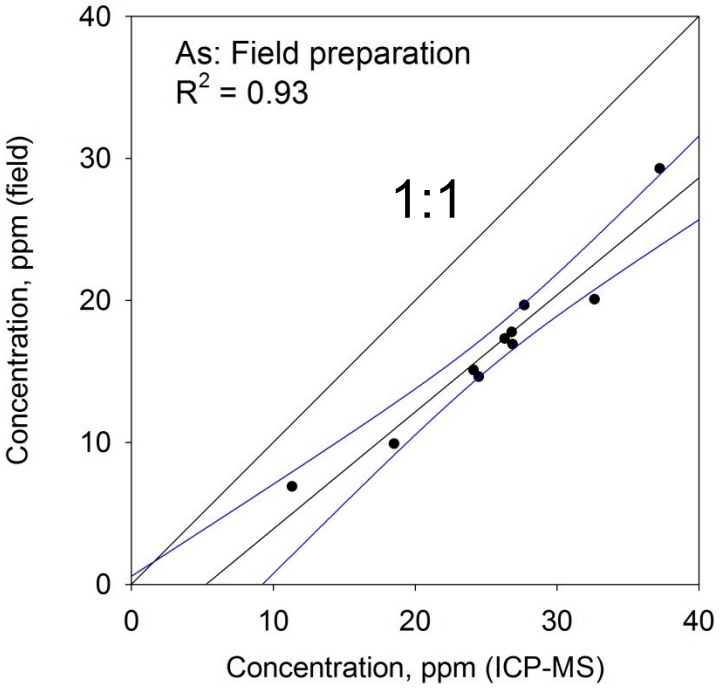

Figure 58: As concentrations measured by FP-XRF in-situ following field preparation against As concentrations measured by ICP-MS following total acid digestion. Black line = fitted linear regression, blue lines = 95% confidence limits.

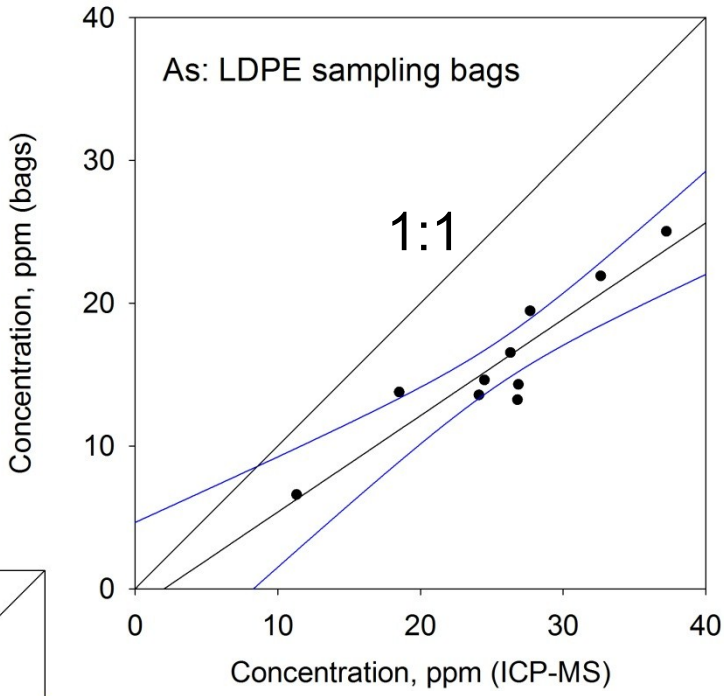

Figure 59: As concentrations measured by FP-XRF ex-situ in LDPE sampling bags against As concentrations measured by ICP-MS following total acid digestion. Black line = fitted linear regression, blue lines = 95% confidence limits.

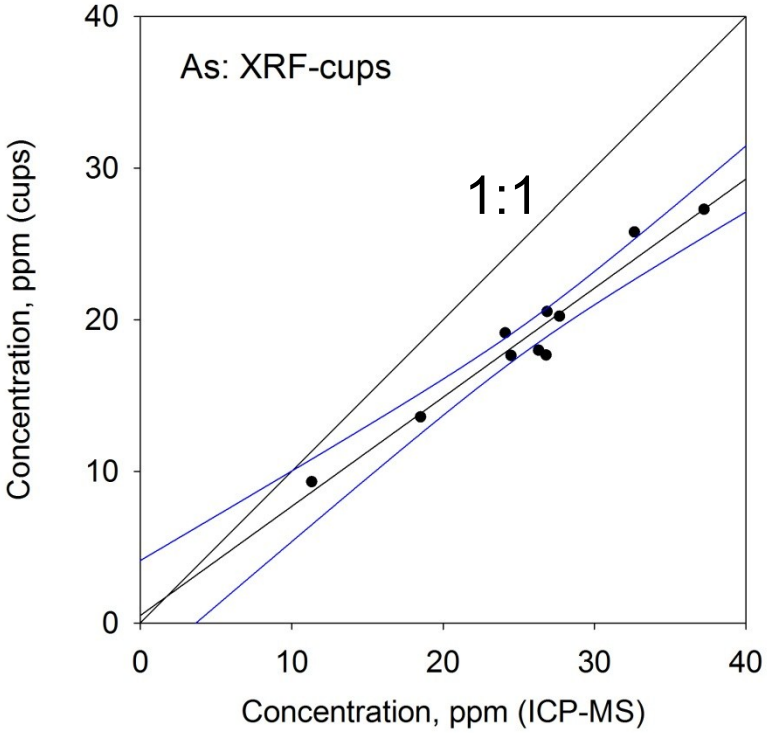

Figure 60: As concentrations measured by FP-X RF ex-situ following thorough sample preparation against As concentrations measured by ICP-MS following total acid digestion. Black line = fitted linear regression, blue lines = 95% confidence limits.

Table 15: Comparison of the precision and accuracy of FP-XRF measurement methods against total digestion/ICP-MS analysis.

Measurement	r^2 between ICP-MS and FP-XRF analysis	RSD% mean of all FP-XRF measurements (range)	Intercept	Slope	U.S. EPA quality level
In-situ – field preparation	0.929	14.4	-4.33	0.82	Q2 – Quantitative screening
Ex-situ – in LDPE sampling bags	0.854	21.6	-1.37	0.68	Q1 - Qualitative screening
Ex-situ – in XRF cups on NETP	0.9483	13.8	0.50	0.72	Q2 – Quantitative screening.

Table 16: Statistical comparisons of FP-XRF data with ICP-MS data.

Measurement	Slope significantly different to 1 (P = 0.05)	Intercept significantly different to 0 (P = 0.05)	Means significantly different (P = 0.05)
In-situ – field preparation	NO	NO	YES
Ex-situ – in LDPE sampling bags	YES	NO	YES
Ex-situ – in XRF cups on NETP	YES	NO	YES

Whilst all preparation methods provided Q3 level linearity compared to ICP-MS analysis (r^2 >0.85) it was found that measurement through LDPE bags did not meet precision requirements required for Q3 or Q2 level data (<20% RSD). Precision was also the limiting quality factor for both field preparations and cup measurements with both sets of measurements failing to achieve definitive (Q3) precision (<10% RSD). As concentrations in the measured soils were consistently underestimated by the internal Niton quantification compared to values obtained using classical ICP-MS determinations. Despite good linearity between ICP-MS and FP-XRF results there were statistically significant differences between ICP-MS results and FP-XRF results obtained via all methods as can be seen from the slope and intercept values given in Table 15 and the statistical comparisons of the groups of data given in Table 16. These differences highlights the need for validation of results by an alternative verified technique which itself should be confirmed with certified reference materials closely matching the samples.

Table 17: Estimations of the detection limit for As by each preparation/analysis method.

Measurement	LOD
In-situ – field preparation	6.84 - 8.53
Ex-situ – in LDPE sampling bags	10.24 - 12.76
Ex-situ – in XRF cups on NETP	5.79 - 7.21

Limits of detection estimated from the standard deviation of the y intercept and standard deviation of residuals from the regression line with ICP-MS analysis are presented in Table 17. Both estimates were calculated via methods presented in Apostol et al. (2009).

Conclusions

Quantitative screening of As with tube source FP-XRF using standard-less calibration modes is possible even at low trace concentrations (< 10 ppm) under field conditions with minimal sample preparation. The combination of the Mo source filter used on the Niton XLt 700 series, resulting in low background radiation at the energy of the arsenic K alpha emission line, the high fluorescent yield of arsenic and the minimal attenuating effect of external filters result in low detection limits even in complex light soil matrices which are prone to extensive scattering. This study shows that one of the most important sources of error in quantitative FP-XRF analysis of soils is the presence of interstitial water which has been underestimated in previous studies. The standard bulk soil calibration mode based on Compton normalisation, used throughout this work, is not effective at correcting for the presence of soil moisture and it is therefore suggested that rapid field drying of samples or soil moisture correction procedures are applied when using standard-less calibrations for quantitative in-situ analysis of arsenic in soils. Despite this limitation it was found that with minimal in-situ preparation of dry soils that limits of detection, precision and accuracy achievable during arsenic analysis were comparable to those obtainable by XRF analysis following thorough preparation under laboratory conditions. The strong bias/underestimation shown by all FP-XRF results for arsenic regardless of preparation method confirms the need for validation of results via an alternative technique such as ICP-MS. Additionally the low precision shown by the field portable instrument at low arsenic concentrations (>13% RSD average for all preparation methods) indicate that repetition of short (100-200 second duration) field analysis is preferable to a fewer analyses with longer count times. For the highest quality quantitative XRF results empirical calibrations based on site specific standards should be used in preference to standard-less soil specific calibration methods. However, in situations where costs associated with logistically challenging field studies in remote areas preclude the prior analysis of site specific standards, standardless FP-XRF analysis modes can represent a viable quantitative technique as long as careful attention is paid to sample preparation.

Chapter 4: A Statistical Investigation of Physicochemical Controls on Arsenic Distribution on the Saône Floodplain

Abstract

This chapter aims to determine the relative importance of physicochemical factors controlling the spatial distribution and variation of arsenic concentrations in moderately contaminated calcareous surface soils (0-10cm) on a section of the riparian floodplain of the Saône. A variety of complimentary techniques including laser granulometry, wet chemistry, geostatistics and field portable X-ray spectrometry were used to generate data which were investigated for correlation with total arsenic concentrations.

Total solid concentrations for 11 elements (obtained by FP-XRF and validated with ICP-MS) in 75 soils at unique geographic locations as well oxidisable organic matter and active carbonate fractions, particle size distribution (PSD) and flooding risk estimates were compared for statistical inter-dependence. Variables found to be strongly positively correlated with measured As concentrations were Fe concentrations ($R = 0.805$, $p < 0.001$), Mn concentrations ($R = 0.74$, $p < 0.001$) and the proportion of the soil clay fraction ($R = 0.613$, $p < 0.001$). In contrast to previous studies, no statistically significant correlation with spatial variables, solid organic matter or carbonate concentration was found to be present. Fine to medium sand sized particles were shown to be strongly anti-correlated with arsenic concentrations whereas the particle size distribution of fractions coarser than 0.5mm showed no statistically significant correlation.

Extensive multi-collinearity between investigated auxiliary variables prevented the determination of their relative importance to a multiple regression model ($R^2 = 0.76$, $p < 0.001$) and indicates that correlations are due to the same real world parameter – the presence of Fe and Mn rich, fine clay particles.

Introduction

Arsenic is the 12th most abundant element in the biosphere and is ubiquitous in the environment. However, arsenic is also a known carcinogen, mutagen and teratogen (National Research Council (U.S.)., 1999). Arsenic distribution in soils and sediments is controlled both by its natural biogeochemical cycle and anthropogenic factors as discussed in Chapter 2.

The mean concentrations of arsenic in top-soils and floodplain sediments in Europe are 11.6 and 12.2 mg kg^{-1} respectively (Salminen, 2005). Geogenic baseline values can however be hard to determine in any given location as they are dependent on factors such as local geology, geology of soil parental material and hydrological regime which vary considerably on a European scale. It is also impossible to differentiate between disperse anthropogenic contamination and geogenic arsenic by classical isotope studies due to the mono-isotopic nature of As (^{75}As).

Arsenic present in European floodplain soils can be traced to a variety of sources including the erosion and weathering of sulphide deposits and highly mineralised primary geology, deposition from industrial atmospheric emissions, the historic and current use of arsenic containing pesticides, wood preservation treatments and additives in poultry feed. These sources are discussed in detail in Chapter 2.

The difficulty in determining baseline arsenic values, compounded by disagreement over the importance of low levels of arsenic exposure on human health (Meharg and Raab, 2010) leads to inconsistency in guideline and action threshold values for arsenic in soils within the European Union (EU). Current national guideline values range from 10 to 500 mg kg^{-1} within the EU and the nomenclature and meaning of these values is also often inconsistent (Carlon, 2007). Whilst exposure levels from arsenic in drinking water can be calculated reasonably well by assuming average water consumption, the risk posed by total soil

concentrations is somewhat more challenging. Exposure from soils can be, for example, due to hand to mouth behaviour in children, consumption of crops grown in arsenic contaminated soil, inhalation of wind-blown particulates or due to infiltration of water supplies.

Total arsenic concentration limits or guideline values in soils therefore must take into account factors including land use, soil influence on water resources, climate, soil chemical conditions and the feasibility of remediation or land use change. Most national legislative limits currently take into account land use, often imposing lower limits for residential soils compared to industrial or agricultural soils. However, many regulatory guidelines do not at present consider soil chemical conditions and factors such as flooding when determining threshold arsenic concentrations.

Soils subjected to periodic flooding (fluvisols) account for 5% of European land (European Commission., 2005)(Figure 61) and moderate contamination of these soils is widespread (Du Laing et al., 2009; Ackermann et al., 2010).

The changes to pH and Eh conditions, CO_2, carbonate and dissolved organic carbon concentrations occurring in flooded soils, which in turn impact arsenic mobility and toxicity are additionally compounded by factors including mineral dissolution and precipitation and the increased solubility of species competing for solid sorption sites (e.g. anionic organics).

The combined effect of these various mechanisms can lead to elevated pore-water arsenic concentrations during flooding events, even in soils containing moderate or low total solid concentrations.

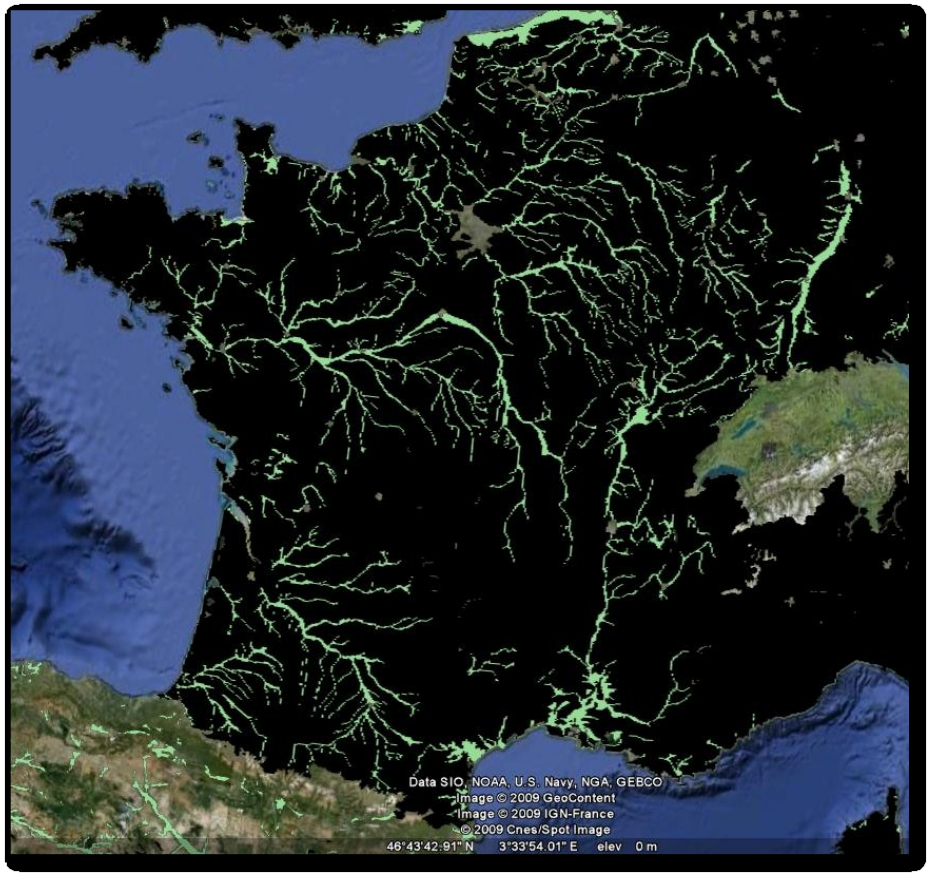

Figure 61: Fluvisols in France (light green) compared to other soil classifications (black) and soil sealed areas (grey)(European Commission., 2005) The area investigated in this study is marked with a red ellipse.

Floodplains also serve roles as areas of high natural biodiversity, controlled overflow areas to reduce the risk of urban flooding and increasingly as highly fertile agricultural land (there is a net increase in agricultural use of alluvial floodplains between CORINE land-cover data from 1996 and 2006 (EEA, 2010). To

function in each of these roles is a delicate balance which is further confounded by contamination with metals and metalloids.

Accurate risk assessment of arsenic contamination in fluvisols is important to ensure safe agricultural practice and avoid contamination of crops and of increasingly used shallow alluvial aquifers. Although many crops traditionally grown on alluvial planes such as wheat and corn have been shown not to accumulate significant concentrations of arsenic in their edible parts (e.g. wheat) (Williams et al., 2007) other crops including rice, vegetables and salads which are also grown on floodplains have been shown to accumulate arsenic to potentially dangerous levels (Meharg and Rahman, 2003; Cao and Ma, 2004; Das et al., 2004).

In the presented study area alone there are 6 active municipal shallow groundwater wells providing local communities with domestic water. In one periodically monitored well, arsenic concentrations of up to 60ug/L of arsenic have been measured, above even the pre-1993 World Health Organisation (WHO) guideline value for drinking water of 50ug/L. Elevated arsenic concentrations in water produced by these 6 municipal wells are reduced to below current WHO and European water standards by ozone treatment prior to distribution via the potable network. Although a limited number of untreated privately owned tube wells in this area are still in use, the water they produce appears not to be used for drinking or cooking.

Although soils on the Saône floodplain are known to be moderately contaminated with arsenic (Comite Syndical de l'EPTB, 2007) the distribution of arsenic in top-soils is poorly defined. The aim of this study is to determine the degree of spatial variation of arsenic contamination in top-soils on part of the floodplain and to infer the underlying chemical and mineralogical associations based on statistical relationships between soil elemental concentrations and physical characteristics. This study could be used as a precursor to risk assessment of agricultural practice and shallow groundwater resource usage.

Methods

Study area

The study area constitutes the east side of the Saône river floodplain between the towns of Pont-de-Vaux and Saint-Didier-Sur-Chalaronne close to the city of Macon in eastern France. This area is approximately 400 km from the source of the Saône river and 80 km from its confluence with the Rhone. All soils were sampled from a 60 km^2 area and within 2 km of the river channel within the extent of the 100 year flood. The extent of the sampling area and the sampling locations are shown in Figure 62.

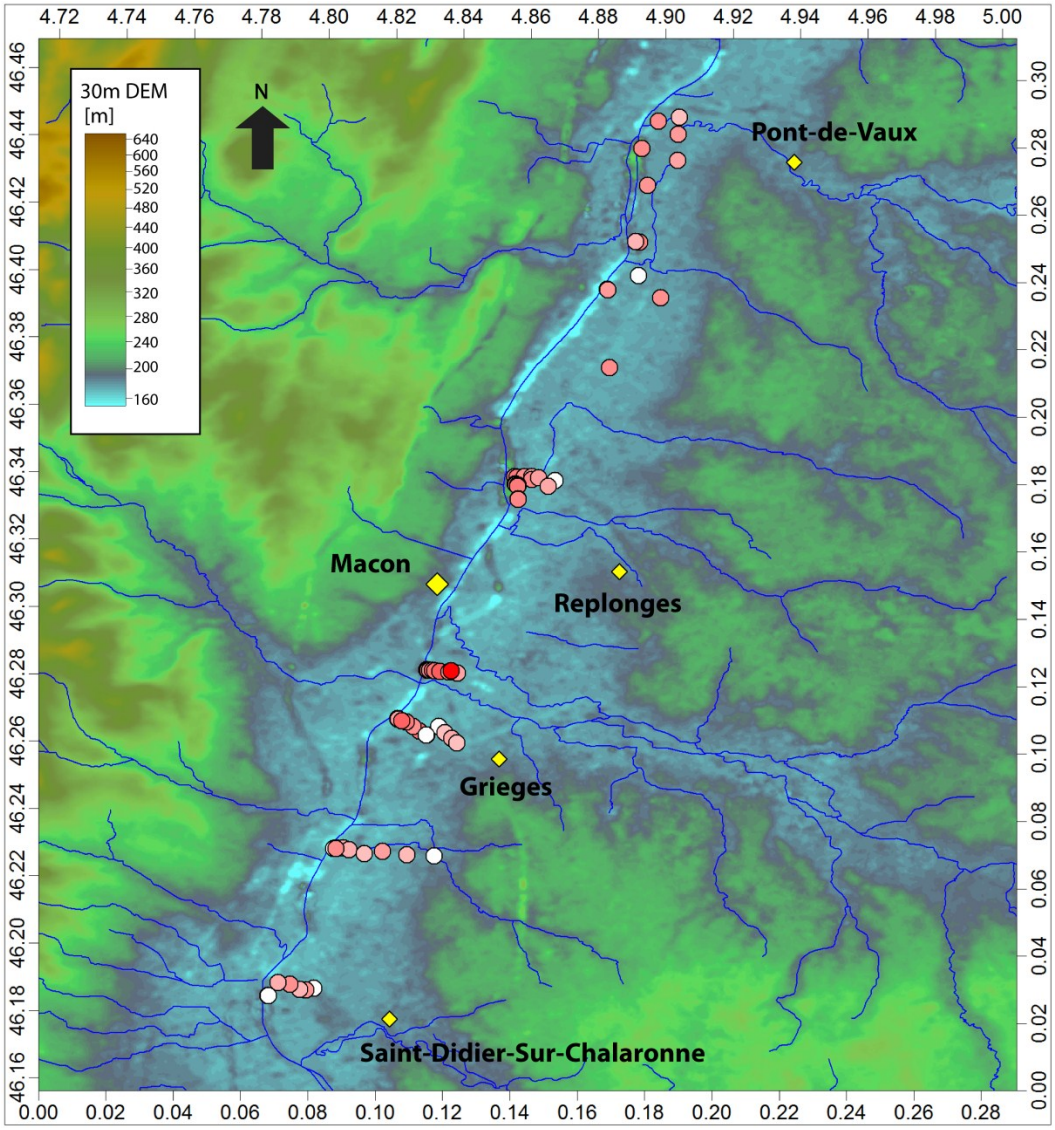

Figure 62: Location of study area showing topography (METI/ERSDAC et al., 2009) the main hydrological network (Institut Geographique National de France, 2010 - blue lines), key towns (yellow diamonds sized by population) and sampling points (circles coloured by arsenic concentration – red = 35 ppm to white = 0 ppm).

Fluvisols are the dominant soil type within this area however variations in soil texture from gleyic to sandy are evident due to changes in the historical fluvial depositional/erosional regime, land use and terrain morphology. Sampling locations were recorded using a European Geostationary Navigation Overlay Service (EGNOS) enabled GPS and sampling was timed using Trimble's planning software to ensure minimal horizontal dilution of precision (HDOP) values (estimated to be <1.5 for all sampling locations).

Determination of multi-elemental concentrations in situ

In situ analysis was performed using NITON® XLt™, 700 Series™ FP-XRF environmental analyser equipped with a miniature 1.0W X-ray tube 40kV/50µA excitation source, an Ag anode target and a high performance peltier cooled Si-PiN X ray detector. Top-soils at each sampling location were prepared with the in-situ method described in detail in Chapter 3, modified from US-EPA 6200 (Sackett and Bedford, 1998) prior to analysis to minimize the limit of detection and maximize the accuracy and precision of the instrument. All samples were analysed within a period of 5 days during August 2009 and the FP-XRF was re-calibrated

between samples using internal standards. Detector temperature was monitored prior to all analyses to ensure stable response.

On board standard-less quantification of elements was performed based on Compton normalization. Elements which occurred consistently below the limit of detection for this device were discarded from the data before statistical analysis, resulting in the final inclusion of 11 elements (K, Ca, Ti, V, Mn, Fe, Ni, Zn, As, Rb and Sr).

Following FP-XRF analysis the field prepared <2mm samples were transferred directly to double sealed polyethylene bags and were transported and stored in cool dark conditions prior to analysis.

The quantitative use of As concentrations was validated by a precision analysis and comparison of 10 representative samples across a range of measured arsenic concentrations (6.9 ppm to 29.3 ppm) using total microwave digestion (1: HNO_3 + HF + H_2O_2, 2: H_3BO_3 + HF) (U.S. EPA, 1996) and inductively coupled plasma mass spectrometry (ICP-MS). All data were acquired using an Agilent 7500c quadrupole ICP-MS (Agilent Technologies, Spain**)** equipped with an octapole reaction system, 103Rh and 193Ir were used as internal standards. The collision/reaction cell was operated with 3.0mL/min of H_2 and 0.5mL/min of He.

Laboratory Pre-treatment of soils:

Prior to analysis of TOC, active carbonates and PSD all soils were further homogenized, lyophilised for a period of 48 hours, to avoid the formation of aggregates and dry sieved again to retain the fine soil fraction (<2mm).

TOC for all soil samples was determined by a modification of the Walkley and Black colorimetric wet oxidation method (Walkley, 1947). In this method carbon is oxidised by dichromate ($Cr_2O_7^{2-}$) and excess dichromate is back titrated with ferrous iron. A correction factor of 1.30 was applied to resulting oxidisable organic carbon concentrations for calcareous soils as suggested by Santi et al., (2006). A range of between 2.5 and 6.6% oxidizable carbon was measured in the sampled soils.

TCO_3 was determined for all soils by the Scheibler volumetric method following ISO standard 10693 (ISO, 1995) whereby CO_2 is released after addition of hydrochloric acid to the sample. A range of 1 to 211 g/kg TCO_3 was measured.

Granulometric Analysis:

PSD was determined by a combination of dry sieving (>1<2mm fraction) and laser diffraction (<1mm fraction). Laser diffraction was conducted using a Malvern Mastersizer 2000 particle size analyser (Malvern Instruments, France) across a measurement range of 0.01 to 1500µm. Lyophilised soils were suspended in water, and subjected to an ultra-sonification step prior to analysis to ensure correct sample dispersion and analysis of elemental particles only. Distributions were calculated as percentage of sample by volume falling into 100 equivalent spherical diameter class sizes.

Phreetic flooding risk estimation:

The investigated area is, like many floodplain soils, at risk from fluvial and phreetic flooding. Whilst over-bank flooding in some areas can be controlled by the construction of defensive barriers and river flow management groundwater rise is significantly more difficult to mitigate. In this study only groundwater rise flood risk is considered as a possible control on arsenic distribution.

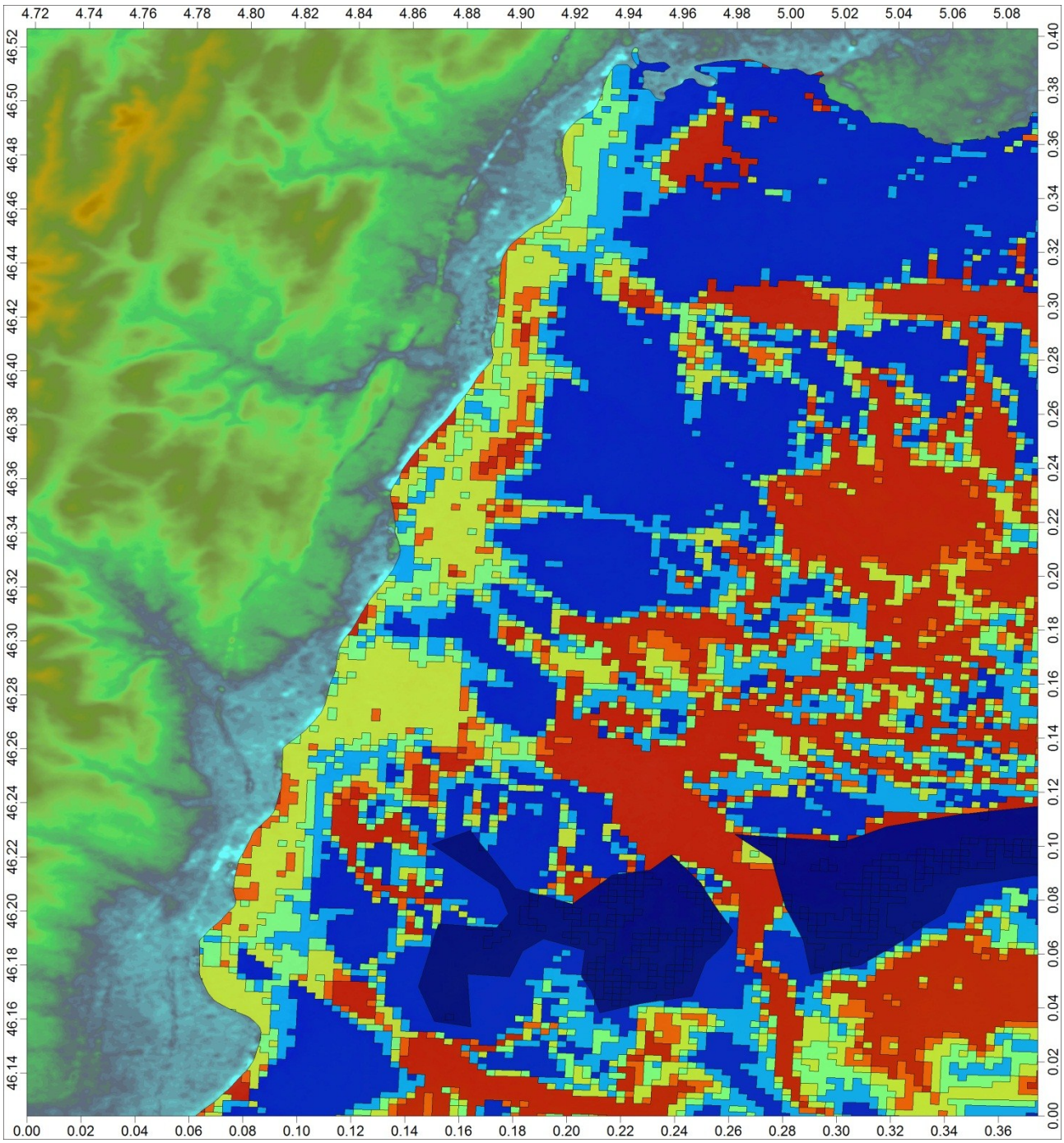

Figure 63: 30m grid digital elevation model of study area (METI/ERSDAC et al., 2009) with the risk of groundwater rise overlay obtained from the BRGM (BRGM, 2006 red = high risk to dark blue = low risk).

Spatial vector data provided by the BRGM which appears to have been converted from a 250m scale raster grid on the susceptibility of an area to groundwater rise and flooding (ranked from 0 – remote risk, to 6 - extremely high risk) was used to quantify risk of groundwater flooding at each sampling point (Figure 63)..

Results and Discussion

Validation of FP-XRF results

FP-XRF results for As were assessed for accuracy via linear regression analysis with ICP-MS results. This analysis demonstrated excellent linearity between field analysed and laboratory validated values (R^2 of 0.93 with a p value of <0.001). The comparison of ICP-MS to FP-XRF results is shown in Figure 64 with the fitted

regression line. Relative standard deviation (RSD) values, were between 6 and 20% (N=2) for all samples demonstrating an acceptable level of precision for quantitative screening (US-EPA, 1998). The slope and intercept were shown to be significantly different to 1 and 0 at the 95% confidence level indicating a bias in the linear regression. The strong linearity between ICP-MS and FP-XRF concentrations for arsenic shows that data is acceptable for correlation type analyses. However, the significant bias demonstrates that results cannot be considered definitively quantitative without correction.

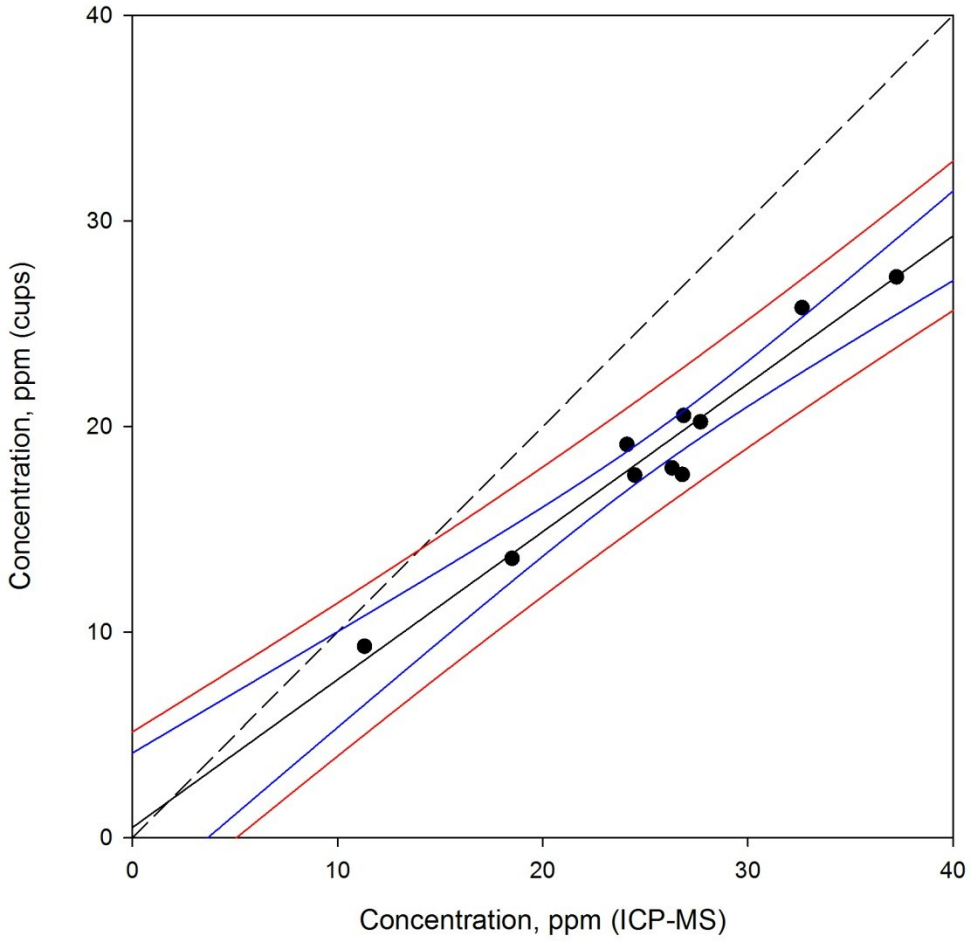

Figure 64: Linear regression of As concentrations obtained by FP-XRF and ICP-MS analyses showing 95% confidence bands on the regression (blue) and 95% prediction bands (red).

Descriptive statistics

Arsenic concentrations in analysed soils, once corrected for FP-XRF measurement bias, varied between 13.6 and 40.8 ppm with a mean concentration of 21.5 ppm and a standard deviation of 4.56 ppm. Approximately 79% of analysed soils were found to contain between 15 and 25 ppm of arsenic with an interquartile range of 17.9 to 24.3 ppm (Figure 65).

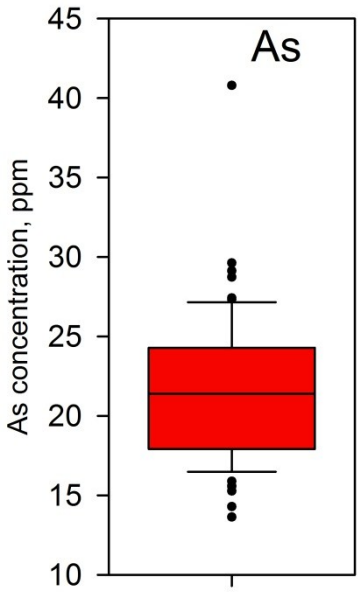

Figure 65: Boxplot of corrected arsenic concentrations. Whiskers correspond to 10th and 90th percentiles, points represent outliers.

The acquired arsenic data failed the Shapiro-wilk test for normality with a W-Statistic of 0.932 and a p value of 0.001 indicating that the data does not follow a normal distribution. This can be clearly seen by the slightly convex plot of concentration and cumulative frequency shown in Figure 66.

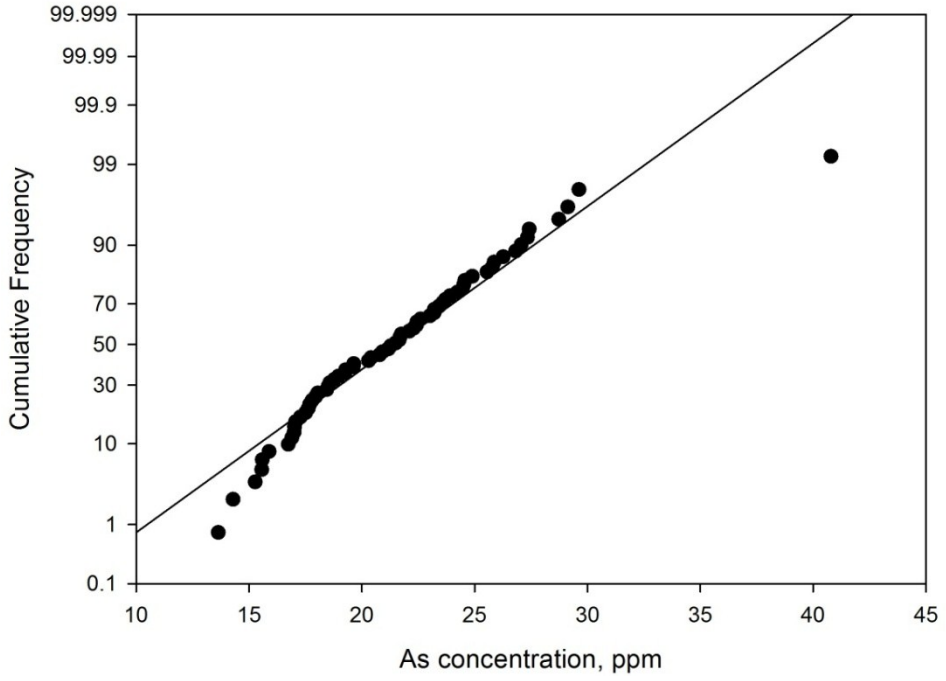

Figure 66: Arsenic concentration cumulative frequency plot. Normally distributed data would be expected to plot on a straight line whereas arsenic concentrations deviate significantly from this.

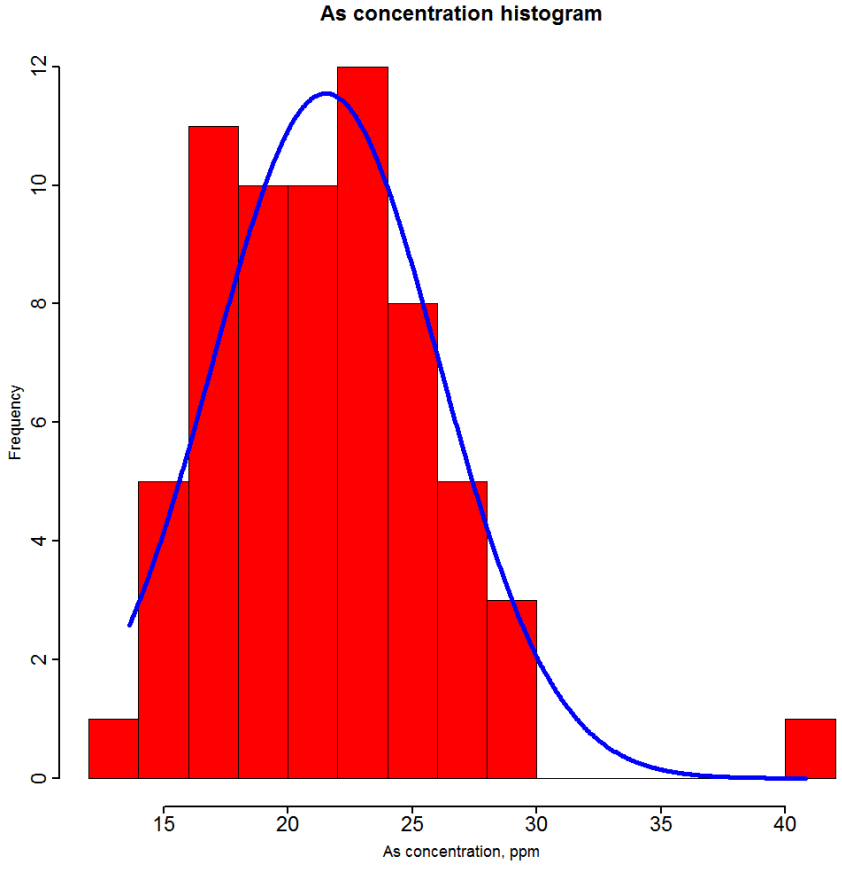

Figure 67: Histogram of arsenic concentrations with a normal distribution curve superimposed in blue demonstrating the slight positive skew to the data.

Figure 67 demonstrates the slight positive skew of the As data which is probably due to the bounding of data at the lower limit due to the centre of the distribution falling just above the analytical limit of detection. In this way the lower tail of the data is truncated as low end values fall below the limit of detection.

Spatial variability

Spatial auto-correlation of arsenic concentrations between sampling locations was evaluated by production of a semi-variogram. As can be seen in Figure 68 arsenic concentrations were found to be spatially auto-correlated within a maximum effective range of approximately 2.5km.

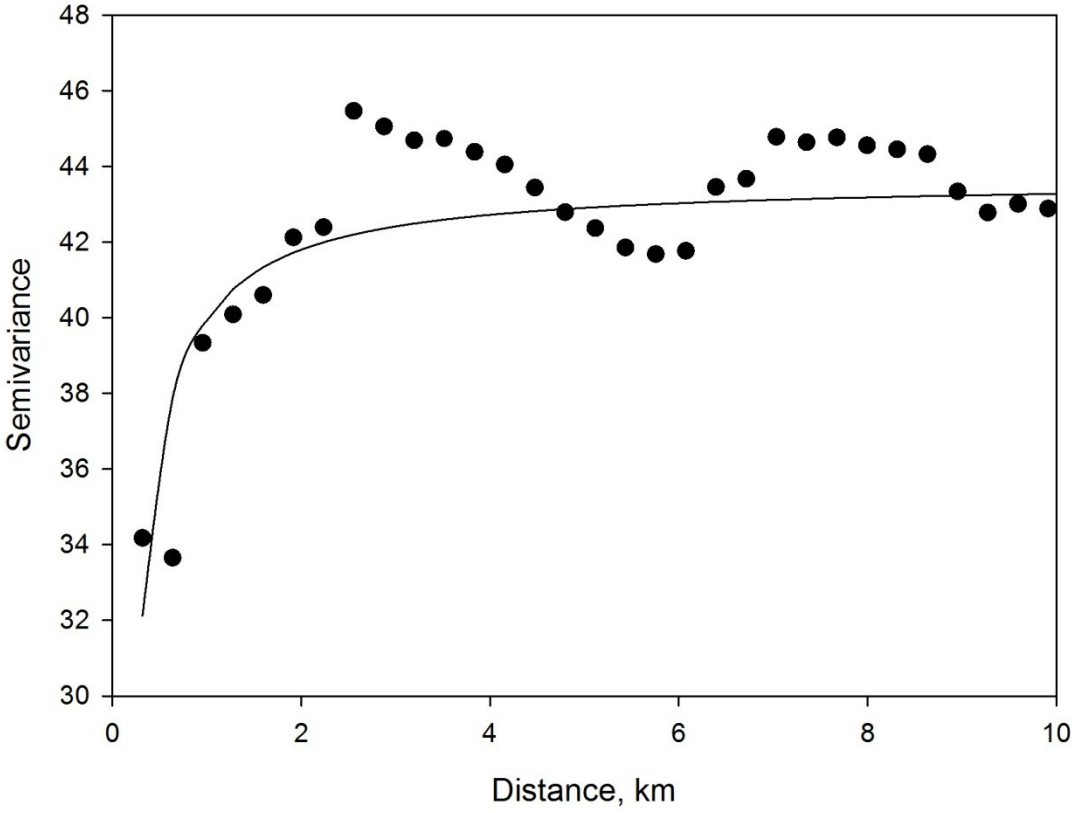

Figure 68: Semi-variogram demonstration spatial autocorrelation of arsenic values with a maximum range of approximately 2.5km. The fitted function of the form y = a + b/x fits the data with R_2= 0.64.

Due to the limited number of sample points and lack of high resolution auxiliary surface data more comprehensive geo-statistical analysis such as ordinary or regression kriging was not attempted. However, the spatial autocorrelation demonstrated in Figure 68 indicates that such techniques would be beneficial if a greater number of data points or high quality surface data (e.g. high resolution digital elevation models) of the investigated area were to become available. As overbank flooding risk is directly related to the distance of a location from the river, distance between each sampling location and the main river channel were calculated using proximity analysis protocols in SAGA GIS (Bock et al., 2010).

Relationships between phreatic flooding risk and elemental concentrations

Flooding risk index was found to be poorly correlated with elemental concentrations. No elements expressed a linear relationship at the 95% confidence level. However subtle trends were apparent. Amongst these potassium, arsenic and manganese were shown to be slightly negatively correlated with flood risk index (R of -0.22, -0.11 and -0.13 respectively) suggesting potential hydraulic redistribution mechanisms on the floodplain. However, as these effects are potentially subtle it is possible that larger sample numbers would be required to prove or disprove their significance.

Inter elemental relationships

A matrix of Pearson correlation coefficients for elemental concentrations was calculated based on FP-XRF data (Gentleman et al., 2009; Dalgaard, 2010). This correlation matrix is plotted in Figure 69 sized and coloured by correlation coefficients. Arsenic is shown to be most strongly correlated with Fe (R=0.75), Mn (R=0.69) and Zn (R=0.59). None of the elements analysed were found to be anti-correlated with As.

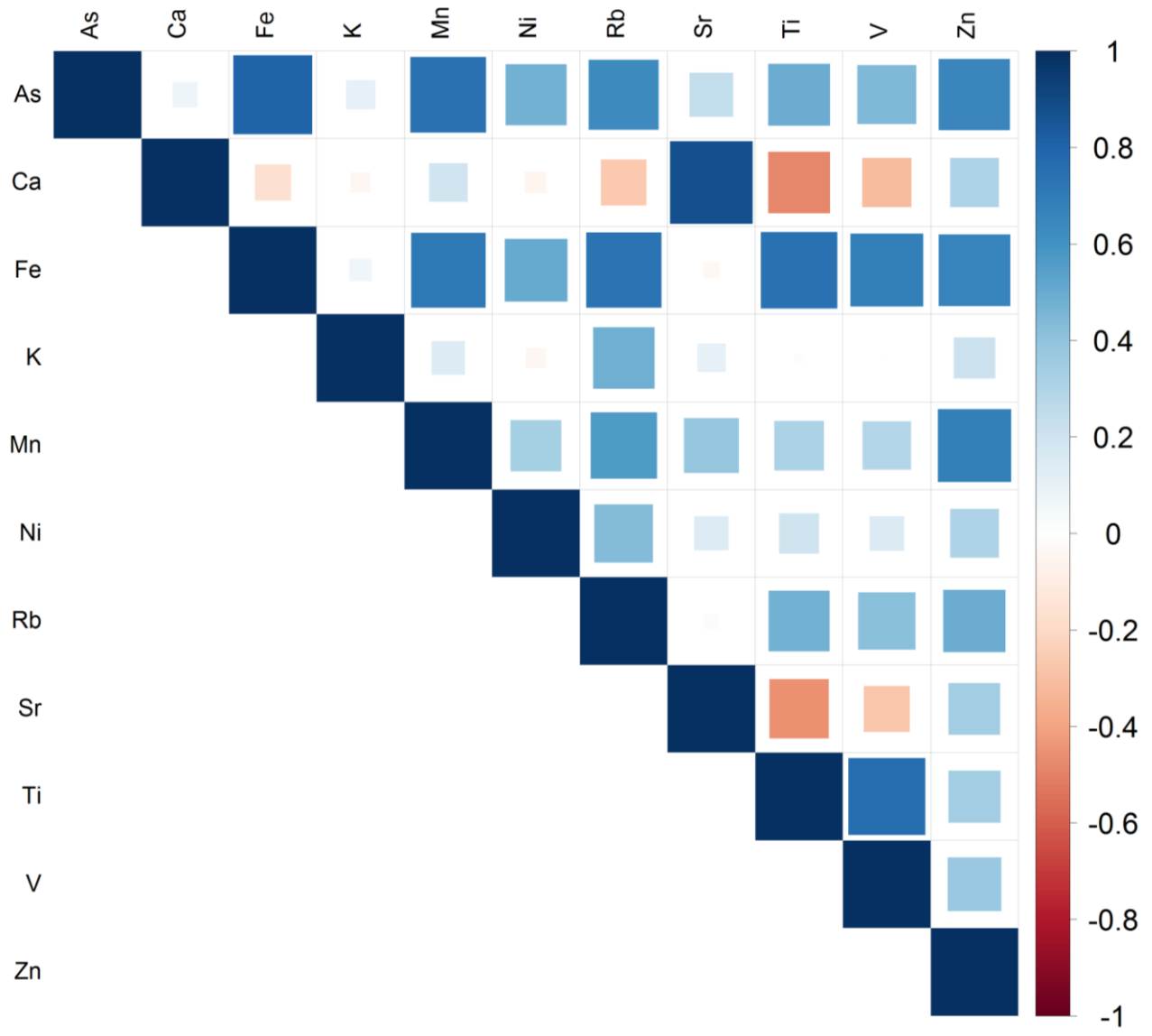

Figure 69*:* Inter-elemental correlation matrix plot, sized and coloured by correlation coefficient (R) values (red = negatively correlated variables, blue = positively correlated variables). Generated using corrplot and ISwR packages in R (Gentleman et al., 2009; Dalgaard, 2010; Wei, 2010).

Chemically there are numerous potential mechanisms by which arsenic may become immobilized in calcareous fluvisols. The most common mechanisms for arsenic immobilization in soils are sorption (either adsorption or absorption to the surface of mineral surfaces), co-precipitation (inclusion in the structure of a mineral during growth) or complexation with organic matter. While correlation does not necessarily imply causality the correlations between As and other analysed elements allow us to hypothesise the probable mineralogical associations of arsenic. The strongest inter elemental correlations with As are with Mn and Fe. Arsenic mobility has already been shown to be controlled in a variety of environments by surface sorption and coprecipitation with iron and manganese (hydr)oxides (Fuller and Davis, 1989; Bowell, 1994).

Equally iron is often a significant structural component in clay minerals e.g. chlorite and illite. Clay minerals have been shown to act as sorbents for both arsenite and de-protonated arsenate species in soils, particularly due to the presence of $AlOH_2$+edge sites. However, their sorption capacities are up to an order of magnitude lower than those of metal oxides, especially within the pH range experience in calcareous soils (Goldberg, 2002). Therefore in calcareous soils at high pH it is very likely that these strong correlations between As, Mn and Fe are due to the sorption or co-precipitation of arsenic with metal (hydr)oxide minerals.

Organic carbon and Arsenic

Although a weak positive correlation was found between oxidisable organic matter and arsenic in the analysed soils (R = 0.32) it was found that this relationship was not significant at the 95% confidence level (p = 0.15). This indicates arsenic complexation directly with solid organic matter is not significant compared to other arsenic immobilisation mechanisms within these soils and that it is not a factor controlling arsenic distribution on the floodplain. This is in contrast to the findings of Chen et al., (2002) who demonstrate a strong positive correlation (R = 0.80 at the 95% confidence level) between total arsenic concentrations and solid organic carbon concentrations in Florida soils. However, numerous studies have shown that organic matter concentration in pore-water is a major controlling factor on arsenic liberation due to both competitive adsorption (negatively charged organic molecules competing for surface sorption sites with anionic arsenic species) and facilitating the development of reducing conditions (Bauer and Blodau, 2006). Therefore whilst solid organic matter concentrations cannot be used as an indicator of arsenic presence they could be used to help determine the risk of arsenic liberation upon the development of reducing conditions.

Particle size distribution (PSD) and spatial soil textural trends

The use of laser diffraction in this study allowed a much more detailed understanding of arsenic distribution between particle size fractions in soil samples with limited textural heterogeneity. Differences between particle size distributions of soils with high and low arsenic concentrations were evident as can be seen in Figure 70). Both soils with high and low arsenic concentrations had a bimodal PSD however the size and position of the peaks were significantly different between the two groups. PSD of soils with high arsenic concentrations (Top 10% of soils by arsenic concentration) peaked at 45µm (4% by volume) and at 375µm (1.5% by volume). PSD of soils with low arsenic concentrations (lowest 10%) peaked at 75µm (3.7% by volume) and at 200µm (4.2% by volume).

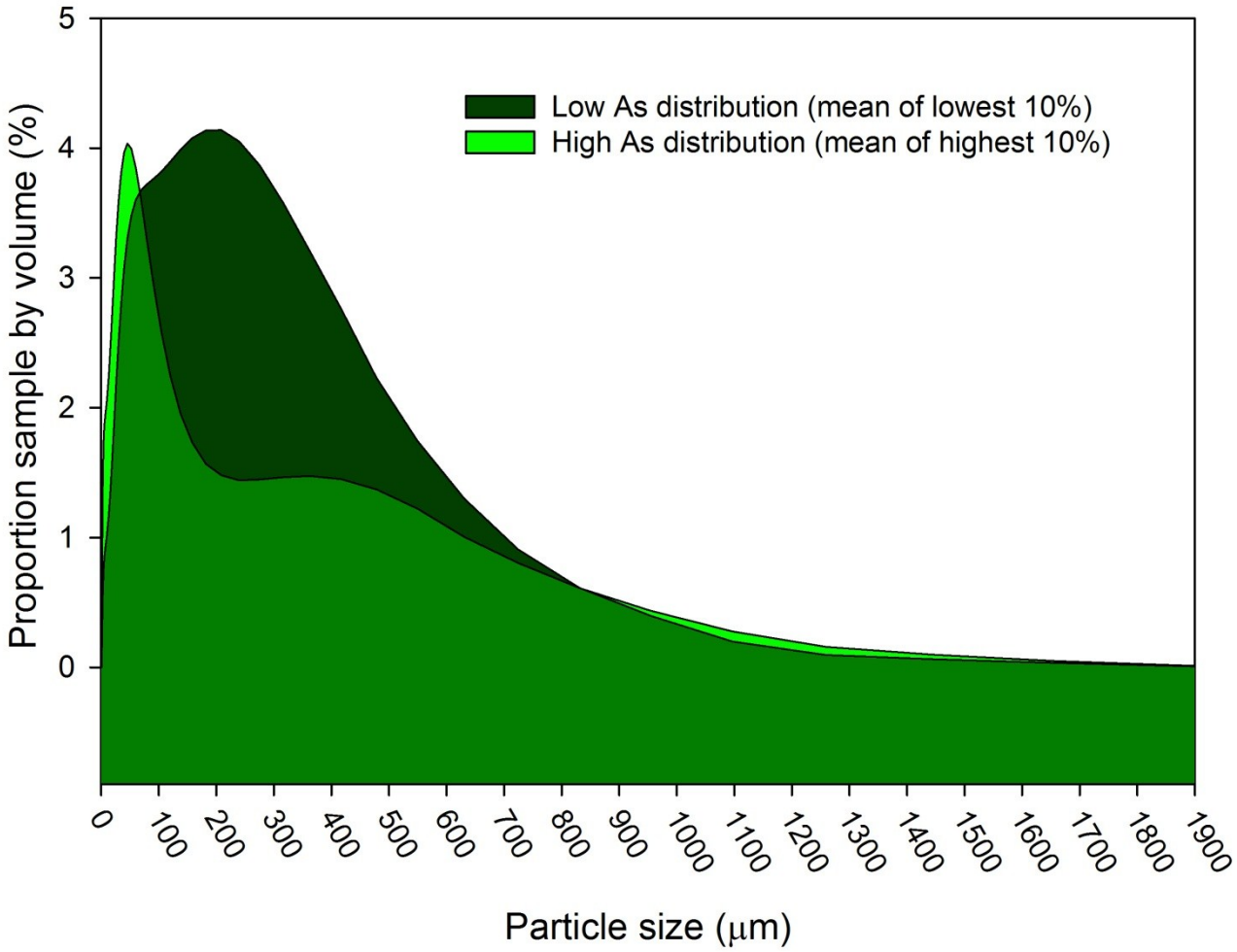

Figure 70: Comparison of the mean particle size distribution of soils containing high arsenic (top 10%) and low arsenic (bottom 10%)

The increased resolution (number of particle size classes) of laser diffraction analysis (compared to traditional sieving and sedimentation techniques) allows statistical analysis of relationships between distinct particle size populations and chemical properties. It can be seen that As, Fe, Mn and organic matter concentrations are all correlated with the finest clay fractions with correlation maxima at between 1µm and 10µm. For As, Fe and to a lesser extent Mn concentrations two more less prominent positive correlation peaks are also present at approximately 40µm (forming a shoulder from the main peak) and 850µm. Organic matter peaks at 65µm and again between 700µm and 1000µm. These relationships are shown in Figure 71.

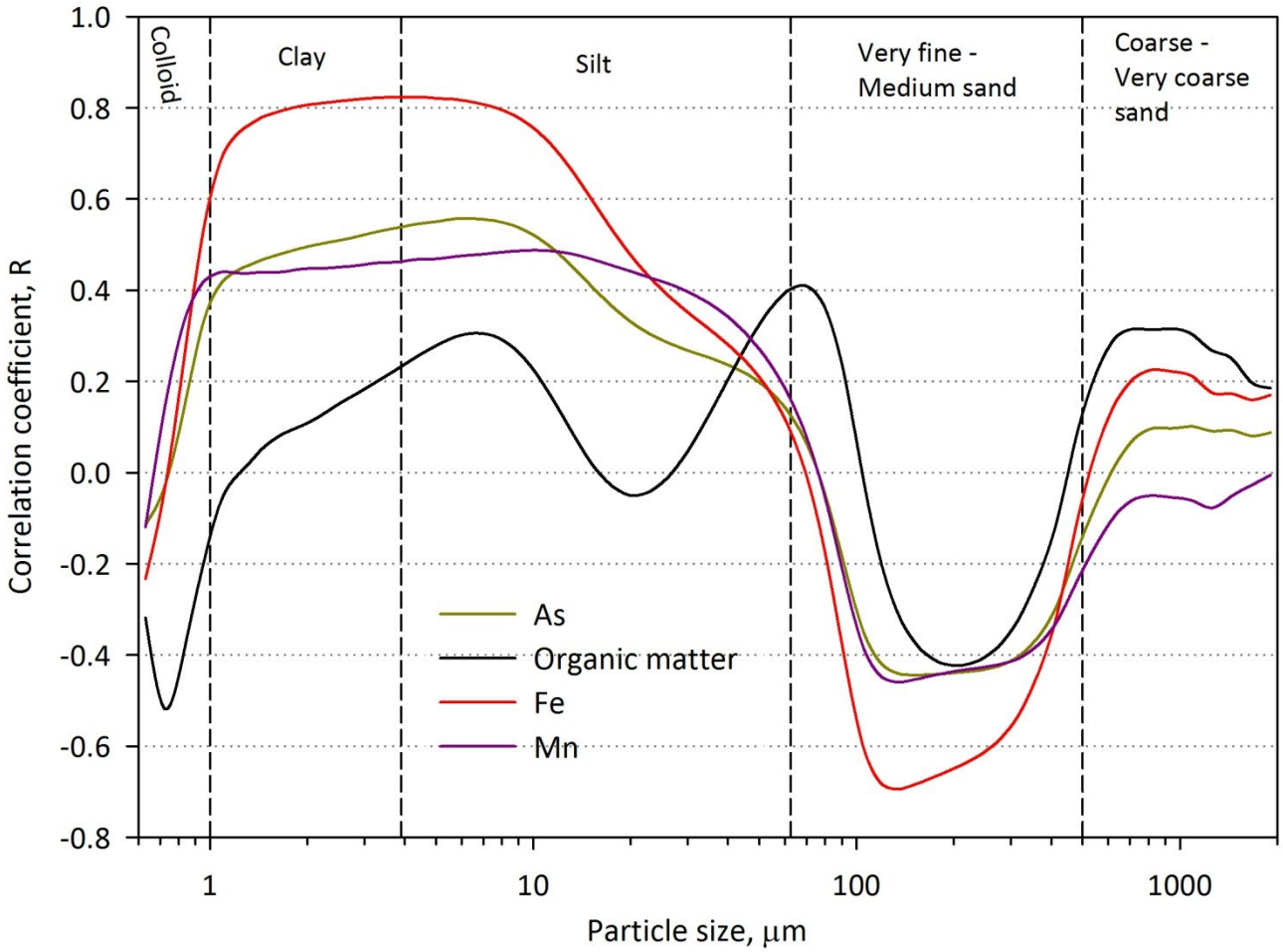

Figure 71: Correlation between sample proportion by particle size and As, Fe, Mn and oxidisable organic matter. Correlation coefficients with a magnitude greater than 0.243 represent a significant correlation at the 95% confidence level (N= 66).

The strong correlations found between arsenic, iron and manganese and particles with a size of 1-10 µm. can be attributed primarily to the increased surface area and hence reactivity of the fine particle size fraction compared to larger sand fractions. The large fractions in soils tend to be dominated by quartz due to its recalcitrant and resistant nature which is broken down less easily during the erosional process than softer and more friable minerals. Quartz also has a near neutral surface charge over a wide range of pH (Schindler and Kamber, 1968) and is therefore less chemically reactive than other minerals such as illite (a mineral found to be present in abundance in the clay fraction (<2µm) of these soils (see Chapter 3)

Typically natural floodplains demonstrate a finer particle size distribution with increasing distance away from the river channel within the extent of the flood (Guccione, 2009). During this study no statistically significant correlation between particle size and distance from the main river channel. This indicates that this either trend is lost due to reworking of the soil at a rate significantly greater than accretion, or that sediment input is controlled to a greater extent by minor channel systems penetrating distally from the main river into the floodplain. Significant reworking of the soil is indeed present on the floodplain due to agricultural activity and due to attempts to control flooding by the construction of damns and flood barriers have probably reduced accretion rates on this part of the floodplain. Due to the presence of extensive artificial flood barriers (digues) along the main river channel numerous gated drainage channels have been

constructed both to allow for flow into channel systems during dry periods and to facilitate the draining of flood-water upon a drop in river height.

Multivariate statistical analysis

Backward stepwise regression analysis was conducted incorporating measured elemental concentrations, active carbonate analysis, PSD and TOC. The most efficient combination of independent variables was found to be Fe, Mn and Clay % (22 observations per independent variable used) from which Equation 1 was derived.

As = 10.421 + (0.000522 * Fe) + (0.0112 * Mn) - (0.352 * Clay %)

This model fits the data with an R^2 value of 0.65 and a p-value of less than 0.001 indicating that the model can explain 67% of arsenic concentration variation in analysed soils and that the fit is significant to the 99.9% confidence limit. The standard error of the estimate provided by this model is 2.7 and the residuals expressed a normal distribution. P values for individual parameters all below 0.05 and so all contributed significantly to the model. Relatively high Variance inflation factors (VIF) found amongst the independent variables (Fe= 4.2, Mn = 1.8 and Clay %= 3.0) indicating multicollinearity. Removal of any of these variables from the model led to significant deterioration of its accuracy indicating that each of these variables are important, however multi-collinearity masks the relative importance of each of these values to the model.

Conclusions

The distribution of arsenic in top-soils of the Saône floodplain has been shown to be diffuse and linked to several physicochemical factors. The most important of the factors analysed was found to be the proportion of Fe and Mn rich fine clay sized particles in the soil matrix. This is thought to be due to the increased chemical reactivity of finer fractions and the important role of micro crystalline iron oxides in the immobilization of pore water arsenic. The inter elemental statistical relationships demonstrate that Fe concentration is the stronger predictor of As concentration suggesting that Fe minerals are the most important sorbents of As in this system even in alkaline soils where alternative minerals such as calcite are expected to play a more important role. . Distance from the main river channel was not found to be a good predictor of arsenic concentrations although data was found to be spatially auto-correlated with a range of 2.5km.

Chapter 5: The Impact of Redox Cycling: Arsenic Attenuation in Contaminated Floodplain Soils

Abstract

Contamination of floodplain soils with arsenic is extensive, particularly in areas with a legacy of industrial activity or prone to geogenic arsenic input.

It is well established that arsenic associated with metal-oxides in soils can be released under the reducing conditions experienced during flooding due to desorption, mineral dissolution and competitive sorption. However, the cumulative effects of seasonal flooding and draining cycles on arsenic mobility are currently poorly understood.

We show through a combination of batch experiments, spectroscopy and thermodynamic and kinetic modelling that the cumulative effects of cyclic flooding can act to attenuate arsenic mobilised during reducing conditions, in part due to depletion of biologically degradable organic carbon (BDOC). We demonstrate that arsenic mobility during cyclic redox conditions can be described by fast (intra-cycle) and slow (inter-cycle) immobilising processes and suggest that effective hydrological management in many redox-oscillating environments may be fundamental to limiting arsenic release.

Introduction

Arsenic is an infamous carcinogen (WHO IARC, 2004), ubiquitous in the environment and subject to a variety of mobility altering processes induced by redox changes experienced in temporally flooded soils (fluvisols). As both the toxicity and mobility of arsenic are highly dependent on oxidation state and chemical speciation (Bissen and Frimmel, 2003), understanding the long term effects of temporal flooding is essential, particularly as recent work has shown that hydrological management may impact arsenic mobility in shallow alluvial aquifers(Benner, 2010; Neumann et al., 2010).

Fluvisols are used extensively for agriculture (Verhoeven and Setter, 2010) despite frequently hosting elevated concentrations of arsenic (Overesch et al., 2007). Common sources of arsenic on floodplains include mine-effluent, pesticides and poultry waste (Smedley and Kinniburgh, 2002), although disperse contamination may also be geogenic (Winkel et al., 2008) or due to atmospheric deposition (Couture et al., 2008). Tracing the origin of arsenic on floodplains is often problematic due to its mono-isotopic nature, lack of durable chemical source signatures and diverse watershed land-use. Fluvisols frequently act as sinks for river-borne contaminants but can also act as contaminant sources due to remobilisation (Roberts et al., 2010). Re-mobilized contaminants threaten human health through accumulation in crops (Meharg and Rahman, 2003) and contamination of increasingly exploited shallow alluvial aquifers (Ahmed et al., 2004).

Much attention has been paid to biogeochemical mechanisms responsible for arsenic mobility in soils upon the development of reducing conditions (McGeehan and Naylor, 1994; Islam et al., 2004) and to hydrological transport processes determining arsenic fluxes from sediments (Mukherjee et al., 2008; Nath et al., 2009). Recently comprehensive field studies have greatly advanced our understanding of the processes affecting arsenic mobility in nature (Neumann et al., 2010) but there is still a scarcity of controlled experimental studies accurately simulating cyclic redox conditions experienced in floodplains, paddy fields and shallow aquifers (Stucki, 2011).

The objectives of this study are to determine both the short and long term geochemical controls on arsenic mobility in one floodplain soil, and to improve our understanding of redox-oscillating environments. To

simulate the natural redox cycles experienced by soils on a heavily managed floodplain, batch redox-oscillation bioreactor experiments were conducted on the top-horizon (0-15cm) of an arsenic-doped calcic fluvisol prone to phreatic and fluvial inundation. Changes within the bioreactors were monitored throughout the experiment using an array of biogeochemical tools. The sampling location, flooding modes and extent are illustrated in Figure 72.

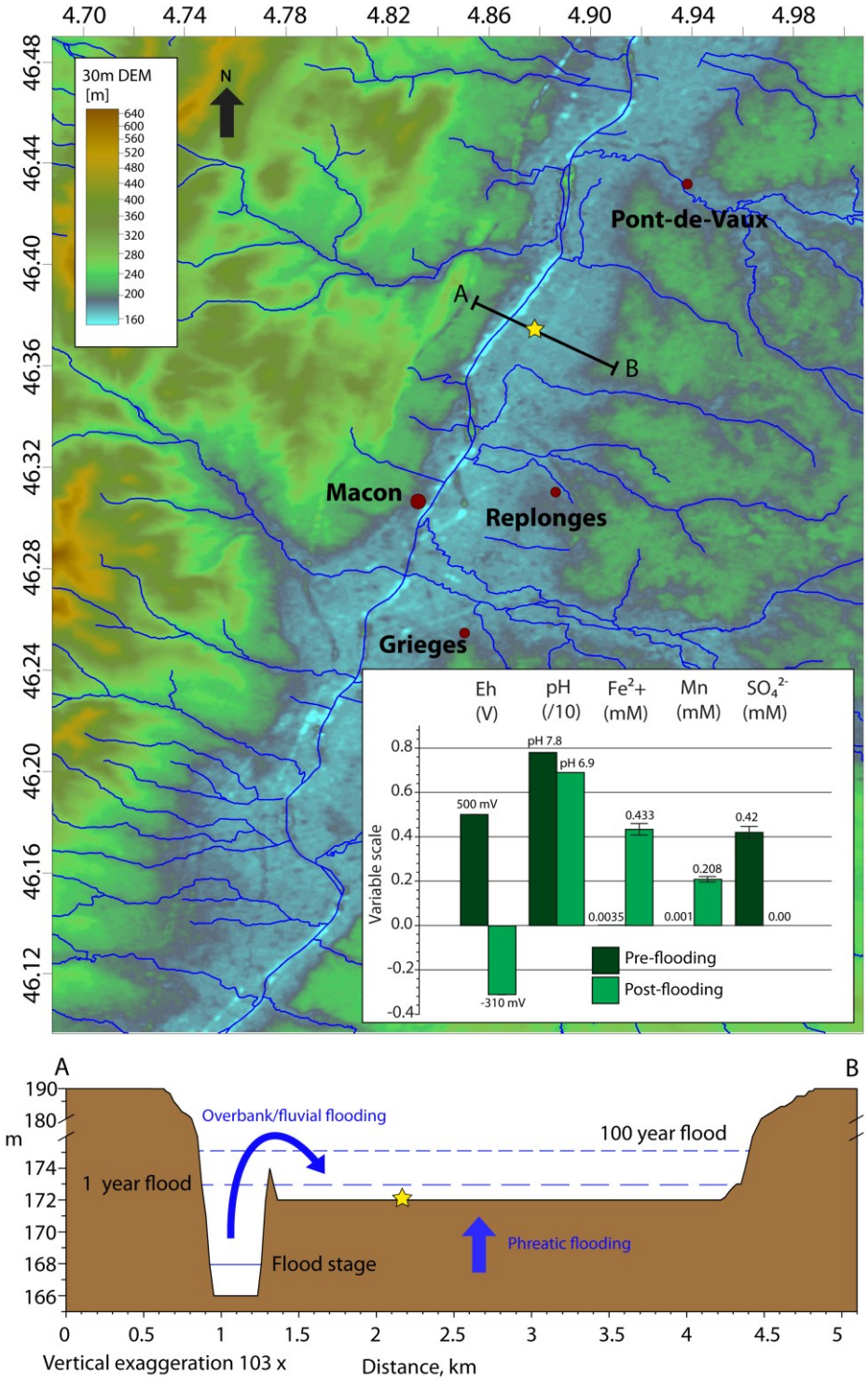

Figure 72: : TOP: Map of the extent of the Saône floodplain showing the sampling location (yellow star), towns (red circles), topography (METI/ERSDAC et al., 2009) and the hydrological network (Institut Geographique National de France, 2010)(in blue). Coordinates are in decimal degrees based on the WGS84 geoid. BOTTOM: An idealised cross-section of the floodplain at the sampling location illustrating the

flooding modes and extent predicted to occur yearly (long dashed line) and every 100 years (short dashed line). INSET: Bar chart comparison of pore water chemistry before and after 30 days of laboratory flooding of soils from the sampling location.

Aqueous chemistry (cations, anions, dissolved organic and inorganic carbon (DOC and DIC)), mineralogy (powder X-ray diffraction (XRD)) and solid arsenic speciation (X-ray absorption spectroscopy (XAS)) were monitored in addition to changes in the bacterial community (16S rRNA). Results were interpreted using thermodynamic and kinetic geochemical modelling implemented in PHREEQC (Parkhurst et al., 1999). The model is used as a diagnostic tool to interpret the measured temporal changes and as a prognostic tool to determine the most probable chemical mechanisms responsible for observed changes in As mobility.

Methods

Soil selection:

The soil used in this study was sampled from the east floodplain of the Saône River close to the town of Macon in eastern France. The soil was taken from the top horizon (0-15cm) of a natural undisturbed mollic-fluvisol occurring on the lower terrace of a minor irrigation channel (46.373107^{o}N, 4.879856^{o}E). Established soil sampling protocols were observed (U.S. EPA Environmental Response Team, 2000) including using only acid washed (5% HNO_3) plastic tools. The sample was transferred directly to a double sealed polyethylene bag and transported on ice. It was subsequently stored at 4^{o}C until the start of experiments.

Soil characterisation:

Elemental composition of the soil was determined by total acidic dissolution (HNO_3 + HF + H_2O_2, H_3BO_3 + HF) (U.S. EPA, 1996) followed by inductively coupled plasma mass spectroscopy (ICP-MS) analysis. The soil was found to contain a moderately elevated arsenic background value of 29.9 ppm which is often observed in mollic fluvisols (Du Laing et al., 2009). Laser granulometric analysis (Malvern Mastersizer 2000) after de-carbonation revealed that the soil was dominated by silt and clay (1% coarse sand, 16% fine sand, 24% coarse silt, 25% fine silt and 34% clay). Bulk mineralogy was analysed by XRD for <2mm, <2μm and <0.2μm fractions; Quartz, Calcite, Illite and Chlorite were identified. Total organic carbon content was determined to be 33.4 g/kg by loss of ignition. These characteristics are indicative of flooding regime with a long periodicity and low flow rates. Total water content was 32.57%. Measured soil pH was 7.8 and was strongly buffered by large quantities of calcite (total $CaCO_3$ was 148 g/kg).

Preliminary experiments: Determination of natural redox fluctuations

To aid experimental design, preliminary laboratory experiments were conducted to determine the extent of redox fluctuation occurring naturally in the investigated soil.

A passive diffusion pore-water sampling device was used to determine the effects of flooding on redox conditions and aqueous chemistry in interstitial pore water. Millipore hydrophilic HAWP membranes with a pore size of 0.45 μM were first washed with 5% HNO_3 and rinsed thoroughly with 18.2MΩ cm water before being fixed over acrylic cells filled with 18.2MΩ cm water. The sampling device was then placed in a flooded soil (15cm of N_2 degassed overlying water) for 30 days to allow for soil reduction and osmotic equilibration before analysis. Eh and pH measurements were taken by gently pushing the electrode into the soil approximately 5cm from the sampler, immediately prior to removal. As saturation of pores in the un-flooded sample was insufficient to allow the use of diffusion membrane samplers, interstitial water was extracted by centrifugation at 8000 rpm for 30 minutes.

An Eh change from +500 to -310mV was recorded, crossing the MnO_2/Mn^{2+}, NO_3^-/NH_4^+, $HAsO_4^{2-}/H_3AsO_3$, $FeOOH/Fe^{2+}$ and SO_4^{2-}/HS^- thermodynamic equilibria (James and Bartlett, 1999), predicting major changes to aqueous chemistry (Figure 72). A concurrent drop in pH from 7.8 to 6.9 occurred despite the presumed production of hydroxide by reductive processes e.g. $FeOOH + H_2O + e^- \rightarrow Fe^{2+} + 3OH^-$. This is attributed to accumulation of CO_2 in pore-water. An increase in $Fe^{2+}_{(aq)}$, $Mn^{2+}_{(aq)}$ and DOC concentrations was also recorded, in addition to elimination of aqueous sulphate, indicative of heterotrophic iron, manganese and sulphate reduction.

Soil preparation:

The field moist soil was removed from polyethylene sampling bags and suspended in a 0.02 mM background sodium chloride electrolyte solution (prepared with 18.2MΩ cm water) at a concentration of approximately 100 g/L (dry-weight equivalent). The suspension was shaken for 5 minutes in a polyethylene bottle and then passed through a 1mm sieve to remove larger rock fragments and large solid organic material. This procedure was repeated until a homogeneous suspension was achieved.

The suspension was doped with 900 ppm / 12 mM of arsenate ($Na_2HAsO_4 \cdot 7H_2O$ – Sigma-aldrich) and left to equilibrate on an agitator for 1 month before the start of reactor experiments.

Experimental design and redox oscillation procedure

A novel redox-cycling bioreactor system, based on a design by Thompson et al (Thompson et al., 2006) was filled with the arsenic doped soil suspension.

The bioreactor consisted of a 2 part Pyrex® glass pressure reaction vessel (Ace- Glass Inc, NJ, USA). The lower part of the reactor contained a working volume of 1 L and used a water jacket to allow for precise temperature control. Ethylene glycol was added to the temperature regulating circuit to avoid fungal and bacterial growth over the duration of the experiment. The upper part of the reactor contained a headspace volume of approximately 300 mL and used ace-glass threaded connections for sampling, electrodes and mechanical agitation (seals secure up to 2.4 bar of internal/external pressure difference). The agitation shaft and blades were Teflon coated and prior to the introduction of soil suspensions the reactor and all glass and plastic parts were washed with 5% HNO_3 then rinsed thoroughly in 18.2MΩ cm water.

Solid polymer open junction Xerolyt electrodes (Mettler-Toledo, France) were selected for their long term stability and low electrolyte leak rates. The Eh and pH electrode signals were connected to FET instrumentation amplifiers with high input impedance. The signal was then passed to an Agilent acquisition/switching unit (34970a) connected to a PC running Agilent BenchLink Data Logger 3 software. Eh and pH data was recorded every 30 seconds.

The suspension was subjected to multiple cycles of reduction and oxidation to replicate flooding and draining experienced in nature and to determine the cumulative effects of such cycling on arsenic mobility. Eh control, based on imposed Eh limits (-310/+500 mV) was implemented by modulating the sparging gas between N_2 and compressed air automatically via the Agilent switching unit, a relay board and a system of solenoid valves. Reducing conditions were stimulated by N_2 sparging (7 days) and oxidising conditions were stimulated by compressed air sparging (7 days). A total of 5.5, 14 day cycles were conducted over a period of 77 days at a constant temperature of 31°C (+/- 1°C). The suspension was sampled on days 1, 4 and 7 of each half cycle, pH and Eh were monitored constantly. Gas flow rate was set to a constant 30 ml/min for both compressed air and nitrogen inputs.

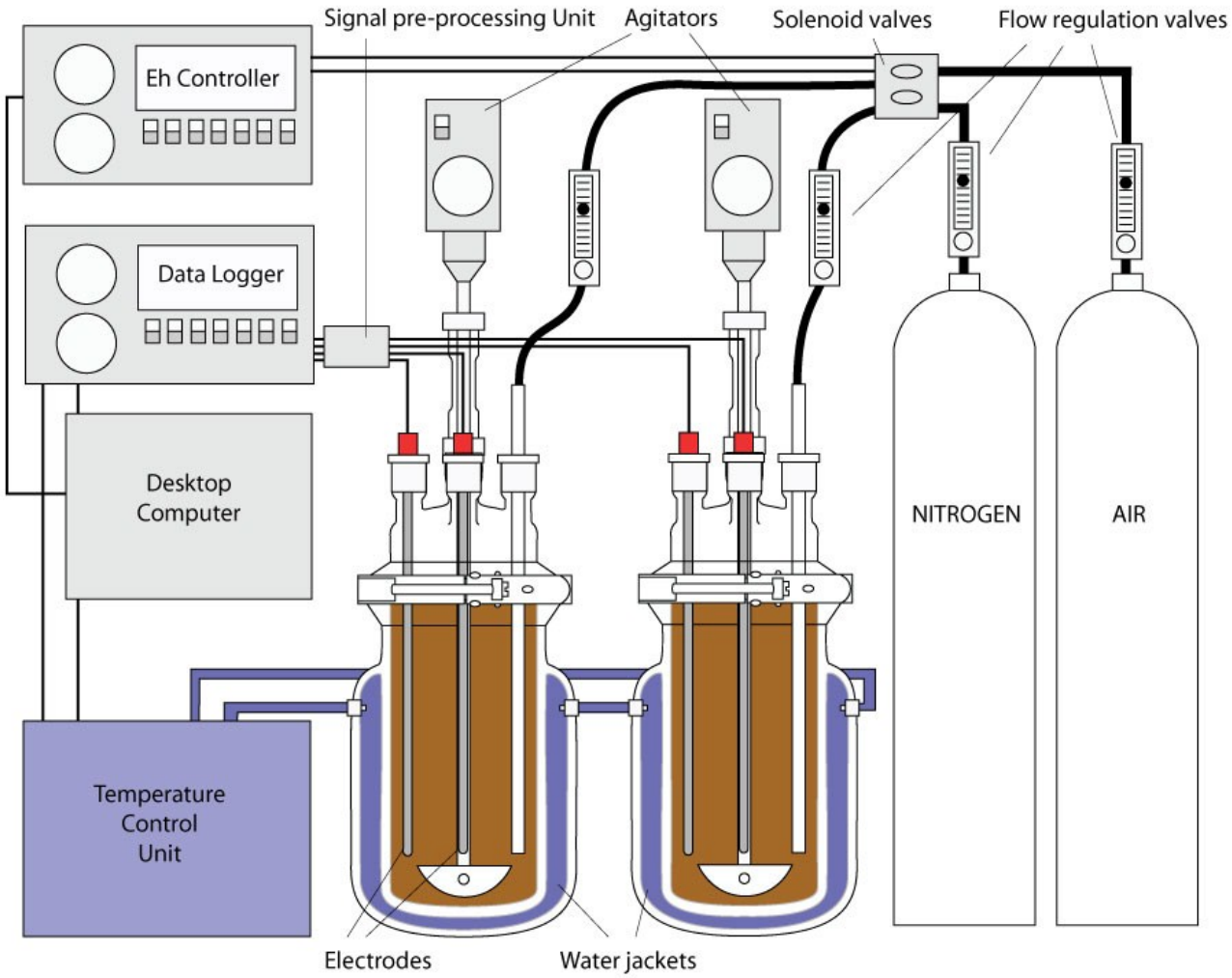

Figure 73: Schematic of the redox-cycling bioreactor system.

Sampling procedure:

9 ml of suspension was sampled through a connection on the top of the reactor by pulling on a syringe connected to a sampling tube. Prior to sampling the syringe and the tube were purged with either air or nitrogen (dependant on the half cycle). The syringe was then sealed and transferred to a 100% N_2 atmosphere glove-box (Jacomex < 0.1ppm oxygen). The suspension was centrifuged at 4300 rpm for 30 minutes to separate solid particles from the aqueous phase (particle size left in suspension < 0.2μm assuming spherical particle geometry and density of 2.65 gcm^3 and a fluid density of 1gcm^3 calculated from Stoke's law). The resulting supernatant was then filtered to 0.22 μm to ensure no large particles were disturbed during supernatant removal. The resulting solution was separated for analysis and the solid pellet frozen immediately in liquid nitrogen where it was stored until it was defrosted (in the glove box) to allow preparation of pellets for XANES and Mössbauer analysis. Aqueous samples for cation analysis were acidified with HNO_3 and stored at 4°C with other samples (TOC and anions) until analysis.

Analytical methods

All chemicals were analytical grade from Fluka, Sigma-Aldrich or Merck and were used as received. Standards and reagents were prepared with high purity 18 MΩ cm water (Millipore).

Pore-water analysis:

Analysis of total Ca, Mn, Fe and As concentrations in the aqueous phase was performed with inductively coupled plasma optical emission spectroscopy (ICP-OES) after appropriate dilution and acidification, using a

Perkin Elmer OPTIMA 300 DV (Perkin Elmer, France). Matrix matched standards were used for all calibrations.

DOC and DIC concentrations were determined using a Shimadzu TOC-5000 (Shimadzu, France) using a sample dilution of 1:100, all glassware was burned at 400^{o}C for 4 hours before use to avoid contamination.

Major anions (Chloride, Nitrate and Sulphate) were analysed by ion chromatography using a Metrohm 761 Compact IC equipped with a conductivity detector, a high capacity analytical separating column (Metrosep A Supp 5 -250) and a low capacity guard column (Metrohm A Supp 5). Samples were injected through a 20 µL loop into a carbonate-bicarbonate mobile phase (H_2CO_3/HCO_3^- 1 mM / 3.2 mM) with a flow rate of 0.7 mL/min and an operating backpressure of 10-12 MPa. This resulted in a total sample run time of approximately 30 minutes per sample.

Eh and pH were recorded constantly within the reactors (every 10 seconds) using Xerolyt Solid polymer open junction electrodes. A 5 point calibration (2, 4, 7, 10, 12) was performed for the pH electrodes at the start and end of the experiment showing that the electrode response had not shifted more than 0.02 pH units (within the pH range used in the experiments) during the 77 day experimental duration.

Measured Eh readings were converted to a redox potential with respect to the Standard Hydrogen Electrode (SHE) by adding the difference of the measurement of the redox potential in a ZoBells solution (3.3 mM $K_3Fe(CN)_6$ and 3.3 mM $K_4Fe(CN)_6$ with its theoretical value of +428 mV. The calculated difference was equal to the electrode manufacturer specification of 207mV. The Eh electrode was found to drift by 4mV upon measuring a ZoBells solution at the end of the 77 day experiment.

Microbial community analysis:

In order to monitor changes in the composition of the bacterial community occurring during the course of the experiment additional 1 ml suspension samples were taken on days 7 (reduced), 67 (oxic) and 77 (reduced). Two gram sub-sections sediment were used for DNA and RNA extractions. Total genomic DNA and RNA were extracted using the PowerSoil RNA kit, with the DNA elution accessory (MOBIO, Carlsbad, USA). The extractions were performed according to the manufacturer's recommendations. RNA extractions were treated with DNASE and then purified using the RNeasy kit (Qiagen, Hilden, Germany). Prior to polymerase chain reaction, the bacterial 16S rRNA gene was reverse transcribed using BioScript reverse-transcriptase with the GM4 primer(Kane et al., 1993). An initial melting step with only the primers was incorporated into the reaction. The 16S rRNA gene for bacteria was amplified from total genomic DNA and cDNA using the GM3F(Muyzer et al., 1995) and GM4R primers. PCRs were performed with TaKaRa Ex Taq (TaKaRa, Otsu Japan) in 50 µl reactions. PCR reactions were performed with the following cycling conditions: 95°C for two minutes, then 30 cycles of 95°C for 30 seconds, 42°C for 30 seconds and 72°C for 3 minutes, followed by a final incubation step at 72°C for 10 minutes. PCR products were visualized on an agarose gel, and the 16S band excised. PCR products were purified using the QIAquick Gel Extraction Kit (Qiagen, Hilden, Germany). Two microliters of purified DNA were ligated in the pGEM T-Easy vector (Promega, Madison, USA) and transformed into competent E. coli TOP10 cells (Invitrogen, Carlsbad, USA) according to the manufacturer's recommendations. Transformation reactions were plated on LB-agarose plates. Overnight cultures were prepared from individual colonies picked from these plates. The 16S inserts were amplified using the T7 and SP6 primers. The amplification products were then purified using Exonuclease I (NEB, Ipswich, USA) and Shrimp Alkaline Phosphatase. The inserts were then sequenced in one direction, with the GM4 primer using the BigDye Terminator v3.1 Cycle Sequencing kit (Applied Biosystems, Foster City, USA). Samples were run on an Applied Biosystems 3100 Genetic Analyser (Foster

City, USA). Phylogenetic analysis were carried out using the ARB (Ludwig et al., 2004) software package with the Silva 98 release database(Pruesse et al., 2007).

Powder X-ray Diffraction Analysis:

Powder XRD analysis of soil mineralogy was conducted on the suspension at day 1 and on the resulting suspension on day 77. Less than 2mm, 2μm and 0.2μm fractions (separated using standard techniques (REF) were analysed using a Bruker D5000 equipped with a Kevex Si(Li) solid detector and a Cu $K_{\alpha 1+2}$ radiation source. Larger fractions were wet ground (18.2MΩ cm water) in a centrifugal mill. Intensities were recorded at 25°C over a range of 2 – 80° 2θ with a step interval of 0.02° 2θ and a counting time of 3 seconds per step. Full-widths at half-maximum intensity (fwhm) were determined for diffraction maxima using the standard EVA program available from Bruker.

X-ray absorption spectroscopy

XAS measurements were performed at the As K-edge (11,867 eV) at the GILDA (BM-08) beamline (Pascarelli et al., 1996) at the European Synchrotron Radiation Facility (ESRF) in Grenoble (France).

Beam-line optics includes a fixed exit monochromator with a pair of Si [311] crystals, and a pair of Pd coated mirrors for efficient harmonic rejection and vertical focusing of the X-ray beam. A dynamic sagittal (horizontal) focusing of the X-ray beam is realized by bending the second monochromator crystal. The bending magnet source and beamline optics provide an intense (typical photon flux at 12 KeV ~10^9 ph·s^{-1}) and submillimetric (spot size ~ 500 (h) x 250(v) μm) beam on the sample. Considering the vertical aperture of the main slits (1mm) and the monochromator crystals, the energy resolution at the As K-edge was about 0.5 eV. In order to reduce the thermal contribution to the Debye-Waller factors and to prevent possible beam-induced redox reactions, all samples were measured in high vacuum (~10^{-5} mbars) and at liquid nitrogen temperature (77 K). Local structure around As was obtained by quantitative refinements of the EXAFS signal. Fits were performed in the back-transformed reciprocal space (k) in the range 4−12 $Å^{-1}$, using a dedicated software package(Monesi et al., 2005) based on MINUIT routines from CERN libraries(James, 1975). The ATOMS(Ravel, 2001) package was used to generate the atomic clusters centered on the absorber atom, which were used as reference structures for calculating theoretical amplitude and phase back-scattering functions with the FEFF8 package (Ankudinov et al., 1998).

Preparation of XAS samples and standards

As(III) and As(V) adsorbed on pure calcite were used as references for LCF. Powder X-ray diffraction analysis was used to verify the crystallography of $CaCO_3$ (≥99% pure, Fluka Chemie AG, CH) as calcite prior to the preparation of standards. As(III) and As(V) solutions were prepared from As_2O_3 (≥99.0% pure, Fluka anal. Sigma Aldrich, CH) and $AsHNa_2O_4.7H_2O$ (≥98.5% pure, Fluka anal. Sigma Aldrich, CH) respectively.

As(III) and As(V) standards were prepared in jacketed glass reactors by adding 20mM As_2O_3 / 30mM $AsHNa_2O_4.7H_2O$ to homogeneous suspensions of calcite (50.045g/L, 0.5M) in ultra-pure water (18.2MΩ cm). Anaerobic conditions were maintained during preparation of As(III) standards by sparging of pure N_2 gas. A constant temperature of 40°C was achieved by use of water jackets and the pH of the suspensions was adjusted by addition of HNO_3 (65%) and NaOH (3M) as required. As(III) standards were prepared at pH 7 and As(V) standards were prepared at pH 6.3. The suspensions were left to equilibrate under these conditions for a period of 6 days.

Solids were collected from reactor suspension samples and arsenic standards by vacuum filtration through 0.22μm cellulose nitrate membranes inside a 100% N_2 atmosphere glove-box (Jacomex < 0.1ppm oxygen). The membranes were dried for 24 hours in the glove box before being sealed with kapton tape and fixed to

XAS sample holders. Loaded sample holders were transferred from the glove box to the sample chamber using double sealed anaerobic jars.

^{57}Fe Mössbauer spectroscopy

Mössbauer spectrometry was performed on solid fractions (obtained by centrifugation) from suspensions sampled on days 4, 14, 70 and 77. The frozen pellets were defrosted in the glove box and deposited on polycarbonate sample holders (diameter 1.5 cm). The sample holders were capped and then sealed with an epoxy resin. They were then transferred in the glove box to a protective container (100% N_2 atmosphere) before being transported for analysis.

The Mössbauer spectra were recorded at 77 K using a constant acceleration spectrometer and a ^{57}Co source diffusing into a rhodium matrix. Velocity calibrations were carried out using α-Fe foil at room temperature (RT, 295 K). All isomer shifts are reported relative to the α-Fe spectrum obtained at RT.

Mössbauer spectra were described using the Mosfit fitting model (MOSFIT: Teillet and Varret unpublished program). This fitting model uses a discrete number of independent quadrupolar doublets of Lorentzian lines where the line width at half-height Γ (mm s^{-1}), the centre shift δ (mm s^{-1}) and the quadrupole splitting ΔE_Q (mm s^{-1}) were refined using a least-squared fitting procedure.

Thermodynamic and kinetic modelling:

The model, implemented in PHREEQC, simulates multiple cycles of biologically mediated oxidation and reduction in a closed system containing organic matter, an active microbial community and typical soil mineralogy. To our knowledge this is the first model to incorporate redox oscillating conditions rather than one-time reduction/oxidation events. Following evidence from 16S rRNA and aqueous chemistry analyses, ferric iron and O_2 are implemented as TEAs in the model. Thermodynamic predictions based upon the initial soil suspension following sodium-arsenate addition suggest strong super-saturation with respect to ferric-arsenate phases which are also often reported in highly contaminated soils (Langmuir et al., 2006). The precipitation of such phases is therefore allowed in the model during the equilibration period prior to cycling.

The reactor suspension is modelled as a homogeneous solution in equilibrium with calcite, illite, scorodite and the reactor head-space atmosphere. Redox equilibrium is controlled primarily by the hematite/magnetite couple (Pang et al., 2007). Selected reactions controlling pore-water chemistry are rate-controlled and are managed in kinetic blocks each corresponding to 7 day half-cycles. These reactions and kinetic formulations are detailed in Table 1.

DOC concentration (CH_2O) is controlled by a combination of production (bacterial hydrolysis of solid organic matter) and consumption/mineralisation processes (aerobic metabolism and heterotrophic iron reduction). Degradation of solid organic matter by hydrolysis is described by the first order kinetic (one-G) model (Van Cappellen and Wang, 1995). An exponential decay function, based upon the decreasing lability of solid organics, was applied to the rate of bacterial hydrolysis, derived from experimental DOC concentrations.

Monod kinetic formulation is used to couple DOC mineralisation to reduction of TEAs (O_2, $Fe(OH)_3$ and FeOOH). DOC consumption processes are therefore dependent on the concentration of DOC and the relevant TEA, a reduction rate constant for each TEA, and an inhibition factor to reflect inhibitory and competitive effects in the presence of more efficient TEAs (R3 and R4) (Canavan et al., 2006). O_2 consumption is also subject to an acceleration constant representative of the lag and growth phase of the

microbial community adapting to the use of a new TEA. All constants, reactions and kinetic formulations are detailed in Tables 19 and 20.

Ferric iron reduction is modelled by a combination of nano-lepidocrocite (γ-FeOOH) and ferrihydrite ($Fe(OH)_3$) (Equations R3 and R4). Both minerals have been previously shown to be subject to microbially mediated reductive dissolution during reducing conditions (Bonneville et al., 2004) and oscillate between super-saturation and under-saturation during cycling (Figure 77).

The rate of slow retention is therefore determined by total reducible ferric iron in the system, the concentration of aqueous arsenic and a rate constant (R6) resulting in highest retention rates during initiation of O_2 sparging and hence ferric (hydr)oxide precipitation in the presence of residual aqueous arsenic, primarily arsenite, mobilised during the reducing half-cycle.

Inner sphere sorption of Fe^{2+} in exchange for H^+ on illite edge sites as reported by Géhin et al. (2007) is implemented with a log k value of -4.7 and 20 g/L illite.

Results and Discussion

Active microbial community during redox-cycling

Bacterial 16S rRNA sequence libraries were generated from RNA extracted from bioreactor samples taken on days, 7, 67 and 77 to identify the active microbial populations during the reducing and oxidising phases, which contributed to the observed geochemical changes. A broad genetic diversity was present in all samples, likely due to the variety of energy generating processes possible in such temporally dynamic chemical environments.

Overall similarity between the samples based on phylotype composition was low (<28%), regardless of the phase. In general, distinct patterns in 16S rRNA phylotypes based on presence or absence; as result of alternating redox conditions were not observed in the libraries. This is unsurprising given that many bacteria are capable of operating under both aerobic and anaerobic conditions. Furthermore, the metabolisms of many phylotypes detected in this study could not be inferred, due to their low identity to properly described bacterial isolates. However, consistent with our experimental results, phylotypes closely related to known heterotrophic bacteria (93/127 sequences) were the largest group of bacteria detected within the bioreactors. Presumably these bacteria were responsible for aerobic and anaerobic oxidation of organic matter within the bioreactors. Phylotypes related to Fe-cycling bacteria, such as *Geobacter* and *Leptothrix* were detected, consistent with our experimental results, which show the importance of iron redox processes in this soil. *Geobacter* sp. are known Fe-reducing bacteria (IRB) (Lovley et al., 1993) and likely contributed to Fe(III)-reduction during the reducing half-cycles. However, these phylotypes were also detected during the oxidising half-cycles. Some Geobacter species when exposed to oxygen are able to use it as terminal electron acceptor (Lin et al., 2004). Therefore, it is possible that these organisms contributed to organic matter oxidation during the oxidising half-cycles. Phylotypes related to Fe-oxidizing bacterium *Leptothrix* sp. (van Veen et al., 1978) were only detected during the oxidising half-cycles, indicating that microbial oxidation of Fe(II) was on going during this period. *Pseudomonas* related phylotypes were detected under both oxidizing and reducing conditions. This group of bacteria contains metabolically diverse groups of heterotrophic bacteria (Moore et al., 2006) including bacteria capable of the oxidation of iron(Straub et al., 1996), sulphide (Mahmood et al., 2009) and arsenate reduction (Freikowski et al., 2010). However, given the presence of many heterotrophic bacterial species in both oxidizing and reducing phases, it is likely that these organisms were responsible for the oxidation of organic matter during both phases.

Phylogenectic affiliation	Closest isolate	Potential role	% Identity closest isolate	RNA		
Beta-, Gammaproteobacteria	*Hydrogenophaga taeniospiralis*, AF078768	Hydrogen oxidizing	98-95	**T=0**	**T=67**	**T=77**
Beta-, Gammaproteobacteria	*Leptothrix cholodnii*, X97070	Heterothropic, Fe-oxidizing	98-95	0	1	0
Beta-, Gammaproteobacteria	*Methyloversatilis universalis*, AY436796	Heterotrophic	98-95	0	4	0
Beta-, Gammaproteobacteria	*Methylibium aquaticum*, DQ664245	Heterotrophic	98	2	0	2
Beta-, Gammaproteobacteria	*Nitrosomonas oligotropha*, AJ298736	Ammmonia oxidizing	90-95	0	0	0
Beta-, Gammaproteobacteria	*Propionivibrio pelophilus*, AF06690	Heterotrophic	90-95	6	0	1
Beta-, Gammaproteobacteria	*Pseudomonas alcaligenes*, DQ115541 *Pseudomonas sp. QZ1*	Heterotrophic Heterotrophic, sulphide oxidizing	97-92 96-92	2	0	0
Beta-, Gammaproteobacteria	*Uncultured sulfur-oxidizing symbiont bacterium*, AM936001	Sulphide oxidation	95	0	7	7
Beta-, Gammaproteobacteria	**Other Beta-, Gammaproteobacteria**	Unknown		9	1	0
Alphaproteobacteria	*Devosia limi*, AJ786801	Uknown	98-92	0	2	9
Alphaproteobacteria	*Magnetospirillum gryphiswaldense*, Y10109	Mixatrophic	92	0	2	0
Alphaproteobacteria	*Mesorhizobium metallidurans*, AM930381	Heterotrophic	98-92	0	0	5
Alphaproteobacteria	*Rhodobium orientis*, D30792	Heterotophic	92	1	0	1
Alphaproteobacteria	*Roseomonas terrae*, EF363716	Heterotophic	98	0	0	0
Alphaproteobacteria	**Other Alphaprotoebacteria**	-		1	1	0
Deltaproteobacteria	*Byssovorax cruenta*, AJ833647	Heterotophic	92	0	4	0
Deltaproteobacteria	*Geobacter ehrlichii*, AY155599	Hetertrophic, Iron reducing	92	0	1	1
Deltaproteobacteria	*Nannocystis sp. 91213*, AY996823	-		0	3	4
Deltaproteobacteria	*Geobacter uraniireducens Rf4*, EF527427	Heterotrophic, Iron reducing	95	4	1	0
Deltaproteobacteria	**Other Deltaproteobacteria**	-		0	0	7
CFB	*Flavobacterium suncheonense*, DQ222428	Heterotophic	95	0	4	1
CFB	*Terrimonas lutea,* AB192292	Heterotophic	95	1	1	0
CFB	**Other CFB**	Heterotophic		8	0	0
Firmicutes	*Gracilibacter thermotolerans*, DQ117465	Heterotophic	92	1	4	4
Firmicutes	*Lysobacter sp. CL4.11*, FM173818	Heterotophic	98	1	0	0
Firmicutes	Filibacter limicola, AJ292316	Heterotophic	95	0	0	0
Firmicutes	Oxobacter pfennigii, X77838	Heterotophic	88	1	0	0
Firmicutes	Sporobacter termitidis, Z4983	Heterotophic	95	1	0	0
Firmicutes	**Other Firmicutes**	Heterotophic		1	0	0
	Other Bacteria	Unknown		2	0	0
	Sum			**41**	6	2

Table 18: Breakdown of bacterial 16S rRNA sequences obtained from the reducing and oxidizing half-cycles.

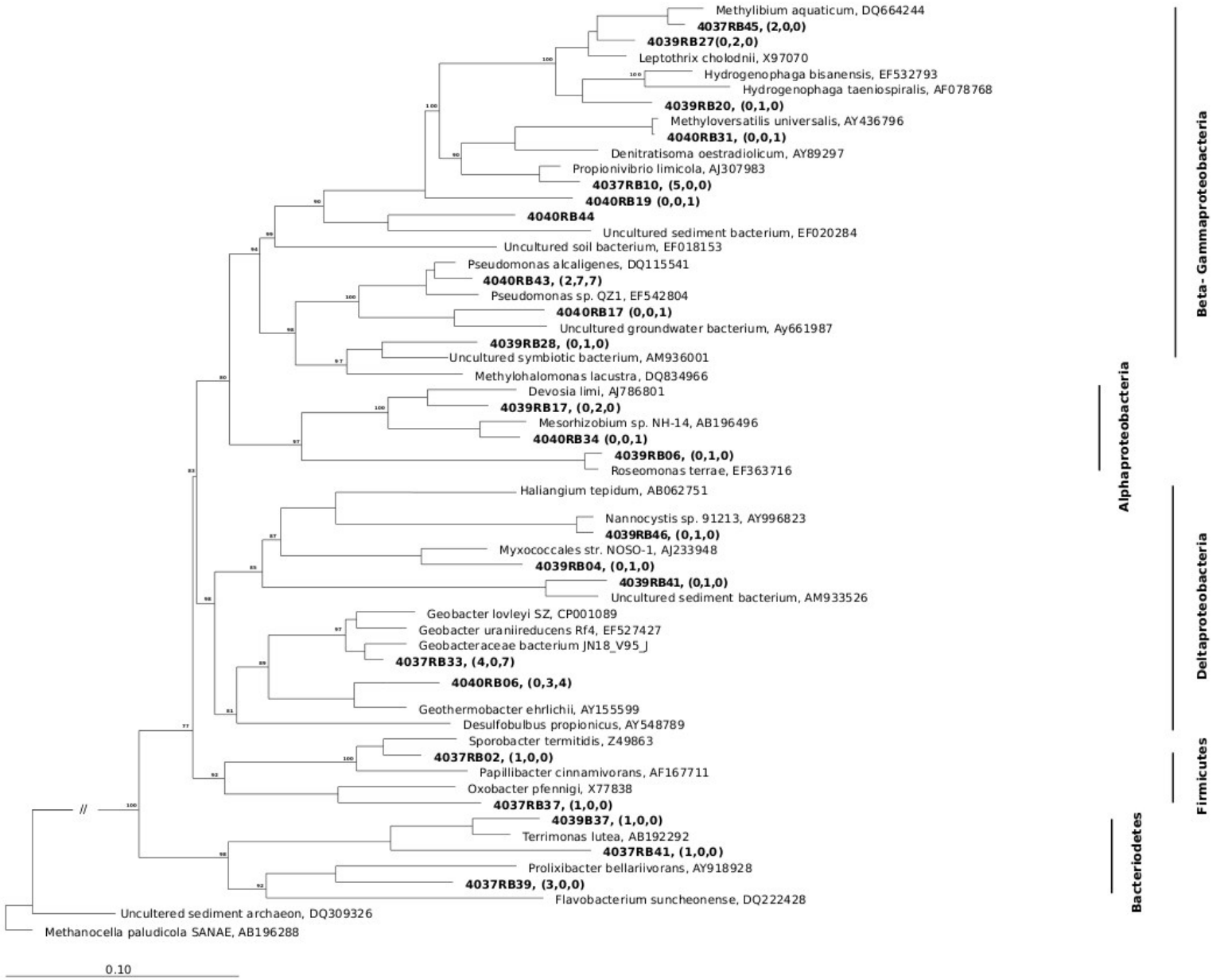

Figure 74: Maximum likelihood phylogenetic tree showing selected sequences obtained from the reactor (bold), and sequences retrieved from the GenBank database. Numbers in brackets are the number of sequences from the reactor at various time points (days 7, 67 and 77) that shared 97 % or greater identify to the displayed sequence. The bootstrap values at the left are percentages out of 1000 replicates. Only values over 70 % are shown. Sequences generated in this study were excluded from bootstrap analysis, and added to the phylogenetic tree using the parsimony tool in ARB.

Potential role	7	67	77	Colour
Heterotrophic	26	23	16	
Heterotrophic, Iron reducing	4	3	11	
Hydrogen oxidising	0	1	0	
Mixatrophic	0	0	5	
Sulphide oxidising	0	1	0	
Ammmonia oxidising	0	0	1	
Iron oxidising	0	4	0	
Unknown	11	10	11	

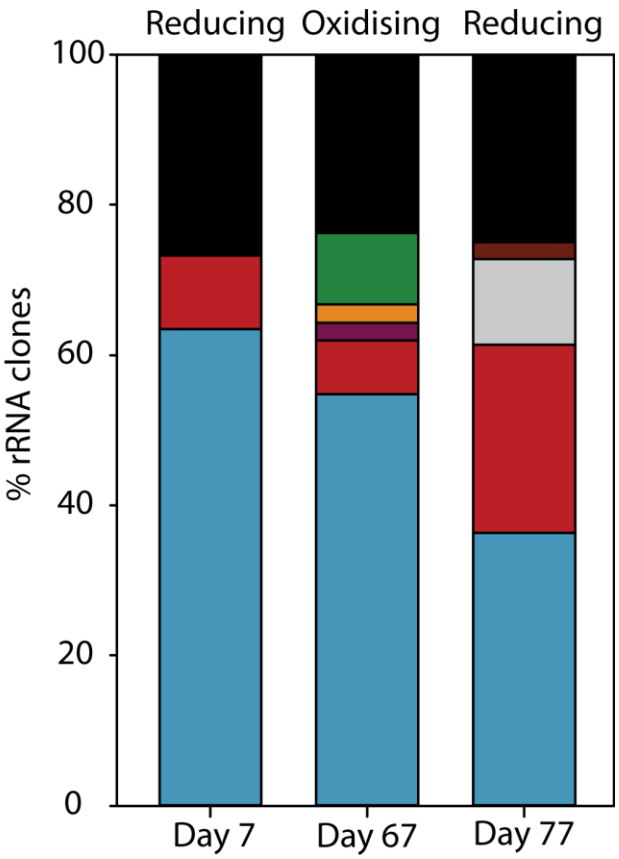

Figure 75: LEFT: Table showing putative roles for bacteria identified by 16S rRNA sequence analysis at different times during this study based on closest cultivated isolate. RIGHT: Stack plot comparing the relative dominance of identified clones in reducing and oxidising half-cycles.

Aqueous chemistry cycling and cumulative effects

As supported by the composition of the microbial community, extensive intra-cycle changes to aqueous chemistry occurred within the suspension during the experiment. Degassing of oxygen in the reactor headspace was analogous to a natural flooding event. The reductive processes, and hence Eh decrease, were driven by the consumption of successive terminal electron acceptors (TEAs) and DOC by the bacterial community present in these samples. This resulted in simultaneous hydroxide production and hence pH rise. The reintroduction of air simulated the initiation of oxidising conditions after a flooding event, whereby reduced species are oxidized by biotic and abiotic processes. Although evidence for reduction of Mn-(hydr)oxides, nitrate and sulphate was apparent (see Table 23) the oxidative capacity of soils is frequently dominated by microbially reducible ferric oxides following exhaustion of residual O_2 (Kirk, 2004) and we propose that reduction of iron is the dominant reductive process in this soil during flooding. Measured geochemical parameters with time are shown in Figure 76 in addition to the results of thermodynamic and kinetic modelling.

Intra-cycle Eh changes are similar to those exhibited in field based Eh monitoring studies in flooded soils (Vorenhout et al., 2004) and cross various redox boundaries (Figure 77). DOC increases during each reducing half-cycle indicate that rates of microbially mediated solubilisation of particulate organic matter (POM) exceeded rates of DOC consumption by heterotrophic metabolism. This DOC increase is also consistent with

data from Grybos et al. (2009) who propose that DOC concentrations increase in soil pore-water during flooding due to bacterial hydrolysis and pH increase (desorption). During subsequent oxidising half-cycles, DOC is removed from solution presumably due to consumption during respiration as pH change is strongly buffered by the presence of calcite. The amplitude of DOC modulation decreases during successive cycles as BDOC is exhausted by bacterial hydrolysis and the labile DOC pool is oxidised to CO_2. This cumulative decrease is representative of organic matter consumption in many managed floodplain soils which are subjected to successive cycles of phreatic but not fluvial flooding, which limits input of fresh organic rich sediment. On floodplains the alluvial aquifer and the river are strongly inter-dependent and often act as one hydrological resource. In these circumstances, as is the case over much of the Saône floodplain, flood barriers are unable to prevent a raise in water levels on the floodplain and hence anoxia during sustained high river levels. Barriers do however prevent overbank or fluvial flooding and the deposition of fresh sediment including labile organic matter. The same cumulative decrease in BDOC is applicable to many other redox-oscillating environments, which receive limited sediment input, including paddy fields which are commonly irrigated by pumping of shallow groundwater.

In such situations, as the most labile organic matter is depleted through successive redox cycles, its availability may limit the rate of heterotrophic metabolism (Neumann et al., 2010), leading to a decrease in reductive processes shown to be responsible for arsenic mobilisation (Islam et al., 2004).

Pore-water Fe^{2+}concentrations remained low (< 70 μM) throughout the experiment despite evidence indicative of iron reduction. Thermodynamic predictions suggest that this is due to the strong stability of magnetite which remains supersaturated with respect to the reactor suspension at all times (Figure 77). This prediction is supported by a wealth of studies on IRB where nano-magnetite is often the final product of reduction (Coker et al., 2008). Additionally fast sorption of Fe^{2+} to a variety of mineral surfaces has been shown to be kinetically favourable compared to precipitation of ferrous minerals at circumneutral to high pH (Charlet et al., 1998). Metal-hydr(oxides) and phyllosilicate minerals (Jaisi et al., 2008) have been shown to offer substantial sorbent surfaces for $Fe^{2+}_{(aq)}$ with phyllosilicates becoming increasingly important at high pH. Illite and chlorite were identified by XRD and analysis and constitute a high proportion of the soil mineral content in this and many other flood-plain soils.

As precipitation of ferrous minerals such as $FeS_{(s)}$ and $FeCO_{3(s)}$ has been shown to limit arsenic mobility in reducing environments (Charlet et al., 2011) fast sorption of Fe^{2+} to redox stable minerals such as recalcitrant metal oxides and phyllosilicates may increase arsenic mobility during reducing conditions.

Intra-cycle mobilisation of arsenic was measured during each reducing half-cycle (up to 335 μM), however, upon re-establishment of oxidising conditions $As_{(aq)}$ was re-immobilised, returning to a base-level of approximately 36 μM close to the analytical limit of quantification (Apostol et al., 2009) (28 μM). During reducing half-cycles the most thermodynamically dominant arsenic species are arsenite anions (H_3AsO_3 and $H_2AsO_3^-$) whereas the conditions established during oxidising half cycles favour the formation of arsenate ($HAsO_4^{2-}$). Arsenite is often considered to be more mobile than arsenate (Borch et al., 2010) due its neutral charge (pK_a1 9.2) and hence relatively limited affinity with positively charged surfaces present at acidic pH compared to arsenate which benefits from electrostatic effects. However, at circumneutral to high pH, soil sorption capacities for arsenite are often greater than for arsenate (Dixit and Hering, 2003) as mineral surfaces become more negatively charged. Transition from arsenate to arsenite during reducing half-cycles does not

therefore satisfactorily resolve observed arsenic mobilisation in calcareous soils at moderate to high pH. Alternative mechanisms shown to release arsenic during reducing conditions include reductive dissolution of As-bearing iron (hydr)oxide (Erbs et al., 2010) and competitive sorption with DOC (Bauer and Blodau, 2006), and it is these mechanisms which we consider most influence measured changes in intra-cycle arsenic mobility.

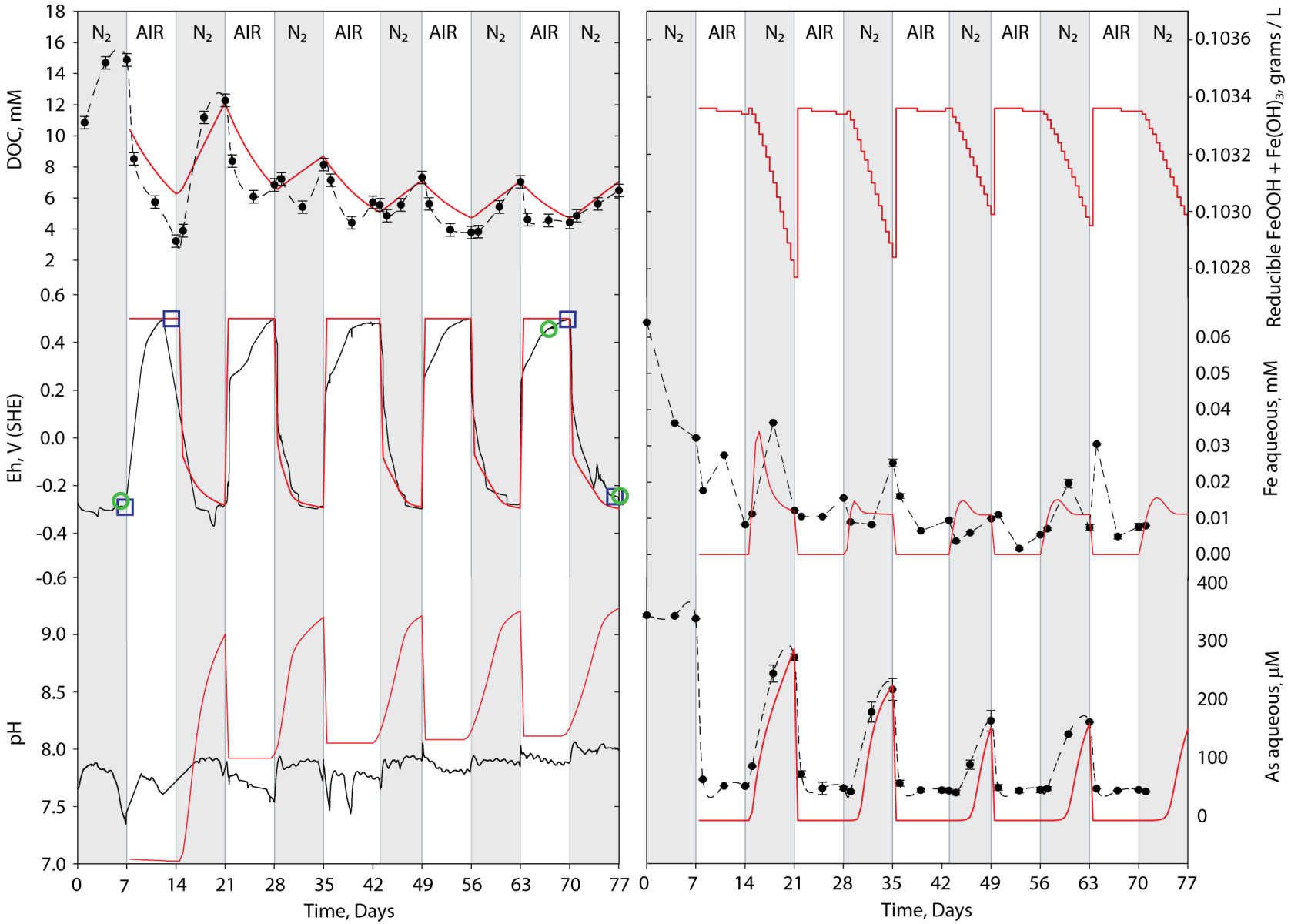

Figure 76: Measured (black) and modelled (red) DOC, Eh, pH, Fe(s) (grams of reducible lepidocrocite and ferrihydrite), $Fe_{(aq)}$ and $As_{(aq)}$ data with time during reactor experiments. Sampling points for XANES and microbial community analysis are shown on the Eh curve (XANES = open blue squares, 16S rRNA = open green circles).

In addition to intra-cycle changes, cumulative effects of redox cycling on arsenic mobility are present, and have not to our knowledge been previously described. Whilst As concentrations during oxidising half-cycles remained relatively constant, successive redox-cycles resulted in a 45% decrease in mobility between the first and fifth reducing half-cycles. Potential causes for the measured decrease in arsenic mobility include: i) a decrease in competition for sorption sites from low molecular weight DOC(Bauer and Blodau, 2006), ii) an increase in the proportion of As that is co-precipitated, or kinetically sorbed, with iron (hydr)oxide phases, or, alternatively, iii) precipitation of As mineral phases.

In order to assess the validity of the hypotheses that co-precipitation with iron oxide minerals or precipitation of discrete arsenic phases may be important processes responsible for measured arsenic attenuation, a model of redox cycling in the bioreactor was developed. Competitive sorption with DOC is not considered in this model due to the complexity of natural organic matter, which may also contribute to the measured decrease in arsenic mobility.

Thermodynamic and kinetic modelling

Intra-cycle oscillation of aqueous arsenic concentration is effectively reproduced by the precipitation and dissolution of ferric-arsenate phases following thermodynamic predictions (Figure 77) although it is probable that this process is also microbially mediated (Cummings et al., 1999). With successive cycles, and hence a decrease in DOC availability, iron reduction rate decreases and hence a lower quantity of ferric arsenate dissolves with each cycle. The measured slow inter-cycle attenuation of As (R5) is successfully captured implementing a arsenic co-precipitation factor, based on work by Erbs et al. (2010) who demonstrate that As co-precipitated with ferrihydrite is significantly less mobile than adsorbed arsenic upon development of reducing conditions.

The model was able to reproduce with good accuracy the measured chemical parameters, except pH which is over predicted. We attribute this failing of the model to problems in estimating fluctuating $CO_{2(aq)}$ concentrations due to a combination of microbial metabolism, slow diffusion of gas to the headspace and subsequent impacts on the carbonate buffering system.

The model demonstrates that the arsenic attenuation measured during redox cycling in batch experiments may be successfully described by a combination of co-precipitation with ferric-(hydr)oxides and a decrease in ferric arsenate dissolution due to depletion of BDOC. This result emphasises the importance of BDOC in arsenic contaminated soils supporting the recent findings of Neumann et al (Neumann et al., 2010) and Benner (Benner, 2010) and indicates the importance of hydrological management on floodplains as a control on arsenic mobility.

Table 19: Key reactions and kinetic formulations used in the model.

Description	Reaction	Kinetic formulation	ID
Hydrolysis of particulate organic matter	$(CH_2O)_{part} \xrightarrow{R_{Hydro}} (CH_2O)_{dis}$	$R_{Hydro}(t) = R^0 e^{(-\alpha t)}$	R1
Respiration	$CH_2\,O\ +\ O_2 \rightarrow CO_2 + H_2O$	$R_{Res} = R_a k_{om}[CH_2O]\left(\frac{[O_2]}{K_{m(O_2)} + [O_2]}\right)$	R2
Reduction of Ferrihydrite	$4Fe(OH)_3 + CH_2O + 8H^+ \rightarrow 4Fe^{2+} + CO_2 + 11H_2O$	$R_{Ferri} = k_{om}[CH_2O]\left(\frac{[Fe(OH)_3]}{K_{m(Ferr)} + [Fe(OH)_3]}\right)\left(\frac{K_{in}}{K_{in} + [O_2]}\right)$	R3
Reduction of Lepidocrocite	$4FeOOH + CH_2O + 8H^+ \rightarrow 4Fe^{2+} + CO_2 + 7H_2O$	$R_{Lepi} = k_{om}[CH_2O]\left(\frac{[FeOOH]}{K_{m(Lepi)} + [FeOOH]}\right)\left(\frac{K_{in}}{K_{in} + [O_2]}\right)$	R4
Slow adsorption of Arsenic	$As(III)_{(mob)} \rightarrow As(III)_{(imob)}$	$R_{AsIm} = k_{imob}[As]([Fe(OH)_3] + [FeOOH])$	R5
Oxidation of Fe^{2+}	$Fe^{2+} + 0.25O_2 + H^+ \rightarrow Fe^{3+} + 0.5H_2O$	$R_{FeOx} = k_{FeOx}[O_2][Fe^{2+}]$	R6

Table 20: Reaction parameters used in the model corresponding to reactions in Table 19. a: Parameter values were obtained as follow: L, from literature; C, constrained by experimental data; M, derived by model fitting.

Parameter	Value	Unit	Source	Ref	Description
R^0	5×10^{-3}	$\mu mol\ s^{-1}$	C		Initial POM hydrolysis rate
α	1.5×10^{-7}	-	C		Attenuation constant for POM hydrolysis
R_α	25	-	M		Acceleration factor for R1
k_{om}	6×10^{-8}	s^{-1}	M		DOC degradation rate constant
K_{in}	24	μM	L	(Van Cappellen and Wang, 1995)	Inhibition of Fe(III) reduction, (R3 and 4)
$K_{m\ (O2)}$	1	μM	L	(Van Cappellen and Wang, 1995)	Half-saturation for oxic respiration (R2)
$K_{m(Ferr)}$	2.6×10^{-2}	$\mu mol\ L^{-1}$	L	(Van Cappellen and Wang, 1995)	Half-saturation for $Fe(OH)_3$ reduction (R3)
$K_{m(Lepi)}$	2.2×10^{-2}	$\mu mol\ L^{-1}$	M		Half-saturation for FeOOH reduction (R4)
			Range		
k_{imob}	1.3×10^{-6}	$\mu M^{-1}\ s^{-1}$	L (1.3×10^{-4})	(Couture et al., 2010)	Rate constant for As co-precipitation with Fe(III)oxyhydoxides (R5)
k_{FeOx}	5×10^{-4}	$\mu M^{-1}\ s^{-1}$	L 5×10^{-4} –1×10^{-8}	(Canavan et al., 2006)	Rate constant for Fe(II) oxidation by O_2 (R6)

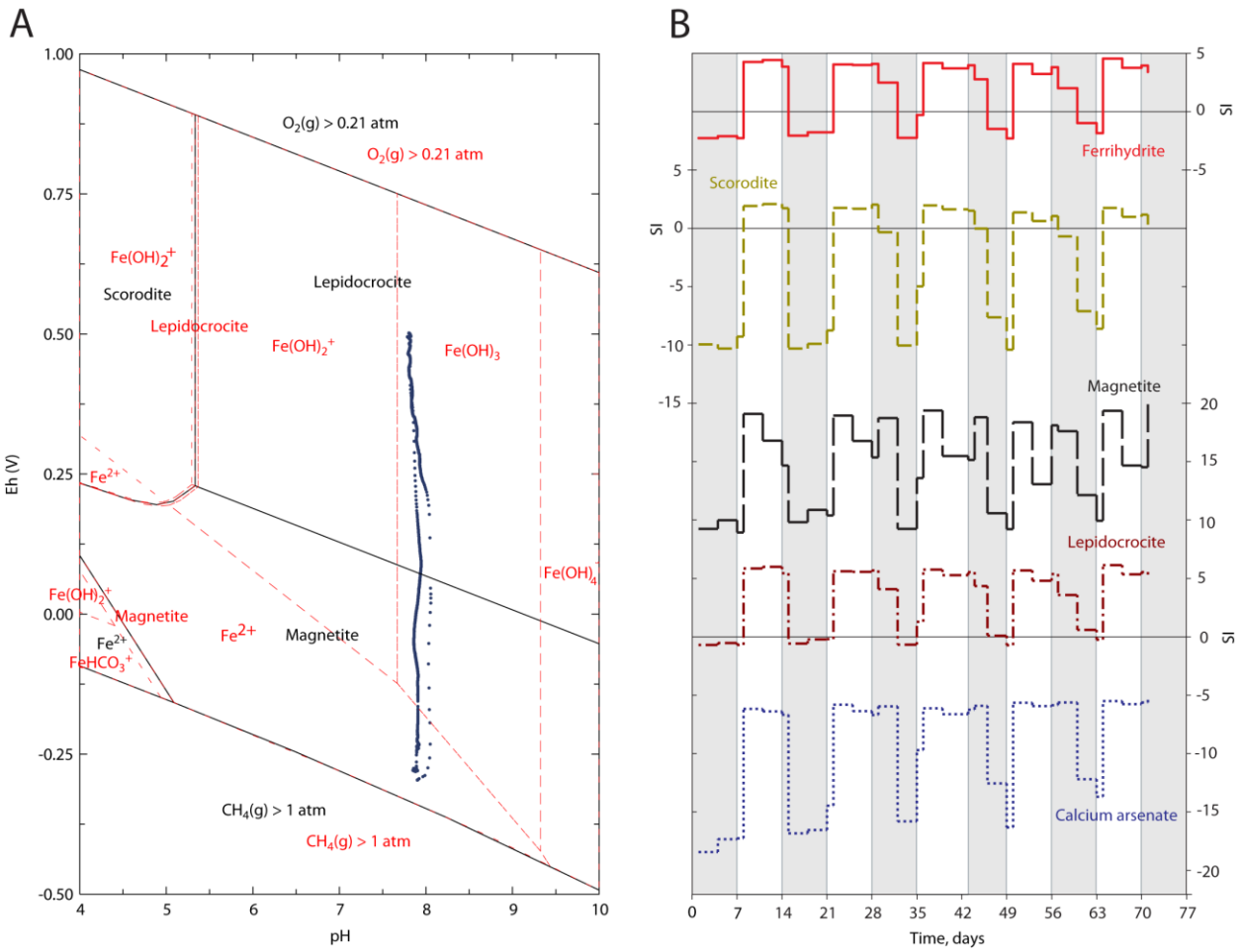

Figure 77: A: Pourbaix diagram of the Fe, As, CO_2 and H_2O system in the reactor suspension with Fe as the principal species. Point data are measured Eh and pH couples from one full cycle. Dominant stability fields are shown with black solid lines and subdominant fields with red dashed lines. B: Saturation indexes of ferrihydrite (solid red line), scorodite (short dashed mustard line), magnetite (long dashed black line), lepidocrocite (dot/dashed line) and calcium arsenate (dotted line) with time during reactor experiments.

Spectroscopic investigation: XAS

To investigate the effect of cyclic redox conditions on solid arsenic oxidation state, X-ray absorption spectra were recorded at the As K-edge on samples taken at the end of the first and last oxidising and reducing cycles (Figure 78). Linear Combination Fitting (LCF) of the samples' XANES spectra using As(III) and As(V) reference spectra, shows that all spectra contain a mix of tri-valent and penta-valent arsenic species, with an increasing ratio of As(III)/As(V) during each reducing cycle. This is consistent with the dissolution of As(V)-bearing minerals predicted by the model.

EXAFS refinements revealed the average local structure around As. In all samples two As-O bonds of differing length (~1.7 and ~1.8 Å) were observed. This structure is compatible with a mixture of As(V) and As(III) oxyanions. Features beyond the first coordination shell were negligibly weak, indicative of an amorphous or highly disordered structure. This is probably due to a combination of outer-sphere sorption and incorporation into poorly crystalline phases such as amorphous ferric arsenate. The lack of further coordination shells also confirms that arsenite uptake into the calcite lattice, observed in more pure carbonate systems (Bardelli et al.,

2011), does not occur to a significant extent in more heterogeneous soil environments. The full results of linear combination fitting, coordination numbers and bond lengths are provided in the Table 21 information.

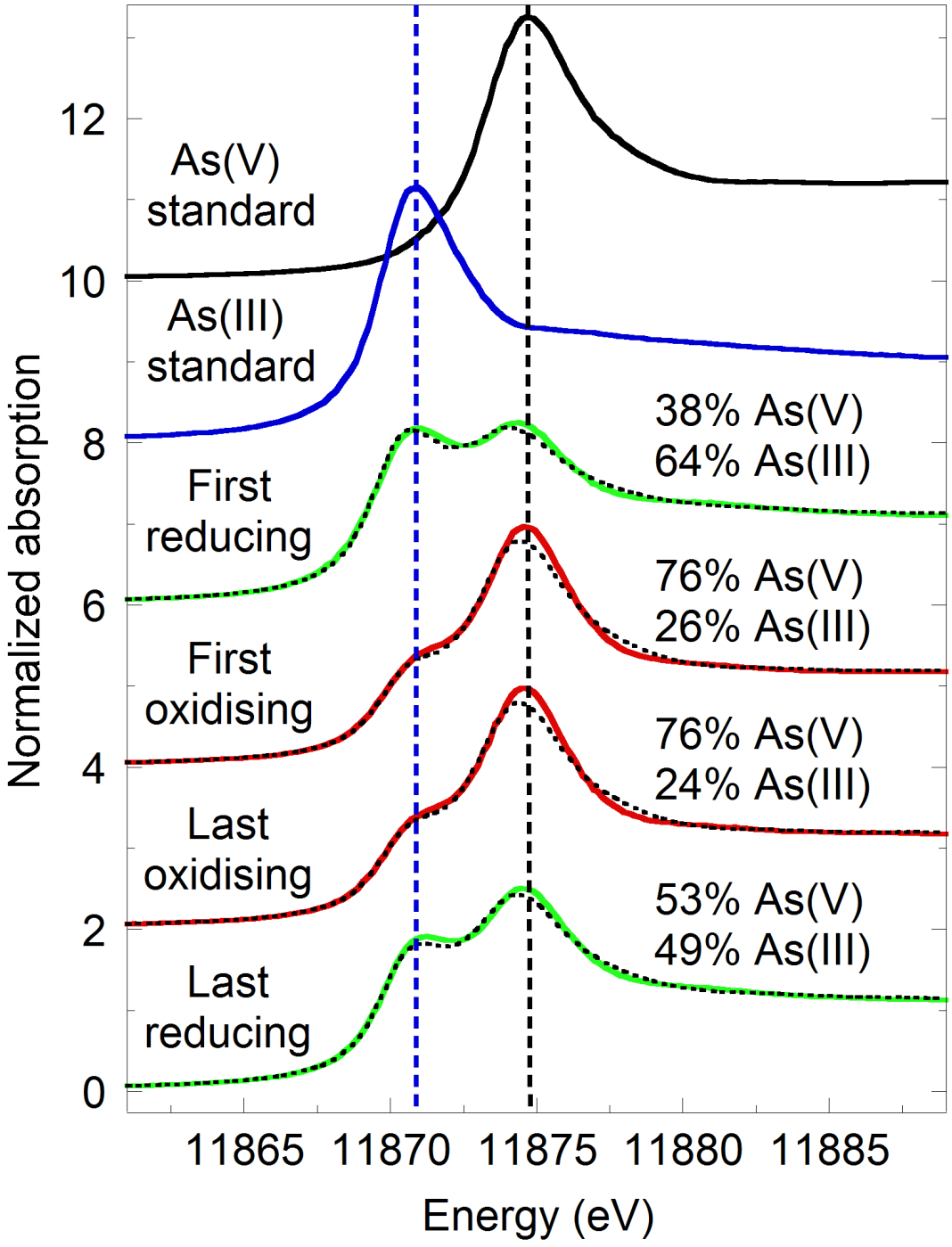

Figure 78: Arsenic K-edge (11,867 eV) XANES spectra recorded at 77K. Spectra from suspension solids are coloured according to time of sampling: green = end of reducing cycle, red = end of oxidising cycle. As(III) and As(V) adsorbed on pure calcite were used as references (black and blue curves, respectively). An estimation of the As(III) and As(V) contributions to natural samples derived from linear combination fitting is shown above each spectrum (the error is about 5%). Dashed lines are the linear combination fits.

Following successive cycles, the ratio of As(III)/As(V) remained constant during oxidising half-cycles, however, decreased considerably during reducing half-cycles. This result is consistent with the model's prediction of arsenate accumulation in a poorly ordered ferric arsenate phase but inconsistent with the immobilisation of arsenite via co-precipitation. The model's over-prediction of As(III)/As(V) may be due to the rapid oxidation of arsenite during co-precipitation by radical species produced by fenton like reactions occurring during oxidation of Fe^{2+} by O_2 (Ona-Nguema et al., 2010). These radical species dramatically accelerate arsenite oxidation at ferrihydrite surfaces (Ona-Nguema et al., 2010) but are not included in the model.

Table 21: Structural parameters (CN, co-ordination numbers; R, atomic distances; σ^2 Debye-Waller factors) and As(III), As(V) proportion derived from LCF using As(III) and As(V) adsorbed on pure calcite as references. The numbers within parenthesis are the errors on the last digit. The error on the determination on the As(III) and As(V) contributions is estimated to be 5-10%. The last two columns report the sum (Σ) of the As(V) and As(III) contributions and the values of the reduced χ square (χ_ν^2) of the LCF, both indicating good matches with the experimental spectra.

Samples	path	CN	R (Å)	σ^2 ($Å^2 \cdot 10^3$)	As(III) As(V)	Σ	χ_ν^2
End of first reducing cycle	As-O1	1.8(5)	1.670(6)	1.1(5)	64	102	0.0031
	As-O2	2.2(5)	1.801(6)		38		
End of first oxidising cycle	As-O1	3.2(5)	1.681(8)	1.2(6)	26	102	0.0029
	As-O2	0.8(5)	1.795(9)		76		
End of last oxidising cycle	As-O1	2.7(5)	1.663(8)	1.8(6)	24	100	0.0041
	As-O2	1.2(5)	1.776(9)		76		
End of last reducing cycle	As-O1	0.1(5)	1.675(2)	1.0(5)	49	102	0.004
	As-O2	3.9(5)	1.788(5)		53		
Standards							
As(V) adsorbed on calcite	As-O	4	1.676(3)	2.2(2)	As(V)		
As(III) adsorbed on calcite	As-O	3	1.775(3)	3.5(3)	As(III)		
Ferrihydrite - $Fe(OH)_3$	As-O	4	1.69(2)	1.4(2)	As(V)		

Spectroscopic investigation: ^{57}Fe Mössbauer

The paramagnetic Mössbauer spectrum obtained on day 77 is shown in Figure 79 with corresponding hyperfine parameters for all spectra provided in Table 22. The spectra can all be successfully modelled with 5 components (2 sextuplets and 3 doublets). Hyperfine parameters for both sextuplets correspond well to those previously recorded for nano-crystalline FeOOH (Fabris et al., 1986; Vandenberghe et al., 1986; Murad, 1987), whereas doublets appear to represent Fe(II) and Fe(III) components of iron rich clay minerals identified during powder XRD analysis (illite and chlorite)(Coey, 1975; Blaauw et al., 1980; Taneja and Jones, 1984; Das et al., 1986). This data strongly supports the presence of nano-crystalline ferric hydroxide minerals within the soil and hence their inclusion in the model despite their absence from XRD spectra.

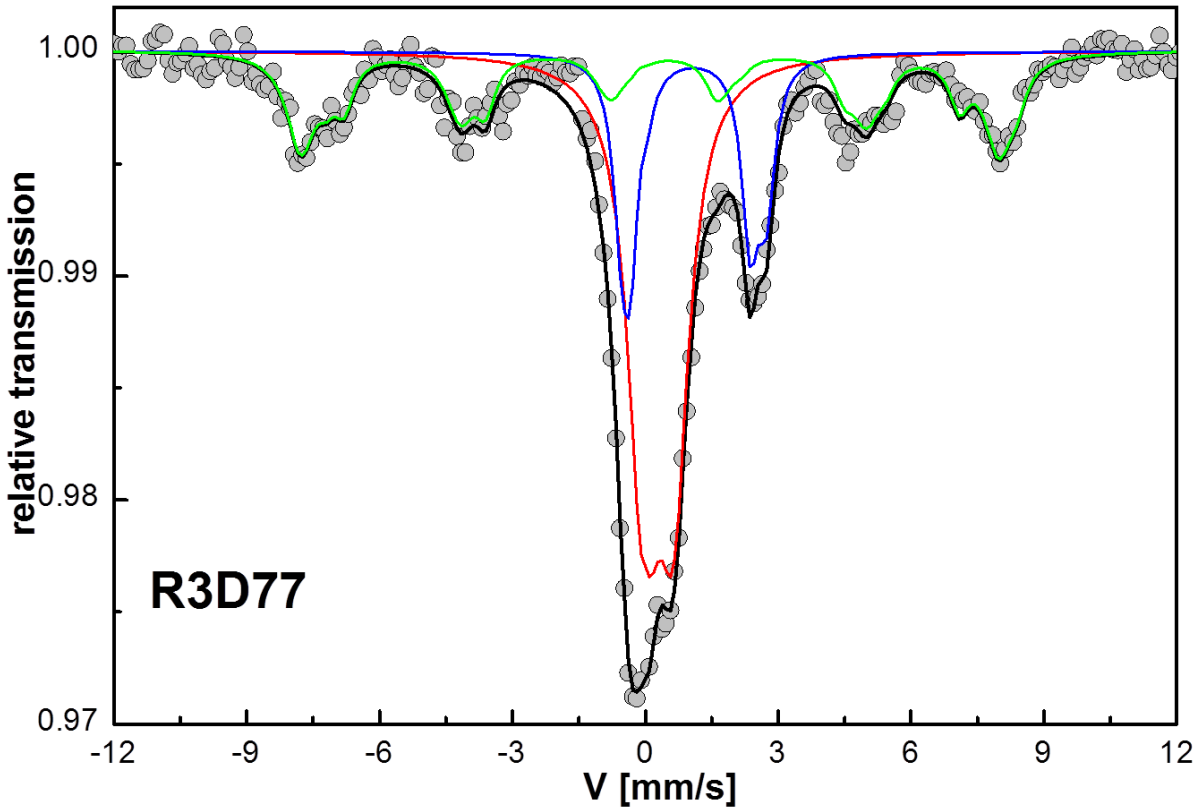

Figure 79: Mössbauer spectra obtained on day 77 at T = 77 K shown together with modelled hyperfine contributions. Green = averaged sextuplet contribution corresponding to Fe(III) present in ferric hydroxides, Red = structural Fe(III) present in clays, Blue = averaged doublet contribution corresponding to structural Fe(II) present in clays.

However, limited variation is observed between Mössbauer spectra obtained during oxidising and reducing cycles or between the first and last samples analysed. This is in contrast to previous wet redox cycling (Thompson et al., 2006) and classic flooding draining cycling experiments (McGeehan, 1998) where clear differences were apparent in the short range order of Fe in FeOOH. The effect of redox cycling on structure and crystallinity of iron (hydr)oxides is still poorly understood with seemingly conflicting results in the limited literature available. Whilst some studies indicate that the effect of flooding and draining result in decreases to crystallinity and hence an increasing surface area and sorption of trace contaminants (McGeehan, 1998), other studies suggest the opposite to be true with repetitive cycling leading to increases in FeOOH crystallinity which may result in increased contaminant mobility during oxic phases due to lower total reactive surface area (Thompson et al., 2006). It is thought that the lack of prominent intercycle changes to Fe(II/III) ratios is to the short periodicity of reducing and oxidising cycles within this study (14 days for 1 full cycle) and that therefore the magnitude of iron reduction and subsequent oxidation was limited compared to the total FeOOH fraction.

Indeed this corresponds well to the prediction of the model that only a small fraction of the ferric iron present is reduced with each cycle but that even this small amount of iron reduction can lead to dramatic changes in arsenic mobility. Unfortunately the lack of sufficient iron cycling to affect bulk properties of the FeOOH iron bearing fraction precludes confirmation or rejection of crystallinity increases or decreases observed in previous studies.

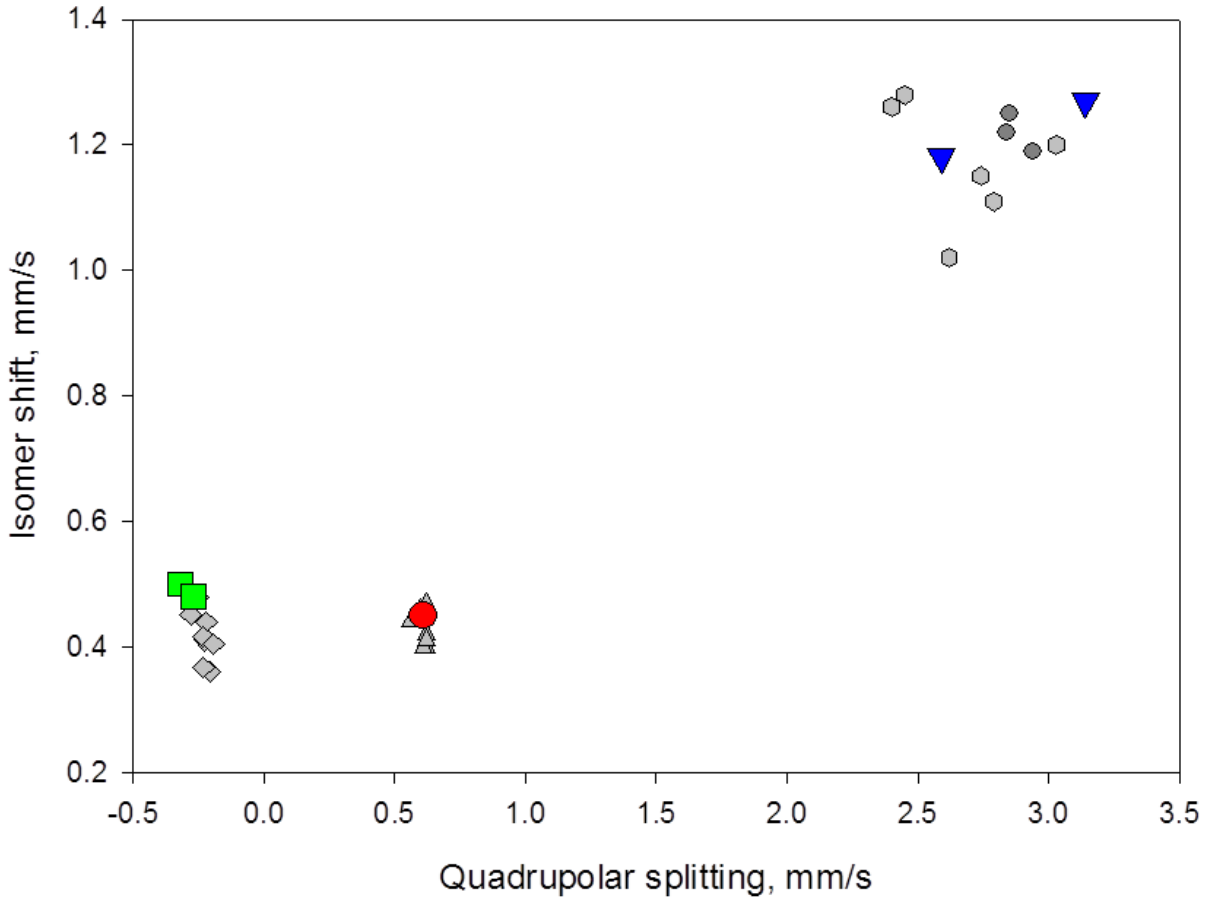

Figure 80: Hyperfine parameters of modeled contributions to soil ^{57}Fe Mössbauer spectra compared to literature values for various iron mineral components. Green squares correspond to modeled sextuplet components, Red circles and blue triangles correspond to modeled doublet components. Grey diamonds correspond to literature values of FeOOH, grey triangles correspond to structural Fe(III) in clays and grey circles correspond to structural Fe(II) in clays.

Table 22: Mössbauer hyperfine parameters of the spectrum presented in Figure 79 in addition to spectra obtained on days 4, 14 and 70.

Sample day	Component	Isomer shift (mm/s)	G (mm/s)	Quadrupole Splitting (mm/s)	Hyperfine field (kOe)	Relative Area (%)
4	Structural Fe(III) in clays	0.43	0.65	0.62		49
	Structural Fe(II) in clays	1.26	0.38	2.82		17
	Fe(III) in FeOOH	0.44	0.60	-0.28	490	22
	Fe(III) in FeOOH	0.27	0.60	-0.20	434	12
14	Structural Fe(III) in clays	0.44	0.63	0.65		51
	Structural Fe(II) in clays	1.21	0.43	2.40		7
	Structural Fe(II) in clays	1.27	0.33	2.90		15
	Fe(III) in FeOOH	0.50	0.55	-0.11	484	18
	Fe(III) in FeOOH	0.38	0.60	-0.43	446	9
70	Structural Fe(III) in clays	0.43	0.62	0.60		46
	Structural Fe(II) in clays	1.23	0.40	2.75		16
	Structural Fe(II) in clays	1.26	0.40	3.08		7
	Fe(III) in FeOOH	0.47	0.60	-0.20	485	24
	Fe(III) in FeOOH	0.60	0.60	-0.15	441	7
77	Structural Fe(III) in clays	0.45	0.83	0.61		49
	Structural Fe(II) in clays	1.18	0.44	2.59		11
	Structural Fe(II) in clays	1.27	0.46	3.14		10
	Fe(III) in FeOOH	0.5	0.60	-0.32	489	19
	Fe(III) in FeOOH	0.48	0.60	-0.27	436	11

Additional reductive processes

The variation in Eh, and to a lesser extent pH, during cycling experiments causes transitions between thermodynamically dominant species for many elements and hence predicts the microbial use of numerous TEAs in addition to ferric iron. Pourbaix diagrams (Figure 81) show the stability fields for the manganese, nitrogen and sulphate systems in the reactor suspension during cycling experiments illustrating the implicated redox couples; MnO_2.Mn^{2+}, NO_3^-.NH_4^+ and SO_4^{2-}.HS^-.

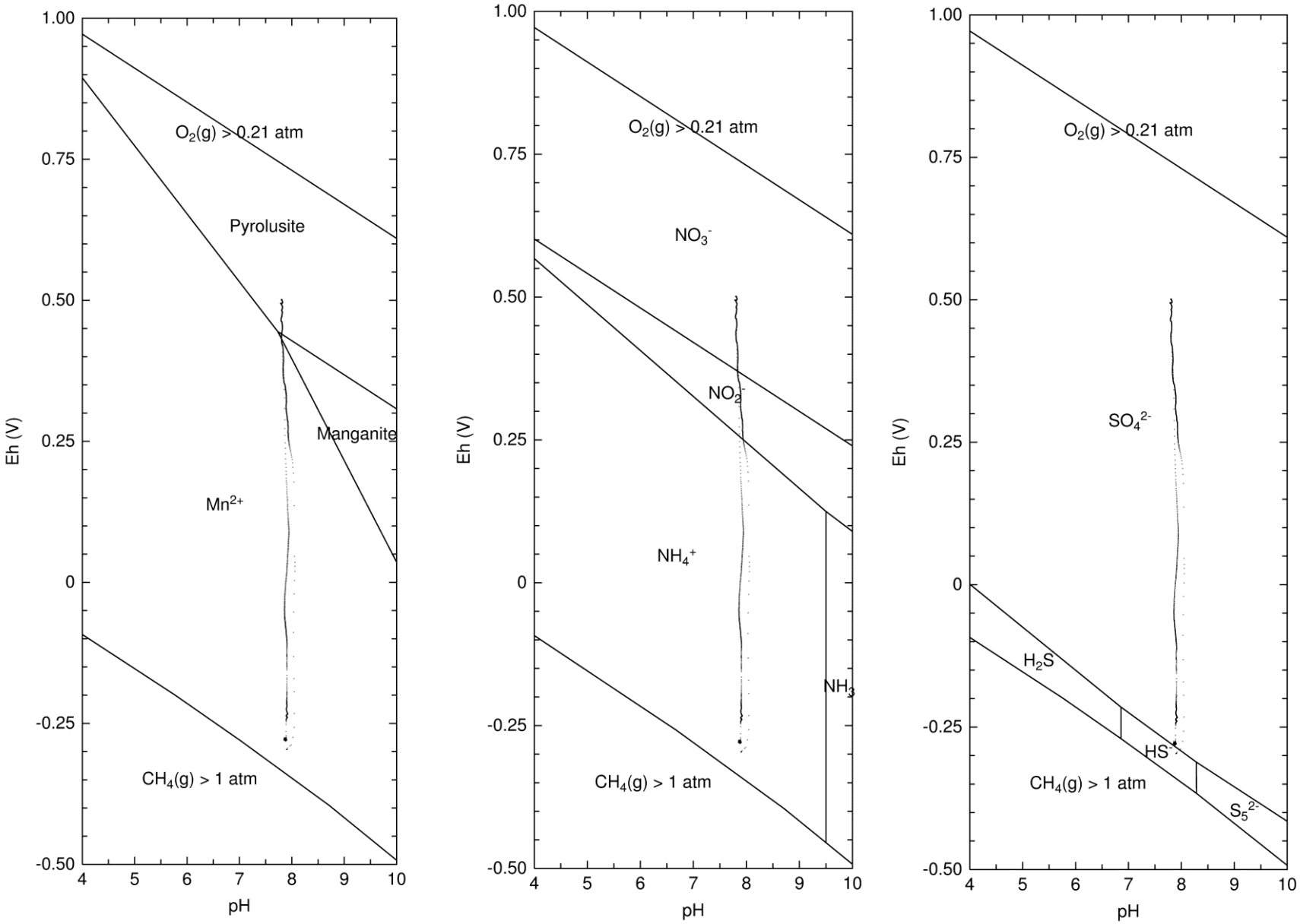

Figure 81: Eh-pH diagrams of LEFT: the Mn, H_2O, CO_2 system, CENTER: the N, H_2O, CO_2 system and RIGHT: the S, H_2O, CO_2 system.

Table 23: Summary of other possible reductive processes within the reactor suspension and the experimental evidence to support or reject reduction during the experiment.

Redox couple	Evidence for reduction	Strength of evidence	Figure
MnO_2.Mn^{2+}	Increasing Mn^{2+} in solution during each reducing cycle.	**Moderate.** A clear pattern of Mn release and removal corresponds well to reducing and oxidising cycles. The release of Mn^{2+} is likely due to the dissolution of Mn(IV)-oxides but may also be partially a result of cation exchange with Ca^{2+} which also increases due to dissolving $CaCO_3$ during reducing cycles due to the absence of CO_2 in the headspace.	Figure 82
NO_3^-.NH_4^+	Decrease of nitrate concentrations during reducing cycles.	**Weak.** Changes in nitrate concentration are small and do not correspond well to reducing and oxidising cycles. Total nitrate levels are low throughout the experiment.	Figure 83
SO_4^{2-}.HS^-	Slight decreases to aqueous sulphate concentrations during some reducing cycles and the activity of close relatives of microbial species known to reduce sulphate.	**Moderate/Weak.** The composition of the microbial community would suggest that sulphate reduction is an important process within this soil. However, during the reactor experiments sulphate reduction appears to have been limited probably due to the length of the reducing cycles/persistence of more energetically favourable terminal electron acceptors.	Figure 83

These reductive processes were considered to be of secondary significance compared to reduction of ferric iron during cycling but experimental evidence for these processes is summarized in Table 5.

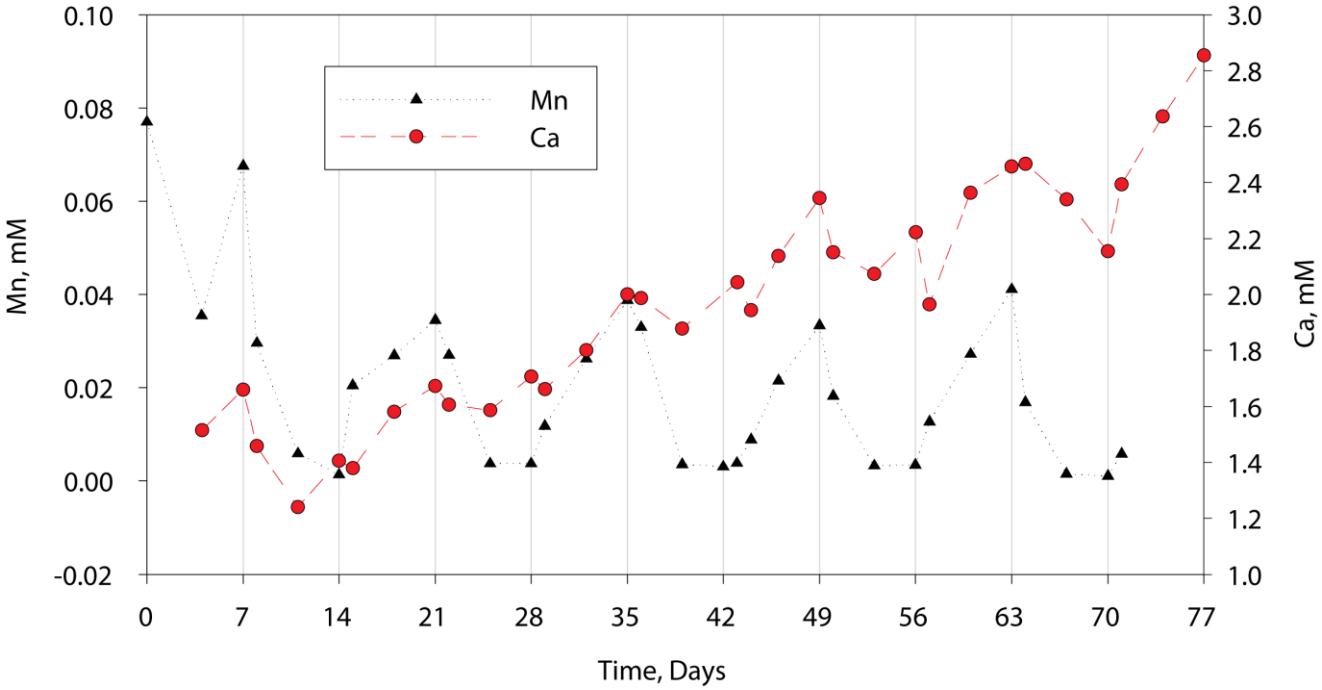

Figure 82: Manganese and calcium pore-water concentration with time in the reactor suspension.

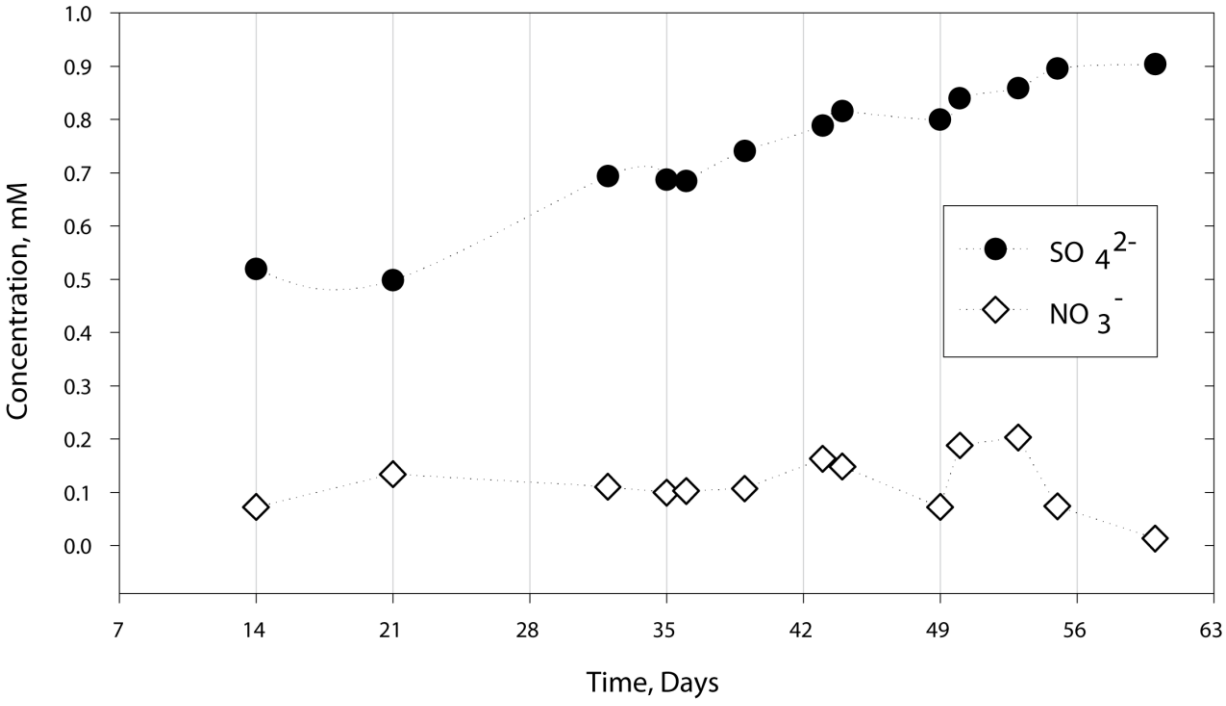

Figure 83: Sulphate and nitrate pore-water concentration with time in the reactor suspension. Nitrate concentration does not systematically decrease with reducing half cycles whereas a limited sulphate decrease is recorded.

Calcite and the carbonate system:

A cumulative increase of Ca^{2+} in solution implies the net dissolution of calcite due to H^+ production in oxidising half-cycles, consistent with decalcification experienced naturally in many soils (Van Den Berg and Loch, 2000). Net decalcification processes diminish the probability that co-precipitation with calcite is responsible for arsenic attenuation. Furthermore, arsenic is rarely found in association with calcite in contaminated soils (Smedley and Kinniburgh, 2002). In natural systems decreased degassing of CO_2 occurs during flooding due to limited diffusion through the soil and overlying water column leading to higher pCO_2 and lower pH in soil solution. As aqueous calcium from dissolving calcite is often then leached from the soil with draining flood water, the soil solution remains under-saturated with respect to calcite upon subsequent CO_2 degassing and pH rise. Whilst pCO_2 was not controlled in this experiment and leaching of Ca^{2+} could not occur due to the nature of the closed solid/aqueous system, the constant degassing of CO_2 and dissolution of calcite is consistent with natural decalcification processes.

Conclusions

In addition to confirming frequently observed changes to arsenic mobility under reduced and oxidised conditions (Frohne et al., 2011) we have shown through batch experiments that successive cycling of redox conditions in arsenic contaminated soils, analogous to flooding and draining, may result in long term changes to arsenic mobility. Previous studies indicate that decreasing As concentrations in pore water during successive cycles of flooding and draining may be due to physical transport of arsenic away from soil in receding floodwater (Roberts et al., 2010). In this instance, evidence from thermodynamic and kinetic modelling, complemented by spectroscopy indicate that decreased mobility of arsenic by 45% during reducing conditions in a closed system can be attributed to co-precipitation processes and depletion of BDOC due to lack of solid organic matter recharge, resulting in decreased rates of heterotrophic iron reduction and ferric arsenate dissolution. We have demonstrated that by using a combination of genetic analyses, geochemical modelling and spectroscopic tools to complement batch and field studies it is possible to increase our understanding of dynamic natural systems over longer time-periods. Further research into the influence of factors such as periodicity, hydrologic regime and mineralogical changes on contaminant mobility under oscillating redox conditions is clearly required, as redox oscillating conditions are prevalent in a variety of arsenic contaminated environments.

Chapter 6: Experimental Redox cycling of Callovo-Oxfordian suspensions contaminated with Cr, As, Hg and U

Abstract

Batch experiments in redox stat reactors were conducted to investigate the periodic and cumulative effects of temporal redox oscillations on the mobility of redox sensitive contaminants in argillaceous marl substrates such as those proposed as final geological barriers in nuclear waste repositories.

Experiments were designed to simulate redox oscillations in the substrate surrounding a near surface low level long lived nuclear waste repository due to seasonal changes in groundwater level. Investigations consisted of the temporal oscillation of redox conditions within powdered Callovo-Oxfordian suspensions in three reactors doped with oxidised Cr, As, Hg and U (R1), As (R2) and Cr (R3). Suspensions were subjected to a total of three full redox cycles entailing phases of compressed air sparing, nitrogen sparing and AH_2DS^{2-} addition. AH_2DS^{2-} was added as a bulk reductant to simulate microbial reduction in lieu of active chemolithotrophic bacteria which are ubiquitous in natural sediments.

Redox changes between -215 and +340 mV resulted in strong intra-cycle changes in the mobility of As, Cr and U with additional cumulative effects apparent for As and Cr. Redox oscillations within this range did not result in changes to aqueous Hg concentration subsequent to the initial period of sorption.

Introduction

Low level long lived nuclear waste (LL-LLW) in France accounts for 7.2% of all nuclear waste by volume but less than 0.009% of total radioactivity (ANDRA, 2010). Currently such waste is stored in surface facilities pending a decision on long term disposal options. Due to the large volumes of waste concerned (estimated at 200,000 m^3 following processing (ANDRA, 2010)) the high costs associated with the deep geological storage and the lower risk posed by low level waste, alternative near surface storage strategies are being investigated. Solutions proposed by the French national nuclear waste management agency (ANDRA) for definitive disposal of LL-LLW include backfilled or excavated near surface repositories in low permeability clay rich layers with a depth of at least 50m. ANDRA's projections indicate that a working definitive solution for the storage of LL-LLW should be available by 2019.

The risks posed by LL-LLW are two-fold. LL-LLW is defined by ANDRA (ANDRA, 2009) as radioactive waste with an activity between 1 and 100,000 Bq per gram which contains isotopes with a half live greater than 30.07 years (^{137}Cs) although such waste commonly contains radioisotopes with far longer half-lives i.e. 1601 years for ^{226}Ra. Such waste will therefore remain a limited radioactive hazard emitting alpha and beta radiation for thousands of years following disposal. Secondly, LL-LLW is often associated with highly toxic non-radioactive inorganic contaminants which will retain their toxicity indefinitely (ANDRA, 2010).

The majority of LL-LLW in France is composed of radium bearing and graphite waste, resulting from processing of minerals for rare earth elements used in electronics and fine metallurgy and decommissioning of first generation nuclear reactors which are moderated with the use of solid

graphite rods. However, radioactive bituminous waste has also been proposed to fall within this category (ANDRA, 2010).

Associated toxic elements of concern to ANDRA include Cd, Sb, B, Cr, As, Hg and U (ANDRA, 2010). Many of these inorganic contaminants including Sb, Cr, As, Hg and U are highly sensitive to changes in redox conditions as discussed in Chapter 1. Whilst deep geological storage results in conditions which are expected to remain anoxic for extended periods of time (ANDRA, 2005), surface storage will likely result in far more dynamic redox conditions due to potential changes in water table level around the repository during its lifespan. Therefore, in a similar way to floodplain top-soils investigated in Chapter 5, contaminants in near surface storage repositories may be subject to cyclic redox conditions in the future following the eventual failure of engineered concrete and metal containers. This chapter aims to elucidate the possible intra cycle and cumulative changes to inorganic contaminant speciation and mobility associated with cyclic redox conditions in a clay rich matrix.

Materials and Methods

Redox control in experimental systems

Redox conditions were controlled in the three clay/contaminant suspensions using a combination of headspace gas control (N_2 or compressed air), as implemented in previous experiments e.g. Patrick et al., (1973); Thompson et al., (2006) and Chapter 5, and injection of an aqueous hydroquinone AH_2DS^{2-} as a bulk reductant substituting for microbial reduction processes.

Dissolved O_2 control

The simplest and most dramatic control on redox conditions within the reactor suspensions was achieved by modulating the concentration of dissolved oxygen in the aqueous phase. During oxidizing cycles the reactor suspension was sparged with compressed air at a rate of 30ml min^{-1} resulting in the diffusion of oxygen from bubbles and the headspace (approximately 20.95% oxygen) to the suspension where it acted as an electron acceptor for redox reactions with reduced solid and aqueous species e.g. Fe(II), S^{-2}, As(III) etc. This lead to a rise in Eh measured at the electrode. During reducing cycles pure N_2 was passed through the headspace at a rate of 30ml min^{-1} causing the diffusion of dissolved oxygen from the suspension to the N_2 headspace and hence the rapid depletion of dissolved oxygen in the aqueous phase leading to a drop in measured Eh. The reactor and gas flow Eh control system used during these experiments is illustrated in Figure 73.

$AQDS^{2-}$ and AH_2DS^{2-} addition as an organic matter substitute and bulk reductant

Whilst depletion of dissolved oxygen in the aqueous phase significantly reduced the oxidizing capacity of the solution, the drop in potential of the solution was not sufficient to cause the reduction of some important oxidized species such as Fe(III) in the absence of an additional electron donor. In natural surface soils and sediments further reduction is driven either directly by natural organic matter (NOM) or by the microbial community which upon oxygen depletion use progressively less efficient electron acceptors such as nitrate, ferric iron and sulphate to oxidize reduced carbon in organic matter (e.g. glucose, where the oxidation state of carbon is 0 is oxidized to CO_2 where the oxidation state of carbon is +4). NOM is also known to function as a catalyst during redox reactions, shuttling electrons between bulk reductants (or microorganisms) and oxidized solid or surface sorbed aqueous species (e.g. As(V), Cr(VI), Fe(III)) (Wolfe and Macalady,

1992; Lovley et al., 1996; Newman and Kolter, 2000; Struyk and Sposito, 2001). Numerous studies suggest that this redox shuttling behaviour is due to quinone like functional groups in which appear to be ubiquitous in natural organic matter (Scott et al., 1999; Struyk and Sposito, 2001; Cory and McKnight, 2005). As these experiments were conducted in the absence of an active anaerobic microbial community which is normally found in natural surface sediments (Hansel et al., 2008), reduction potential was controlled by the direct injection of the hydroquinone, 9,10-anthraquinol 2-6-disulfonate (AH_2DS^{2-}) which is the reduced form of 9,10-anthraquinone-2,6-disulfonate ($AQDS^{2-}$). $AQDS^{2-}$ is often used as a substitute for electron shuttling NOM in model mineral/microbial systems (Lovley et al., 1996).

The reduction of $AQDS^{2-}$ to AH_2DS^{2-} (via a semi-quinone radical species $AHDS^{3-}$ at high pH) is reversible and involves the transfer of 2 electrons and 2 protons (shown in Figure 84).

The experimentally derived 2 electron reduction potential for $AQDS^{2-}/AH_2DS^{2-}$ (Eh^0) is 0.228 V versus the standard hydrogen electrode (SHE) (Rosso et al., 2004), therefore -0.160 V at pH 7. This maximum reduction potential is similar to those documented for humic substances in the literature (Straub and Schink, 2003; Bauer et al., 2007). This Eh is well within the limits of measured potentials in reduced flooded natural soils and sediments (Mansfeldt, 2003; Vorenhout et al., 2004) or in landfill leachate plumes (Lyngkilde and Christensen, 1992). The direct addition of small quantities of AH_2DS^{2-} therefore allows a conservative simulation of natural reducing conditions whilst avoiding the use of other strong chemical reductants such as sodium dithionite which have been shown to not accurately simulate reduction processes in natural systems (Ribeiro et al., 2009; Stucki, 2011). Whilst the reduction potential for AH_2DS^{2-} does allow reduction of ferric iron it is not low enough to favour sulphate reduction of methane production.

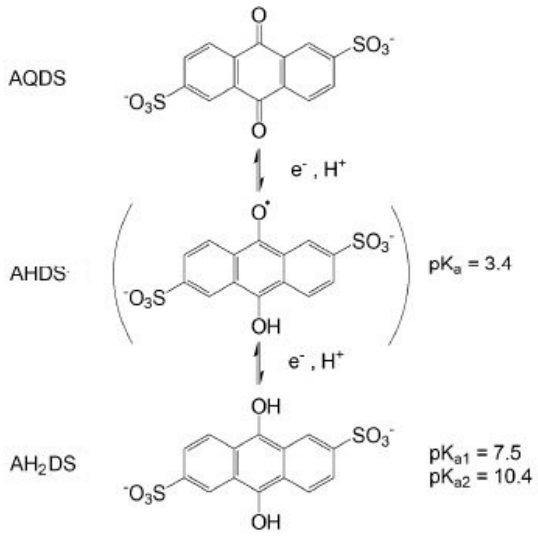

Figure 84: Two electron reduction of $AQDS^{2-}$ to AH_2DS^{2-} modified from Aeschbacher 2007.

A total of five AH_2DS^{2-} additions were applied to each reactor during the experimental period on days 6, 13, 20, 27 and 34. Each addition consisted of 10 mL of 30mM L^{-1} AH_2DS^{2-} solution (with the exception of day 27 in reactor 1 when 30 mL of 30 mM L^{-1} solution was added to test the influence of AH_2DS^{2-} quantity or reductive potential was limiting reductive processes) prepared from disodium AQDS salt and reduced following the method detailed below.

Reduction of $AQDS^{2-}$ to AH_2DS^{2-} by Hydrogen

Reduction of $AQDS^{2-}$ may be achieved chemically, electrochemically, or biologically (Coates et al., 1998; Lovley et al., 1999; Aeschbacher, 2007). Electrochemical and chemical reduction procedures were trialled prior to the start of experiments and for reasons of practicality, chemical reduction was selected. It was found that while both trialled methods worked well chemical reduction was

achieved more rapidly using simpler apparatus and without the need for supporting electrolytes which reduced the solubility of AH_2DS^{2-}.

As AH_2DS^{2-} was used as a bulk reductant in these experiments as opposed to its most common use as an electron shuttle (Lovley et al., 1996) highly concentrated 30mM L^{-1} solutions were prepared. As solubility of $AQDS^{2-}$ is less than that of AH_2DS^{2-} and is limited further by the presence of additional cations in solution, $AQDS^{2-}$ solutions were prepared by dissolving 98% pure disodium AQDS salt purchased from TCI Europe (Belgium) in 18.2mΩ water at 70°C in an ultrasonic bath. Once fully dissolved the warm solution was transferred immediately to a reaction vessel containing palladium coated pellets in order to avoid re-precipitation of disodium AQDS due to cooling. The reaction vessel was sealed with two unidirectional valves, the first to allow the entry of hydrogen gas into the bottom of the reactor and the second to allow for the exhaust of hydrogen from the reactor headspace. The solution was sparged with hydrogen gas and the solution changed from colourless to bright red indicative of the formation of AH_2DS^{2-}. The reduced solution was then extracted from the reaction vessel via syringe through a rubber septum, sealed and transferred to a 100% N_2 atmosphere glove box where it was filtered to 0.22µm.

Suspension composition

Solid phase preparation

A core sample of the Jurassic COx clay from the Parisian basin in northern France was used as the solid phase in the reactor suspensions. The core (EST 40952) was extracted in ANDRA's laboratory of Meuse/Haute-Marne. Prior to addition to the reactors this core was broken up and ground in an agate ball mill until all material passed a 0.63µm sieve. As each reactor had a total suspension capacity of 1 L, ~2 g of clay was used to give a clay loading of 2 g L^{-1}. Precise clay loadings are detailed in Table 24.

Table 24: Precise clay loadings in each reactor.

Reactor	Clay loading g L^{-1}
1 Cr, As, Hg, U	2.0030
2 As	2.0032
3 Cr	2.0028

Solid phase chemical and mineralogical properties

Although the mineralogy of core EST 40952 has not been characterized directly, extensive mineralogical investigation of the COx layer has been conducted previously (ANDRA, 2005).

The COx is composed of three main mineralogical phases:

Clays (25-60% of the total rock mass) comprising of illite, smectite, micas, kaolinite and chlorite.

Carbonates – (20-40% of the total rock mass) consisting primarily of calcite with a few per cent of dolomite.

Quartz – (20-30% of the total rock mass) with a fine particle size distribution consisting mostly of silt.

In addition to the bulk mineralogical components, accessory phases such as pyrite (2-3wt% total rock mass maximum) are also present (Elion, 2005).

X-ray diffraction and total elemental concentration analyses from cores close to EST 40952 indicate that the proportion of phyllosilicates in this layer is comparatively high, that background contaminant concentrations are low to moderate and that little lateral variation occurs within the layer (Made, 2010). The range in mineralogy of samples and their background contaminant concentrations analysed from borehole PGZ 1001 are shown in Table 25 and Table 26.

Table 25: Mineralogical composition of solid phase. From Made (2010).

Mineral	Percent of rock mass (wt. %)
Phyllosilicates	**50-55**
Mica/illite	21-24
Illite/Smectite (R=1 + R=0)	24-27
Kaolinite	2-4
Chlorite	2-4
Tectosilicates	**23-25**
Quartz	20-22
Carbonates	**18-20**
Calcite	15-18
Pyrite	**<1.5**

Table 26: Background contaminant concentrations in solid phase prior to additions. From Made (2010).

Contaminant	Concentration, mg kg^{-1}
Arsenic	20
Chromium	90-100
Uranium	2

Reductive capacity

Redox conditions in the COx are mildly reducing (pore water Eh of between -180 and -150mV) and are thought to be buffered in this range by pyrite/Fe(III) and pyrite/sulphate redox couples (EURATOM, 2010). In addition the COx contains up to 2% reduced organic matter and reactive surface adsorbed Fe(II). These characteristics give the solid phase used in these experiments a moderate initial reductive capacity.

Contaminant solution preparation

A 1L solution containing all contaminants to be investigated was prepared for each reactor under oxic conditions and adjusted to pH 7 using dilute HCl and NaOH. These solutions were added to the reactors before the ground clay material to avoid super saturation and precipitation of contaminant mineral phases prior to the start of Eh controlled experiments.

Chromium, arsenic and uranium were each added to the solutions as oxidized salts to concentrations of 50µM L^{-1} (8.098 mg L^{-1} of sodium chromate (Na_2CrO_4), 15.601 mg L^{-1} of sodium arsenate hepta-hydrate ($Na_2HAsO_4.7H_2O$) and 25.1065 mg L^{-1} of uranyl-nitrate hexa-hydrate ($UO_2(NO_3)_2.6H_20$)). Mercury was added to the solution in reactor 1 using 1000ppm standard solutions in a 0.5 M L^{-1}

HNO_3 matrix from SPEX plasma to a concentration of 0.175 µM L^{-1}. The precise additions for each reactor are provided in Table 27.

Table 27: Precise elemental additions to contaminant solutions.

Contaminant added (Day 0)	Reactor 1, mg (uM L^{-1})	Reactor 2, mg (uM L^{-1})	Reactor 3, mg (uM L^{-1})
Sodium chromate	8.5 (52.479)	-	8.7 (53.714)
Sodium arsenate hepta-hydrate	16.3 (52.240)	15.9 (50.958)	-
Mercury 1000ppm standard	-(0.175)	-	-
Uranyl nitrate hexa-hydrate	25.3 (50.385)	-	-

As the availability of background contaminant concentrations in the COx is not known Table 28 shows the maximum contaminant concentrations possible in solution assuming 100% mobility of background contaminants within the added solid phase and 100% mobility of added contaminants.

Table 28: Maximum possible contaminant concentrations in solution assuming 100% mobility of added contaminants and background contaminants.

Contaminant	Reactor 1, uM L^{-1}	Reactor 2, uM L^{-1}	Reactor 3, uM L^{-1}
Chromium	56.331	-	57.566
Arsenic	52.775	51.493	-
Mercury	0.175	-	-
Uranium	50.402	-	-

Second contaminant addition to Reactor 1

On day 30 of the experiment additional contaminants were added to reactor 1 followed by a period of intensive sampling in order to ascertain the rates of contaminant immobilization and to test the immobilization capacity of the COx for each contaminant. Exact additions are detailed in Table 29.

Table 29: Precise elemental additions to reactor 1 on day 30 of the experiment and concentrations assuming 0.844L volume (i.e. assuming no evaporative losses prior to additions).

Element added (Day 30)	Reactor 1 (mg / uM L^{-1})
Sodium chromate	13.3 (97.292)
Sodium arsenate hepta-hydrate	22.3 (84.680)
Mercury 1000ppm standard	(0.207)
Uranyl nitrate hexa-hydrate	35.0 (82.587)

Sampling procedure and suspension separation

Each sample consisted of 7ml of suspension which was extracted through a connection on the top of the reactor by pulling on a syringe connected to a sampling tube. Prior to sampling the syringe and the tube were purged with either air or nitrogen (Dependent on the half cycle). The syringe was then sealed and transferred to a 100% N_2 atmosphere glove-box (JACOMEX) (O_2, CO_2 <1 ppmv). The

suspension was subsequently centrifuged at 4300rpm for 30 minutes to separate solid particles from the aqueous phase (particle size left in suspension < 0.2µm assuming spherical particle geometry and density of 2.65 gcm^3 and a fluid density of 1 gcm^3 calculated from Stoke's law). The resulting supernatant was then filtered to 0.22µm to ensure only truly aqueous or colloidal material remained and that any larger particles disturbed during supernatant removal after centrifugation were removed. The remaining filtrate was stored at 4°C prior to further analysis.

Analytical methods

ORP and pH Measurement

Oxidation/Reduction potential (ORP) and pH were measured continuously in each reactor using Mettler-Toledo DXT series, solid-polymer Xerolyt® electrolyte, open-junction electrodes (Mettler-Toledo France, Analyse Industrielle). A five point pH calibration (2, 4, 7, 10, 12) was performed for all pH electrodes at the start and end of the experiment showing that the electrode response had not shifted more than 0.02 pH units (within the pH range used in the experiments) during the 36 day experiments.

Measured ORP readings were converted to a redox potential with respect to the Standard Hydrogen Electrode (SHE) by adding the difference of the measurement of the redox potential in a ZoBell's solution (0.0033M $K_3Fe(CN)_6$ and 0.0033M $K_4Fe(CN)_6$ with its theoretical value of +428mV. The calculated difference was equal to the electrode manufacturer specification of 207 mV. The Eh electrodes were found to drift by 3 mV upon measuring a ZoBell's solution at the end of the 36 day experiments.

Solid and Aqueous Mercury concentrations

Total Hg concentrations in the aqueous phase were analysed using a Leco 254 Advanced Mercury Analyser following a method described by (Costley et al., 2000). Using this technique samples are placed in a nickel holder which is inserted into a quartz combustion tube with a catalyst consisting of cobalt oxalate, manganese oxide, cobalt and calcium acetate. Samples are then dried before combustion in a pure oxygen atmosphere at 750°C. At this temperature all mercury is vaporized and then trapped on a gold amalgamator whilst other interfering elements are removed. Once interfering elements have been exhausted the amalgamator trap is heated to 900°C in order to re-release the trapped Hg into the gas phase where it is transported to a heated cuvette. The total mercury in the gas phase may then be determined by atomic absorption spectroscopy using a silicon diode detector due to the absorption peak for mercury at 253.6 nm. All samples were analysed in triplicate (500mg per measurement). After insertion of samples a drying cycle was conducted for a period of 200 seconds, followed by combustion for 200 seconds and finally analysis. Blanks were measured before analysis and after every 10 samples. Mercury measured in the blanks was consistently lower than 30pg for dry blanks (0.15ppb for 18.2mΩ blanks). The standard deviation between triplicates was calculated to determine the total quantifiable error for this technique which in 92% of cases was less than 2 ppb.

Aqueous total elemental concentrations: Na, Al, Ca, Cr, Mn, Fe, As and U

To measure the concentration of major and trace elements (Na, Ca, Cr, Mn, Fe, As and U) in solution, an Agilent 720ES inductively coupled plasma atomic emission spectrometer (ICP-OES) was used (Agilent Technologies Europe).

Following filtration, samples were diluted to ensure that concentrations of all elements were within the linear response range of the ICP-OES and acidified to 2% HNO_3 so that losses were not experienced due to precipitation of oxides from solution prior to analysis. Matrix-matched standards prepared from 1000ppm stock solutions were used for quantification purposes. All samples were analysed in triplicate (3 separate injections) and the margins of error reported represent the relative standard deviation between injections for each sample.

Concentrations of major anions: Chloride, Nitrite, Nitrate, and Sulphate

To measure the concentration of major anions in sample filtrate a Waters 4000 Capillary Ion analyzer was used. Ions quantified were chloride (Cl^-), nitrite (NO_2^-), nitrate (NO_3^-), and sulphate (SO_4^{2-}). Phosphate (PO_4^{3-}) was below the limit of detection in all samples and carbonate was not quantified due to equilibration of solutions with atmospheric CO_2 concentrations prior to analysis. Limits of detection for each anion were determined to be: 0.13, 0.097, 0.415 and 0.452 ppm for Cl^-, SO_4^{2-}, NO_3^-, and NO_2^- respectively. Measurements of triplicates demonstrated a typical relative standard deviation of <3% for each element.

Verification of $AQDS^{2-}$ reduction

The complete reduction of $AQDS^{2-}$ was verified by UV/Vis spectrometry using a Perkin Elmer Lamba 35 spectrometer using a method documented by (Aeschbacher, 2007) and (Wang et al., 2011) (Figure 85). Absorption spectra from initial $AQDS^{2-}$ solutions showed a peak at 328nm, characteristic of oxidized $AQDS^{2-}$. Reduction resulted in the disappearance of the absorbance peak at 328nm and the appearance of peaks at 386nm, characteristic of reduced AH_2DS^{2-} which is the dominant species at pH 7 and 406nm characteristic of $AHDS^{3-}$ which is also expected as a less dominant species.

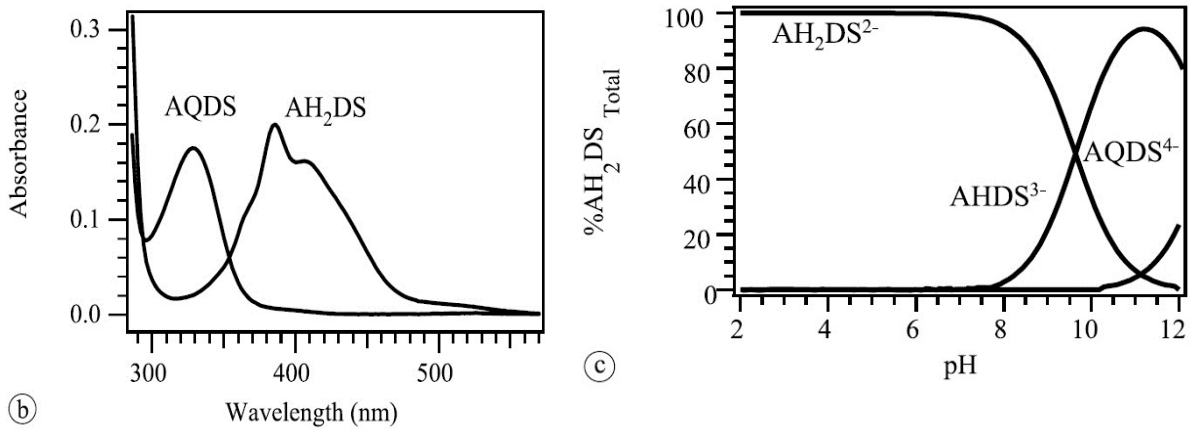

Figure 85: Absorption spectra of AQDS and reduction products at pH 6.5 (from Wang et al. (2011)).

Results & Discussion

Performance of experimental setup

Oscillation of redox conditions between approximately -215 mV and +340 mV was achieved consistently within all reactors over the course of the experimental period (Figures 87, 88, 89 and 90). These values are consistent with Eh values found in a range of near surface soil and sediment environments prone to redox oscillating conditions (Mansfeldt, 2003).

Temperature within the reactors was maintained at 22°C +/-2°C for the entire experimental period (see Figure 86). Peaks in temperature observed on days 16, 17, 23, 24, 30 and 31 are thought to be due to increases in environmental temperature within the room where the reactors were installed rather than the result of exothermic reactions within the reactors themselves.

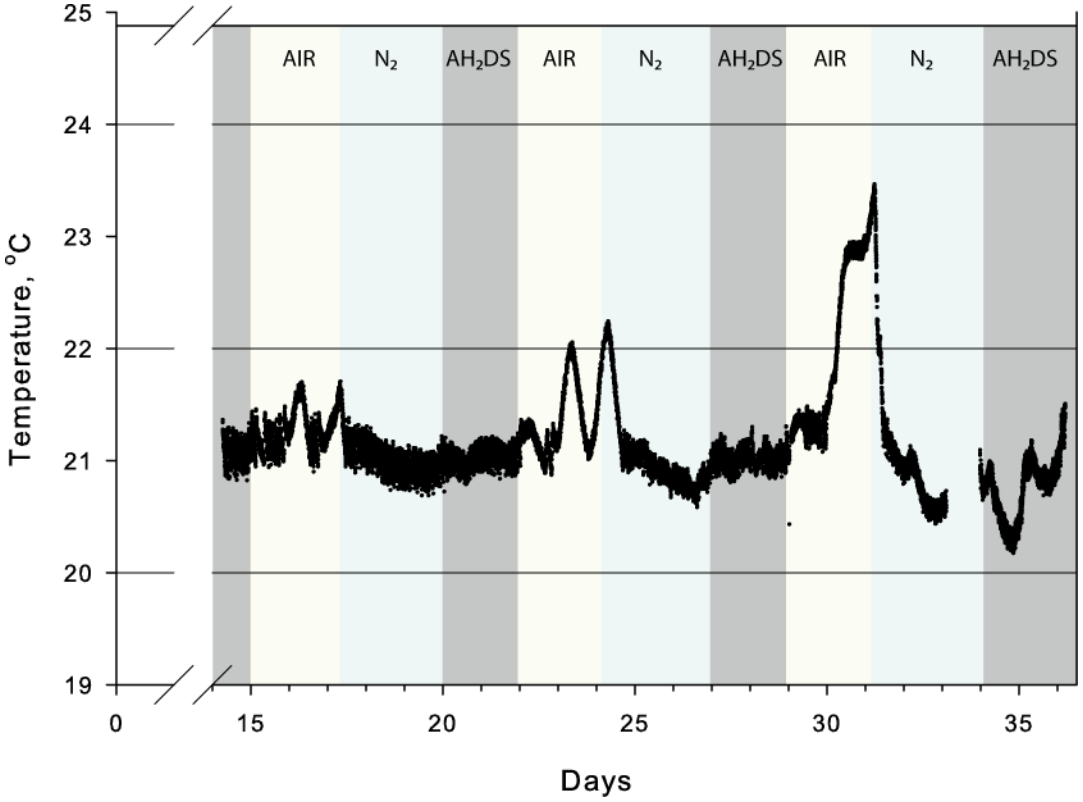

Figure 86: Temperature variation within the reactors during the experimental period (22 +/- 2°C).

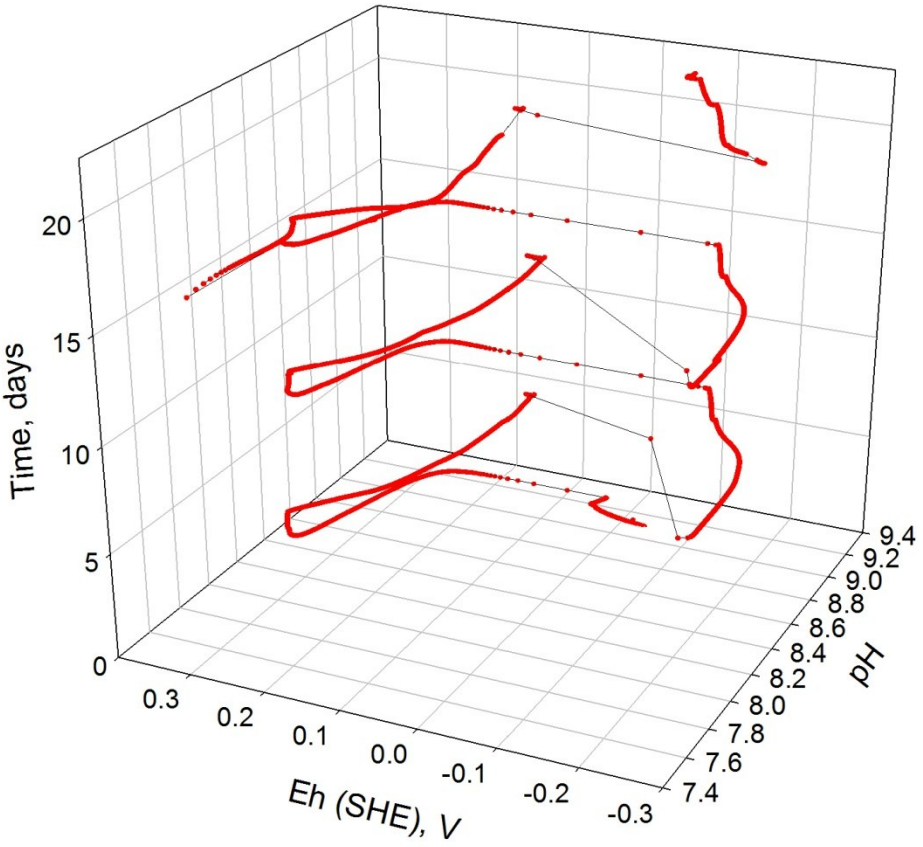

Figure 87: The variation of Eh and pH conditions in reactor 1 with time illustrating the consistency of the imposed redox oscillations.

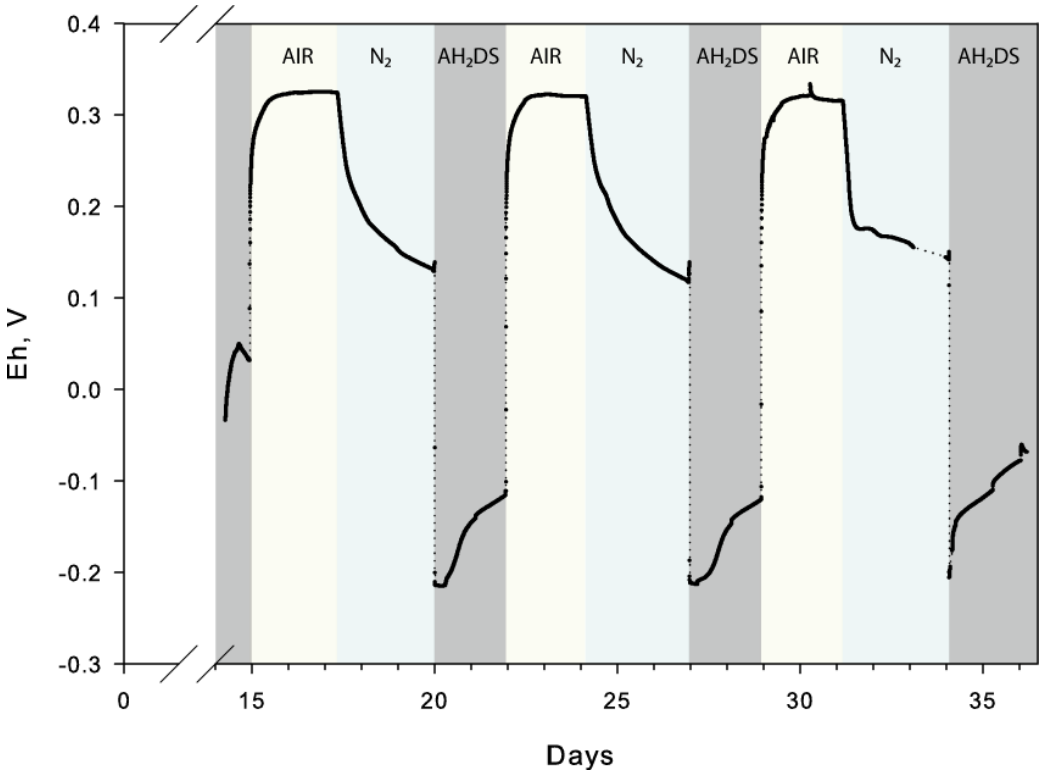

Figure 88: Eh (SHE) with time measured within the reactor 1 suspension, reference shading

indicates; light yellow = initiation of air sparging, light blue = initiation of N_2 sparging, grey = addition of AH_2DS^{2-} reductant solution.

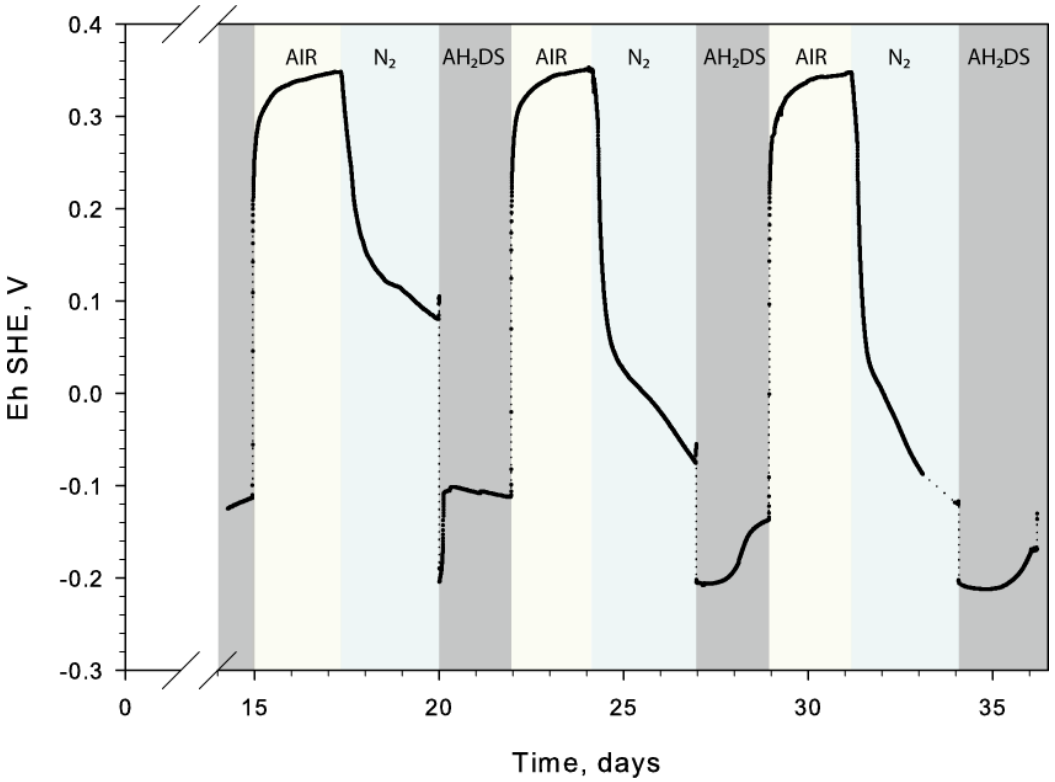

Figure 89: Eh (SHE) with time measured within the reactor 2 suspension, reference shading indicates; light yellow = initiation of air sparging, light blue = initiation of N_2 sparging, grey = addition of AH_2DS^{2-} reductant solution

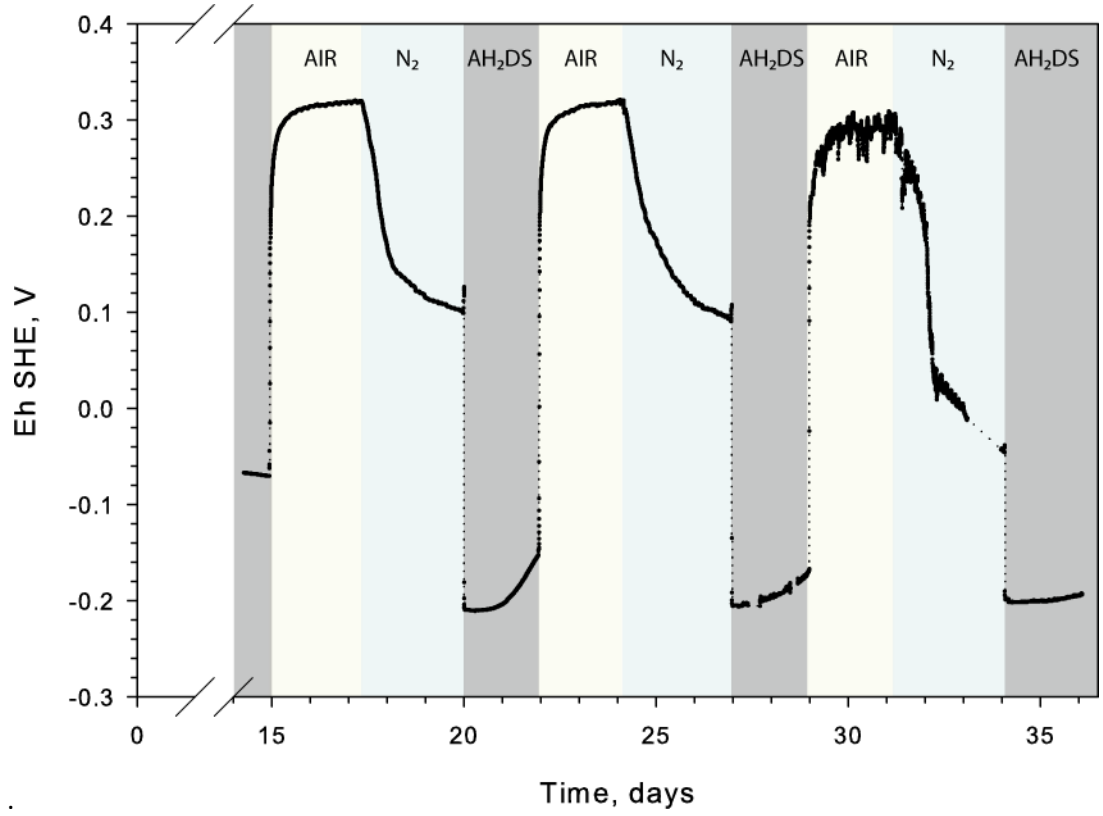

.

Figure 90: Eh (SHE) with time measured within the reactor 3 suspension, reference shading indicates; light yellow = initiation of air sparging, light blue = initiation of N_2 sparging, grey = addition of AH_2DS^{2-} reductant solution.

The experimental installation performed well throughout the experiment with a minimum data resolution of 30s achieved for Eh, pH and temperature measurements, with a few regrettable exceptions. The most notable of these occurred on day 14 of the experiment when a power supply failure in the computer controlling the experiment and recording data caused the complete loss of two internal hard drives.

The computer system had been designed so that two independent disks were arranged in a RAID 1 (Redundant Array of Independent Disks) configuration so that data was recorded simultaneously to two independent disks. This configuration allows for a degree of redundancy in that data is protected from failure of a single hard drive. Unfortunately in this case two hard drives failed simultaneously and catastrophically leading to the loss of all Eh, pH and temperature data between days 0 and 14. For this reason all data presented and interpreted in this chapter considers only days 14 to 36 (three full redox oscillations) although experimental procedures remained constant for the duration of the experiments (five full redox oscillations).

The 2nd equipment failure affecting data quality during the experimental period occurred on day 27 of the experiments when the mechanical stirrer for reactor 3 malfunctioned. The fault was identified as a burned out electronic component on the speed controller circuit board, however immediate repair was not possible. Therefore, agitation in the reactor 3 suspension stopped on day 27 resulting in partitioning of the reactor via sedimentation of suspended particles. The electrode tips were both covered by sediment resulting in noisy Eh/pH data between days 27 and 36. Whilst it is not believed that sedimentation would have resulted in intense redox stratification due to the lack of an active microbial community, diffusion between the sampled supernatant and interstitial pore water measured via the pH and Eh electrodes may have been limiting for some species.

For future long running experiments, to reduce the chance of deterioration or loss of data, it is recommended that mechanical, electrical and data redundancy be increased.

Whilst active mechanical redundancy is difficult to implement on such a small scale, provisioning of spare parts for crucial mechanical (i.e. suitable mechanical stirrers and stirring shafts) is recommended.

Electrical redundancy should be implemented via uninterruptable power supplies, of sufficient power to provide electricity to data processors, data loggers, computer equipment, water bath pumps and heating elements.

Data redundancy should be increased via the implementation of automatic network backup of acquired data rather than relying on RAID style backups within one physical computer.

In addition to equipment failures limitations of the experimental setup were noted. Most importantly high rates of evaporation were observed from the reactor suspensions due to the constant sparging of the suspension with dry compressed air or nitrogen. While direct measurement of evaporation rate was not possible, chloride is often used as an environmental tracer to determine evaporation or recharge rates (Grunberger et al., 2008). The recorded increases in chloride

concentration within the reactors act as a good indicator of increasing ionic strength caused by evaporation (Figure 91).

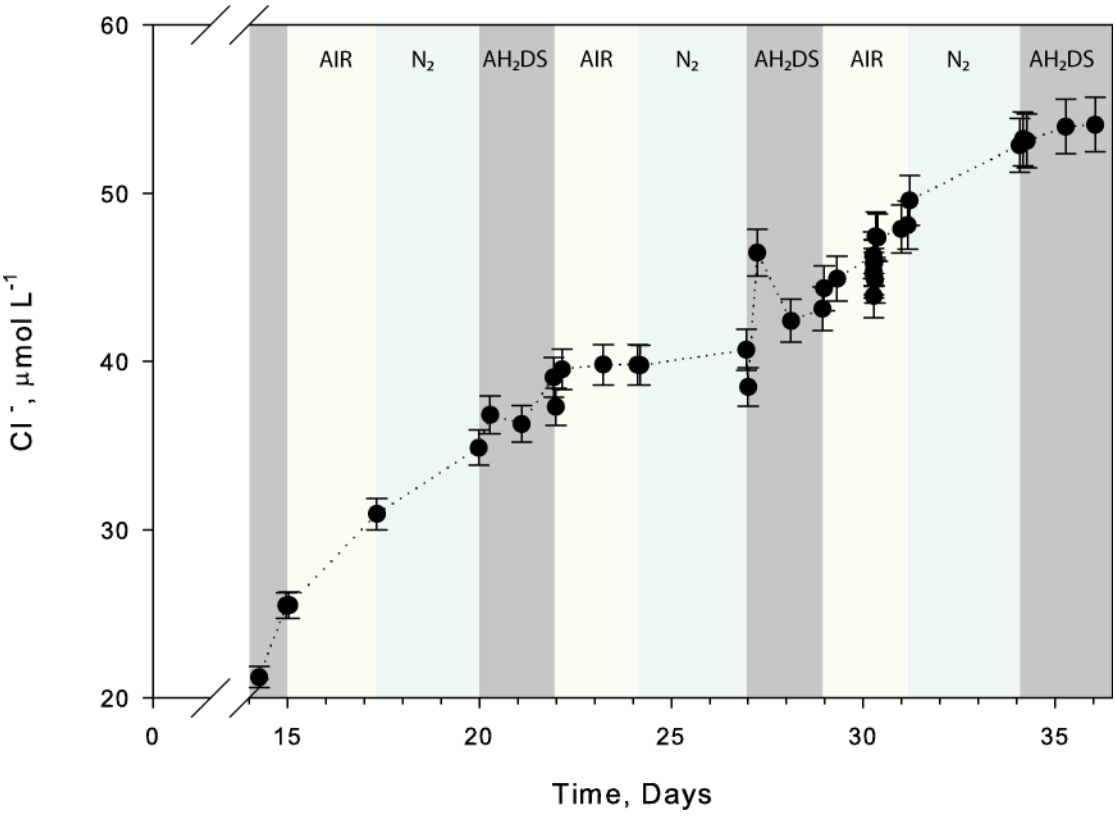

Figure 91: Chloride concentration in the reactor 1 suspension over time. The increase is considered to be due to evaporation and to a lesser extent addition of HCl during pH balancing of AH_2DS^{2-} solutions on days 20 and 27.

In order to avoid these evaporative losses and hence increasing ionic strength in future experiments online humidifiers should be added to incoming air and nitrogen lines and condenser coils added to exhaust ports.

Electron balance upon addition of AH_2DS^{2-}

Following degassing of oxygen from the suspensions by 2-3 days of nitrogen sparging AH_2DS^{2-} was added as a reductant. Each addition of AH_2DS^{2-} to the reactor suspensions lowered the measured Eh to approximately -215 mV and reduced oxidized species due to the addition of two electrons by the oxidation of each reduced quinone molecule. Considering the half reaction for the oxidation of each 10 mL, 30 mM L^{-1} AH_2DS^{2-} addition (Equation 12), a total of 0.6 mM of electrons should be available for reduction of oxidized species (with the exception of day 27 in reactor 1 where 1.8 mM of electrons were made available). This assumes that all AH_2DS^{2-} was oxidized following addition and that no oxidation of AH_2DS^{2-} to $AQDS^{2-}$ occurred prior to injection.

Equation 12 $AH_2DS^{2-} \rightarrow AQDS^{2-} + 2H^+ + \mathbf{2e^-}$

Oxidized species thermodynamically predicted to dominate in the reactors prior to AH_2DS^{2-} addition include Fe(III), U(VI), As(V), Cr(VI), Hg(II) and SO_4^{2-} (see corresponding Pourbaix diagrams for reactor

1 in Figures 92, 93, 94, 95, and 97). However, the availability of each of these oxidized species as electron acceptors and the kinetics of their reduction is radically different.

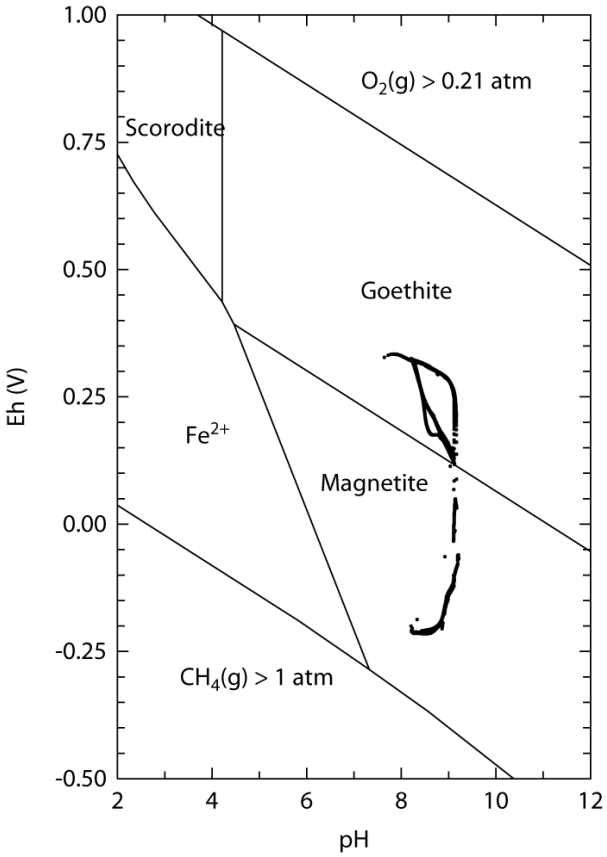

Figure 92: The Fe-As–H_2O–CO_2 system at 298.15K and 10^5 Pa. $\sum Fe = 10^{-10}$. Measured Eh pH conditions are overlaid in black.

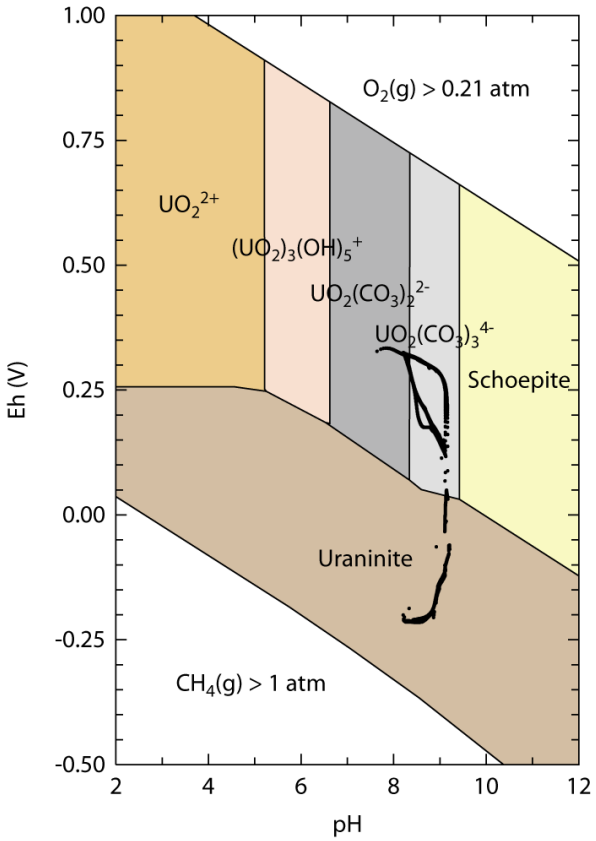

Figure 93: The U–CO_2–H_2O system at 298.15K and 10^5 Pa. $\sum U = 10^{-10}$. Measured Eh pH conditions are overlaid in black.

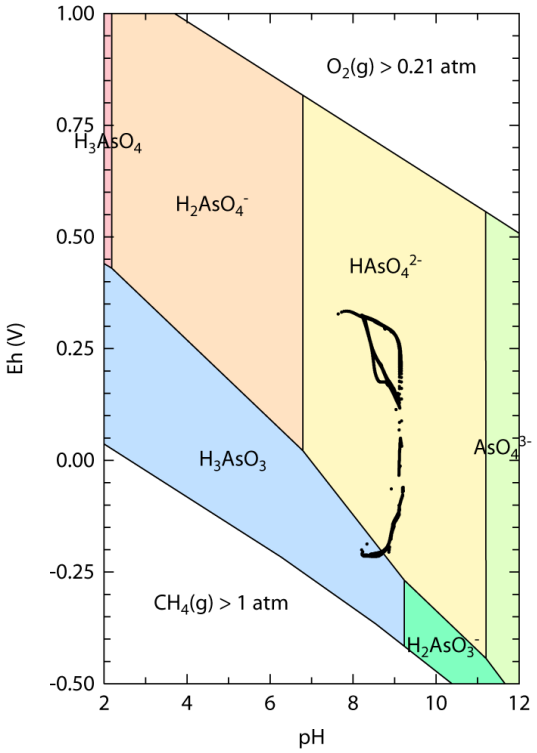

Figure 94: The As–CO_2–H_2O system at 298.15K and 10^5 Pa. ∑As = 10^{-10}. Measured Eh pH conditions are overlaid in black.

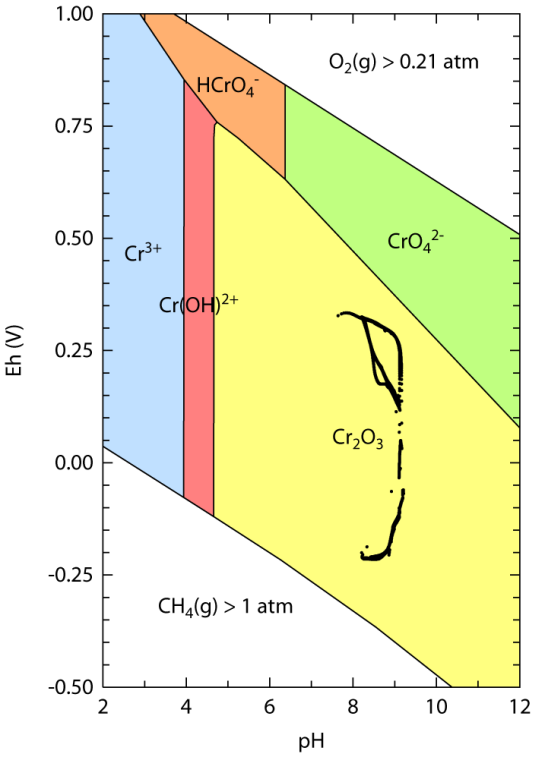

Figure 95: The Cr–CO_2–H_2O system at 298.15K and 10^5 Pa. ∑Cr = 10^{-10}. Measured Eh pH conditions are overlaid in black.

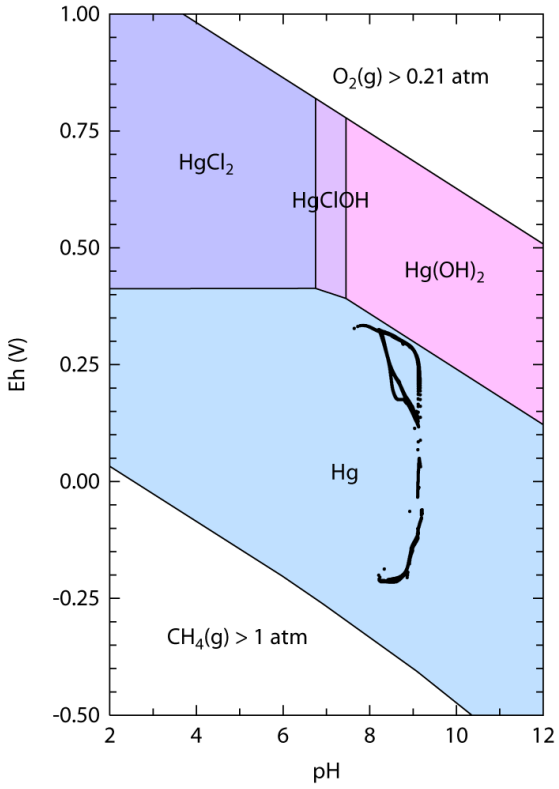

Figure 96: The Hg–Cl-CO_2–H_2O system at 298.15K and 10^5 Pa. ∑Hg = 10^{-10}. Measured Eh pH conditions are overlaid in black.

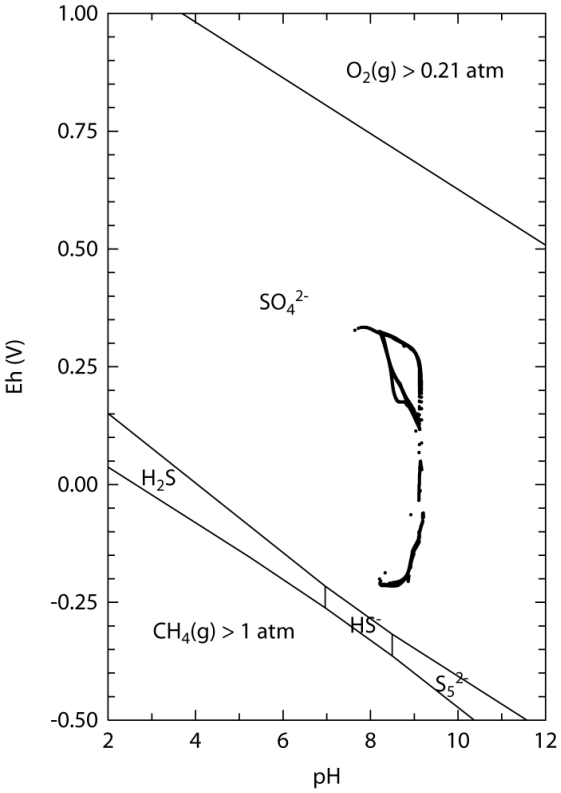

Figure 97: The S–CO_2–H_2O system at 298.15K and 10^5 Pa. ∑S = 10^{-10}. Measured Eh pH conditions are overlaid in black.

The precipitation of Manganite is thermodynamically predicted in each of the reactors during the oxic phase as illustrated by Figure 98. However, oxidation of $Mn^{2+}_{(aq)}$ is a relatively slow kinetic process in the absence of manganese oxidizing bacteria such as Leptothrix species even in strongly favourable conditions (Zhang et al., 2002). Therefore, despite the thermodynamic prediction we expect limited Manganite precipitation and subsequent dissolution during cycling.

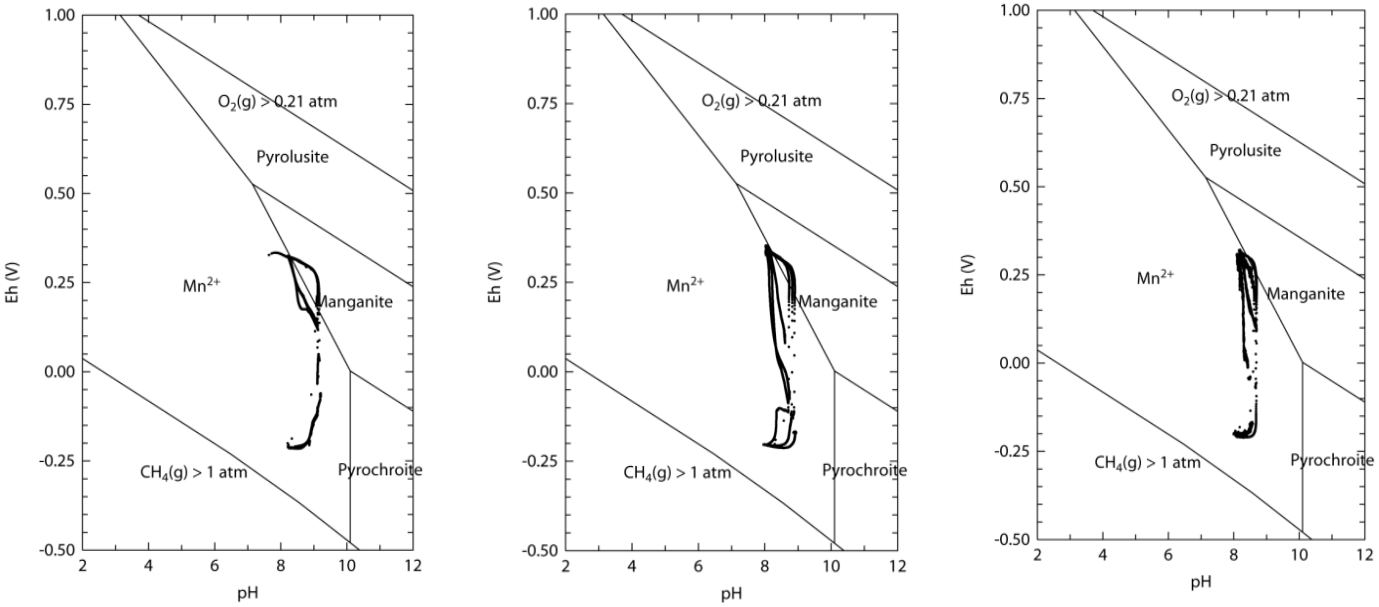

Figure 98: Pourbaix diagrams of the Mn – CO_2 – H_2O system at 298.15K and 10^5 Pa. ∑ Mn = 10^{-5} from LLNL data. Measured Eh pH conditions in reactor suspensions are overlaid in black (reactor 1 left, reactor 2 middle and reactor 3 right).

Initial concentrations of oxidized contaminants (Cr, As, Hg and U) are known, as Cr, As and U were added as oxidized salts and, in the case of mercury, as a free cation which will have rapidly hydrolyzed to $Hg(OH)_2$ under prevailing conditions in the suspension. In contrast the total concentration of oxidized iron is more difficult to estimate.

A large proportion of the total iron content within the COx sample is present in the structure of phyllosilicate minerals and as such is significantly less available for redox processes than the iron contained within pyrite. As pyrite concentrations within the powdered COx sample are known to be < 1.5 % a theoretical maximum Fe(III) concentration within the oxidized suspension can be calculated as 0.2501 mM, based on total oxidative dissolution of pyrite during the first oxidizing cycle and suspension equilibration period, if initial concentrations of possible surface adsorbed Fe(II) and structural clay Fe(II) are neglected.

Although complete and rapid oxidative dissolution of pyrite may seem improbable, it has been shown that oxidation of pyrite by molecular oxygen increases with pH and that the presence of carbonate and bicarbonate ions accelerates pyrite oxidation under moderately alkali conditions (Caldeira et al., 2010) . Bicarbonate and to a lesser extent carbonate ions (due to pH) are predicted to occur in this system due to dissolution of $CO_{2(g)}$ in the headspace during oxidizing cycles (Equation 14).

Equation 13 $CO_{2(g)} \rightleftharpoons CO_{2(aq)}$

Equation 14 $CO_{2(aq)} + H_2O \rightleftharpoons H_2CO_{3(aq)} \rightleftharpoons HCO_3^-{}_{(aq)} + H^+{}_{(aq)} \rightleftharpoons CO_3^{2-}{}_{(aq)} + 2H^+{}_{(aq)}$

It has long been considered that the rate limiting step in pyrite oxidation is the oxidation of Fe(II), in acidic (Singer and Stumm, 1970) solutions. Recent work on the mechanism of accelerated pyrite dissolution in carbonate solutions by Caldeira et al (Caldeira et al., 2010) suggests that this is also the case in alkali conditions but that soluble iron carbonate complexes near to the pyrite surface help accelerate electron transfer (Figure 99).

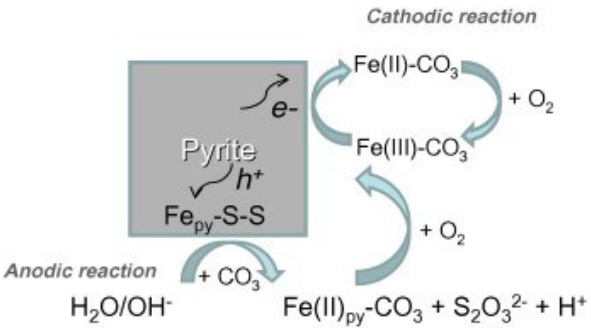

Figure 99: Schematic illustration of the mechanism of accelerated pyrite dissolution in carbonate containing media proposed by (Caldeira et al., 2010).

The oxidation of pyrite in carbonate containing solutions has been shown to result in the preferential precipitation of ferrihydrite over other oxides (such as hematite) which have been shown to form in hydroxide media (Caldeira et al., 2003). It is therefore probable that the ferric oxide resulting from pyrite oxidation by molecular oxygen in the COx is ferrihydrite. Freshly precipitated ferrihydrite has been shown to have an average size of between 2 and 6nm (Michel et al., 2007) and hence a high surface area (> 200 $m^2\ g^{-1}$)(Weidler, 1997) which would make it a highly suitable electron acceptor for reduction by AH_2DS^{2-}.

Subsequent to the full oxidation of pyrite to Fe(III) and SO_4^{2-}, summarized in the sequence of equations (15, 16, 17 and 18) shown below, the re-reduction of Fe(III) to Fe(II) by added AH_2DS^{2-} is thermodynamically predicted and kinetically favourable. However the reduction of sulphate to sulphide is not (Figure 97).

Equation 15 $FeS_2 + 3O_2 + 2H_2O \rightarrow Fe^{2+} + 2SO_4^{2-} + 4H^+$ (Gray, 1997)

Equation 16 $Fe^{2+} + 0.25O_2 + H^+ \rightarrow Fe^{3+} + 0.5H_2O$ (Konhauser, 2007)

Equation 17 $Fe^{3+} + 3H_2O \rightarrow Fe(OH)_3 + 3H^+$ (Konhauser, 2007)

Equation 18 $FeS_2 + 14Fe^{3+} + 8H_2O \rightarrow 15Fe^{2+} + 2SO_4^{2-} + 16H^+$ (Edwards et al., 2000)

The half reactions for the thermodynamically predicted reduction of key oxidized species within the reactor suspensions are given in Table 30. Evaluating the quantity of reducible oxidized species

within the reactors and the number of electrons required for their reduction to thermodynamically predicted oxidation states, it is possible to show that there is a slight deficit of reductant with the initial AH_2DS^{2-} addition (see Table 30). This deficit would of course diminish during the experiment due to sampling of the suspension.

Table 30: Evaluation of electron requirements for complete reduction of key oxidized species in reactor 1 during the first AH_2DS^{2-} addition.

Half reaction for reduction of oxidized reactor species	Electrons transferred per atom of contaminant	Protons transferred per atom of contaminant	Maximum quantity of oxidized species estimated in suspension, mM	Electrons required for complete reduction of oxidized species, mM	Quantity of protons consumed during complete reduction of oxidized species mM
$FeOOH + 3H^+ + e^- \rightarrow Fe^{2+} + 2H_2O$	1	3	0.2501	0.2501	0.7503
$HAsO_4^{2-} + 4H^+ + 2e^- \rightarrow H_3AsO_3 + H_2O$	2	4	0.0528	0.1056	0.2112
$UO_2(CO_3)_3^{4-} + 3H^+ + 2e^- \rightarrow UO_2 + 3HCO_3^-$	2	3	0.0504	0.1008	0.1512
$CrO_4^{2-} + 8H^+ + 3e^- \rightarrow Cr^{3+} + 4H_2O$	3	8	0.0563	0.1689	0.4504
			Total:	**0.6254**	**1.5631**

As the capacity of the reductant to supply electrons for reduction is approximately equal to the capacity for oxidized species to accept electrons it is reasonable to postulate that, following AH_2DS^{2-} additions all available Fe(III), present as disordered ferric oxides, was reduced to Fe^{2+} and liberated into solution accounting for the peaks in measured aqueous/colloidal iron concentration following AH_2DS^{2-} additions (Figures 100, 101 and 102). However, measured aqueous iron concentrations do not correspond well to the concentrations calculated stoichiometrically assuming almost total Fe(III) reduction. Assuming almost total Fe(III) reduction by AH_2DS^{2-} additions it is possible to disparity this by subtracting iron adsorbed to surfaces or forming secondary ferrous phases:

Equation 19 $Fe(III)_{tot} = \Delta[Fe^{2+}]measured + Fe^{2+}$ adsorbed + Fe^{2+} precipitated.

Potential ferrous precipitates could include FeS, $FeCO_3$ and Fe_3O_4 however the reduction potential of AH_2DS^{2-} is insufficient to reduce sulphate to sulphide, therefore it is reasonable to assume that the suspension is never supersaturated with respect to iron sulphide minerals. As the suspension had been sparged with pure $N_{2(g)}$ for nearly 3 days prior to AH_2DS^{2-} addition, free carbonates present during oxidizing cycles would likely have degassed as $CO_{2(g)}$ before $Fe^{2+}_{(aq)}$ formation and hence the suspension would have remained under-saturated with respect to siderite. Equally even under supersaturated conditions, precipitation kinetics of siderite and magnetite are extremely slow (Jensen et al., 2002) especially when compared to the rapid adsorption of Fe(II) at neutral to high pH (Charlet et al., 1998) therefore it can be assumed that neither siderite or magnetite formation occured immediately following AH_2DS^{2-} additions.

Assuming therefore that there was no precipitation of ferrous minerals:

Equation 20 $Fe(III)_{tot} = \Delta[Fe^{2+}]measured + Fe^{2+}$ adsorbed

This would indicate therefore that between 0.250 and 0.237 mM of Fe^{2+} is adsorbed by the 2g COx solid phase following AH_2DS^{2-} additions, or 0.125 mM g^{-1}. This figure corresponds to between 10 and 20% of the recorded sorption capacities of phyllosilicate minerals for Fe(II) in the literature (Jaisi et al., 2007) demonstrating the feasibility of this interpretation.

Previous work conducted by Charlet et al (Charlet et al., 1998) shows that adsorption of Fe^{2+} at high pH is an extremely fast process and it is reasonable to assume that a large proportion of reduced iron was immediately adsorbed following reductive dissolution, prior to separation of aqueous and particulate phases. Dependent on the extent of saturation of cation sorption sites on mineral surfaces it is possible that this could generate competition for sites and desorption of other sorbed ions.

As can be seen in Figures 100, 101 and 102, there are substantial differences in the measured aqueous/colloidal iron concentrations between the three reactors following AH_2DS^{2-} additions. While in reactor 3 (chromium contaminated: Figure 102) well defined peaks in aqueous Fe concentrations on days 20, 27 and 34 mirror AH_2DS^{2-} injections and Fe(II) release due to reductive dissolution of ferrihydrite, these features are far less clear in reactor 2 (arsenic: Figure 101) where surface protonation changes caused by pH shift between O_2, N_2 and AH_2DS^{2-} controlled cycles appears to play a far greater role. The difference between the iron peaks measured in reactor 1 on days 20, 34 and day 27 is due to the different quantity of AH_2DS added on day 27 of the experiment. On day 27, 30 mL of 30 mM L^{-1} AH_2DS^{2-} was added to test practically whether the quantity of reductant was limiting reduction in the suspension.

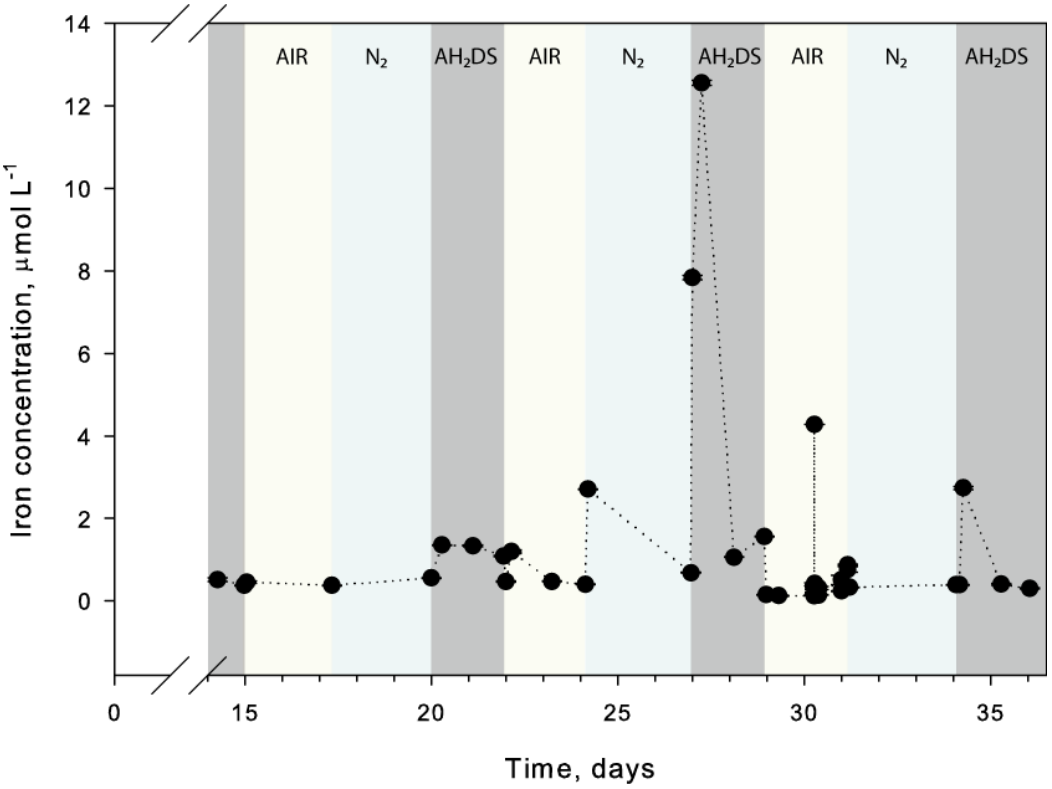

Figure 100: Aqueous/colloidal iron concentration in the reactor 1 suspension over time. The increases occurring on days 20, 27 and 34 are thought to be due to the release of $Fe^{2+}_{(aq)}$ following reduction by added AH_2DS^{2-}.

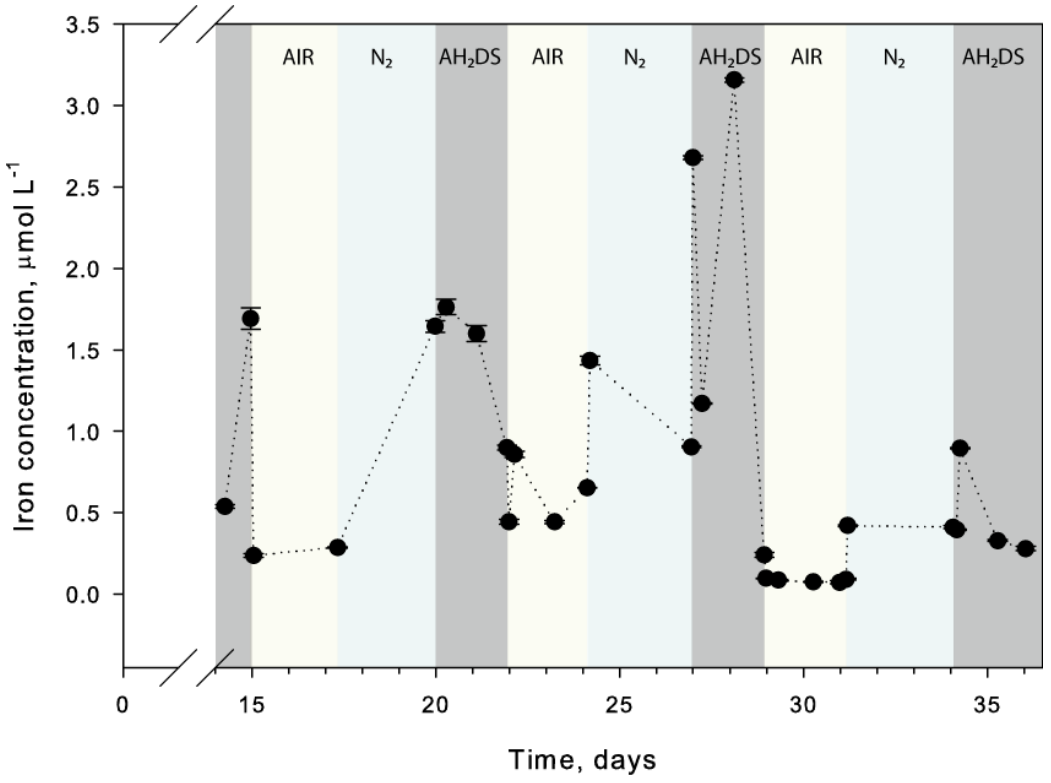

Figure 101: Aqueous/colloidal iron concentration in the reactor 2 suspension over time. The changes in concentration are more complicated than in reactor 1 and appear to be due to a

combination of $Fe^{2+}_{(aq)}$ release following reduction by AH_2DS^{2-} and $Fe^{2+}_{(aq)}$ adsorption/desorption due to pH changes.

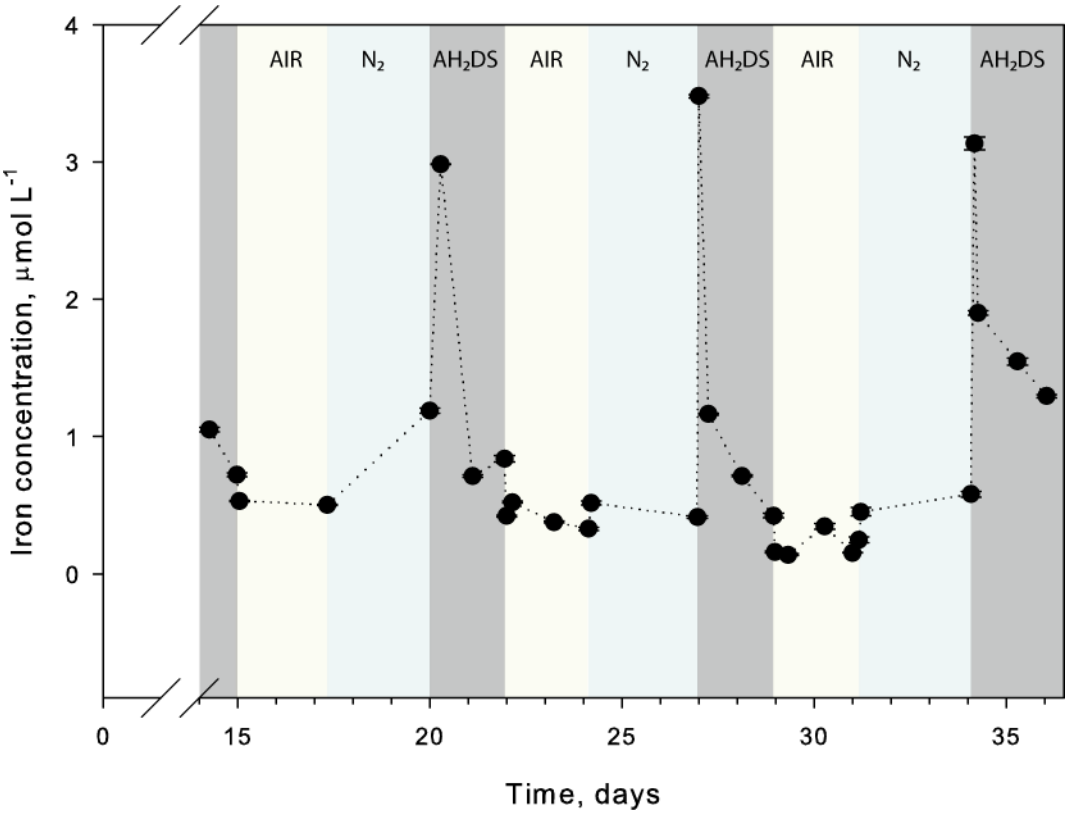

Figure 102: Aqueous/colloidal iron concentration in the reactor 3 suspension over time. The increase in measured concentration on days 20, 27 and 34 appear to be due to $Fe^{2+}_{(aq)}$ release due to reduction by AH_2DS^{2-}. Increases of approximately 0.2µmol L^{-1} can also be seen on days 24 and 31 corresponding to pH changes due to O_2 to N_2 gas change.

Proton balance upon addition of AH_2DS^{2-}

In addition to an increase in electron availability with each AH_2DS^{2-} injection, proton balance and hence pH was also heavily affected, as can be seen in Figures 103, 104 and 105. Following AH_2DS^{2-} additions, pH dropped dramatically in each reactor, by between 0.7 and 0.9 pH units.

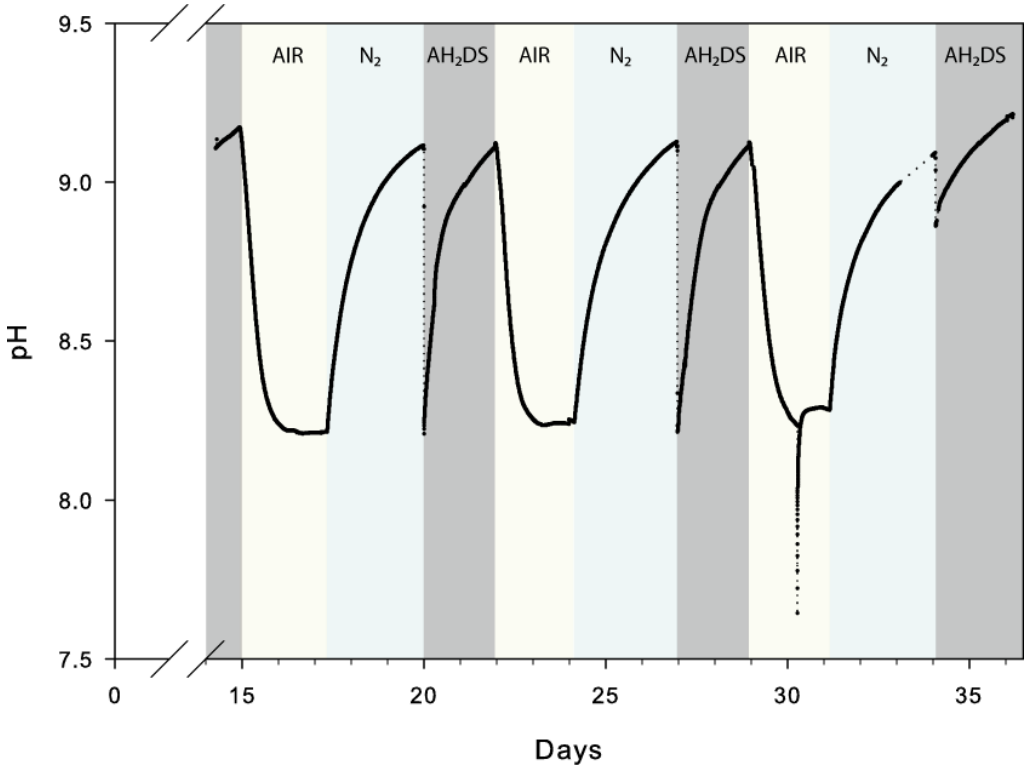

Figure 103: pH with time measured within the reactor 1 suspension, reference shading indicates; light yellow = initiation of air sparging, light blue = initiation of N_2 sparging, grey = addition of AH_2DS^{2-} reductant solution.

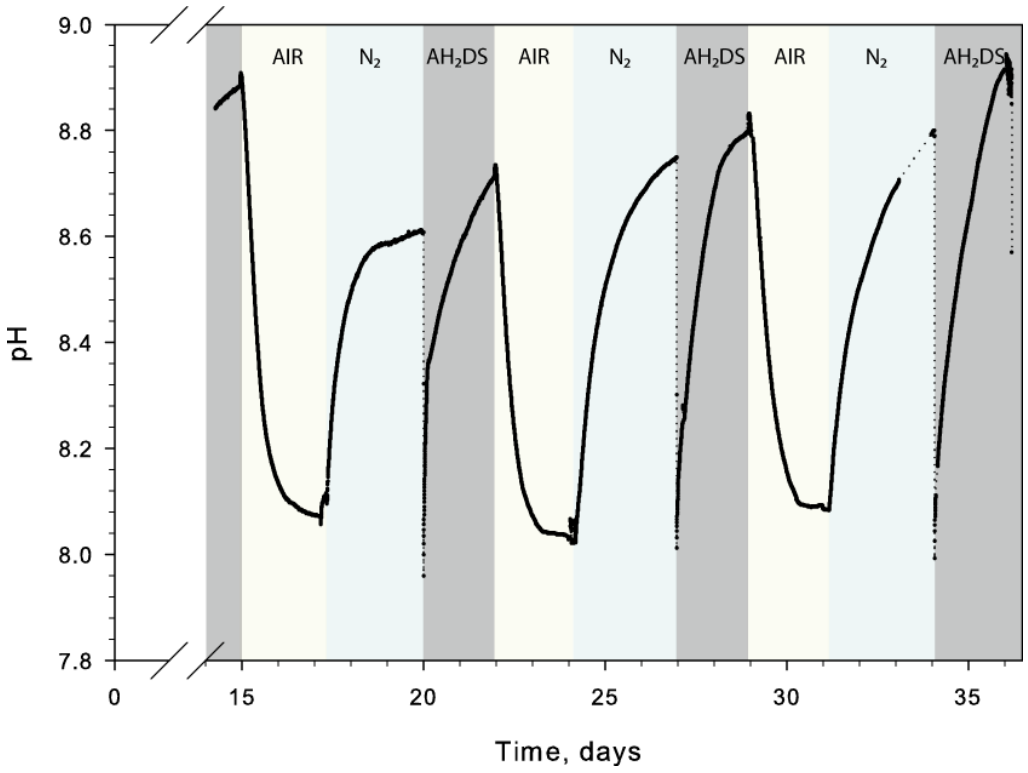

Figure 104: pH with time measured within the reactor 2 suspension, reference shading indicates; light yellow = initiation of air sparging, light blue = initiation of N_2 sparging, grey = addition of AH_2DS^{2-} reductant solution.

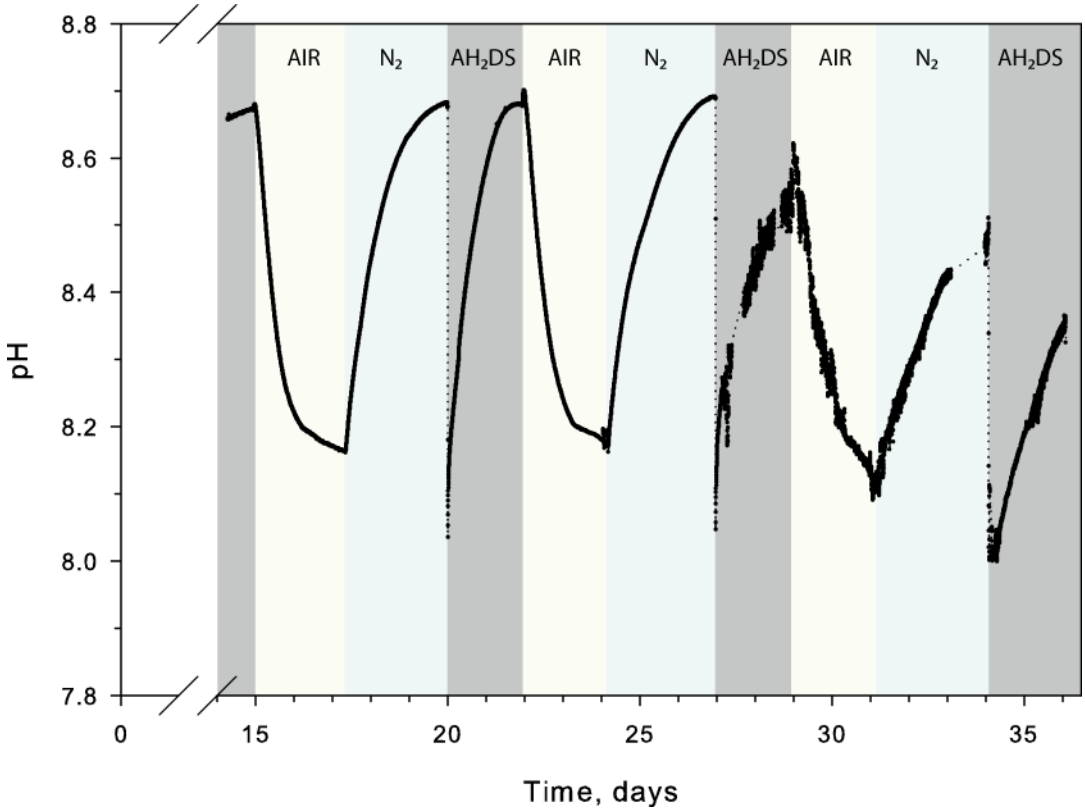

Figure 105: pH with time measured within the reactor 3 suspension, reference shading indicates; light yellow = initiation of air sparging, light blue = initiation of N_2 sparging, grey = addition of AH_2DS^{2-} reductant solution.

As shown in the previous section, the oxidation of one molecule of AH_2DS^{2-} to $AQDS^{2-}$ necessitates the loss of 2 electrons and 2 protons and hence the release of 0.6 mM of H^+ ions (Equation 12). However, as the pK_a1 of AH_2DS^{2-} is 7.5 it is expected that the added AH_2DS^{2-} should rapidly de-protonate to $AHDS^{3-}$ causing the release of 0.3 mM of H^+ into solution via de-protonation and 0.3 mM via subsequent oxidation of $AHDS^{3-}$ to $AQDS^{2-}$. However, the half reactions for the reduction of Fe(III), As(V), Cr(VI) and U(VI) (shown in Table 30) all consume protons resulting in the net consumption of 0.9631 mM (1.5631 mM -0.6 mM) of protons assuming complete AH_2DS^{2-} de-protonation, $AHDS^{3-}$ oxidation and the reduction of Fe(III) and contaminants. AH_2DS^{2-} addition would therefore be expected to cause a pH rise in the suspension rather than a pH drop.

The measured drop in pH following AH_2DS^{2-} addition is therefore thought to be due to the mixing of a low pH AH_2DS solution, with the higher pH reactor suspension (~ pH 9). The supply of protons in AH_2DS^{2-} addition counters the proton consumption via redox reactions and results in the dramatic pH drops measured. This pH drop is buffered by the dissolution of calcite (Equation 21) resulting in the observed peaks in aqueous calcium concentration immediately after AH_2DS^{2-} additions.

Equation 21 $CaCO_{3(s)} + H^+ \rightleftharpoons Ca^{2+} + HCO_3^-$

This aqueous calcium increase is shown in Figures 106, 107 and 108 where peaks corresponding to 10 mL, 30 mM L^{-1} additions induce approximately 0.05 mM L^{-1} increases in aqueous calcium concentrations in reactors 1 and 2 (e.g. 0.0549 in R1 on day 20 and 0.0432 in R2 on day 27) and increases of approximately 0.12 mM L^{-1} in reactor 3 (0.1233 on day 20).

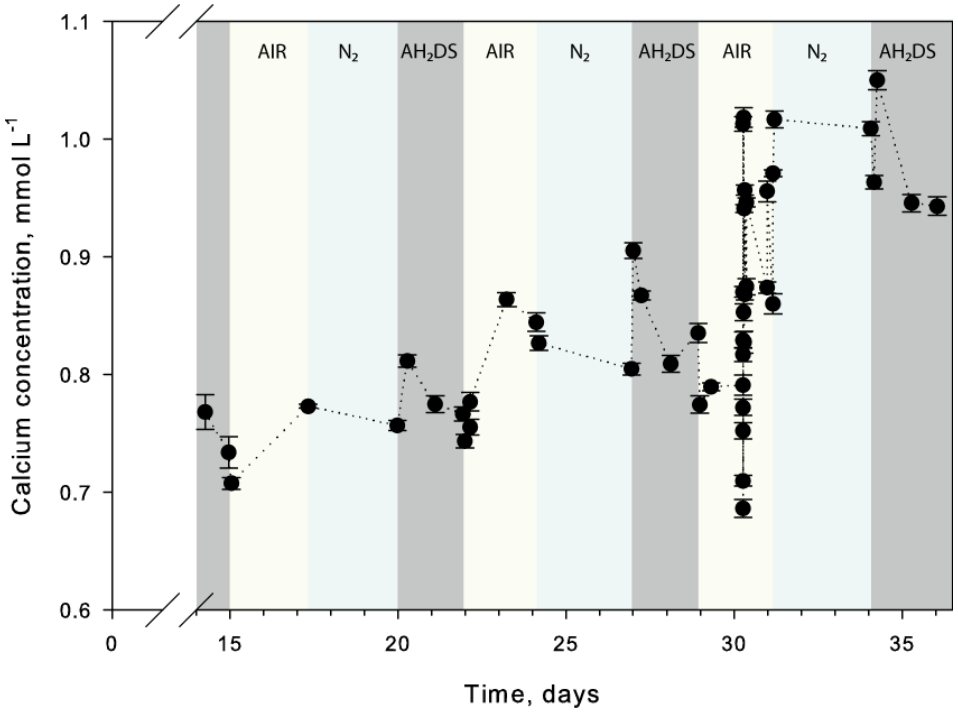

Figure 106: Aqueous/colloidal calcium concentration in the reactor 1 suspension over time.

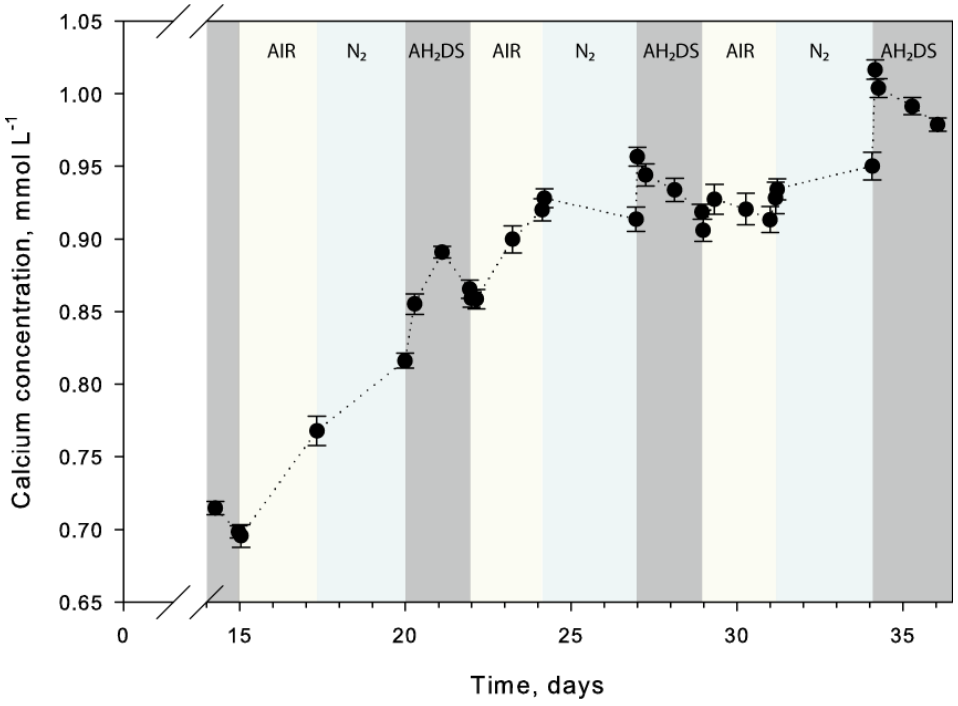

Figure 107: Aqueous/colloidal calcium concentration in the reactor 2 suspension over time.

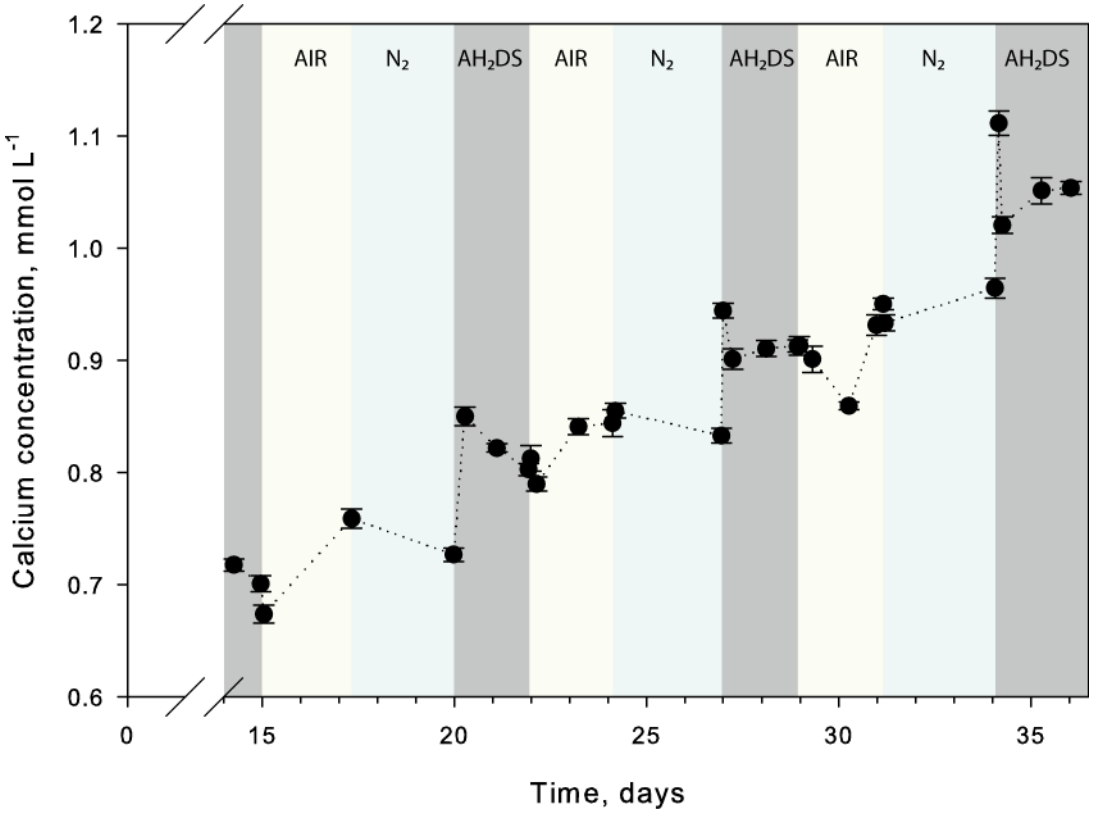

Figure 108: Aqueous/colloidal calcium concentration in the reactor 3 suspension over time.

Whilst it is possible to conclude, from Equation 21, assuming total reduction of oxidized species, that:

Equation 22 $\Delta[H^+]_{measured} = [H^+]_{added} - [H^+]_{consumed} - \Delta[Ca^{2+}]_{measured} - \Delta[Ca^{2+}]_{adsorbed}$

Where:

$[H^+]_{added}$ includes all H^+ added via AH_2DS injection (solution mixing, de-protonation and oxidation processes.

$[H^+]_{consumed}$ concerns H^+ consumed via reduction of contaminants and iron (equations shown in Table 30).

Unfortunately it is not possible to test the assumption of total reduction of oxidized species (Cr(VI), U(VI), As(V) etc) or to quantify reduction by using this equation as the $\Delta[Ca^{2+}]_{adsorbed}$ term is unknown.

The differences in $\Delta[Ca^{2+}]_{measured}$ between reactors 1, 2 and 3, despite identical solid phase composition and AH_2DS additions are therefore directly attributable to differences in proton consumption due to reduction reactions involving contaminants, resulting in a greater of lesser degree of calcite dissolution. For example, the rapid oxidation of Cr^{3+} is not expected by molecular oxygen following reduction of the added CrO_4^{2-} in reactor 3, whereas oxidation of As(III) and Fe(II) species in reactors 1 and 2 is predicted with molecular oxygen, resulting in a greater quantity of reducible oxidized species in reactors 1 and 2 prior to AH_2DS^{2-} additions than in reactor 3. What is surprising is the similarity between $\Delta[Ca^{2+}]_{measured}$ in reactors 1 and 2 as reactor 1 should contain

significantly more reducible species (due to the additional presence of U(VI)) than reactor 2, therefore less calcite dissolution and a lower $\Delta[Ca^{2+}]_{measured}$ should be observed in reactor 1 assuming redox reactions involving uranium and mercury. The similarity of $\Delta[Ca^{2+}]_{measured}$ between reactors 1 and 2 and the strong difference compared to $\Delta[Ca^{2+}]_{measured}$ in reactor 3 indicates that cyclic reduction occurs for iron and arsenic in the reactors but not for chromium or uranium.

Calcite present in the COx also acts as a pH buffer, via dissolution, during oxidizing cycles where oxidation of reduced species results in the generation of acidity (e.g. via the oxidative dissolution of pyrite shown in Equations 15, 16, 17 and 18, and via the reverse of the half reactions shown in Table 30). This dissolution is, in part, responsible for the increase in aqueous calcium concentrations measured during cycles of oxidation (Figures 106, 107 and 108). Other mechanisms which are of importance when considering calcium release include cation exchange due to a reduction in pH during oxidizing cycles and the dissolution of calcite due to the addition of CO_2 and hence acidity, via air sparing (shown in Equations 23 and 24)

Equation 23 $CO_{2(aq)} + H_2O \rightleftharpoons H^+ + HCO_3^-$

Equation 24 $CaCO_{3(s)} + CO_{2(aq)} + H_2O \rightleftharpoons Ca^{2+} + 2HCO_3^-$

Upon switching to N_2 sparging the increase in pH (e.g. from 8.2 to 9.1 measured in reactor 1) can be attributed to the re-precipitation of calcite due to equilibration with the decreased CO_2 partial pressure associated with the pure N_2 headspace (Equation 25), this interpretation is supported by the decreases in measured aqueous calcium concentrations recorded following N_2 sparging. While there are exceptions to this (e.g. between days 31 and 34 in reactor 3 where calcium concentration increases) these exceptions are attributed to the effect of evaporation and hence constantly increasing ionic strength.

Equation 25: $[Ca^{2+}] = (10^{-6.6} [P_{CO2}])^{(1/3)}$

CEC Balance upon contaminant and AH_2DS^{2-} addition

Whilst the cation exchange capacity of the solid component of the reactor suspensions will change during the course of the experiments due to dissolution and re-precipitation of redox sensitive mineral phases expected in natural redox oscillating environments (e.g. pyrite and ferrihydrite), experimental procedure and design also result in changes to cation balance within the reactors.

As mentioned previously, increases in chloride concentration within the aqueous phase indicate that evaporation had a strong influence on the reactor suspension due to constant sparging with dry gases. This increase in ionic strength is evident from measured concentrations of major cations (Na^+ & Ca^{2+}, Figures 106 to 111). In addition to concentration of the reactor suspensions by evaporation, ionic strength increased due to additions of sodium with each AH_2DS^{2-} addition (prepared from disodium salt) and the contaminant additions (Cr and As additions prepared from sodium salts).

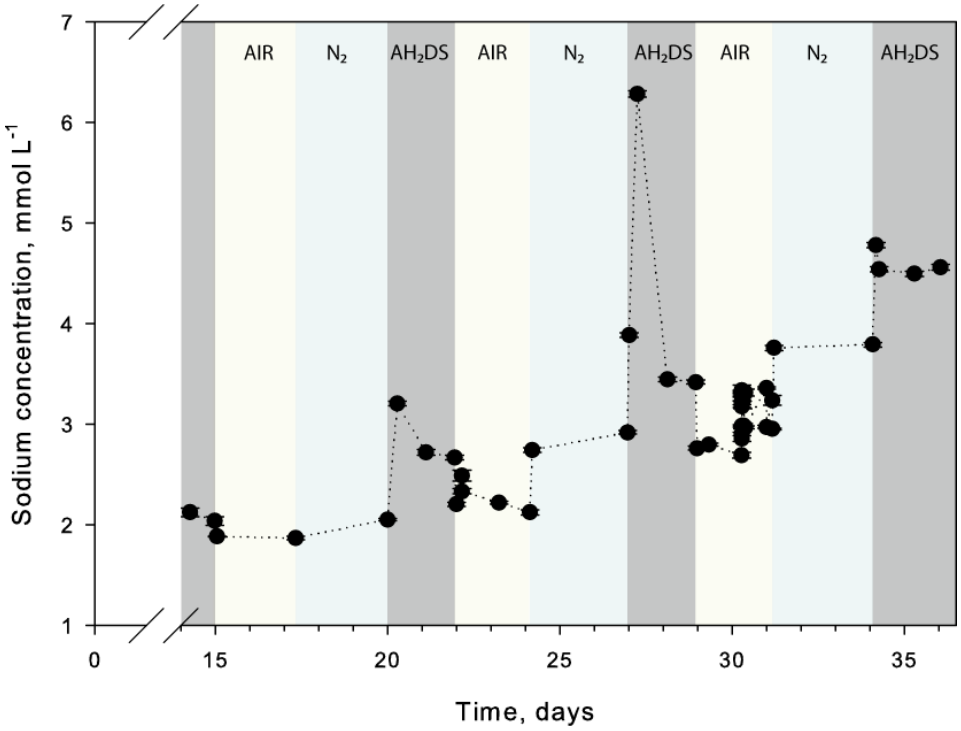

Figure 109: Aqueous sodium concentration measured in the suspension from reactor 1. Δ[Na] on days 20, 27 and 34 correspond well to Na concentrations added via AH_2DS^{2-} additions (1.2, 3.6 and 1.2 mM respectively).

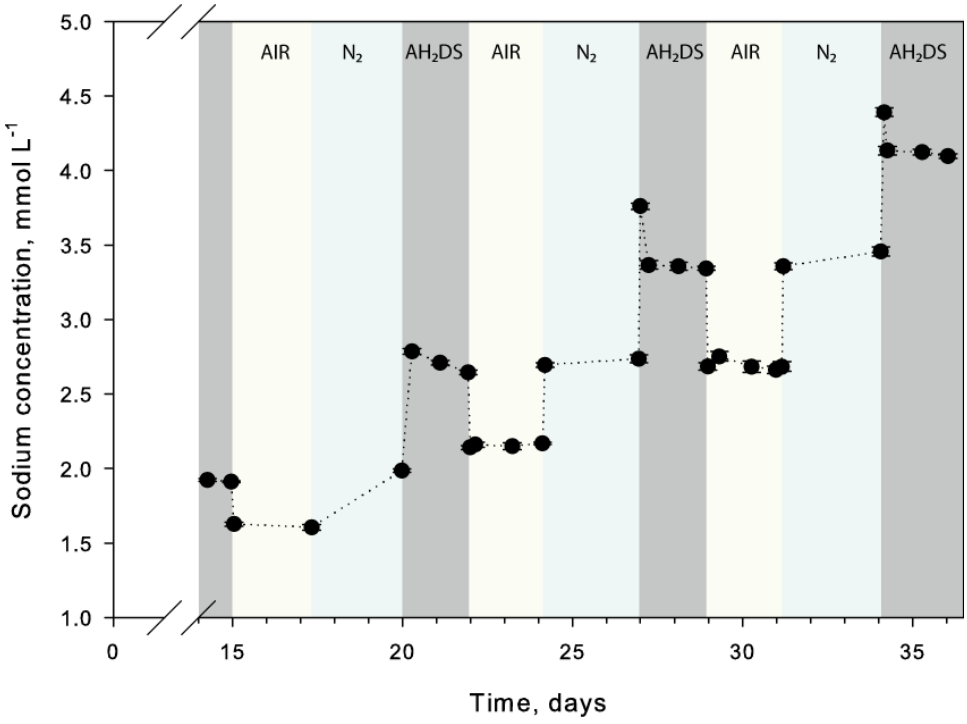

Figure 110: Aqueous sodium concentration measured in the suspension from reactor 2. Δ[Na] on days 20, 27 and 34 correspond well to Na concentrations added via AH_2DS^{2-} additions of 1.2 mM.

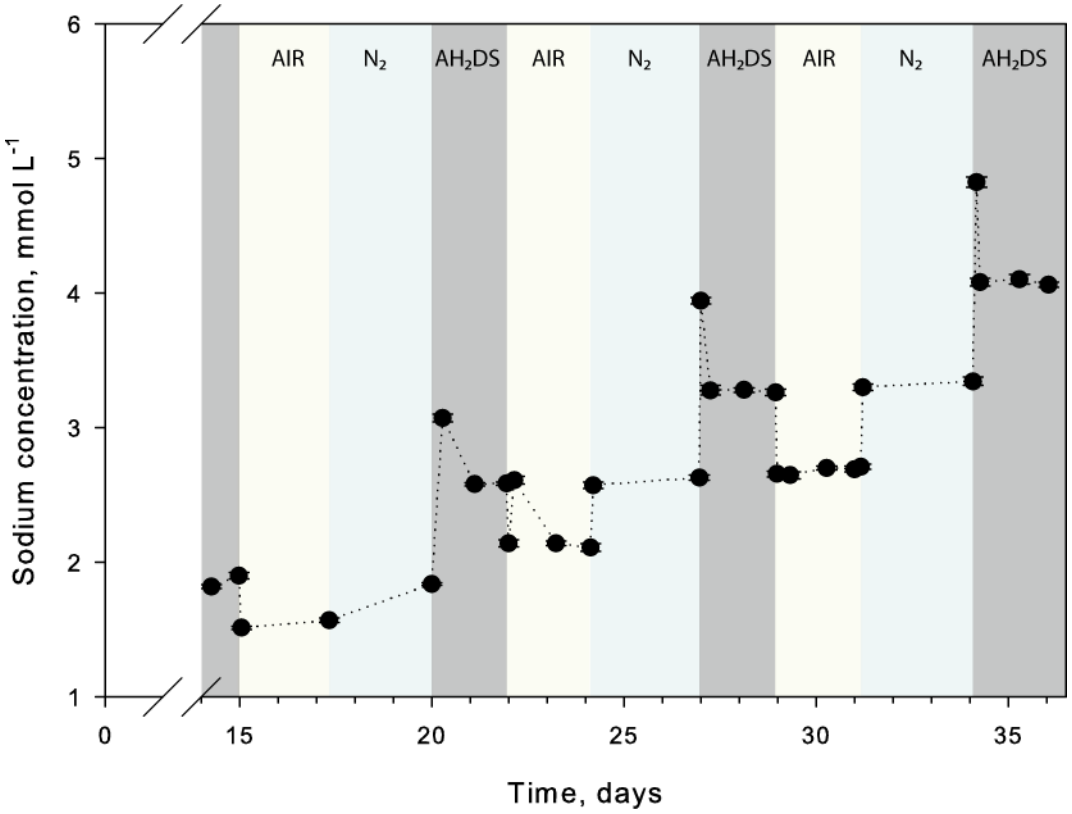

Figure 111: Aqueous sodium concentration measured in the suspension from reactor 2. Δ[Na] on days 20, 27 and 34 correspond well to Na concentrations added via AH_2DS^{2-} additions of 1.2 mM.

It is interesting to observe the differences in sorption behaviour of Na^+ after AH_2DS^{2-} addition to each reactor. Whilst rapid adsorption of sodium occurs after each AH_2DS^{2-} addition in all reactors, a clear decrease in adsorption is observed between injections on day 34 compared to day 20 in reactor 1 (the injection on day 27 must be excluded from this interpretation due to the 3x addition of AH_2DS^{2-} on this day). The same trend is evident in reactor 2 following AH_2DS^{2-} additions on days 27 and 34, whereas such differences in adsorption are not measured in reactor 3. Although sampling resolution is not sufficient to draw strong conclusions from this effect it appears that a greater number of surface sorption sites for Na^+ are free in reactor 3 towards the end of the experiments than in reactors 1 and 2 indicating an increasing saturation of cation exchange capacity. A decrease in sorption or sorption rate of Ca^{2+} after AH_2DS^{2-} additions (leading to calcite dissolution) between days 20, 27 and 34 is not apparent in any of the reactors. This demonstrates the preferential sorption of divalent Ca^{2+} compared to monovalent Na^+.

Effects of redox cycling on investigated contaminants

Arsenic

Arsenic was added to both reactor 1 and reactor 2 in its oxidized i.e. As(V) form as sodium arsenate. As can be seen from the Pourbaix diagrams (Figures 112 and 113) Eh conditions following AH_2DS^{2-} additions thermodynamically favour reduction to As(III) as the fully protonated arsenite species via Equation 26.

Equation 26 $HAsO_4^{2-} + 4H^+ + 2e^- \rightarrow H_3AsO_3 + H_2O$

Upon the switching to air sparging once again Eh conditions thermodynamically favour oxidation to As(V) as the double de-protonated arsenate species, via the reversal of Equation 26. However, due to the relatively slow kinetics of arsenic oxidation and reduction arsenic speciation is often found to be in disequilibrium in natural environments. In some natural flooded soils it has been shown that appreciable reduction of As(V) species to As(III) species does not occur for the first 15 days after flooding (Ackermann et al., 2008).

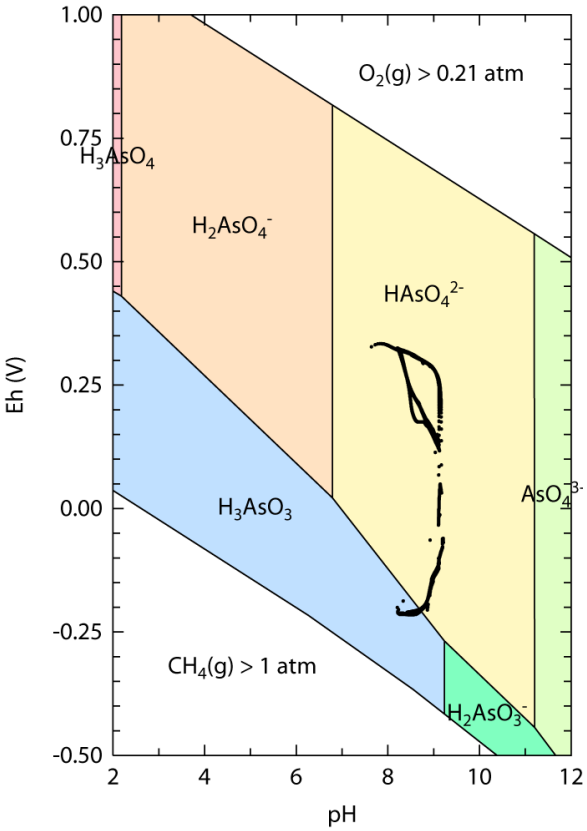

Figure 112: Pourbaix diagram of the As-H_2O-CO_2 system at 298.15K and 10^5 Pa from LLNL data with Eh pH conditions in reactor 1 drawn in black.

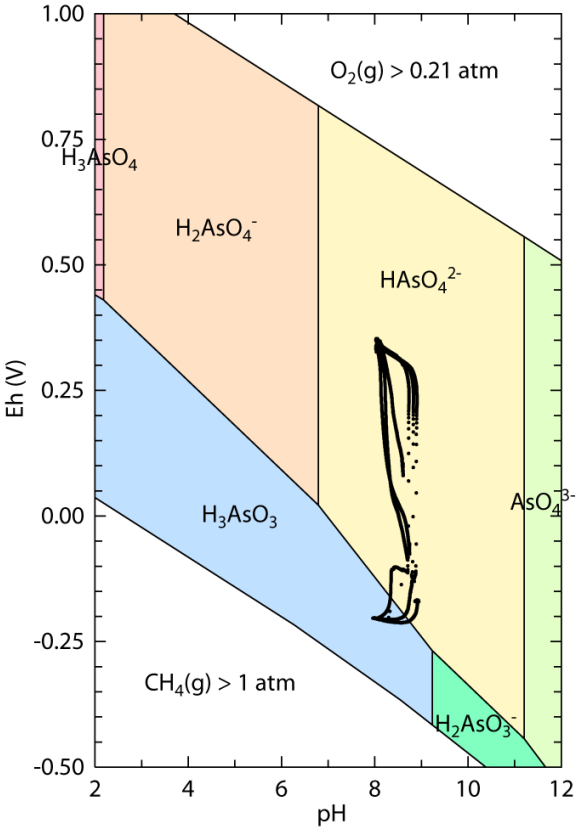

Figure 113: Pourbaix diagram of the As-H_2O-CO_2 system at 298.15K and 10^5 Pa from LLNL data with Eh pH conditions in reactor 2 drawn in black.

Measured arsenic concentrations varied considerably within the aqueous phase during cycling (Figures 114 and 115). A common trend of increased arsenic mobility during reducing cycles and decreased mobility during oxidising cycles is present in both reactor suspensions.

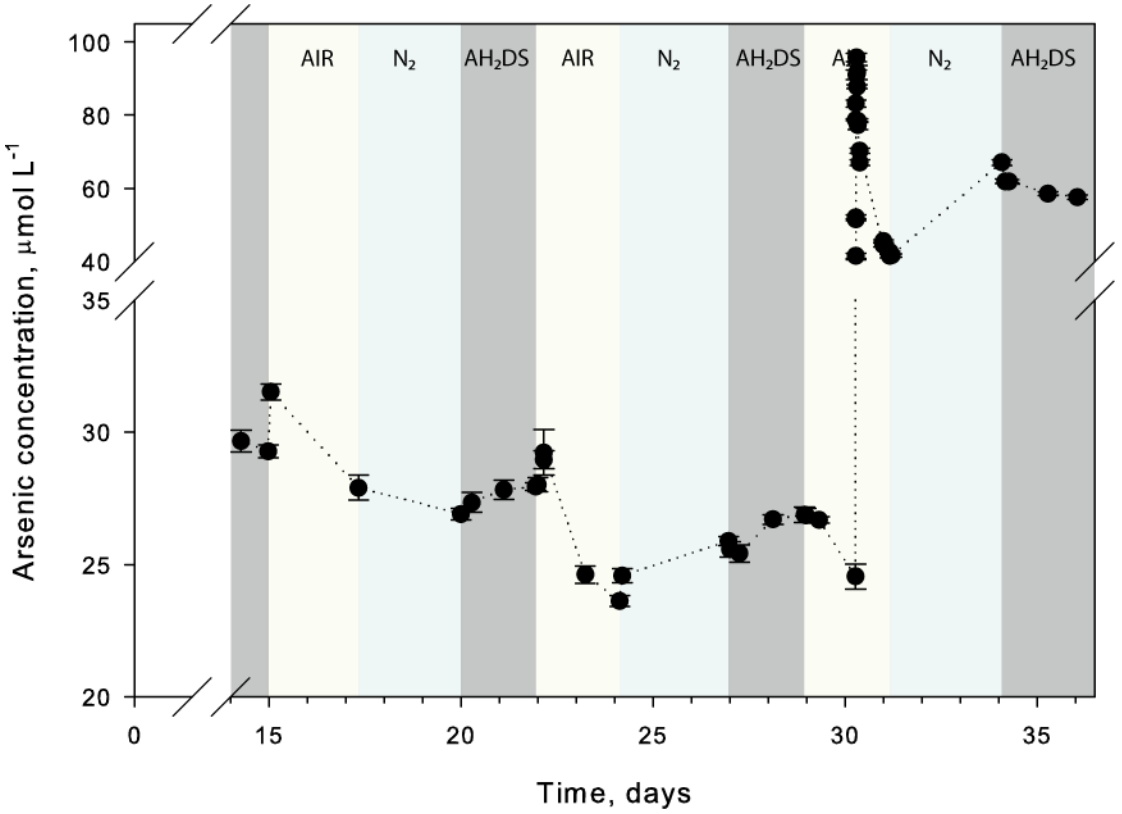

Figure 114: Aqueous/colloidal arsenic concentration in the reactor 1 suspension over time.

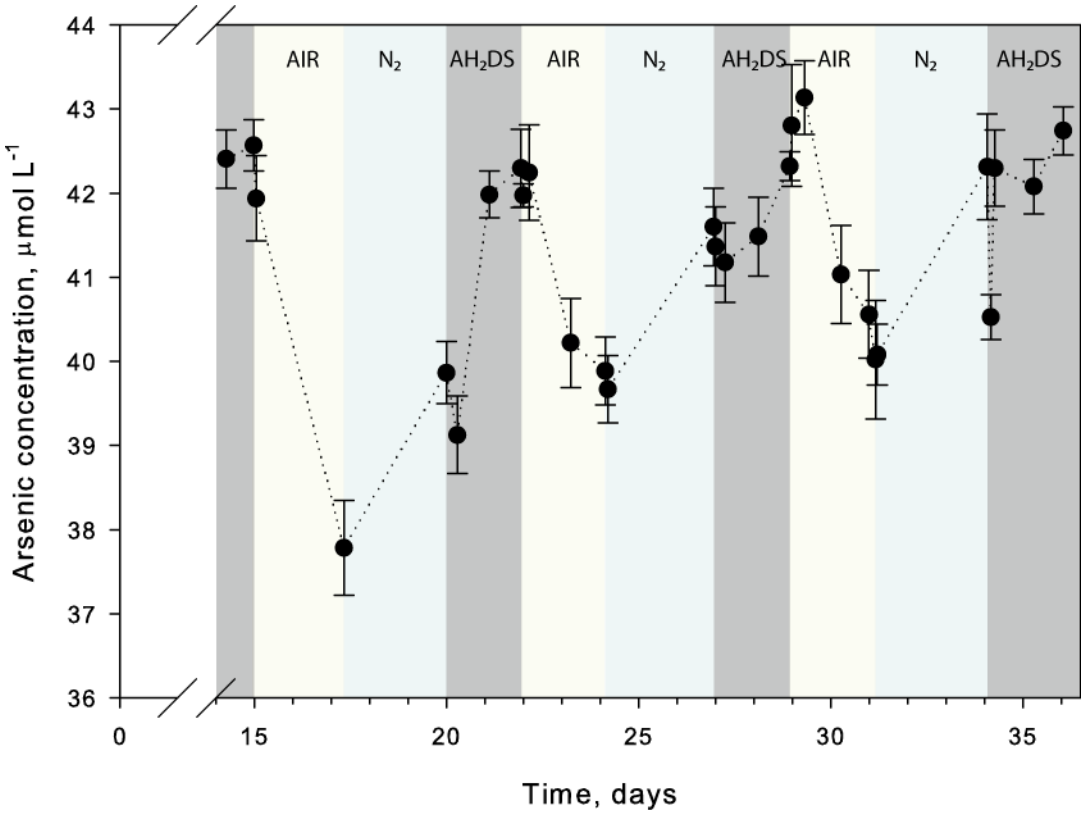

Figure 115: Aqueous/colloidal arsenic concentration in the reactor 2 suspension over time.

Despite similar intra cycle trends in arsenic mobility between reactors distribution coefficients (Kd values) and cumulative trends vary substantially (Figures 116 and 117). Kd values in reactor 1 range from between 328 and 616 L/kg compared to between 97 and 181 L/kg in reactor 2. These values are significantly lower than those obtained for other contaminants investigated demonstrating the high mobility of arsenic under all Eh and pH conditions imposed experimentally. Kd values in both reactors were found to be negatively correlated with pH conditions as shown in Figures 116 and 117 (R^2 of 0.42 to 0.50).

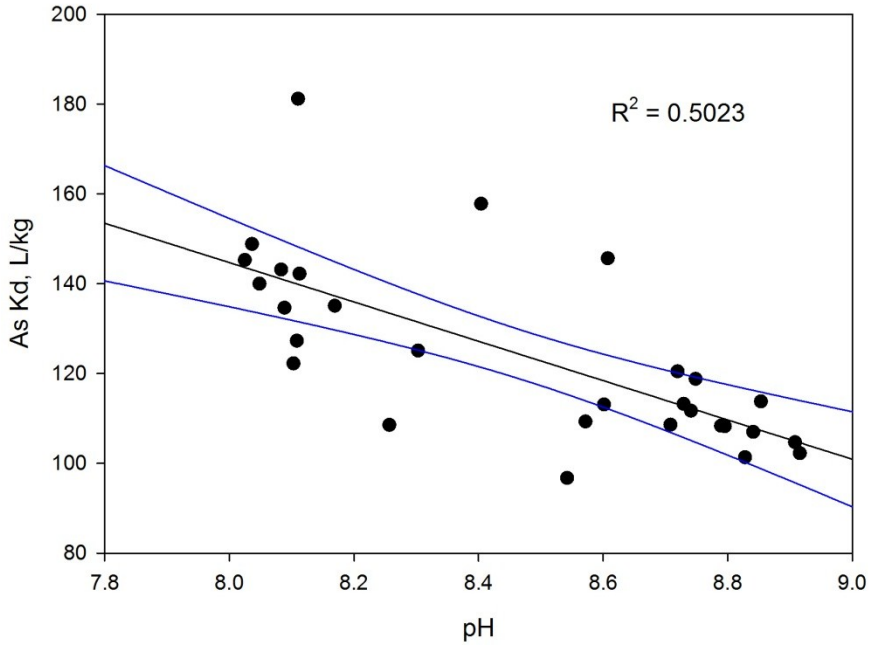

Figure 116: Distribution coefficient against pH for As in reactor 2. Blue banding lines represent a 95% confidence on the regression.

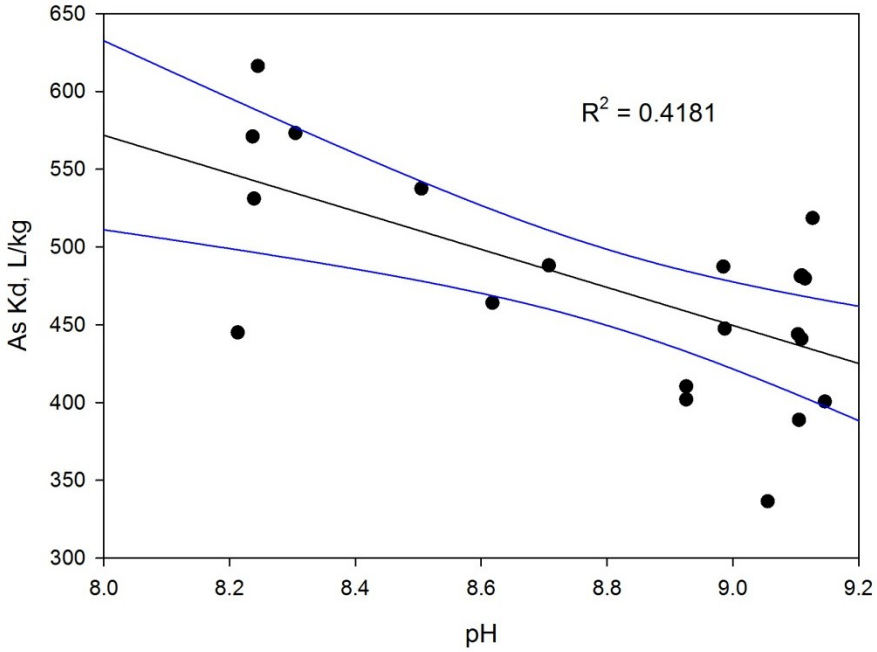

Figure 117: Distribution coefficient against pH for As in reactor 1. Blue banding lines represent a 95% confidence on the regression.

This negative trend is indicative of the arsenic speciation within the reactors. Surface sorption of negatively charged arsenate species is expected to decrease with increasing pH due to repulsion from increasingly negatively charged clay and oxide surfaces. Experimentally derived sorption envelopes for the expected principal sorbents in this system; phyllosilicate minerals and ferric

hydroxides (Goldberg, 2002) clearly demonstrate desorption at high pH. As deprotonated arsenite does not become a dominant species until pH 9.2 negative mineral surface charge does not act as a significant barrier to arsenite adsorption resulting in relatively flat sorption envelopes (Goldberg, 2002). Therefore the negative correlation present between As Kd values and pH indicates that a significant proportion of As is present as As(V) even under reducing conditions and that therefore the assumption of complete arsenate reduction due to sufficient addition of reductant is false.

The redox reaction between reduced humic substances and As(V) is often conceptualized as scenario A in Figure 120. As redox reactions between AH_2DS^{2-} as a model humic substance and As(V) proceed via an intermediate semi-quinone step scenario B in Figure 120 offers a more realistic representation.

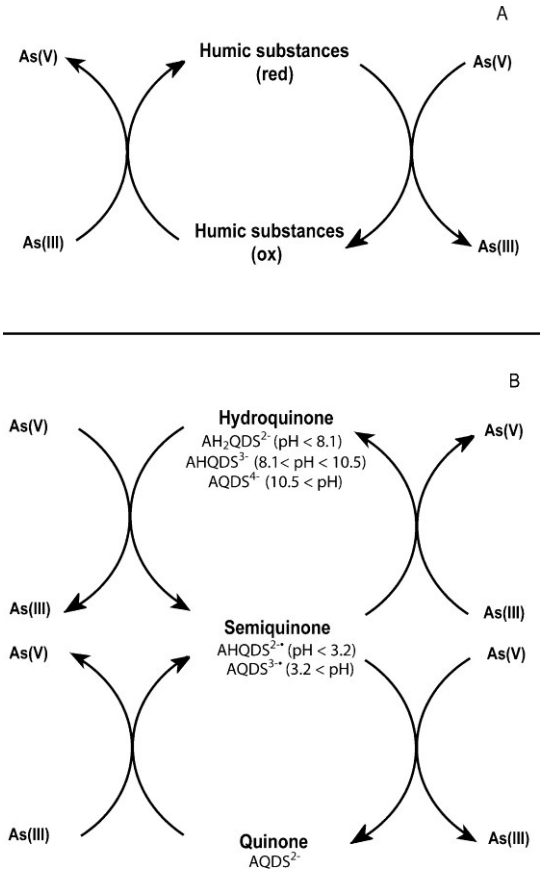

Figure 118: Scheme illustrating reduction of As(V) and oxidation of As(III) (A) by reduced and oxidized humic substances (HS) or (B) by the fully reduced (hydroquinone), partially reduced (semiquinone) and oxidized form (quinone) of anthraquinone-2,6-disulfonate ($AQDS^2$). From Jiang et al. (2009).

Whilst this may be a good approximation of reactions between reduced humic substances and inorganic arsenic in the natural environment the reality has been shown to be more complicated. Jiang et al. (2009) demonstrate that during chemical or microbial reduction of AQDS strongly oxidising radical species are formed. These species are capable of the oxidation of arsenite species and therefore counter the effect of AH_2DS^{2-} as a reductant. This effect is enhanced with increasing pH and increasing AQDS/As ratio as can be seen in Figure 119. As experiments were conducted at approximately pH 8-9 with a high proportion of AQDS/As it is highly likely that this type of oxidation did occur in the reactor suspensions. This potential for arsenite oxidation by radical species does help to explain the consistent presence of arsenate and hence the observed correlation between Kd and pH. However, such effects detract from the representativeness of AH_2DS^{2-} as an analogue of reductive microbial activity.

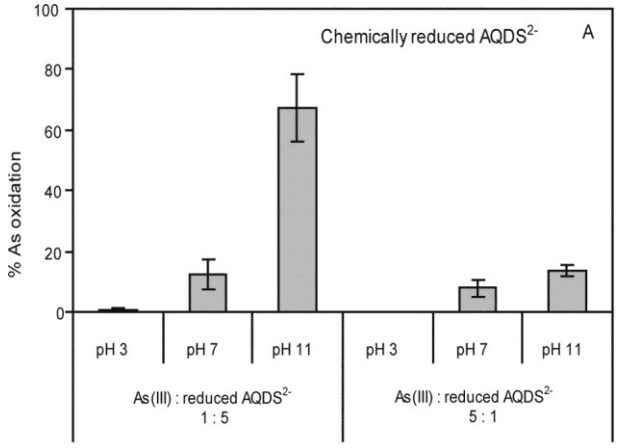

Figure 119: Oxidation of As(III) by chemically reduced $AQDS^{2-}$. The initial concentrations were 90 µM As(III) and 450 µM reduced $AQDS^{2-}$ (molar ratio 1:5) or 330 µM As(III) and 67 µM reduced $AQDS^{2-}$ (molar ratio 5:1). From Jiang et al. (2009).

Despite correlation between pH and Kd values, pH alone is not enough to explain As mobility trends as can be seen in Figures 120 and 121 where arsenic concentrations normalized with respect to pH are expressed as a function of time. Cyclic trends are also present indicating that other factors such as co-precipitation and aqueous speciation change are also controlling As mobility during experiments.

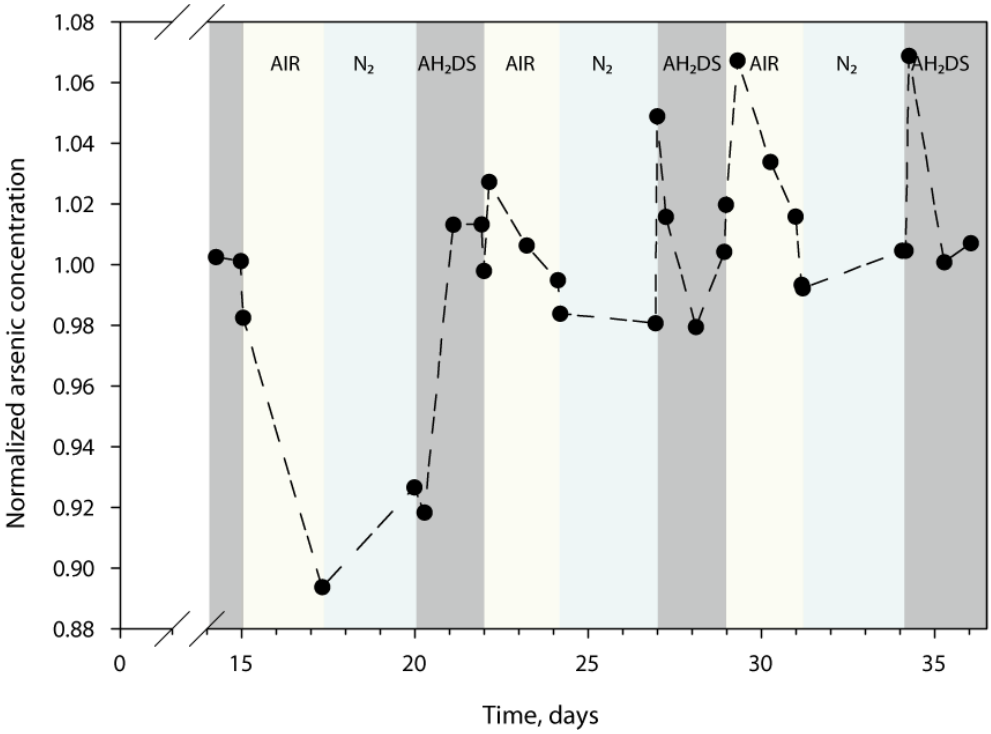

Figure 120: As concentration normalized with respect to pH during redox cycling in reactor 2.

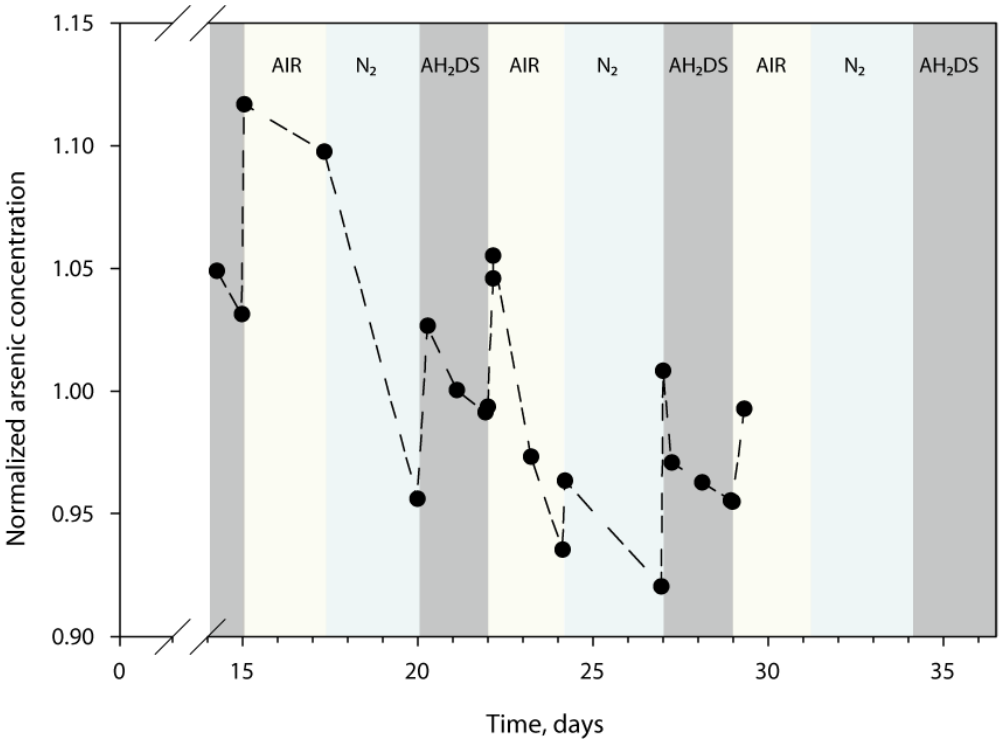

Figure 121: As concentration normalized with respect to pH during redox cycling in reactor 1.

Cumulative changes

Cumulative changes in arsenic mobility are observed in both reactors after multiple cycles of redox oscillation (Figures 114 and 115) even when the effects of pH change on sorption are eliminated by normalisation (Figures 120 and 121). In reactor 1, a decrease in arsenic mobility is measured with an increasing number of redox cycles (Figures 114 and 121). Several possible mechanisms may be responsible for this successive immobilisation, firstly increased co-precipitation/kinetic sorption with ferric hydroxides as observed in Chapter 5 may be responsible. An alternative mechanism which may be applicable to the Cox suspensions is an increasing proportion of ferric hydroxides with each cycle. If the most redox active component in the COx is the pyrite fraction it could be considered that with each oxidising cycle grains of pyrite shrink due to oxidative dissolution, the subsequent precipitation of ferric hydroxides act as a substantial sorbent for both As(III) and As(V) species. With each successive oxidising cycle a greater proportion of the pyrite grain may be dissolved leading to a greater proportion of ferric hydroxide in the system until the complete dissolution of pyrite grains. As sulphate reduction is not favoured thermodynamically by AH_2DS^{2-} addition replenishment of ferrous sulphide or pyrite mineralogy would not be expected during each reducing cycle.

In contrast, in reactor 2 no cumulative trend in arsenic mobility is observed during reducing cycles (following AH_2DS^{2-}additions) with consistent concentrations of 42 to 43 µmol L^{-1}. However, a cumulative effect of redox cycling is apparent during oxidising cycles and when normalised to remove the effect of pH on sorption (Figure 120). This cumulative increase of arsenic mobility in reactor 2 in contrast to the cumulative decrease in reactor 1 may be attributable to evaporative concentration which was greater in reactor 2 than reactor 1 however definitive conclusions cannot be drawn in the absence of further spectroscopic data or investigative modelling.

Chromium

Chromium was added to both reactor 1 and reactor 3 in its oxidized i.e. Cr(VI) form as sodium chromate. As can be seen from the Pourbaix diagrams (in Figures 124 and 125) Eh conditions in the reactors thermodynamically favour reduction to Cr(III) and precipitation of Cr_2O_3 via Equation 27. This is true even during air sparging cycles and therefore following AH_2DS^{2-} additions reduction to Cr(III) is strongly favoured. In addition even in thermodynamically favourable solutions, oxidation rates of Cr(III) by molecular oxygen are very slow (Schroeder and Lee, 1975; Rai et al., 1989), which leads to the predominance of Cr(III) in the subsurface, especially in the absence of a MnO_2, which, due to slow precipitation kinetics usually requires the presence of a manganese oxidizing microbial or fungal community in redox oscillating conditions (Thompson et al., 2005; Tebo et al., 2011).

Equation 27 $2CrO_4^{2-} + 16H^+ + 14e^- \rightarrow Cr_2O_3 + 8H_2O$

Chromium mobility within the suspensions was low both during oxidising and reducing conditions with Kd values of between 21,642 and 715,059 L/kg in reactor 1 and 41,207 and 2,333,530 in reactor 3. No significant correlation between pH and Kd was found in either suspension indicating that unlike for arsenic, pH changes within the experimental range were not an important mobility controlling factor for Chromium. Kd values did vary significantly with redox cycling in both suspensions (e.g. Figure 126). It was found that in both reactors Chromium was mobile during reducing cycles and less mobile in oxidising cycles (Figures 122 and 123). If all chromium is present

as Cr^{3+} it is expected that lower pH associated with oxidising cycles and immediately following AH_2DS^{2-} additions should result in a decrease in surface sorption and therefore release of chromium into the aqueous phase. The opposite trend is shown to be true and is more indicative of anionic contaminant behaviour. This suggests that the increased mobility of chromium during N_2 sparging cycles may be due to the presence of small quantities of Cr(VI) species. This Cr(VI) may be residual i.e. added Cr(VI) which was not reduced or may be the result of oxidation of Cr(III) by radical species shown to be produced during AQDS reduction and capable of arsenite oxidation at high pH and high AQDS/As ratios (Jiang et al., 2009).

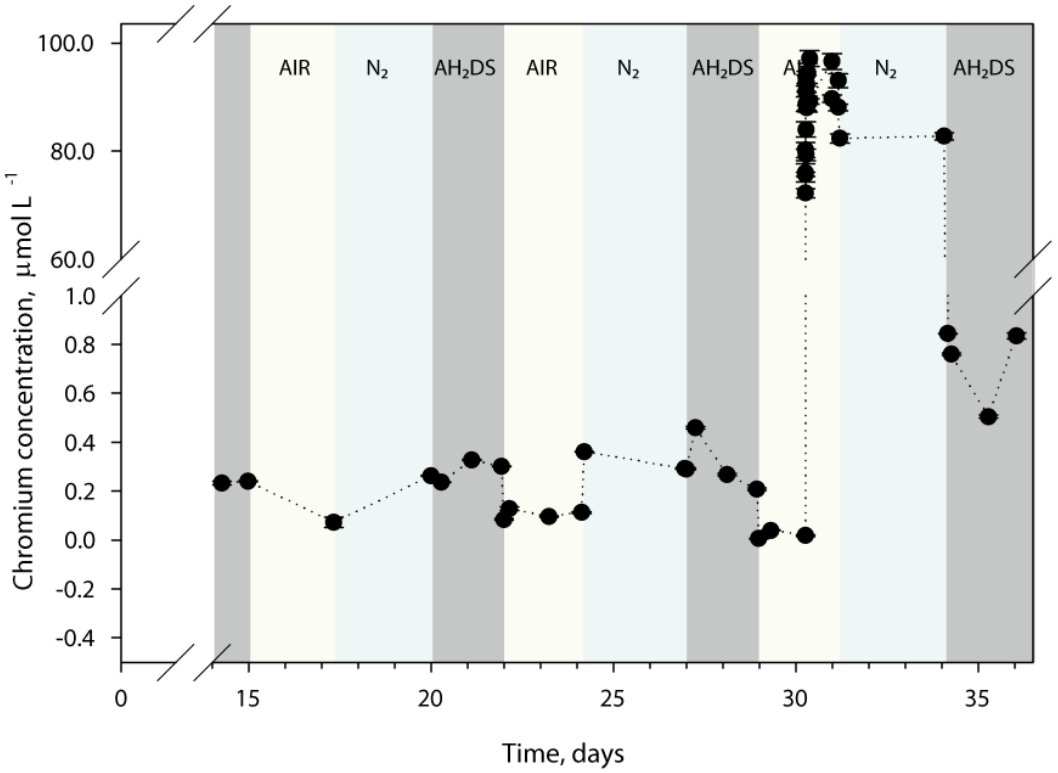

Figure 122: Aqueous/colloidal chromium concentration in the reactor 1 suspension over time.

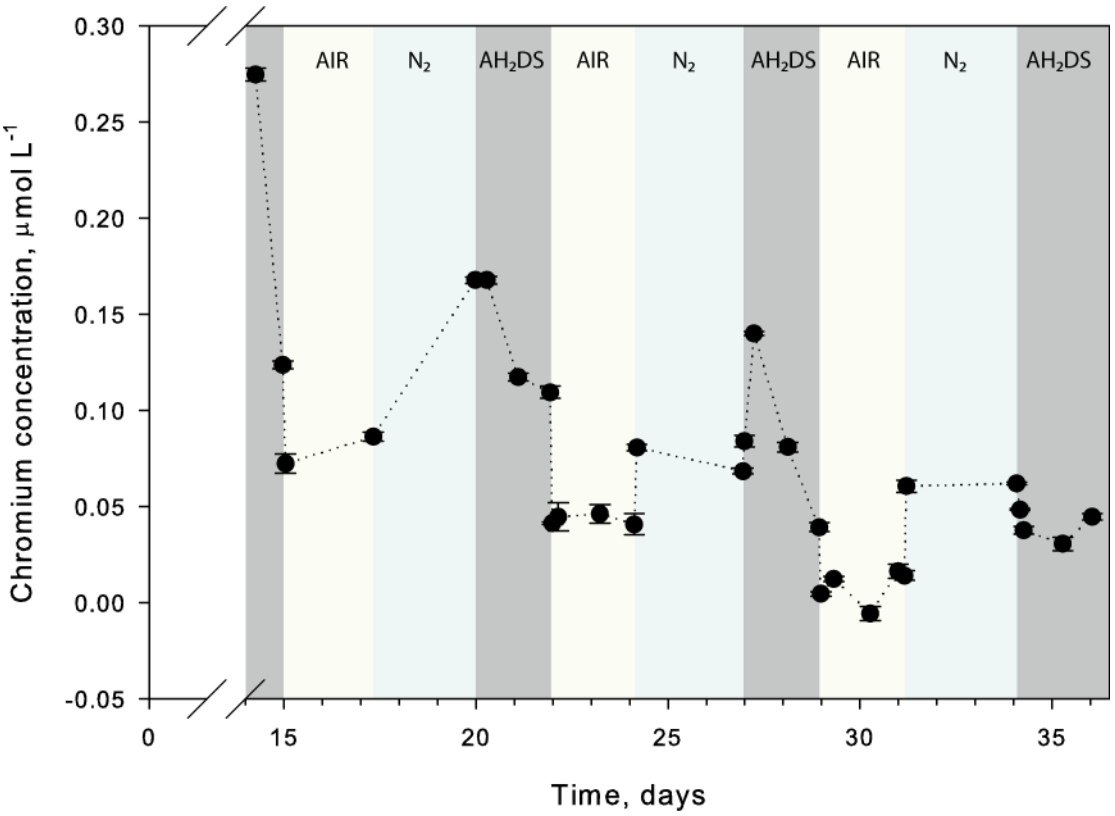

Figure 123: Aqueous/colloidal chromium concentration in the reactor 3 suspension over time

As surface reduction of chromate by several minerals, including pyrite and siderite has been conclusively demonstrated (Zouboulis et al., 1995; Erdem et al., 2004; Mullet et al., 2007), it is possible to postulate that reduction occurred even prior to AH_2DS^{2-} additions during the oxic equilibration period, unfortunately due to the loss of data from the start of the experiments it is impossible to confirm with certainty if this did or did not occur in the un-cycled COx suspension. From data obtained following the 2nd contaminant addition in reactor 1 on day 30 (under oxidizing conditions) it appears that reduction did not occur until the addition of AH_2DS^{2-} on day 34 due to the high mobility of chromium during the oxidising cycle (Figure 122). However, at this point in the experiment the suspension had been exposed to four full redox cycles. Due to the lack of sulphate reduction in suspensions during reducing conditions it is probable that depletion of pyrite occurred during the experiment via oxidative dissolution and therefore that the capacity of the suspension for surface reduction of Cr(VI) was diminished.

It can however be assumed that following the first reducing cycle (addition of AH_2DS^{2-}), almost all chromate was reduced to Cr(III) resulting in a radically reduced mobility within the suspension (approaching the sensitivity limit of the ICP-OES).

One question resulting from this interpretation is the form under which immobile Cr(III) is present subsequent to reduction. As explained within the 1st chapter of this thesis, while the most thermodynamically favourable species is Cr_2O_3 kinetic controls exist which rarely allow the precipitation of such a solid in natural systems. The two most probable interpretations are the precipitation of $(Fe_{1-x},Cr_x)OH_3$ in solid solution or the sorption of $Cr^{3+}_{(aq)}$ to negatively charged clay surfaces (Arnfalk et al., 1996).

The increased release of $Fe^{2+}_{(aq)}$ and $Ca^{2+}_{(aq)}$ following the addition of AH_2DS^{2-} in reactor 1 on day 34, compared to releases following AH_2DS^{2-} addition on day 20 (Figures 100 and 106), favours the hypothesis that a significant proportion of the freshly reduced $Cr^{3+}_{(aq)}$ was adsorbed to clay surfaces rather than precipitated as a discrete mineral.

Assuming a greater degree of proton consumption due to increased availability of reducible species following the addition of oxidized contaminants on day 30, it would be expected that fewer protons would be available to cause calcite dissolution. However, as $\Delta[Ca^{2+}]_{measured}$ increases corresponding to an assumed proton decrease, a logical conclusion is that Ca^{2+} and Fe^{2+} were exchanged on clay surfaces due to the preferential adsorption of the freshly available trivalent Cr^{3+} ions.

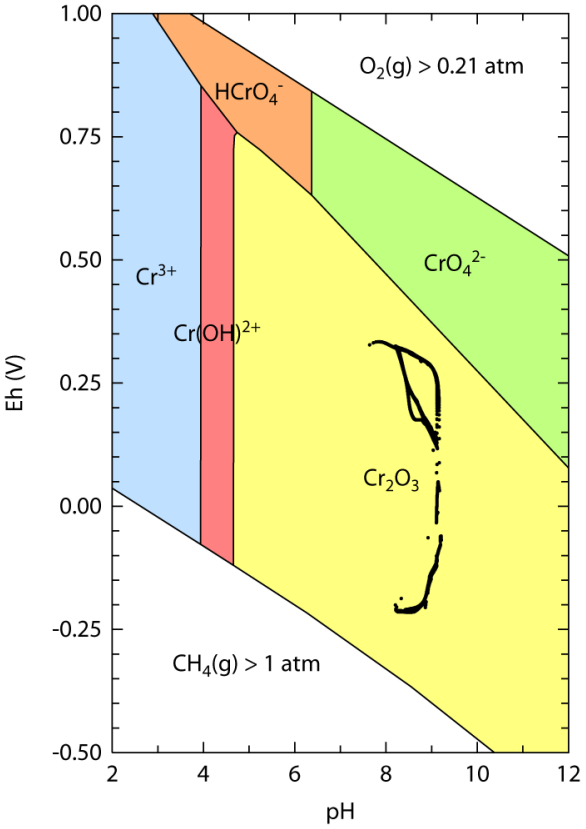

Figure 124: Pourbaix diagram of the Cr-H_20-CO_2 system at 298.15K and 10^5 Pa from LLNL data with Eh pH conditions in reactor 1 drawn in black.

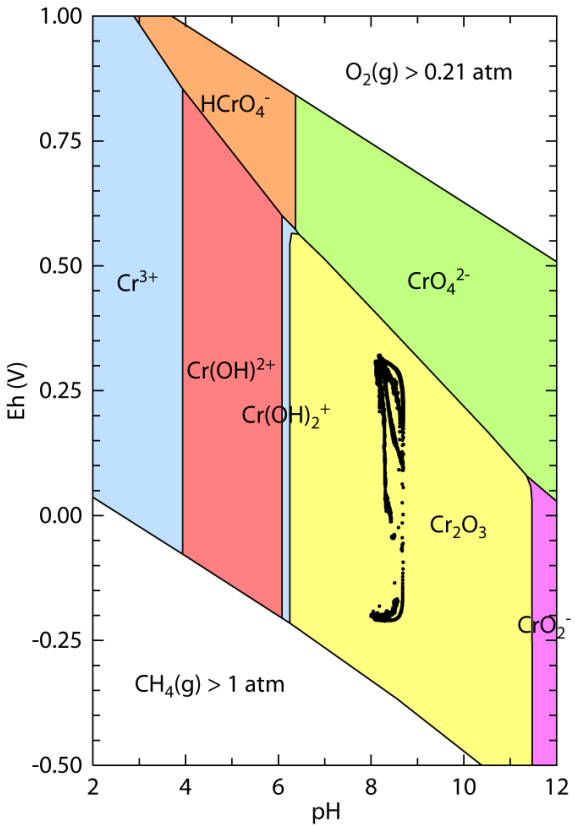

Figure 125: Pourbaix diagram of the Cr-H_2O-CO_2 system at 298.15K and 10^5 Pa from LLNL data) with Eh pH conditions in reactor 3 drawn in black.

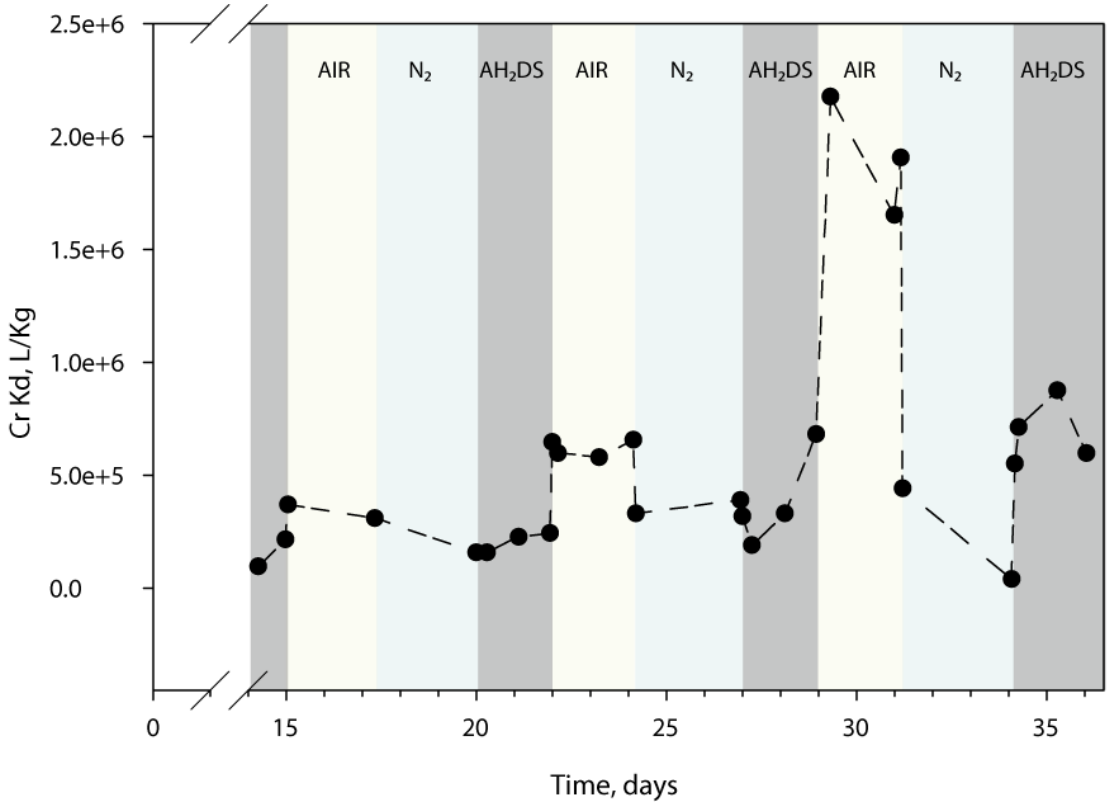

Figure 126: Distribution coefficient for Chromium against time in reactor 3.

Cumulative trends

In reactor 3 a clear decreasing trend in chromium concentrations is recorded with successive redox cycles. As discussed previously the pattern of immobilization/mobilization with redox cycling and pH change is more representative of an anionic aqueous species than a cationic species indicating that the measured trend may be the result of diminishing chromate in the reactor suspensions following initial chromium addition as sodium chromate. Peaks of aqueous Cr present immediately following AH_2DS^{2-} additions may therefore be due to the release of residual chromate previously immobilised due to co-precipitation with ferric hydroxide minerals. Reductive dissolution of ferric hydroxides initiated by reductant addition would result in the liberation of this residual chromate and subsequent reduction to Cr(III). This interpretation corresponds well to the observed decrease in chromium mobility during reducing conditions after the initial chromium release. Aqueous chromium liberated in this way is therefore considered to be re-immobilized during the remainder of the AH_2DS^{2-} cycle, either by re-adsorption to alternative sorbents such as clay minerals or due to precipitation as discrete Cr(III) phases. This interpretation adequately describes the cumulative decrease in chromium concentration following successive AH_2DS^{2-}additions as a greater proportion of Cr^{3+} is adsorbed to phyllosilicate minerals unaffected by reductive dissolution. However, whilst this interpretation appears to describe the experimental data well, spectroscopic investigation or sequential extractions could elucidate the mechanisms responsible for increasing chromium immobilisation.

Uranium

Uranium was added to reactor 1 in its oxidized i.e. U(VI) form as uranyl-nitrate. As can be seen from the Pourbaix diagram (Figure 127) Eh conditions following AH_2DS^{2-} additions thermodynamically favour reduction to U(IV) and precipitation of uraninite. Upon the switching to air sparging once again Eh conditions thermodynamically favour U(VI) as uranyl di and tri carbonate species. However, due to the relatively slow kinetics of uranium oxidation and reduction uranium speciation is often found to be in disequilibrium in natural environments (Wan et al., 2005; Zheng and Wan, 2005).

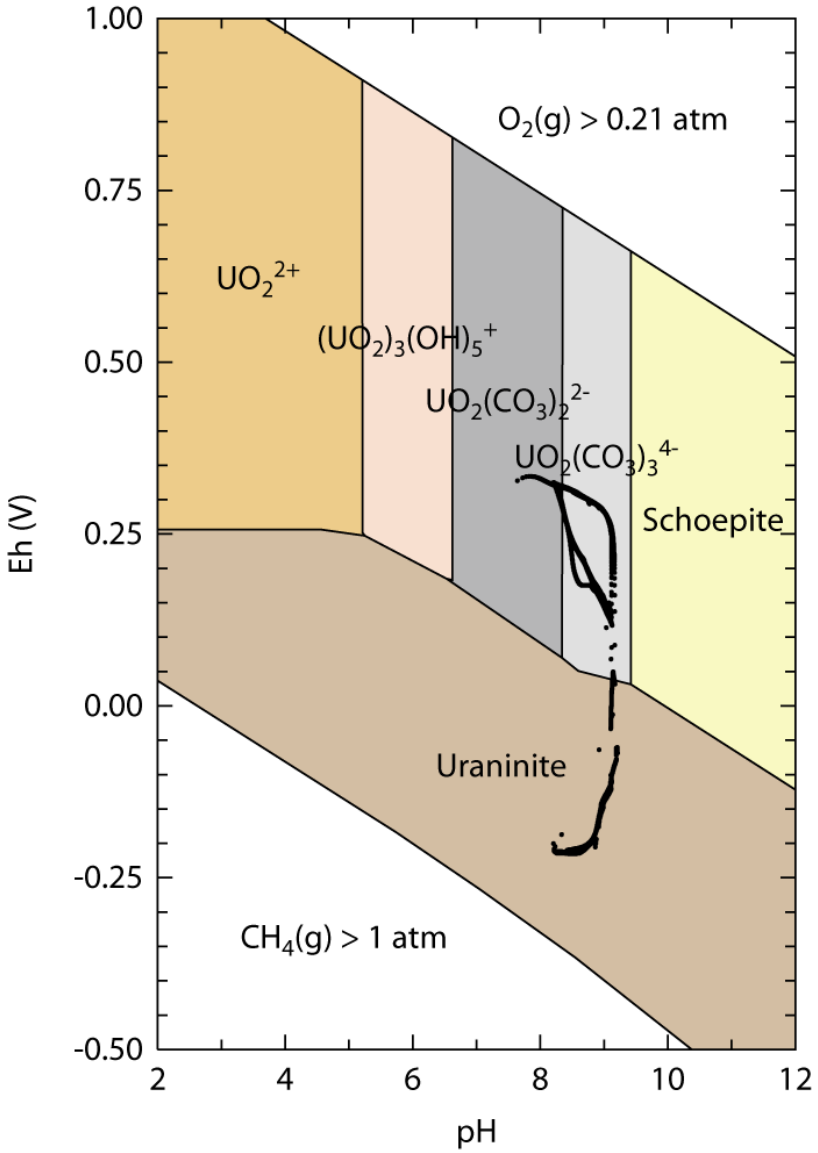

Figure 127: Pourbaix diagram of the U-H_2O-CO_2 system at 298.15K and 10^5 Pa from LLNL data with Eh pH conditions in reactor 1 drawn in black.

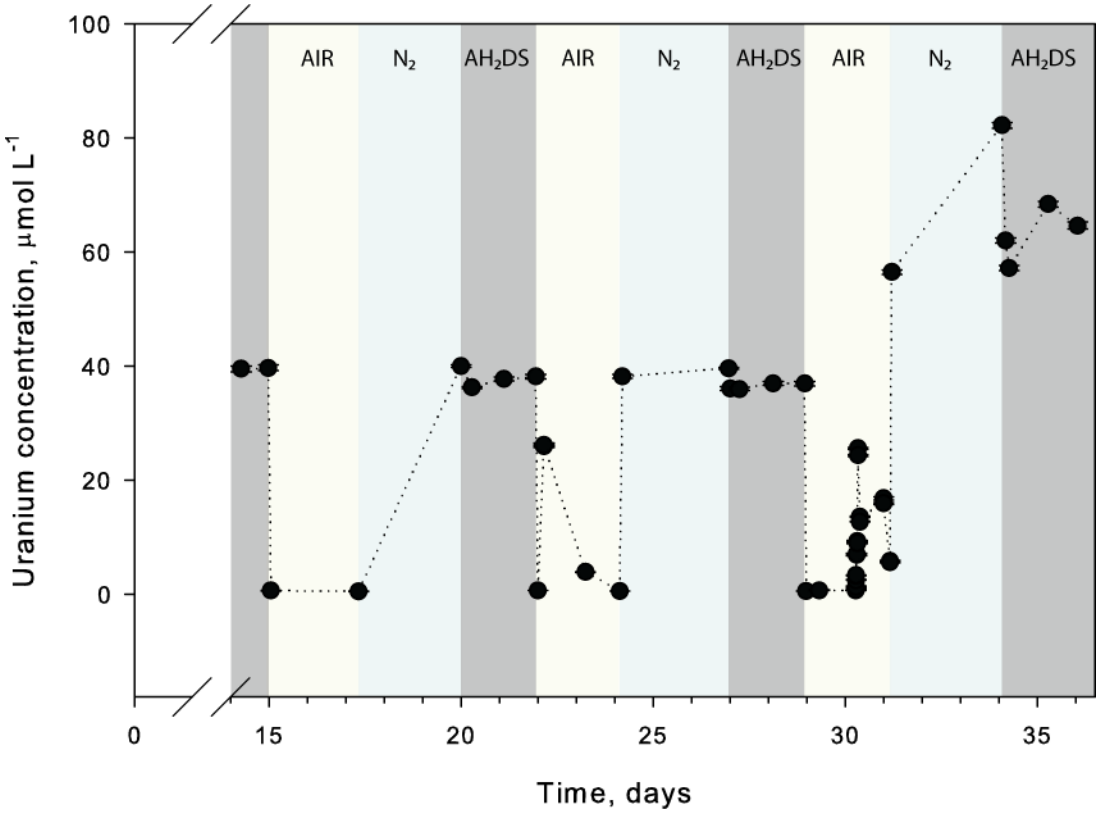

Figure 128: Aqueous/colloidal uranium concentration in the reactor 1 suspension over time.

Uranium mobility varied considerably during the experiment with decreased mobility during oxidising conditions. During reducing cycles uranium was found to be highly mobile with a Kd value in the suspension of approximately 129 L/kg, however upon air sparging this value dropped to approximately 53,570 L/kg demonstrating a high degree of immobilisation. This trend is counter intuitive as often microbial reduction of uranyl ions under anoxic conditions results in immobilisation of uranium as uraninite in natural soils and sediments (Dong et al., 2006). It is often assumed therefore that low Eh conditions are synonymous with uranium retention. Conversely the uranyl ion, thermodynamically predicted under oxidising conditions, which may complex with many inorganic and organic ligands in solution is considered highly mobile. Despite the thermodynamic predictions illustrated in Figure 127, recent studies reveal that reduction of U(VI) may be seriously limited by slow electron transfer processes, particularly at high pH where large oligomeric molecules such as $UO_2(CO_3)_3^{4-}$ are favoured (Wang et al., 2011). Consequently uranyl reduction to uraninite is considered to be very limited during these experiments. Therefore despite strongly varying Eh conditions $UO_2(CO_3)_3^{4}$ is expected to be the dominant species at all times during the reactor experiment with subdominant concentrations of $(UO_2)_2CO_3OH_3^-$ and $UO_2(CO_3)_2^{2-}$. In the absence of uraninite surface complexation is expected as the dominant immobilisation mechanism for U(VI) species.

As all predicted aqueous uranyl species are negatively charged ferric hydroxides are thought to act as strong sorbents below their point of zero charge in addition to incorporating U(VI) species into their structure (Duff et al., 2002; Kerisit et al., 2011). Additionally silanol and aluminol edge sites of phyllosilicate minerals offer a substantial capacity for complexation of uranyl-carbonate complexes

(Bachmaf and Merkel, 2010). It is the combination therefore of sorption processes between ferric hydroxides and clay edge sites which are thought to control uranium mobility in reactor suspensions.

There is significant variation to uranyl sorption envelopes between clays of different mineralogy as demonstrated by Bachmaf and Merkel (2010). Smectites which represent 12-13.5% of the COx mineralogical composition exhibit fewer aluminol edge sites and a greater number of silanol sites than Kaolinite type clays (2-4% of COx). Smectites demonstrate a parabolic sorption envelope for U(VI) species with significant desorption between pH 5 and 9 whereas Kaolinites act as significantly stronger sorbents of U(VI) at neutral and high pH.

During cycles of air sparging pH was consistently lower (~pH 8.2) than for cycles of nitrogen sparging (~ pH 9), partially due to the equilibrium of calcite at atmospheric pCO_2 and partially due to oxidation of reduced species resulting in proton production. This pH change is thought to have resulted in the dramatic changes in U(VI) mobility observed by a combination of two mechanisms. Firstly increasing pH will have resulted in desorption of uranyl-carbonate complexes from silanol edge sites. Secondly increasing pH from 8-9 crosses the point of zero charge of many metal oxides resulting in additional desorption of negatively charged uranyl-carbonate complexes from these surfaces.

The importance of pH changes on mobility of U(VI) species has been reported by several authors including Barnett et al. (2002) who predict large increases of aqueous U(VI) species upon pH increases such as those experienced in reactor suspensions.

Mercury

Mercury was added to reactor 1 in its oxidized i.e. Hg(II) form as a free cation at low pH. As can be seen from the Pourbaix diagrams (Figure 129) Eh conditions following AH_2DS^{2-} additions thermodynamically favour reduction to Hg(0), a liquid metal at room temperature, via Equation 28.

Equation 28 $Hg(OH)_2 + 2H^+ + 2e^- \rightarrow Hg^0 + 2H_2O$

Upon the switching to air sparging once again Eh conditions approach the dominant field of Hg(II) as a dual hydroxylated species via the reversal of Equation 28. It is therefore expected that under oxidising conditions $Hg(OH)_2$ should be present in the suspension as a subdominant species to Hg(0).

Aqueous mercury concentrations were found to be very low under reactor conditions with Kd values ranging between 25,560 and 330,094 L/kg, this suggests that either transformation to Hg(0) did not occur or that Hg(0) was volatilised and lost into the gas phase.

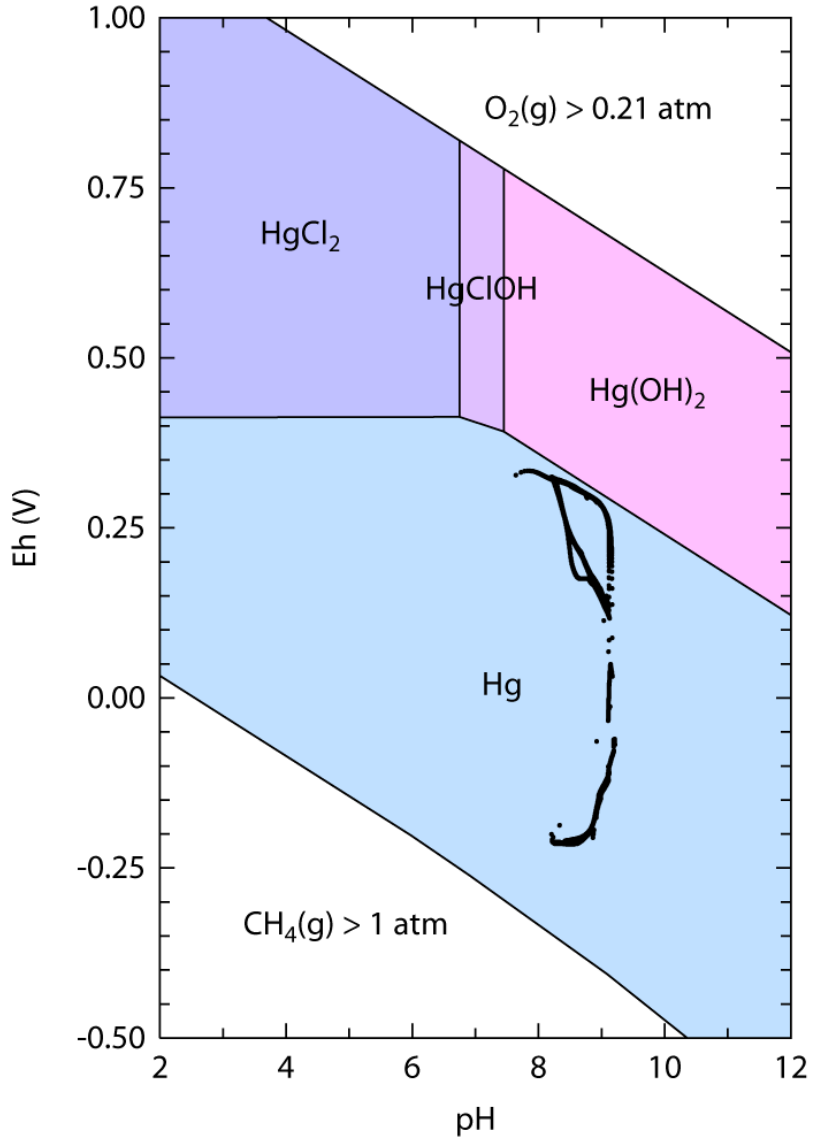

.

Figure 129: Pourbaix diagram of the Hg-H_2O-CO_2-Cl system at 298.15K and 10^5 Pa with Eh pH conditions in reactor 1 drawn in black.

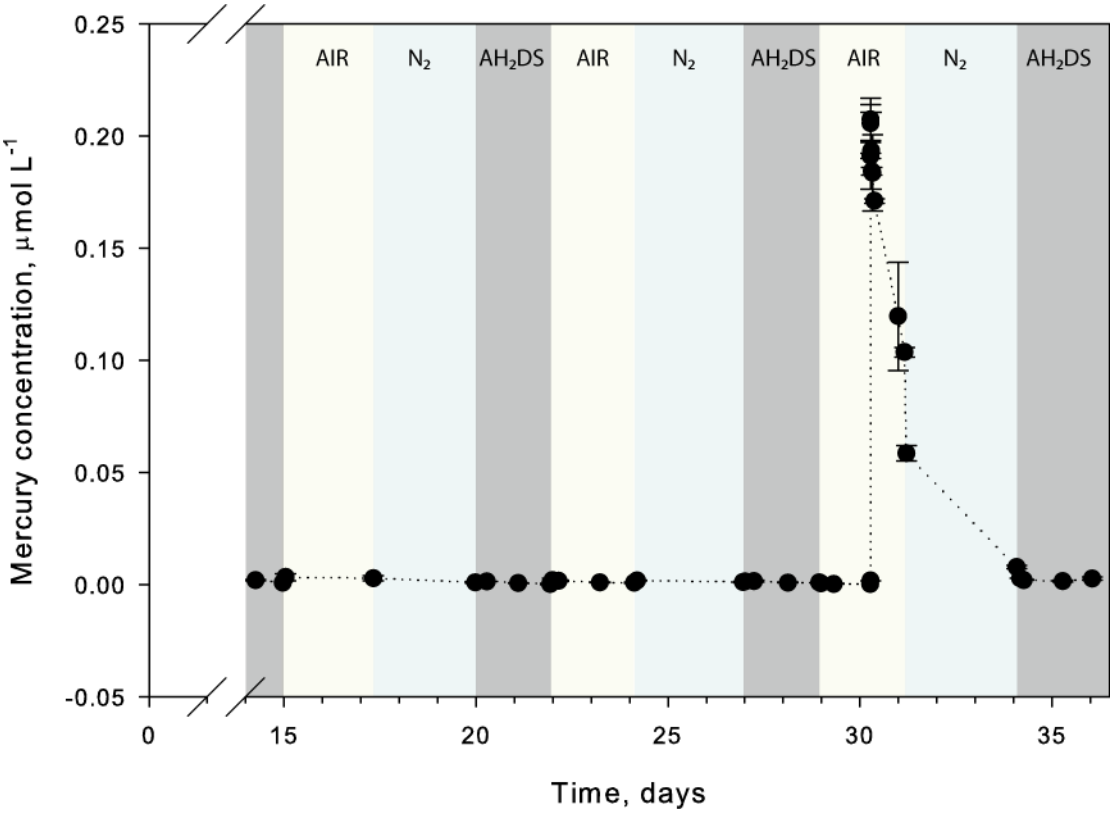

Figure 130: Aqueous/colloidal mercury concentration in the reactor 1 suspension over time.

Abiotically controlled mercury mobility within the COx can therefore be considered to be low over the range of Eh and pH conditions expected even with extensive redox cycling. As mercury immobilisation is not thought to be dependent on a particular redox sensitive mineral phase but the result of speciation cumulative trends are also unlikely and were not observed during this experiment. Even under conditions of sulphate reduction, not experienced during the experimental period, Hg is unlikely to be mobilised due to the formation of HgS (cinnabar).

Despite these findings Hg mobility in soils is strongly influenced by organic matter and microbial activity which have not been thoroughly evaluated within this experiment. Further experiments in the presence of an active microbial community are required to establish if low mercury mobility is also applicable to natural conditions in such clay rich media.

Conclusions

In carbonate rich clay layers such as the Callovo-oxfordian (COx), pH is well buffered by calcite and dolomite and is unlikely to drop significantly below pH 7 with cycles of oxidation and reduction unless significant decalcification occurs. Within the pH and Eh conditions expected Cr, As, Hg and U may undergo significant changes to their speciation. Additionally cumulative changes to the substrate are expected due the varying mineral stability which will have a secondary effect on the mobility of contaminants.

These initial experiments show changes to the intra-cycle mobility of As, Cr and U in addition to cumulative changes in As and Cr mobility following successive redox cycling. A summary of the range of distribution coefficients calculated from this study is provided in Table 31 in addition to the key trends observed. Mercury and Chromium were found to be highly immobile over the whole

range of experimental conditions due presumably to formation of stable Hg(0) and a combination of Cr^{3+} sorption and precipitation processes following reduction of Cr(VI) by reduced ferrous minerals and AH_2DS^{2-}. Conversely arsenic was found to be highly mobile throughout redox cycling under both oxidising and reducing conditions. Incomplete reduction of As(V) to As(III) is presumed due to pH dependence of Kd values and literature evidence of radical oxidising species in chemically reduced AH_2DS^{2-} (Jiang et al., 2009). Subsequent re-oxidation of arsenite to arsenate by molecular oxygen, catalysed by mineral surfaces is thought presumed to occur upon each oxidising cycle.

Mobility of uranium under redox oscillating conditions was found to vary significantly due to changes in aqueous speciation and changing mineral surface charge due to oscillating pH. In contrast to often reported uranium immobilisation under reducing conditions (Anderson et al., 2003), uranium mobility was high under reducing conditions in the reactor environment due presumably to inefficient electron transfer between AH_2DS^{2-} and large uranyl-carbonate complexes impeding reduction to uraninite. The observed high mobility under reducing conditions is therefore attributed to loss of positive charge on metal oxide surfaces due to pH change and subsequent uranyl-carbonate desorption.

Table 31: Summary of the range of Kd values obtained experimentally during redox cycling and the intra-cycle and cumulative trends observed.

Contaminant	Kd max observed L/kg	Kd min observed L/kg	Key intra-cycle trends	Cumulative trends
Arsenic	616	97	Increased mobility during reducing cycles	Decreasing mobility with successive redox cycles
Chromium	2,333,530	21,642	Increased mobility during reducing cycles	Decreasing mobility with successive redox cycles
Mercury	330,094	25,560	No clear trends	No clear trends
Uranium	53,569	129	Increased mobility during reducing cycles	No clear cumulative trends

Mercury was shown to be rapidly immobilised upon addition to the Cox suspensions and its subsequent mobility was not shown to vary significantly intra cycle or cumulatively due to redox oscillations. However, Hg mobility has been shown to be strongly affected by microbial processes such as methylation and therefore further similar experiments using a substrate from the near surface with an active microbial community should be conducted to better evaluate Hg mobility around any future near surface repository.

Cumulative effects of redox cycling were shown for both arsenic and chromium which appear to be attenuated due to cumulative mineralogical changes induced by successive redox cycles. Two hypotheses are presented including increased co-precipitation of these contaminants with ferric hydroxide minerals and an increasing proportion of ferric hydroxides with cycling due to the successive dissolution of pyrite during cycling.

All calculations presented in this chapter assume that the reactor environment acts as a closed system with respect to contaminants and that all added contaminants remain within either the aqueous or solid phase. While this assumption is valid for contaminants with low volatility such as uranium and chromium, arsenic and mercury have been shown to be subject to methylation and subsequent volatilisation in the environment(Compeau and Bartha, 1985; Mestrot et al., 2011). Although this volatilisation is highly unlikely in the abiotic experimental environment, such processes could lead to greater contaminant mobility in the near surface environment and therefore should be considered in further experiments, especially in the presence of a more natural near surface substrate and an active microbial community.

Whilst this experiment offers a preliminary view of contaminant mobility in a clay rich substrate under cyclic redox conditions, many of the mechanisms responsible for contaminant mobility may only be hypothesised in the absence of further spectroscopic data. Additionally, although AH_2DS^{2-} was carefully selected as a bulk reductant to mimic reduction by microbial activity, re-oxidation of reduced species by radical species produced during AQDS reduction hinder its effective use at high pH and high AQDS/contaminant ratios. The potential of AH_2DS^{2-} is also not sufficiently low to cause sulphate reduction, a process which is crucial to understanding contaminant mobility in the subsurface, particularly in sulphide bearing clay layers subjected to redox oscillation. Sulphides often act as sorbents for contaminants under reducing conditions and the lack of sulphate reduction during these experiments may have led to artificially low Kd values for contaminants under reducing conditions in the absence precipitating sulphides.

To further understand such a complex dynamic system further experiments in the presence of an active microbial community, supported by spectroscopic analyses and kinetic modelling are required. These experiments would also benefit from the control of pCO_2 concentrations in the sparging gas to avoid strong changes to pH which have been shown to affect contaminant mobility in the reactor environment but which are not necessarily present to the same extent under natural redox oscillating conditions.

Chapter 7: Conclusions, Perspectives and Future Research

The pedosphere as a sink and a source for contaminants

Traditionally clay rich floodplain and wetland soils are regarded as sinks for inorganic contaminants in the hydro/pedosphere. The evidence presented in this thesis challenges this view, demonstrating that in addition to immobilizing a variety contaminants supplied by hydrological or atmospheric transport, floodplain soils can act as sources of contaminants, re-releasing significant contaminant concentrations to the aqueous phase due to highly dynamic chemical conditions driven by cyclic flooding.

Indeed Chapter 2 of this thesis highlights the current poor understanding of arsenic fluxes to and from the pedosphere in addition to the large margins of error present in flux estimates between other arsenic pools in the environment. This is particularly true when frequently used estimates for anthropogenic atmospheric arsenic fluxes are considered in light of increasing coal combustion and metal production.

Implications for soil risk assessment

Release of arsenic previously considered to be immobilized in soils in Europe could pose a risk to human health by increasing contaminant transfer factors to crops and by contaminating increasingly important shallow alluvial aquifers and surface water. Results presented in this thesis clearly show that partitioning coefficients (K_d values) for arsenic and other trace contaminants in calcareous soils can vary considerably dependent on prevailing soil redox and pH conditions and that therefore, even moderate total solid soil arsenic concentrations can result in periodically high aqueous concentrations. This draws attention to the fact that total contaminant concentrations in the soil solid phase cannot be used in isolation as adequate indicators of risk and that risk assessments for any given land use also require an understanding of soil mineralogy, hydrologic regime and contaminant speciation. The wide range of soil arsenic concentrations specified as national guideline and action values, demonstrates the lack of consensus and legislative consistency between countries, even within the European Union. If harmonization of environmental legislation between European member states is to be achieved, consideration must be paid both to variations in background concentrations of geogenic contaminants in soils between states/regions and to factors affecting solid, aqueous and gaseous partitioning for contaminants with varying chemical properties in different soils.

In the case of the Saône floodplain top-soils, results included within Chapter 5 demonstrate that during periods of pore-saturation, caused either by overbank flooding or by groundwater rise, soils moderately contaminated with arsenic may release significant quantities of arsenic to interstitial water, mediated by a variety of processes.

Implications for near surface storage of low-level long-lived nuclear waste

The results presented in Chapter 6 show that redox changes within clay barrier materials surrounding near surface geological storage repositories, even in the absence of an active microbial community, can have a dramatic impact on contaminant mobility. Mobility is shown to vary considerably between contaminants and between oxidising and reducing conditions. Despite carefully controlled redox conditions via dosing of reduced AQDS and oxygen sparging, trends in contaminant mobility show that contaminant speciation differs significantly from thermodynamic

predictions and demonstrates that kinetic controls on speciation change and redox transformations play an important role in determining contaminant mobility. This is particularly true in the case of uranium where wet chemistry data support the formation of highly mobile uranyl-carbonate complexes which are thought to remain stable due to electrostatic repulsion between the electron donor (AH_2DS^{2-}) and the negatively charged uranyl-carbonate complex in addition to very slow electron transfer from reduced aqueous species (e.g. Fe^{2+}) to the uranyl core. Mobility of Cr, As, Hg and U may be described by a combination of surface complexation, precipitation, cation exchange and co-precipitation which differs substantially dependent on contaminant speciation and substrate specific mineralogy. Arsenate, arsenite and uranyl-carbonate complexes are shown to be the most mobile contaminant species investigated at high pH (8-9) and variable Eh conditions. Although these experiments offer an insight into the important processes controlling contaminant mobility in a calcareous clay rich media, abiotic reduction by AH_2DS^{2-} is shown to differ significantly from microbial reductive processes reported in natural soils and sediments. Therefore to ensure adequate understanding of contaminant mobility during water level changes in a substrate around a nuclear waste repository wet chemistry experiments must be conducted using site specific substrate supported by solid characterisation techniques and investigative modelling such as used in Chapter 5.

The importance of cumulative redox cycling effects

Beyond demonstrating the importance of varying solid/aqueous phase distribution dependent on flooding and hence Eh conditions, the results presented in Chapters 5 and 6 of this thesis clearly show that the repetitive oscillation of redox conditions can result in additional cumulative effects to partition coefficients due to kinetic controls on mineralogy and mineralization of labile organic matter fractions. Whilst this may seem logical, very few investigations into the cumulative effects of redox oscillating conditions exist and fewer still have formally considered the effects of bulk mineralogical/structural changes on contaminant distribution coefficients.

Under experimental conditions multiple cycles of reduction and oxidation are clearly shown to result in the attenuation of aqueous As and Cr concentrations suggesting that redox cycling may be an effective form of natural attenuation of toxic contaminants in the environment. In the Callovo-oxfordian clay and calcareous fluvisol from the Saône floodplain various mineralogical and microbial processes are considered to be responsible for the observed cumulative effects on mobility. These mechanisms include increased co-precipitation processes, gradual oxidative dissolution of pyrite grains resulting in an increased ferric hydroxide fraction and decreased microbial activity/reductive dissolution resulting from depletion of labile organic matter.

The remainder of chapter 7 summarizes the physical and chemical distribution of arsenic on the investigated riparian floodplain, the key processes observed experimentally during this thesis which control mobility of arsenic and other contaminants, the relevance of these findings to other environments and finally the limitations of experimental and modelling approaches used during this thesis.

Distribution of arsenic on the Saône floodplain

An investigation of the distribution of arsenic on part of the Saône floodplain in Chapter 4 leads to several key conclusions. The first regards the source of the arsenic contamination. As no clear spatial trends were observed with respect to arsenic concentrations in top soils, either perpendicular

or parallel to the river flow it is possible to conclude that the contamination does not originate from a point source on this part of the floodplain. The diffuse nature of the contamination indicates that contamination originates from outside of the sampled area, imported with floodwater as aqueous species or suspended particles or alternatively by atmospheric deposition. Whilst diffuse contamination could be a result of historic arsenic application directly to soils by farmers, the variety of land-use (pasture land, salad production, corn production, natural wet land) which all display comparable arsenic contamination, makes this interpretation improbable. Comparison between elemental concentrations in soils and the risk of groundwater rise hints that a hydraulic re-distribution of contaminants on the floodplain does occur. However due to the low total number of sampling points, the correlation could not be proven to be statistically significant at the 95% confidence level. What was clear from this study is that the distribution of arsenic was dependent on one key physico-chemical variable, the presence of iron and manganese containing particles between 2 and 10 μm in diameter. Whilst it is possible that this could be indicative of phyllosilicate minerals it seems more probable that poorly crystalline metal oxyhydroxides phases, subsequently identified by Mössbauer spectroscopy, control mobility of arsenic on the floodplain.

Key biogeochemical processes observed

Depletion of labile organic matter

Dissolved organic matter in pore water has been linked by several recent studies to the liberation of arsenic in shallow alluvial aquifers and paddy field soil. In Chapter 5 the cycling of dissolved organic matter in a floodplain soil under redox cycling conditions is shown to be gradually attenuated due to depletion via rapid aerobic metabolism under oxidising conditions and comparatively slow replenishment by particulate organic matter hydrolysis. This depletion of labile organic matter is shown to result in decreased microbial reduction of metal hydroxide minerals which act to immobilise arsenic via sorption and co-precipitation processes and hence a decrease in arsenic mobility. This scenario is analogous to groundwater rise and fall where pore saturation is achieved without the influx of fresh sediment to replenish labile organic matter pools in soil.

Dissimilatory reductive dissolution and subsequent oxidative precipitation of iron and manganese oxyhydroxides

Iron and manganese (hydr)oxide minerals have been shown by many previous studies to be key mineralogical controls on arsenic mobility in soils and sediments due to their large surface area and hence extensive sorption capacity for anionic aqueous species in addition to immobilisation of such species by co-precipitation processes. As both Fe(III) and Mn(IV) may serve as a terminal electron acceptor for anaerobic microbial metabolism following oxygen depletion in flooded soils, both iron and manganese hydroxide minerals are subject to reductive dissolution during flooding. Contaminants such as arsenic associated with Fe or Mn hydroxides have been shown to be released into the aqueous phase upon reductive dissolution of these minerals. Evidence for all of these processes including aqueous chemistry, spectroscopic and microbial ecology data is presented in Chapter 5. In addition to confirming these processes in soils of the Saône floodplain results presented in Chapter 5 demonstrate that successive cycles of oxidation and reduction result in the decreased mobility of arsenic under reducing conditions. The presented thermodynamic and kinetic model of the experimental system suggests that the previously undocumented attenuation of

aqueous arsenic is in part due to an increased proportion of co-precipitated arsenic compared to surface sorbed arsenic with each cycle.

De-carbonation

One of the key cumulative effects of redox cycling on bulk chemistry, identified experimentally in both calcareous floodplain soils and the Callovo-Oxfordian clay material used within this thesis, is that of de-carbonation. Oxidation processes which occur following draining of floodplain soils produce acidity which is neutralized by dissolution of carbonates and hence the release of metal ions (in this case of calcite Ca^{2+}).

Experimentally an increase in aqueous Ca^{2+} concentrations was observed during each redox oscillation experiment. Whilst in a more perfectly closed system (e.g. without degassing of CO_2 produced during microbial metabolism) carbonate dissolution may be countered by re-precipitation, upon development of reducing conditions and proton consumption, hydraulic transport of liberated Ca with receding floodwater may prevent such re-precipitation. De-carbonated was not considered to influence arsenic mobility substantially during the short experimental periods of this thesis, particularly as arsenic is shown not to be strongly associated with carbonate fractions by statistical methods (Chapter 4). However, this gradual change in the mineralogical matrix is likely to have dramatic long term effects. Upon the complete depletion of the carbonate fraction, the main pH buffering phase in calcareous soils, subsequent pH drop is highly probable. The effects of the potentially dramatic pH drop are likely to important for contaminant mobility, I.e. Contaminants which occur as monoatomic cations will become more mobile whereas oxyanions will become less mobile.

Processes not observed

Immobilisation of arsenic by FeS_2 or $FeCO_3$

Neither ^{57}Fe Mössbauer spectrometry or X-ray diffraction analysis revealed the presence of ferrous sulphide or carbonate minerals which have been shown by numerous authors to be sorbents of arsenic under reducing conditions (Charlet et al., 2011). It could therefore be concluded that immobilisation of arsenic by such phases in this soil are of limited importance. Further evidence to support this conclusion comes from Charlet et al. (1998) who demonstrate that at high pH conditions rapid sorption of Fe^{2+} to clay minerals may limit precipitation of thermodynamically favourable ferrous phases. However, disparities between experimental conditions and the natural environment may also contribute to the lack of $FeCO_3$ and FeS_2 in reactor suspensions. Although Eh conditions achieved during reactor experiments oscillated within the range of those experienced by soils during natural flooding, homogenisation of soils by mechanical agitation resulted in the destruction of natural soil structure. Soil structure would normally result in many chemical micro-environments where sulphide reduction could more readily occur. Additionally periods of flooding on the Saône floodplain can last for periods greater than a month, comparatively periods of reduction in reactor suspensions of up to 7 days were very short and may not have been sufficient to allow for the onset of sulphate reduction.

Redox behaviour of structural clay components

Recently Ribeiro et al. (2009) and Stucki (2011) have reported that structural ferric iron in clays can be redox active and accessible to iron reducing bacteria as a terminal electron acceptor. The results of Mössbauer spectroscopy presented in Chapter 5 show that no strong changes to the Fe(II/III) ratio in clays were recorded between the end of reducing and oxidizing cycles indicating that significant reduction of structural Fe(III) did not occur under experimental conditions. However, this does not contradict the results of Stucki (2011) and Ribeiro et al. (2009) due to the limited periods of reducing conditions in the reactor suspensions. It is reasonable to assume that reduction of structural Fe(III) is significantly less energetically efficient than reduction of poorly crystalline ferric (hydr)oxide minerals. Therefore structural Fe(III) may only become a viable terminal electron acceptor upon exhaustion of the more labile ferric iron fraction. Indeed, despite the strong evidence for microbial iron reduction during reducing half cycles there was limited decrease to the total proportion of ferric iron present as poorly crystalline FeOOH and the PHREEQC model of the system does not predict exhausted of labile ferric iron within the 7 day reducing periods. This result suggests that even relatively small changes to poorly crystalline ferric oxide fractions, imperceptible via bulk spectroscopy may cause large changes to arsenic mobility.

Further research needs

Applicability of findings to other redox oscillating environments: The experimental redox cycling aspects of this thesis were conducted on one type of calcareous fluvisol and one well classified clay rich sedimentary rock sample from the Callovo-oxfordian formation. Whilst a variety of different techniques have been used to determine the processes key to controlling arsenic mobility under in the investigated substrates during experimental conditions, the question remains as to what extent these processes are applicable to other soils and sediments subjected to temporal redox oscillations. The complexity of flooded soil systems under redox oscillating conditions, even when experimentally simplified as homogeneous zero suspensions warrants greater attention than was possible within the framework of this thesis. One logical continuation of this research theme would be to apply the same experimental methodology to soils with differing mineralogical composition, varying proportions and types of organic matter and over a range of pH and temperature conditions to assess the importance of the different arsenic liberating and attenuating processes observed during this thesis. Particularly whether the observed attenuation of arsenic released following successive redox cycles is applicable in a range of redox oscillating environments. As the PHREEQC model indicates that both organic matter depletion and increased precipitation contribute to this trend, further experiments isolating these factors are required. This could be achieved by simply adding additional dissolved organic carbon to replace the exhausted labile pool at the onset of each oxidizing half cycle. Further experiments could also be conducted to determine whether this observed trend is applicable to aged contaminated soils, i.e. soils which have been contaminated for several years and may have reached an equilibrium state with respect to fast and slow sorption processes, or whether the observed attenuation is applicable uniquely to recently contaminated soils (equivalent to the doping of experimental soils with arsenic one month prior to the onset of cycling).

Dynamic climate/hydraulic variation: The results presented in this thesis clearly demonstrate that many processes controlling contaminant mobility in floodplain soils are kinetically controlled. Oscillating redox conditions induced by flooding and draining also include time controlled

parameters. Further questions raised based on this observation include the effects of temporal flooding parameters such as the speed of oscillation between reducing and oxidizing conditions and the length of each oxidizing or reducing half cycle. As the periodicity, intensity and timing of flooding are expected to change due to changing global and regional climatic conditions an understanding of how these changes may alter contaminant mobility in contaminated soils would be extremely valuable.

Improvements to experimental design and alternative experimental methodologies: Whilst laboratory based representations of complex natural systems always entail a degree of compromise it is my opinion that significant improvements could be made to the experimental design used during this thesis in order to more accurately represent natural flooded conditions.

One of the key simplifications of the suspended sediment systems used within this work is the destruction of soil spatial heterogeneity. As discussed in Chapter 1, the micro-structure present in soils results in the creation of many micro environments with strong variations in Eh and pH conditions. The lack of significant sulphate reduction during reactor cycling experiments when evidence from static flooding experiments under similar Eh pH conditions indicate substantial sulphate reduction may be partially explained by the removal of this range of Eh – pH environments in soils which contribute to bulk measured values. This disparity may also be due destruction of microbial habitat effectively limiting the creation of biofilms necessary for full soil microbial function.

A further key experimental simplification of this system is the constant level of soil moisture in the reactors. Whilst wet oxidation is induced in this experimental system by the rapid diffusion of oxygen from the headspace to the aqueous phase, it is feasible that the changes to mineralogy observed under wet oxidation and reduction conditions may differ to those observed to wet reduction and dry oxidation cycling.

Additional experimental possibilities include the coupling of oscillating redox conditions with diffusive and advective transport models. Zero dimensional geochemical modelling conducted in PHREEQC serves as a strong diagnostic and prognostic tool to aid understanding of important processes determining mobility of contaminants in dynamic soil and sediment systems. However mobility in this context refers to the partitioning between immobile solid phases and mobile aqueous or colloidal phases. While this is useful in itself, a key question posed by modellers of waste repositories is the spatial mobility of contaminants in the environment. The results of coupling of the developed PHREEQC code to 1D transport models, fed by and validated by experimental column studies would be of great interest to waste repository modellers who tend to traditionally view the matrix in porous media as a relatively static entity with little variation with time.

References

Abbott, J.L., 1948. X-ray fluorescence analysis. The Iron Age 58-62.

Ackermann, J., Vetterlein, D., Kuehn, T., Kaiser, K., Jahn, R., 2010. Minerals controlling arsenic distribution in floodplain soils. European Journal of Soil Science 61, 588-598.

Ackermann, J., Vetterlein, D., Tanneberg, H., Neue, H.-U., Mattusch, J., Jahn, R., 2008. Speciation of Arsenic under Dynamic Conditions. Engineering in Life Sciences 8, 589-597.

Aeschbacher, M., 2007. Extent and Magnitude of the Apparent 15N-KineticIsotope Effect During Reduction of NitroaromaticCompounds by Anthraquinol 2,6-disulfonate.

Aggett, J., Aspell, A.C., 1980. Arsenic contamination in an apple orchard. Environmental Pollution Series A, Ecological and Biological 22, 39-46.

Aggett, J., O'Brien, G.A., 1985. Detailed model for the mobility of arsenic in lacustrine sediments based on measurements in Lake Ohakuri. Environmental Science & Technology 19, 231-238.

Ahern, F., Eckert, J.M., Payne, N.C., Williams, K.L., 1985. Speciation of chromium in sea water. Analytica Chimica Acta 175, 147-151.

Ahmed, K.M., Bhattacharya, P., Hasan, M.A., Akhter, S.H., Alam, S.M.M., Bhuyian, M.A.H., Imam, M.B., Khan, A.A., Sracek, O., 2004. Arsenic enrichment in groundwater of the alluvial aquifers in Bangladesh: an overview. Applied Geochemistry 19, 181-200.

Aiuppa, A., D'Alessandro, W., Federico, C., Palumbo, B., Valenza, M., 2003. The aquatic geochemistry of arsenic in volcanic groundwaters from southern Italy. Applied Geochemistry 18, 1283-1296.

Alexandratos, V.G., Elzinga, E.J., Reeder, R.J., 2007. Arsenate uptake by calcite: Macroscopic and spectroscopic characterization of adsorption and incorporation mechanisms. Geochimica et Cosmochimica Acta 71, 4172-4187.

Allard, B., Arsenie, I., 1991. Abiotic reduction of mercury by humic substances in aquatic system — an important process for the mercury cycle. Water, Air, & Soil Pollution 56, 457-464.

Aller, R.C., 1994. Bioturbation and remineralization of sedimentary organic matter: effects of redox oscillation. Chemical Geology 114, 331-345.

Amini, M., Abbaspour, K.C., Berg, M., Winkel, L., Hug, S.J., Hoehn, E., Yang, H., Johnson, C.A., 2008. Statistical Modeling of Global Geogenic Arsenic Contamination in Groundwater. Environmental Science & Technology 42, 3669-3675.

Amirbahman, A., Reid, A.L., Haines, T.A., Kahl, J.S., Arnold, C., 2002. Association of Methylmercury with Dissolved Humic Acids. Environmental Science & Technology 36, 690-695.

Anderson, R.T., Vrionis, H.A., Ortiz-Bernad, I., Resch, C.T., Long, P.E., Dayvault, R., Karp, K., Marutzky, S., Metzler, D.R., Peacock, A., White, D.C., Lowe, M., Lovley, D.R., 2003. Stimulating the In Situ Activity of Geobacter Species To Remove Uranium from the Groundwater of a Uranium-Contaminated Aquifer. Appl. Environ. Microbiol. 69, 5884-5891.

Andersson, A., 1979. Mercury in Soils, in: The Biogeochemistry of mercury in the environment. Elsevier/North-Holland Biomedical Press ;;Sole distributors for the U.S.A. and Canada Elsevier/North-Holland, Amsterdam ;;New York ;New York, pp. 79–122.

ANDRA, 2005. Phenomenological evolution of a geological repository, Dossier 2005 Argile. Agence nationale pour la gestion des dechets radioactifs.

ANDRA, 2009. Inventaire National 2009 (Rapport de Synthese). Agence nationale pour la gestion des dechets radioactifs.

ANDRA, 2010. Plan National de gestion des matieres et des dechets radioactifs 2010-2012. Agence nationale pour la gestion des dechets radioactifs.

Andreae, M.O., 1980. Arsenic in Rain and the Atmospheric Mass Balance of Arsenic. J. Geophys. Res. 85, 4512-4518.

Ankudinov, A.L., Rehr, J.J., Conradson, S.D., 1998. Real-space multiple-scattering calculation and interpretation of x-ray-absorption near-edge structure. Phys. Rev. B 58, 7565-7576.

Apostol, I., Miller, K., Ratto, J., Kelner, D., 2009. Comparison of different approaches for evaluation of the detection and quantitation limits of a purity method: A case study using a capillary isoelectrofocusing method for a monoclonal antibody. Analytical Biochemistry 385, 101-106.
Appelo, C., 2005. Geochemistry, groundwater and pollution, 2nd ed. Balkema, Leiden ;;New York.
Appelo, C.A.J., Van Der Weiden, M.J.J., Tournassat, C., Charlet, L., 2002. Surface Complexation of Ferrous Iron and Carbonate on Ferrihydrite and the Mobilization of Arsenic. Environmental Science & Technology 36, 3096-3103.
APVMA, 2005. The Reconsideration of Registrations of Arsenic Timber Treatment Products (CCA and arsenic trioxide) and Their Associated Labels (REPORT OF REVIEW FINDINGS AND REGULATORY OUTCOMES SUMMARY REPORT). Australian Pesticides and Veterinary Medicines Authority, Canberra, Australia.
Armstrong, W., 1964. Oxygen Diffusion from the Roots of Some British Bog Plants. Nature 204, 801-802.
Armstrong, W., 1980. Aeration in Higher Plants. Academic Press, pp. 225-332.
Arnfalk, P., Wasay, S.A., Tokunaga, S., 1996. A comparative study of Cd, Cr(III), Cr(VI), Hg, and Pb uptake by minerals and soil materials. Water, Air, & Soil Pollution 87, 131-148.
Arnold, R.G., DiChristina, T.J., Hoffmann, M.R., 1988. Reductive dissolution of fe(III) oxides by Pseudomonas sp. 200. Biotechnology and Bioengineering 32, 1081-1096.
Arnold, R.G., Hoffmann, M.R., DIChristina, T.J., Picardal, F.W., 1990. Regulation of Dissimilatory Fe(III) Reduction Activity in Shewanella putrefaciens. Appl. Environ. Microbiol. 56, 2811-2817.
Australasian Institute of Mining and Metallurgy.;Queensland., 2002. Green processing 2002. Australasian Institute of Mining and Metallurgy, Carlton Vic.
Bachmaf, S., Merkel, B., 2010. Sorption of uranium(VI) at the clay mineral–water interface. Environmental Earth Sciences 1-10-10.
Bachmaf, S., Planer-Friedrich, B., Merkel, B.J., 2008. Effect of sulfate, carbonate, and phosphate on the uranium(VI) sorption behavior onto bentonite. Radiochimica Acta 96, 359-366.
Bardelli, F., Benvenuti, M., Costagliola, P., Di Benedetto, F., Lattanzi, P., Meneghini, C., Romanelli, M., Valenzano, L., 2011. Arsenic uptake by natural calcite: An XAS study. Geochimica et Cosmochimica Acta 75, 3011-3023.
Barkay, T., Miller, S.M., Summers, A.O., 2003. Bacterial mercury resistance from atoms to ecosystems. FEMS Microbiology Reviews 27, 355-384.
Barnett, M.O., Jardine, P.M., Brooks, S.C., 2002. U(VI) Adsorption to Heterogeneous Subsurface Media: Application of a Surface Complexation Model. Environmental Science & Technology 36, 937-942.
Barnett, M.O., Turner, R.R., Singer, P.C., 2001. Oxidative dissolution of metacinnabar ([beta]-HgS) by dissolved oxygen. Applied Geochemistry 16, 1499-1512.
Bartlett, R., James, B., 1979. Behavior of Chromium in Soils: III. Oxidation1. J. Environ. Qual. 8, 31-35.
Bauer, M., Blodau, C., 2006. Mobilization of arsenic by dissolved organic matter from iron oxides, soils and sediments. Science of The Total Environment 354, 179-190.
Bauer, M., Heitmann, T., Macalady, D.L., Blodau, C., 2007. Electron Transfer Capacities and Reaction Kinetics of Peat Dissolved Organic Matter. Environmental Science & Technology 41, 139-145.
Beckhoff, B., 2006. Handbook of practical X-ray fluorescence analysis. Springer, Berlin ;;New York.
Behrends, T., Vancappellen, P., 2005. Competition between enzymatic and abiotic reduction of uranium(VI) under iron reducing conditions. Chemical Geology 220, 315-327.
Bencko, V., Rossner, P., Havrankova, H., Puzanova, A., Tucek, M., 1978. Effects of the combined action of selenium and arsenic on mice versus suspension culture of mice fibroblasts, in: Fouts, J., Gut, I. (Eds.), Industrial and environmental xenobiotics : in vitro versus in vivo biotransformation and toxicity : proceedings of an international conference held in Prague, Czechoslovakia, 13-15 September 1977. Excerpta Medica ;;sole distributors for the USA and Canada Elsevier/North-Holland, Amsterdam ;New York, pp. 312-316.
Benner, S., 2010. Hydrology: Anthropogenic arsenic. Nature Geosci 3, 5-6.

Bernick, M.B., Kalnicky, D.J., Prince, G., Singhvi, R., 1995. Results of field-portable X-ray fluorescence analysis of metal contaminants in soil and sediment. Journal of Hazardous Materials 43, 101–110.

Bethke, C.M., Yeakel, S., 2009. The Geochemist's Workbench® Reference Manual - Release 8.0. University of Illinois, Rockware, Illinois.

Bhattacharya, P., Jacks, G., Frisbie, S., Smith, E., Naidu, R., Sarkar, B., 2002. Arsenic in the Environment: A Global Perspective, in: Heavy metals in the environment. Marcel Dekker, New York, pp. 147-215.

Billen, G., Joiris, C., Wollast, R., 1974. A bacterial methylmercury-mineralizing activity in river sediments. Water Research 8, 219-225.

Bissen, M., Frimmel, F.H., 2003. Arsenic — a Review. Part I: Occurrence, Toxicity, Speciation, Mobility. Acta hydrochim. hydrobiol. 31, 9-18.

Blaauw, C., Stroink, G., Leiper, W., 1980. Mössbauer analysis of talc and chlorite. J. Phys. Colloques 41, C1-411-C1-412.

Bloom, A.J., 1996. Nitrogen dynamics in plant growth systems. Life Support Biosph Sci 3, 35-41.

Blowes, D.W., Ptacek, C.J., Jambor, J.L., Weisener, C.G., 2003. The Geochemistry of Acid Mine Drainage, in: Treatise on Geochemistry. Pergamon, Oxford, pp. 149-204.

Bock, M., Bohner, J., Conrad, O., Kothe, R., Ringeler, A., 2010. SAGA GIS: System for Automated Geoscientific Analyses.

de Boer, L.M., 1999. On the "ultimate" elemental correction equations for arsenic and selenium. Royal Society of Chemistry Special Publication 241, 27-33.

Bonneville, S., Van Cappellen, P., Behrends, T., 2004. Microbial reduction of iron(III) oxyhydroxides: effects of mineral solubility and availability. Chemical Geology 212, 255-268.

Borch, T., Kretzschmar, R., Kappler, A., Cappellen, P.V., Ginder-Vogel, M., Voegelin, A., Campbell, K., 2010. Biogeochemical Redox Processes and their Impact on Contaminant Dynamics. Environmental Science & Technology 44, 15-23.

Bowell, R.J., 1994. Sorption of arsenic by iron oxides and oxyhydroxides in soils. Applied Geochemistry 9, 279-286.

Bowen, H., 1979. Environmental chemistry of the elements. Academic Press, London ;;New York.

Bragg, L.J., Oman, J.K., Tewalt, S.J., Oman, C.J., Rega, N.H., Washington, P.M., Finkelman, R.B., 1997. Coal Quality (CoalQual) Database: Version 2.0 (Open-file report No. 97-134). U.S Geological Survey.

Brennecka, G.A., Wasylenki, L.E., Bargar, J.R., Weyer, S., Anbar, A.D., 2011. Uranium Isotope Fractionation during Adsorption to Mn-Oxyhydroxides. Environmental Science & Technology 45, 1370-1375.

BRGM, 2006. Remontées de nappes,Débordements,Ruissellements,Inondations,Crues.

BRGM, 2010. InfoTerre. BRGM, Orléans.

Brooks, W.E., 2010. Arsenic (2009 Minerals Yearbook). United States Geological Survey, Virginia, U.S.A.

Burgess, J., 1978. Metal ions in solution. Ellis Horwood ;;distributed by Halsted Press, Chichester ;New York.

Burgos, W.D., McDonough, J.T., Senko, J.M., Zhang, G., Dohnalkova, A.C., Kelly, S.D., Gorby, Y., Kemner, K.M., 2008. Characterization of uraninite nanoparticles produced by Shewanella oneidensis MR-1. Geochimica et Cosmochimica Acta 72, 4901-4915.

Burton, E.D., Bush, R.T., Sullivan, L.A., Johnston, S.G., Hocking, R.K., 2008. Mobility of arsenic and selected metals during re-flooding of iron- and organic-rich acid-sulfate soil. Chemical Geology 253, 64-73.

Cáceres, V.L., Gruttner, D.E., Contreras, N.R., 1992. Water Recycling in Arid Regions: Chilean Case. Ambio 21, 138-144.

Cai, Y., Cabrera, J.C., Georgiadis, M., Jayachandran, K., 2002. Assessment of arsenic mobility in the soils of some golf courses in South Florida. The Science of The Total Environment 291, 123-134.

Caldeira, C.L., Ciminelli, V.S.T., Dias, A., Osseo-Asare, K., 2003. Pyrite oxidation in alkaline solutions: nature of the product layer. International Journal of Mineral Processing 72, 373-386.

Caldeira, C.L., Ciminelli, V.S.T., Osseo-Asare, K., 2010. The role of carbonate ions in pyrite oxidation in aqueous systems. Geochimica et Cosmochimica Acta 74, 1777-1789.

Canavan, R.W., Slomp, C.P., Jourabchi, P., Van Cappellen, P., Laverman, A.M., van den Berg, G.A., 2006. Organic matter mineralization in sediment of a coastal freshwater lake and response to salinization. Geochimica et Cosmochimica Acta 70, 2836-2855.

Cao, X., Ma, L.Q., 2004. Effects of compost and phosphate on plant arsenic accumulation from soils near pressure-treated wood. Environmental Pollution 132, 435-442.

Van Cappellen, P., Wang, Y., 1995. Metal cycling in surface sediments: Modeling the interplay of transport and reaction., in: Metal Contaminated Aquatic Sediments. Ann Arbor Press, Chelsea.

Carlon, C., 2007. Derivation methods of soil screening values in Europe: A review and evaluation of national procedures towards harmonisation (JRC Scientific and Technical Report No. EUR 22805-EN). European Commission. Joint Research Cenre, Ispra, Italy.

Carroll, S.A., Bruno, J., Petit, J.C., Dran, J.C., 1992. Interactions of U(VI), Nd and Th(IV) at the calcite-solution interface. Radiochimica Acta 58-59, 245-252.

Chakraborty, S., Favre, F., Banerjee, D., Scheinost, A.C., Mullet, M., Ehrhardt, J.-J., Brendle, J., Vidal, L., Charlet, L., 2010. U(VI) Sorption and Reduction by Fe(II) Sorbed on Montmorillonite. Environmental Science & Technology 44, 3779-3785.

Chakraborty, S., Wolthers, M., Chatterjee, D., Charlet, L., 2007. Adsorption of arsenite and arsenate onto muscovite and biotite mica. Journal of Colloid and Interface Science 309, 392-401.

Charlet, L., Manceau, A., 1992a. Structure, Formation and Reactivity of Hydrous Oxide Particles; Insights from X-ray Absorption Spectroscopy, in: Buffle, J. (Ed.), Environmental particles. Lewis Publishers, Boca Raton FL, pp. 117-164.

Charlet, L., Manceau, A.A., 1992b. X-ray absorption spectroscopic study of the sorption of Cr(III) at the oxide-water interface : II. Adsorption, coprecipitation, and surface precipitation on hydrous ferric oxide. Journal of Colloid and Interface Science 148, 443-458.

Charlet, L., Morin, G., Rose, J., Wang, Y., Auffan, M., Burnol, A., Fernandez-Martinez, A., 2011. Reactivity at (nano)particle-water interfaces, redox processes, and arsenic transport in the environment. Comptes Rendus Geoscience 343, 123-139.

Charlet, L., Silvester, E., Liger, E., 1998. N-compound reduction and actinide immobilisation in surficial fluids by Fe(II): the surface [6-point triple bond; length half of m-dash]FeIIIOFeIIOHo species, as major reductant. Chemical Geology 151, 85-93.

Chen, J.M., Hao, O.J., 1998. Microbial Chromium (VI) Reduction. Critical Reviews in Environmental Science and Technology 28, 219-251.

Chen, M., Ma, L.Q., 2001. Comparison of Three Aqua Regia Digestion Methods for Twenty Florida Soils. Soil Science Society of America Journal 65, 491.

Chen, M., Ma, L.Q., Harris, W.G., 2002. Arsernic Concentrations in Florida Surface Soils: Influence of Soil Type and Properties. Soil Science Society of America Journal 66, 632-340.

Cheng, C.N., Focht, D.D., 1979. Production of arsine and methylarsines in soil and in culture. Applied and Environmental Microbiology 38, 494.

Chilvers, D.C., Peterson, P.J., 1987. Global Cycling of Arsenic, in: Hutchinson, T.C., Meema, K.M. (Eds.), Lead, Mercury, Cadmium and Arsenic in the Environment, Scientific Commitee on Problems of the Environment (SCOPE). John Wiley & Sons, Chichester, New York, Brisbane, Toronto.

Chirenje, T., Ma, L.Q., Clark, C., Reeves, M., 2003. Cu, Cr and As distribution in soils adjacent to pressure-treated decks, fences and poles. Environmental Pollution 124, 407-417.

Chisholm-Brause, C.J., Berg, J.M., Matzner, R.A., Morris, D.E., 2001. Uranium(VI) Sorption Complexes on Montmorillonite as a Function of Solution Chemistry. Journal of Colloid and Interface Science 233, 38-49.

Chiu, V.Q., Hering, J.G., 2000. Arsenic Adsorption and Oxidation at Manganite Surfaces. 1. Method for Simultaneous Determination of Adsorbed and Dissolved Arsenic Species. Environmental Science & Technology 34, 2029-2034.

Christensen, T.H., Kjeldsen, P., Albrechtsen, H.-J., Heron, G., Nielsen, P.H., Bjerg, P.L., Holm, P.E., 1994. Attenuation of landfill leachate pollutants in aquifers. Critical Reviews in Environmental Science and Technology 24, 119-202.

Clarkson, T.W., 1993. Mercury: Major Issues in Environmental Health. Environmental Health Perspectives 100, 31-38.

Coates, J.D., Ellis, D.J., Blunt-Harris, E.L., Gaw, C.V., Roden, E.E., Lovley, D.R., 1998. Recovery of Humic-Reducing Bacteria from a Diversity of Environments. Appl. Environ. Microbiol. 64, 1504-1509.

Coey, J.M.D., 1975. Iron in a post-glacial lake sediment core; a Mössbauer effect study. Geochimica et Cosmochimica Acta 39, 401-415.

Coker, V.S., Bell, A.M.T., Pearce, C.I., Pattrick, R.A.D., van der Laan, G., Lloyd, J.R., 2008. Time-resolved synchrotron powder X-ray diffraction study of magnetite formation by the Fe(III)-reducing bacterium Geobacter sulfurreducens. American Mineralogist 93, 540-547.

Colon, M., Hidalgo, M., Iglesias, M., 2009. Correction strategies over spectral interferences for arsenic determination in aqueous samples with complex matrices by quadrupole ICP-MS. J. Anal. At. Spectrom. 24, 518.

Comite Syndical de l'EPTB, 2007. Rapport au Comite Syndical: Contrat de Vallee Inondable de la Saone. Resultats de l'etude de caracterisation des masses d'eau du bassin Saone. Etablissement Public Territorial du Bassin, Macon.

Compeau, G.C., Bartha, R., 1985. Sulfate-Reducing Bacteria: Principal Methylators of Mercury in Anoxic Estuarine Sediment. Appl. Environ. Microbiol. 50, 498-502.

Cory, R.M., McKnight, D.M., 2005. Fluorescence Spectroscopy Reveals Ubiquitous Presence of Oxidized and Reduced Quinones in Dissolved Organic Matter. Environmental Science & Technology 39, 8142-8149.

Costley, C.T., Mossop, K.F., Dean, J.R., Garden, L.M., Marshall, J., Carroll, J., 2000. Determination of mercury in environmental and biological samples using pyrolysis atomic absorption spectrometry with gold amalgamation. Analytica Chimica Acta 405, 179-183.

Couture, R.-M., Gobeil, C., Tessier, A., 2008. Chronology of Atmospheric Deposition of Arsenic Inferred from Reconstructed Sedimentary Records. Environmental Science & Technology 42, 6508-6513.

Couture, R.-M., Gobeil, C., Tessier, A., 2010. Arsenic, iron and sulfur co-diagenesis in lake sediments. Geochimica et Cosmochimica Acta 74, 1238-1255.

Cummings, D.E., Caccavo, Fendorf, S., Rosenzweig, R.F., 1999. Arsenic Mobilization by the Dissimilatory Fe(III)-Reducing Bacterium Shewanella alga BrY. Environmental Science & Technology 33, 723-729.

Cutting, R.S., Coker, V.S., Fellowes, J.W., Lloyd, J.R., Vaughan, D.J., 2009. Mineralogical and morphological constraints on the reduction of Fe(III) minerals by Geobacter sulfurreducens. Geochimica et Cosmochimica Acta 73, 4004-4022.

Dalgaard, P., 2010. ISwR: Introductory Statistics with R.

Das, D., Chakrabarti, M., Majumdar, C., Bose, M., 1986. Mössbauer spectroscopy of green shale from banded iron formation. Pramana 27, 331-336.

Das, H.K., Mitra, A.K., Sengupta, P.K., Hossain, A., Islam, F., Rabbani, G.H., 2004. Arsenic concentrations in rice, vegetables, and fish in Bangladesh: a preliminary study. Environment International 30, 383-387.

Datta, R., Sarkar, D., Sharma, S., Sand, K., 2006. Arsenic biogeochemistry and human health risk assessment in organo-arsenical pesticide-applied acidic and alkaline soils: An incubation study. Science of The Total Environment 372, 39-48.

Davis, J.A., Yabusaki, S.B., Steefel, C.I., Zachara, J.M., Curtis, G.P., Redden, G.D., Criscenti, L.J., Honeyman, B.D., 2004. Assessing of Conceptual Models for Subsurface Reactive Transport of Inorganic Contaminants. Eos Trans. AGU 85.

Dayan, A.D., Paine, A.J., 2001. Mechanisms of chromium toxicity, carcinogenicity and allergenicity: Review of the literature from 1985 to 2000. Human & Experimental Toxicology 20, 439 -451.

Van Den Berg, G.A., Loch, J.P.G., 2000. Decalcification of soils subject to periodic waterlogging. European Journal of Soil Science 51, 27-33.

Dick, J.G., Wan, C.C., Difruscia, R., 1977. The calculation of mylar film absorption correction coefficients in X-ray spectrochemical analysis of aqueous samples. X-Ray Spectrom. 6, 212-214.

Disnar, J.R., Sureau, J.F., 1990. Organic matter in ore genesis: Progress and perspectives. Organic Geochemistry 16, 577-599.

Dixit, S., Hering, J.G., 2003. Comparison of Arsenic(V) and Arsenic(III) Sorption onto Iron Oxide Minerals: Implications for Arsenic Mobility. Environmental Science & Technology 37, 4182-4189.

Dixon, H.B.F., 1996. The Biochemical Action of Arsonic Acids Especially As Phosphate Analogues. Academic Press, pp. 191-227.

Dong, W., Xie, G., Miller, T.R., Franklin, M.P., Oxenberg, T.P., Bouwer, E.J., Ball, W.P., Halden, R.U., 2006. Sorption and bioreduction of hexavalent uranium at a military facility by the Chesapeake Bay. Environmental Pollution 142, 132-142.

Drahota, P., Paces, T., Pertold, Z., Mihaljevic, M., Skrivan, P., 2006. Weathering and erosion fluxes of arsenic in watershed mass budgets. Science of The Total Environment 372, 306-316.

Drexel, R.T., Haitzer, M., Ryan, J.N., Aiken, G.R., Nagy, K.L., 2002. Mercury(II) Sorption to Two Florida Everglades Peats: Evidence for Strong and Weak Binding and Competition by Dissolved Organic Matter Released from the Peat. Environmental Science & Technology 36, 4058-4064.

Driscoll, C.T., Blette, V., Yan, C., Schofield, C.L., Munson, R., Holsapple, J., 1995. The role of dissolved organic carbon in the chemistry and bioavailability of mercury in remote Adirondack lakes. Water, Air, & Soil Pollution 80, 499-508.

Duff, M.C., Coughlin, J.U., Hunter, D.B., 2002. Uranium co-precipitation with iron oxide minerals. Geochimica et Cosmochimica Acta 66, 3533-3547.

Eary, L.E., Rai, D., 1987. Kinetics of chromium(III) oxidation to chromium(VI) by reaction with manganese dioxide. Environmental Science & Technology 21, 1187-1193.

Eckert, J.M., Judd, R.J., Lay, P.A., Symons, A.D., 1991. Response of chromium(V) to the diphenylcarbazide spectrophotometric method for the determination of chromium(VI). Analytica Chimica Acta 255, 31-33.

Edelstein, D.L., 2011. Copper (2009 Minerals Yearbook). United States Geological Survey, Virginia, U.S.A.

Edwards, D., 2006. Revised Reregistration Eligibility Decision for MSMA, DSMA, CAMA, and Cacodylic Acid (Reregistration Eligibility Decision Document No. EPA 738-R-06-021). United States Environmental Protection Agency: Office of Prevention, Pesticides and Toxic Substances.

Edwards, K.J., Bond, P.L., Gihring, T.M., Banfield, J.F., 2000. An Archaeal Iron-Oxidizing Extreme Acidophile Important in Acid Mine Drainage. Science 287, 1796 -1799.

EEA, 2010. Corine Land Cover 2000 and 2006 raster data. European Environment Agency, The European Topic Centre on Land Use and Spatial Information.

EEA-EC-JRC, UN-WHO, 2008. Impacts of Europe's changing climate - 2008 indicator-based assessment - Joint EEA-JRC-WHO report. European Environment Agency, European

Commission Joint Research Centre and The United Nations World Health Organisation, Copenhagen, Denmark.
Eggleston, C., Jordan, G., 1998. A new approach to pH of point of zero charge measurement: crystal-face specificity by scanning force microscopy (SFM). Geochimica et Cosmochimica Acta 62, 1919-1923.
Elion, P., 2005. Le modèle géologique du Callovo-Oxfordien à l'état initial - Site de Meuse / Haute-Marne (No. n° C.NT.ASMG.03.0101.). Andra.
Embrick, L.L., Porter, K.M., Pendergrass, A., Butcher, D.J., 2005. Characterization of lead and arsenic contamination at Barber Orchard, Haywood County, NC. Microchemical Journal 81, 117-121.
Erbs, J.J., Berquo, T.S., Reinsch, B.C., Lowry, G.V., Banerjee, S.K., Penn, R.L., 2010. Reductive dissolution of arsenic-bearing ferrihydrite. Geochimica et Cosmochimica Acta 74, 3382-3395.
Erdem, M., Gur, F., Tumen, F., 2004. Cr(VI) reduction in aqueous solutions by siderite. Journal of Hazardous Materials 113, 217-222.
Essington, M., 2004. Soil and water chemistry an integrative approach. CRC Press, Boca Raton.
EURATOM, 2010. Final Scientific and Technical Report of the Integrated Project "Fundamental Processes of Radionuclide Migration". EURATOM.
European Commission., 2005. Soil atlas of Europe.
Faassen, H.G., 1973. Effects of mercury compounds on soil microbes. Plant and Soil 38, 485-487.
Fabris, J., Resende, M., Allan, J., Coey, J., 1986. Mössbauer analysis of Brazilian Oxisols. Hyperfine Interactions 29, 1093-1096.
FAO, 2011. FAOSTAT: ForesSTAT. Food and Agirculture Organization of the United Nations, Rome, Italy.
Farquhar, M.L., Charnock, J.M., Livens, F.R., Vaughan, D.J., 2002. Mechanisms of Arsenic Uptake from Aqueous Solution by Interaction with Goethite, Lepidocrocite, Mackinawite, and Pyrite: An X-ray Absorption Spectroscopy Study. Environmental Science & Technology 36, 1757-1762.
Fendorf, S., Eick, M.J., Grossl, P., Sparks, D.L., 1997. Arsenate and Chromate Retention Mechanisms on Goethite. 1. Surface Structure. Environmental Science & Technology 31, 315-320.
Fendorf, S., Nico, P.S., Kocar, B.D., Masue, Y., Tufano, K.J., 2010. Arsenic Chemistry in Soils and Sediments, in: Synchrotron-Based Techniques in Soils and Sediments. Elsevier, pp. 357-378.
Fernandez-Martinez, A., Roman-Ross, G., Cuello, G.J., Turrillas, X., Charlet, L., Johnson, M.R., Bardelli, F., 2006. Arsenic uptake by gypsum and calcite: Modelling and probing by neutron and X-ray scattering. Physica B: Condensed Matter 385-386, 935-937.
Finkelman, R.B., Belkin, H.E., Zheng, B., 1999. Health impacts of domestic coal use in China. Proceedings of the National Academy of Sciences of the United States of America 96, 3427 - 3431.
La Force, M.J., Hansel, C.M., Fendorf, S., 2000. Arsenic Speciation, Seasonal Transformations, and Co-distribution with Iron in a Mine Waste-Influenced Palustrine Emergent Wetland. Environmental Science & Technology 34, 3937-3943.
Foster, A.L., Brown, G.E., Tingle, T.N., Parks, G.A., 1998. Quantitative arsenic speciation in mine tailings using X-ray absorption spectroscopy. American Mineralogist 83, 553-568.
Freikowski, D., Winter, J., Gallert, C., 2010. Hydrogen formation by an arsenate-reducing *Pseudomonas putida*, isolated from arsenic-contaminated groundwater in West Bengal, India. Applied Microbiology and Biotechnology 88, 1363-1371.
Friberg, L., Nordberg, G., 1973. Inorganic mercury—a toxicological and epidemiological appraisal, in: Miller, M., Clarkson, T.W. (Eds.), Mercury, mercurials, and mercaptans. Thomas, Springfield Ill.
Frohne, T., Rinklebe, J., Diaz-Bone, R.A., Du Laing, G., 2011. Controlled variation of redox conditions in a floodplain soil: Impact on metal mobilization and biomethylation of arsenic and antimony. Geoderma 160, 414-424.

Froideval, A., Del Nero, M., Gaillard, C., Barillon, R., Rossini, I., Hazemann, J.L., 2006. Uranyl sorption species at low coverage on Al-hydroxide: TRLFS and XAFS studies. Geochimica et Cosmochimica Acta 70, 5270-5284.

Fuller, C.C., Davis, J.A., 1989. Influence of coupling of sorption and photosynthetic processes on trace element cycles in natural waters. Nature 340, 52-54.

Gabriel, M., Williamson, D., 2004. Principal Biogeochemical Factors Affecting the Speciation And Transport of Mercury through the terrestrial environment. Environmental Geochemistry and Health 26, 421-434-434.

Gehin, A., Greneche, J.-M., Tournassat, C., Brendle, J., Rancourt, D.G., Charlet, L., 2007. Reversible surface-sorption-induced electron-transfer oxidation of Fe(II) at reactive sites on a synthetic clay mineral. Geochimica et Cosmochimica Acta 71, 863-876.

Gentleman, R., Ihaka, R., Chambers, J., 2009. The R project for Statistical Computing.

Germani, M.S., Zoller, W.H., 1988. Vapor-phase concentrations of arsenic, selenium, bromine, iodine, and mercury in the stack of a coal-fired power plant. Environmental Science & Technology 22, 1079-1085.

Giambelluca, T.W., Nullet, M.A., Schroeder, T.A., 1986. Rainfall Atlas of Hawai'i (No. R76). Water Resources Research Center, University of Hawaii at Manoa.

Giammar, D.E., Hering, J.G., 2001. Time Scales for Sorption−Desorption and Surface Precipitation of Uranyl on Goethite. Environmental Science & Technology 35, 3332-3337.

Gill, R., 1997. Modern analytical geochemistry : an introduction to quantitative chemical analysis for earth, environmental, and materials scientists. Longman, Harlow Essex England.

Goldberg, S., 2002. Competitive adsorption of arsenate and arsenite on oxides and clay minerals. Soil Science Society of America journal 66.

Goldberg, S., Johnston, C.T., 2001. Mechanisms of Arsenic Adsorption on Amorphous Oxides Evaluated Using Macroscopic Measurements, Vibrational Spectroscopy, and Surface Complexation Modeling. Journal of Colloid and Interface Science 234, 204-216.

Gómez-Parrales, I., Bellinfante, N., Tejada, M., 2011. Study of mineralogical speciation of arsenic in soils using X ray microfluorescence and scanning electronic microscopy. Talanta 84, 853-858.

Grandstaff, D.E., 1976. A kinetic study of the dissolution of uraninite. Econ Geol 71, 1493-1506.

Gray, N.F., 1997. Environmental impact and remediation of acid mine drainage: a management problem. Environmental Geology 30, 62-71.

Greenwood, N., 1989. Chemistry of the elements, 2nd ed. Butterworth-Heinemann, Oxford ;;Boston.

Greskowiak, J., Prommer, H., Massmann, G., Nützmann, G., 2006. Modeling Seasonal Redox Dynamics and the Corresponding Fate of the Pharmaceutical Residue Phenazone During Artificial Recharge of Groundwater. Environmental Science & Technology 40, 6615-6621.

Griffin, R.A., Au, A.K., Frost, R.R., 1977. Effect of pH on adsorption of chromium from landfill-leachate by clay minerals. Journal of Environmental Science and Health . Part A: Environmental Science and Engineering 12, 431 - 449.

Grunberger, O., Macaigne, P., Michelot, J.-L., Hartmann, C., Sukchan, S., 2008. Salt crust development in paddy fields owing to soil evaporation and drainage: Contribution of chloride and deuterium profile analysis. Journal of Hydrology 348, 110-123.

Grybos, M., Davranche, M., Gruau, G., Petitjean, P., Pedrot, M., 2009. Increasing pH drives organic matter solubilization from wetland soils under reducing conditions. Geoderma 154, 13-19.

Guberman, D.E., 2011. Lead (2009 Minerals Yearbook). United States Geological Survey, Virginia, U.S.A.

Guccione, M.J., 2009. Grain-Size Distribution of Overbank Sediment and Its Use to Locate Channel Positions, in: Alluvial Sedimentation. Blackwell Publishing Ltd., pp. 185-194.

Guo, H., Li, Y., Zhao, K., Ren, Y., Wei, C., 2011. Removal of arsenite from water by synthetic siderite: Behaviors and mechanisms. Journal of Hazardous Materials 186, 1847-1854.

Hamza, M.A., Anderson, W.K., 2005. Soil compaction in cropping systems: A review of the nature, causes and possible solutions. Soil and Tillage Research 82, 121-145.

Han, F., Su, Y., Monts, D., Plodinec, M.J., Banin, A., Triplett, G., 2003. Assessment of global industrial-age anthropogenic arsenic contamination. Naturwissenschaften 90, 395-401.

Hansel, C.M., Fendorf, S., Jardine, P.M., Francis, C.A., 2008. Changes in Bacterial and Archaeal Community Structure and Functional Diversity along a Geochemically Variable Soil Profile. Appl. Environ. Microbiol. 74, 1620-1633.

Harduin, J.C., Royer, P., Piechowski, J., 1994. Uptake and Urinary Excretion of Uranium after Oral Administration in Man. Radiation Protection Dosimetry 53, 245 -248.

Harris-Hellal, J., Vallaeys, T., Garnier-Zarli, E., Bousserrhine, N., 2009. Effects of mercury on soil microbial communities in tropical soils of French Guyana. Applied Soil Ecology 41, 59-68.

Hem, J.D., 1977. Reactions of metal ions at surfaces of hydrous iron oxide. Geochimica et Cosmochimica Acta 41, 527-538.

Henke, B.L., Gullikson, E.M., Davis, J.C., 1993. X-ray interactions: photoabsorption, scattering, transmission, and reflection at E, Atomic data and nuclear data tables. Academic Press.

Henke, B.L., Gullikson, E.M., Davis, J.C., 2011. CXRO X-Ray Interactions With Matter [WWW Document]. URL http://henke.lbl.gov/optical_constants/

Henke, K., 2009. Arsenic environmental chemistry, health threats and waste treatment. Wiley, Chichester U.K.

Hillel, D., 1980. Applications of soil physics. Academic Press, New York.

Hoeft, S.E., Kulp, T.R., Stolz, J.F., Hollibaugh, J.T., Oremland, R.S., 2004. Dissimilatory Arsenate Reduction with Sulfide as Electron Donor: Experiments with Mono Lake Water and Isolation of Strain MLMS-1, a Chemoautotrophic Arsenate Respirer. Appl. Environ. Microbiol. 70, 2741-2747.

Holley, E.A., James McQuillan, A., Craw, D., Kim, J.P., Sander, S.G., 2007. Mercury mobilization by oxidative dissolution of cinnabar ([alpha]-HgS) and metacinnabar ([beta]-HgS). Chemical Geology 240, 313-325.

Hossain, M.B., Jahiruddin, M., Panaullah, G.M., Loeppert, R.H., Islam, M.R., Duxbury, J.M., 2008. Spatial variability of arsenic concentration in soils and plants, and its relationship with iron, manganese and phosphorus. Environmental Pollution 156, 739-744.

Hubbell, J.H., Seltzer, S.M., 2009. NIST Physical Reference Data: X-Ray Mass Attenuation Coefficients.

Hughes, M.F., 2002. Arsenic toxicity and potential mechanisms of action. Toxicology Letters 133, 1-16.

Hyun, S.P., Cho, Y.H., Hahn, P.S., Kim, S.J., 2001. Sorption mechanism of U(VI) on a reference montmorillonite: binding to the internal and external surfaces. J. Radioanal. Nucl. Chem. 250, 55-62.

Icopini, G.A., Long, D.T., 2002. Speciation of Aqueous Chromium by Use of Solid-Phase Extractions in the Field. Environmental Science & Technology 36, 2994-2999.

Ilton, E.S., Haiduc, A., Moses, C.O., Heald, S.M., Elbert, D.C., Veblen, D.R., 2004. Heterogeneous reduction of uranyl by micas: Crystal chemical and solution controls. Geochimica et Cosmochimica Acta 68, 2417-2435.

Institut Geographique National de France, 2010. BD Carthage - Réseau hydrographique français.

International Atomic Energy Agency., 1989. The Application of the principles for limiting releases of radioactive effluents in the case of the mining and milling of radioactive ores. International Atomic Energy Agency, Vienna.

Islam, F.S., Gault, A.G., Boothman, C., Polya, D.A., Charnock, J.M., Chatterjee, D., Lloyd, J.R., 2004. Role of metal-reducing bacteria in arsenic release from Bengal delta sediments. Nature 430, 68-71.

ISO, 1995. Soil quality - Determination of carbonate content - Volumetric method.

Jacks, G., Bhattacharya, P., 1998. Arsenic contamination in the environment due to the use of CCA-wood preservatives, in: Arsenic in Wood Preservatives, Kemi Report 3/98. pp. 7-75.

Jackson, T., 1998. Mercury in Aquatic Ecosystems, in: Langston, W. (Ed.), Metal metabolism in aquatic environments. Chapman & Hall, London ;;New York.

Jain, A., Loeppert, R.H., 2000. Effect of Competing Anions on the Adsorption of Arsenate and Arsenite by Ferrihydrite. J. Environ. Qual. 29, 1422-1430.

Jaisi, D.P., Dong, H., Liu, C., 2007. Influence of biogenic Fe(II) on the extent of microbial reduction of Fe(III) in clay minerals nontronite, illite, and chlorite. Geochimica et Cosmochimica Acta 71, 1145-1158.

Jaisi, D.P., Liu, C., Dong, H., Blake, R.E., Fein, J.B., 2008. Fe2+ sorption onto nontronite (NAu-2). Geochimica et Cosmochimica Acta 72, 5361-5371.

James, B., Bartlett, R., 1999. Redox phenomena, in: Sumner, M. (Ed.), Handbook of Soil Science. CRC Press, Boca Raton, FL, p. B169–B194.

James, F., 1975. Minuit - a system for function minimization and analysis of the parameter errors and correlations. Computer Physics Communications 10, 343-367.

Janeczek, J., Ewing, R., 1992. Dissolution and alteration of uraninite under reducing conditions. Journal of Nuclear Materials 190, 157-173.

Jang, M., 2010. Application of portable X-ray fluorescence (pXRF) for heavy metal analysis of soils in crop fields near abandoned mine sites. Environmental Geochemistry and Health 32, 207-216.

Jenkins, R., 1995. Quantitative x-ray spectrometry, 2nd ed. M. Dekker, New York.

Jensen, D.L., Boddum, J.K., Tjell, J.C., Christensen, T.H., 2002. The solubility of rhodochrosite (MnCO3) and siderite (FeCO3) in anaerobic aquatic environments. Applied Geochemistry 17, 503-511.

Jernelov, A, 1969. Conversion of mercury compounds, in: Miller, M. W, Berg, G. G. (Eds.), Chemical fallout. Charles C Thomas, Springfield, Il, pp. 68–74.

Jew, A. D., Rytuba, J. J., Spormann, A. M., Brown, G. E., 2007. Bacterial Influence on the Solubility of Cinnabar and Metacinnabar at New Idria, CA. Presented at the American Geophysical Union, Fall Meeting 2007.

Jia, Y., Xu, L., Fang, Z., Demopoulos, G.P., 2006. Observation of Surface Precipitation of Arsenate on Ferrihydrite. Environmental Science & Technology 40, 3248-3253.

Jiang, J., Bauer, I., Paul, A., Kappler, A., 2009. Arsenic Redox Changes by Microbially and Chemically Formed Semiquinone Radicals and Hydroquinones in a Humic Substance Model Quinone. Environmental Science & Technology 43, 3639-3645.

Jonsson, J., Sherman, D.M., 2008. Sorption of As(III) and As(V) to siderite, green rust (fougerite) and magnetite: Implications for arsenic release in anoxic groundwaters. Chemical Geology 255, 173-181.

Jorgensen, N., Laursen, J., Viksna, A., Pind, N., Holm, P.E., 2005. Multi-elemental EDXRF mapping of polluted soil from former horticultural land. Environment International 31, 43-52.

Joubert, A.V.P., Lucas, L., Garrido, F., Joulian, C., Jauzein, M., 2007. Effect of temperature, gas phase composition, pH and microbial activity on As, Zn, Pb and Cd mobility in selected soils in the Ebro and Meuse Basins in the context of global change. Environmental Pollution 148, 749-758.

Kaise, T., Yamauchi, H., Horiguchi, Y., Tani, T., Watanabe, S., Hirayama, T., Fukui, S., 1989. A comparative study on acute toxicity of methylarsonic acid, dimethylarsinic acid and trimethylarsine oxide in mice. Appl. Organometal. Chem. 3, 273-277.

Kalnicky, D.J., Patel, J., Singhvi, R., 1992. Factors affecting comparability of field XRF and laboratory analyses of soil contaminants, in: Proceedings of the Forty-First Annual Conference on Applications of X-Ray Analysis. Presented at the The Forty-First Annual Conference on Applications of X-Ray Analysis, Colorado Springs, CO. USA.

Kalnicky, D.J., Singhvi, R., 2001. Field portable XRF analysis of environmental samples. Journal of hazardous materials 83, 93–122.

Kane, M.D., Poulsen, L.K., Stahl, D.A., 1993. Monitoring the enrichment and isolation of sulfate-reducing bacteria by using oligonucleotide hybridization probes designed from environmentally derived 16S rRNA sequences. Appl. Environ. Microbiol. 59, 682-686.

Keigwin, R.P., 2009. Amendment to Organic Arsenicals RED.
Kerisit, S., Felmy, A.R., Ilton, E.S., 2011. Atomistic Simulations of Uranium Incorporation into Iron (Hydr)Oxides. Environmental Science & Technology 45, 2770-2776.
Kershisnik, M., Kalamegham, R., Ash, K., Nixon, D., Ashwood, E., 1992. Using 16O35Cl to correct for chloride interference improves accuracy of urine arsenic determinations by inductively coupled plasma mass spectrometry. Clin Chem 38, 2197-2202.
Khan, B.I., Jambeck, J., Solo-Gabriele, H.M., Townsend, T.G., Cai, Y., 2006. Release of Arsenic to the Environment from CCA-Treated Wood. 2. Leaching and Speciation during Disposal. Environmental Science & Technology 40, 994-999.
Khan, B.I., Solo-Gabriele, H.M., Townsend, T.G., Cai, Y., 2006. Release of Arsenic to the Environment from CCA-Treated Wood. 1. Leaching and Speciation during Service. Environmental Science & Technology 40, 988-993.
Kilbride, C., Poole, J., Hutchings, T.R., 2006. A comparison of Cu, Pb, As, Cd, Zn, Fe, Ni and Mn determined by acid extraction/ICP-OES and ex situ field portable X-ray fluorescence analyses. Environmental Pollution 143, 16-23.
Kirk, G., 2004. The biogeochemistry of submerged soils. Wiley, Chichester ;;Hoboken N.J.
Kirpichtchikova, T.A., Manceau, A., Spadini, L., Panfili, F., Marcus, M.A., Jacquet, T., 2006. Speciation and solubility of heavy metals in contaminated soil using X-ray microfluorescence, EXAFS spectroscopy, chemical extraction, and thermodynamic modeling. Geochimica et Cosmochimica Acta 70, 2163-2190.
Klein, C.B., 1996. Carcinogenicity and genotoxicity of chromium, in: Toxicology of metals. Lewis Publishers, Boca Raton, pp. 205-219.
Kocourková, E., Sracek, O., Houzar, S., Cempírek, J., Losos, Z., Filip, J., Hršelová, P., 2011. Geochemical and mineralogical control on the mobility of arsenic in a waste rock pile at Dlouhá Ves, Czech Republic. Journal of Geochemical Exploration.
Konhauser, K., 2007. Introduction to geomicrobiology. Blackwell Pub., Malden MA.
Lacey, D.T., Lawson, F., 1970. Kinetics of the liquid-phase oxidation of acid ferrous sulfate by the bacterium Thiobacillus ferrooxidens. Biotechnol. Bioeng. 12, 29-50.
Lado, L.R., Polya, D., Winkel, L., Berg, M., Hegan, A., 2008. Modelling arsenic hazard in Cambodia: A geostatistical approach using ancillary data. Applied Geochemistry 23, 3010-3018.
Du Laing, G., Rinklebe, J., Vandecasteele, B., Meers, E., Tack, F.M.G., 2009. Trace metal behaviour in estuarine and riverine floodplain soils and sediments: A review. Science of The Total Environment 407, 3972-3985.
Langford, A., 2005. Practical skills in forensic science. Pearson Prentice Hall, Harlow England ;;New York.
Langford, Ferner, 1999. Toxicity of mercury. Journal of human hypertension 13.
Langmuir, D., Mahoney, J., Rowson, J., 2006. Solubility products of amorphous ferric arsenate and crystalline scorodite (FeAsO4.2H2O) and their application to arsenic behavior in buried mine tailings. Geochimica et Cosmochimica Acta 70, 2942-2956.
Lantzy, R.J., Mackenzie, F.T., 1979. Atmospheric trace metals: global cycles and assessment of man's impact. Geochimica et Cosmochimica Acta 43, 511-525.
Leckie, J.O., 1986. Adsorption and transformation of trace element species at sediment/water interfa, in: The importance of chemical "speciation" in environmental processes : report of the Dahlem Workshop on The Importance of Chemical "Speciation" in Environmental Processes, Berlin 1984, Sept. 2-7. Springer, Berlin u.a.
Levine, J., 1991. Global biomass burning : atmospheric, climatic, and biospheric implications. MIT Press, Cambridge Mass.
Lide, D., 2009. CRC Handbook of Chemistry and Physics, 90th ed. CRC Press.
Liger, E., Charlet, L., Van Cappellen, P., 1999. Surface catalysis of uranium(VI) reduction by iron(II). Geochimica et Cosmochimica Acta 63, 2939-2955.

Liikanen, E., 2003. COMMISSION DIRECTIVE 2003/2/ECof 6 January 2003relating to restrictions on the marketing and use of arsenic (tenth adaptation to technical progressto Council Directive 76/769/EEC) (Official Journal of the European Communities). European Commission, Brussels.

Lin, W.C., Coppi, M.V., Lovley, D.R., 2004. Geobacter sulfurreducens Can Grow with Oxygen as a Terminal Electron Acceptor. Appl. Environ. Microbiol. 70, 2525-2528.

Lin, Z., Puls, R.W., 2000. Adsorption, desorption and oxidation of arsenic affected by clay minerals and aging process. Environmental Geology 39, 753-759.

Lipiec, J., Hatano, R., 2003. Quantification of compaction effects on soil physical properties and crop growth. Geoderma 116, 107-136.

Livesey, N.T., Huang, P.M., 1981. Adsorption of Arsenate By Soils and Its Relation To Selected Chemical Properties and Anions. Soil Science 131.

Lloyd, J.R., Leang, C., Hodges Myerson, A.L., Coppi, M.V., Cuifo, S., Methe, B., Sandler, S.J., Lovley, D.R., 2003. Biochemical and genetic characterization of PpcA, a periplasmic c-type cytochrome in Geobacter sulfurreducens. Biochem. J. 369, 153-161.

Loebenstein, R., 1994. The Materials Flow of Arsenic in the United States (Information Circular No. IC 9382). Bureau of Mines, U.S. Department of the Interior, Denver.

Lovley, D.R., Coates, J.D., Blunt-Harris, E.L., Phillips, E.J.P., Woodward, J.C., 1996. Humic substances as electron acceptors for microbial respiration. Nature 382, 445-448.

Lovley, D.R., Fraga, J.L., Coates, J.D., Blunt-Harris, E.L., 1999. Humics as an electron donor for anaerobic respiration. Environmental Microbiology 1, 89-98.

Lovley, D.R., Giovannoni, S.J., White, D.C., Champine, J.E., Phillips, E.J.P., Gorby, Y.A., Goodwin, S., 1993. Geobacter metallireducens gen. nov. sp. nov., a microorganism capable of coupling the complete oxidation of organic compounds to the reduction of iron and other metals. Archives of Microbiology 159, 336-344.

Lovley, D.R., Phillips, E.J.P., 1986. Organic Matter Mineralization with Reduction of Ferric Iron in Anaerobic Sediments. Appl. Environ. Microbiol. 51, 683-689.

Lovley, D.R., Roden, E.E., Phillips, E.J.., Woodward, J.., 1993. Enzymatic iron and uranium reduction by sulfate-reducing bacteria. Marine Geology 113, 41-53.

Ludwig, W., Strunk, O., Westram, R., Richter, L., Meier, H., Yadhukumar, Buchner, A., Lai, T., Steppi, S., Jobb, G., Förster, W., Brettske, I., Gerber, S., Ginhart, A.W., Gross, O., Grumann, S., Hermann, S., Jost, R., König, A., Liss, T., Lüßmann, R., May, M., Nonhoff, B., Reichel, B., Strehlow, R., Stamatakis, A., Stuckmann, N., Vilbig, A., Lenke, M., Ludwig, T., Bode, A., Schleifer, K., 2004. ARB: a software environment for sequence data. Nucleic Acids Research 32, 1363 -1371.

Luo, W., Gu, B., 2011. Dissolution of Uranium-Bearing Minerals and Mobilization of Uranium by Organic Ligands in a Biologically Reduced Sediment. Environmental Science & Technology 45, 2994-2999.

Luo, Z., Wadhawan, A., Bouwer, E., 2010. Sorption behavior of nine chromium (III) organic complexes in soil. International Journal of Environmental Science and Technology 7, 1-10.

Lyngkilde, J., Christensen, T.H., 1992. Redox zones of a landfill leachate pollution plume (Vejen, Denmark). Journal of Contaminant Hydrology 10, 273-289.

Maclean, J.L., Dawe, D.C., Hettel, G.P., Hardy, B. (Eds.), 2002. Rice Almanac, Third Edition. ed. CABI Publishing, Oxon, U.K.

Macur, R.E., Jackson, C.R., Botero, L.M., Mcdermott, T.R., Inskeep, W.P., 2004. Bacterial Populations Associated with the Oxidation and Reduction of Arsenic in an Unsaturated Soil. Environmental Science & Technology 38, 104-111.

Made, B., 2010. Personal communication: Composition moyenne sur échantillons niveau laboratoire (forage PGZ 1001).

Mahmood, Q., Zheng, P., Hu, B., Jilani, G., Azim, M.R., Wu, D., Liu, D., 2009. Isolation and characterization of Pseudomonas stutzeri QZ1 from an anoxic sulfide-oxidizing bioreactor. Anaerobe 15, 108-115.

Majzlan, J., Navrotsky, A., Schwertmann, U., 2004. Thermodynamics of iron oxides: Part III. Enthalpies of formation and stability of ferrihydrite (~Fe(OH)3), schwertmannite (~FeO(OH)3/4(SO4)1/8), and [epsilon]-Fe2O3. Geochimica et Cosmochimica Acta 68, 1049-1059.

Manceau, A., Marcus, M.A., Tamura, N., 2002. Quantitative Speciation of Heavy Metals in Soils and Sediments by Synchrotron X-ray Techniques. Reviews in Mineralogy and Geochemistry 49, 341-428.

Manning, B.A., Fendorf, S.E., Goldberg, S., 1998. Surface Structures and Stability of Arsenic(III) on Goethite: Spectroscopic Evidence for Inner-Sphere Complexes. Environmental Science & Technology 32, 2383-2388.

Manning, B.A., Goldberg, S., 1996. Modeling Competitive Adsorption of Arsenate with Phosphate and Molybdate on Oxide Minerals. Soil Sci. Soc. Am. J. 60, 121-131.

Mansfeldt, T., 2003. In situ long-term redox potential measurements in a dyked marsh soil. Z. Pflanzenernähr. Bodenk. 166, 210-219.

Masson, M., Schafer, J., Blanc, G., Pierre, A., 2007. Seasonal variations and annual fluxes of arsenic in the Garonne, Dordogne and Isle Rivers, France. Science of The Total Environment 373, 196-207.

Matschullat, J., 2000. Arsenic in the geosphere -- a review. The Science of The Total Environment 249, 297-312.

McBride, M., 1994. Environmental chemistry of soils. Oxford University Press, New York.

McGeehan, S.L., 1998. Alteration of arsenic sorption in flooded-dried soils. Soil Science Society of America journal 62, 828-833.

McGeehan, S.L., Naylor, D.V., 1994. Sorption and Redox Transformation of Arsenite and Arsenate in Two Flooded Soils. Soil Sci. Soc. Am. J. 58, 337-342.

McLaren, S.J., Kim, N.D., 1995. Evidence for a seasonal fluctuation of arsenic in New Zealand's longest river and the effect of treatment on concentrations in drinking water. Environmental Pollution 90, 67-73.

Meharg, A.A., Raab, A., 2010. Getting to the bottom of arsenic standards and guidelines. Environmental Science & Technology 44, 4395-4399.

Meharg, A.A., Rahman, M.M., 2003. Arsenic Contamination of Bangladesh Paddy Field Soils: Implications for Rice Contribution to Arsenic Consumption. Environmental Science & Technology 37, 229-234.

Mercuro, D., 2010. Thermo Scientific Niton XLt Analyzer [WWW Document]. Niton XLt/XLp and XLi Handheld XRF Analyzers. URL http://www.niton.com/Niton-Analyzers-Products/xltpi/xlt.aspx?sflang=en

Merry, R.H., Tiller, K.G., Alston, A.M., 1983. Accumulation of copper, lead and arsenic in some Australian orchard soils. Australian Journal of Soil Research 21, 549-561.

Mestrot, A., Feldmann, J., Krupp, E.M., Hossain, M.S., Roman-Ross, G., Meharg, A.A., 2011. Field Fluxes and Speciation of Arsines Emanating from Soils. Environmental Science & Technology 45, 1798-1804.

METI/ERSDAC, NASA/LPDAAC, USGS/EROS, 2009. ASTER Global DEM Validation (Summary report for the 30m world-coverage dataset).

Michel, F.M., Ehm, L., Antao, S.M., Lee, P.L., Chupas, P.J., Liu, G., Strongin, D.R., Schoonen, M.A.A., Phillips, B.L., Parise, J.B., 2007. The Structure of Ferrihydrite, a Nanocrystalline Material. Science 316, 1726 -1729.

Millward, G.E., Liu, Y.P., 2003. Modelling metal desorption kinetics in estuaries. The Science of The Total Environment 314-316, 613-623.

Monesi, C., Meneghini, C., Bardelli, F., Benfatto, M., Mobilio, S., Manju, U., Sarma, D., 2005. Local structure in LaMnO3 and CaMnO3 perovskites: A quantitative structural refinement of Mn K-edge XANES data. Phys. Rev. B 72.

Moon, H.S., Komlos, J., Jaffé, P.R., 2007. Uranium Reoxidation in Previously Bioreduced Sediment by Dissolved Oxygen and Nitrate. Environmental Science & Technology 41, 4587-4592.

Moore, E., Tindall, B., Santos, V., Pieper, D., Ramos, J.-L., Palleroni, N., 2006. Nonmedical: Pseudomonas, in: The Prokaryotes. Springer New York, pp. 646-703.

Morel, F.M.M., Kraepiel, A.M.L., Amyot, M., 1998. THE CHEMICAL CYCLE AND BIOACCUMULATION OF MERCURY. Annu. Rev. Ecol. Syst. 29, 543-566.

Mudahar, G.S., Modi, S., Makhan, S., 1991. Total and partial mass attenuation coefficients of soil as a function of chemical composition. International Journal of Radiation Applications and Instrumentation. Part A. Applied Radiation and Isotopes 42, 13-18.

Mukherjee, A., Bhattacharya, P., Savage, K., Foster, A., Bundschuh, J., 2008. Distribution of geogenic arsenic in hydrologic systems: Controls and challenges. Journal of Contaminant Hydrology 99, 1-7.

Mullet, M., Demoisson, F., Humbert, B., Michot, L.J., Vantelon, D., 2007. Aqueous Cr(VI) reduction by pyrite: Speciation and characterisation of the solid phases by X-ray photoelectron, Raman and X-ray absorption spectroscopies. Geochimica et Cosmochimica Acta 71, 3257-3271.

Munthe, J., McElroy, W.J., 1992. Some aqueous reactions of potential importance in the atmospheric chemistry of mercury. Atmospheric Environment. Part A. General Topics 26, 553-557.

Murad, E., 1987. Mössbauer spectra of nontronites: Structural implications and characterization of associated iron oxides. Z. Pflanzenernaehr. Bodenk. 150, 279-285.

Murphy, E.A., Aucott, M., 1998. An assessment of the amounts of arsenical pesticides used historically in a geographical area. The Science of The Total Environment 218, 89-101.

Mustafa, S. Mustafa, Jamal, A. Jamal, Naeem, A. Naeem, Rehana, N. Rehana, 2001. Chromate Anion Adsorption on Iron Hydroxide. Adsorption Science & Technology 19, 701-710.

Muyzer, G., Teske, A., Wirsen, C., Jannasch, H., 1995. Phylogenetic relationships of*Thiomicrospira* species and their identification in deep-sea hydrothermal vent samples by denaturing gradient gel electrophoresis of 16S rDNA fragments. Archives of Microbiology 164, 165-172.

Nath, B., Chakraborty, S., Burnol, A., Stuben, D., Chatterjee, D., Charlet, L., 2009. Mobility of arsenic in the sub-surface environment: An integrated hydrogeochemical study and sorption model of the sandy aquifer materials. Journal of Hydrology 364, 236-248.

National Research Council (U.S.)., 1999. Arsenic in drinking water. National Academy Press, Washington D.C.

Navas, A., Machin, J., 2002. Spatial distribution of heavy metals and arsenic in soils of Aragon (northeast Spain): controlling factors and environmental implications. Applied Geochemistry 17, 961-973.

Neumann, R.B., Ashfaque, K.N., Badruzzaman, A.B.M., Ashraf Ali, M., Shoemaker, J.K., Harvey, C.F., 2010. Anthropogenic influences on groundwater arsenic concentrations in Bangladesh. Nature Geosci 3, 46-52.

Neumann, R.B., St. Vincent, A.P., Roberts, L.C., Badruzzaman, A.B.M., Ali, M.A., Harvey, C.F., 2011. Rice Field Geochemistry and Hydrology: An Explanation for Why Groundwater Irrigated Fields in Bangladesh are Net Sinks of Arsenic from Groundwater. Environmental Science & Technology 45, 2072-2078.

Newman, D.K., Kolter, R., 2000. A role for excreted quinones in extracellular electron transfer. Nature 405, 94-97.

Nicolli, H.B., Suriano, J.M., Gomez Peral, M.A., Ferpozzi, L.H., Baleani, O.A., 1989. Groundwater contamination with arsenic and other trace elements in an area of the pampa, province of Córdoba, Argentina. Environmental Geology 14, 3-16.

Nicou, R., 1986. Influence of soil ploughing on soil physical properties and growth of annual crops in semiarid West Africa: Relevance to tree planting. Forest Ecology and Management 16, 103-115.

Nikolausz, M., Kappelmeyer, U., Szekely, A., Rusznyak, A., Marialigeti, K., Kastner, M., 2008. Diurnal redox fluctuation and microbial activity in the rhizosphere of wetland plants. European Journal of Soil Biology 44, 324-333.

Nikolausz, M., Marialigeti, K., Kovacs, G., 2004. Comparison of RNA- and DNA-based species diversity investigations in rhizoplane bacteriology with respect to chloroplast sequence exclusion. Journal of Microbiological Methods 56, 365-373.

Nordstrom, D.K., 2002. Worldwide Occurrences of Arsenic in Ground Water. Science 296, 2143 - 2145.

Nriagu, J.O., Pacyna, J.M., 1988. Quantitative assessment of worldwide contamination of air, water and soils by trace metals. Nature 333, 134-139.

Ona-Nguema, G., Morin, G., Juillot, F., Calas, G., Brown, G.E., 2005. EXAFS Analysis of Arsenite Adsorption onto Two-Line Ferrihydrite, Hematite, Goethite, and Lepidocrocite. Environmental Science & Technology 39, 9147-9155.

Ona-Nguema, G., Morin, G., Wang, Y., Foster, A.L., Juillot, F., Calas, G., Brown, G.E., 2010. XANES Evidence for Rapid Arsenic(III) Oxidation at Magnetite and Ferrihydrite Surfaces by Dissolved O2 via Fe2+-Mediated Reactions. Environmental Science & Technology 44, 5416-5422.

Oremland, R.S., Stolz, J.F., 2003. The Ecology of Arsenic. Science 300, 939-944.

Overesch, M., Rinklebe, J., Broll, G., Neue, H.-U., 2007. Metals and arsenic in soils and corresponding vegetation at Central Elbe river floodplains (Germany). Environmental Pollution 145, 800-812.

Pabalan, R.T., Turner, D.R., Paul Bertetti, F., Prikryl, J.D., 1998. UraniumVI Sorption onto Selected Mineral Surfaces: Key Geochemical Parameters, in: Adsorption of Metals by Geomedia. Academic Press, San Diego, pp. 99-130.

Paces, Pacesova, 2001. Weathering of rocks in soil budgets of trace metals, in: Water-Rock interaction : proceedings of the tenth international symposium on water-rock interaction : WRI-10, Villasimius, Italy, 10.-15. July 2001. A.A.Balkema, Lisse The Netherlands.

Pacyna, J.M., 1986. Atmospheric trace elements from natural and anthropogenic sources, in: Toxic metals in the atmosphere, Advances in Environmental Science and Technology. Wiley, New York.

Paktunc, D., Bruggeman, K., 2010. Solubility of nanocrystalline scorodite and amorphous ferric arsenate: Implications for stabilization of arsenic in mine wastes. Applied Geochemistry 25, 674-683.

Pallud, C., Kausch, M., Fendorf, S., Meile, C., 2010. Spatial Patterns and Modeling of Reductive Ferrihydrite Transformation Observed in Artificial Soil Aggregates. Environ. Sci. Technol. 44, 74-79.

Palmer, N., von Wandruszka, R., 2010. Humic acids as reducing agents: the involvement of quinoid moieties in arsenate reduction. Environmental Science and Pollution Research 17, 1362-1370.

Pang, S.C., Chin, S.F., Anderson, M.A., 2007. Redox equilibria of iron oxides in aqueous-based magnetite dispersions: Effect of pH and redox potential. Journal of Colloid and Interface Science 311, 94-101.

Parikh, S.J., Lafferty, B.J., Meade, T.G., Sparks, D.L., 2010. Evaluating Environmental Influences on AsIII Oxidation Kinetics by a Poorly Crystalline Mn-Oxide. Environmental Science & Technology 44, 3772-3778.

Parkhurst, D.L., Appelo, C.A.J., (US), G.S., 1999. User's guide to PHREEQC (Version 2): A computer program for speciation, batch-reaction, one-dimensional transport, and inverse geochemical calculations. US Geological Survey Reston, VA.

Pascarelli, S., Boscherini, F., D'Acapito, F., Hrdy, J., Meneghini, C., Mobilio, S., 1996. X-ray Optics of a Dynamical Sagittal-Focusing Monochromator on the GILDA Beamline at the ESRF. J Synchrotron Rad 3, 147-155.

Patrick, W.H., Jugsujinda, A., 1992. Sequential Reduction and Oxidation of Inorganic Nitrogen, Manganese, and Iron in Flooded Soil. Soil Sci. Soc. Am. J. 56, 1071-1073.

Patrick, W.H., Williams, B.G., Moraghan, J.T., 1973. A Simple System for Controlling Redox Potential and pH in Soil Suspensions. Soil Sci Soc Am J 37, 331-332.

Payne, R.B., Gentry, D.M., Rapp-Giles, B.J., Casalot, L., Wall, J.D., 2002. Uranium Reduction by Desulfovibrio desulfuricans Strain G20 and a Cytochrome c3 Mutant. Applied and Environmental Microbiology 68, 3129-3132.

Payne, T.E., Brendler, V., Comarmond, M.J., Nebelung, C., n.d. Assessment of surface area normalisation for interpreting distribution coefficients (Kd) for uranium sorption. Journal of Environmental Radioactivity In Press, Corrected Proof.

Peters, H.A., Croft, W.A., Woolson, E.A., Darcey, B.A., Olson, M.A., 1984. Seasonal Arsenic Exposure from Burning Chormium-Copper-Arsenate-Treated Wood. Journal of the American Medical Associaton 251, 2393-2396.

Petrick, J.S., Ayala-Fierro, F., Cullen, W.R., Carter, D.E., Vasken Aposhian, H., 2000. Monomethylarsonous Acid (MMAIII) Is More Toxic Than Arsenite in Chang Human Hepatocytes. Toxicology and Applied Pharmacology 163, 203-207.

Plant, J.A., Kinniburgh, D.G., Smedley, P.L., Fordyce, F.M., Klinck, B.A., 2003. Arsenic and Selenium, in: Treatise on Geochemistry. Pergamon, Oxford, pp. 17-66.

Polya, D.A., Lythgoe, P.R., Abou-Shakra, F., Gault, A.G., Brydie, J.R., Webster, J.G., Brown, K.L., Nimfopoulos, M.K., Michailidis, K.M., 2003. IC-ICP-MS and IC-ICP-HEX-MS determination of arsenic speciation in surface and groundwaters: preservation and analytical issues. Mineral Mag 67, 247-261.

Ponnamperuma, F.N., 1972. The Chemistry of Submerged Soils. Academic Press, pp. 29-96.

Potts, P.J., Williams-Thorpe, O., Webb, P.C., 1997. The Bulk Analysis of Silicate Rocks by Portable X-Ray Fluorescence: Effect of Sample Mineralogy in Relation to the Size of the Excited Volume. Geostandards and Geoanalytical Research 21, 29-41.

Prietzel, J., Thieme, J., Salomé, M., 2010. Assessment of sulfur and iron speciation in a soil aggregate by combined S and Fe micro-XANES: microspatial patterns and relationships. J Synchrotron Rad 17, 166-172.

Pruesse, E., Quast, C., Knittel, K., Fuchs, B.M., Ludwig, W., Peplies, J., Glöckner, F.O., 2007. SILVA: a comprehensive online resource for quality checked and aligned ribosomal RNA sequence data compatible with ARB. Nucleic Acids Research 35, 7188 -7196.

Puzon, G.J., Roberts, A.G., Kramer, D.M., Xun, L., 2005. Formation of Soluble Organo−Chromium(III) Complexes after Chromate Reduction in the Presence of Cellular Organics. Environmental Science & Technology 39, 2811-2817.

Puzon, G.J., Tokala, R.K., Zhang, H., Yonge, D., Peyton, B.M., Xun, L., 2008. Mobility and recalcitrance of organo-chromium(III) complexes. Chemosphere 70, 2054-2059.

Qafoku, N., Icenhower, J., 2008. Interactions of aqueous U(VI) with soil minerals in slightly alkaline natural systems. Reviews in Environmental Science and Biotechnology 7, 355-380-380.

Raab, G.A., Bartling, M.H., Stapanian, M.A., Cole, W.H., Tidwell, R.L., Cappo, K.A., 1991. The Homogenization of Environmental Soil Samples in Bulk, in: Hazardous waste measurements. Lewis, Chelsea Mich.

Radu, T., Subacz, J.L., Phillippi, J.M., Barnett, M.O., 2005. Effects of Dissolved Carbonate on Arsenic Adsorption and Mobility. Environmental Science & Technology 39, 7875-7882.

Rai, D., Eary, L.E., Zachara, J.M., 1989. Environmental chemistry of chromium. Science of The Total Environment 86, 15-23.

Ravel, B., 2001. ATOMS: crystallography for the X-ray absorption spectroscopist. J Synchrotron Rad 8, 314-316.

Raven, K.P., Jain, A., Loeppert, R.H., 1998. Arsenite and Arsenate Adsorption on Ferrihydrite: Kinetics, Equilibrium, and Adsorption Envelopes. Environmental Science & Technology 32, 344-349.

Ravichandran, M., 2004. Interactions between mercury and dissolved organic matter--a review. Chemosphere 55, 319-331.

Ravichandran, M., Aiken, G.R., Reddy, M.M., Ryan, J.N., 1998. Enhanced Dissolution of Cinnabar (Mercuric Sulfide) by Dissolved Organic Matter Isolated from the Florida Everglades. Environmental Science & Technology 32, 3305-3311.

Ravichandran, M., Aiken, G.R., Ryan, J.N., Reddy, M.M., 1999. Inhibition of Precipitation and Aggregation of Metacinnabar (Mercuric Sulfide) by Dissolved Organic Matter Isolated from the Florida Everglades. Environmental Science & Technology 33, 1418-1423.

Read, D., 2003. Report on Copper, Chromium and Arsenic (CCA) Treated Timber (Literature review and intepretation). Environmental Risk Management Authority New Zealand, Wellington, New Zealand.

Reddy, M.M., Aiken, G.R., 2001. Fulvic Acid-Sulfide Ion Competition for Mercury Ion Binding in the Florida Everglades. Water, Air, & Soil Pollution 132, 89-104.

Reeder, R.J., Nugent, M., Tait, C.D., Morris, D.E., Heald, S.M., Beck, K.M., Hess, W.P., Lanzirotti, A., 2001. Coprecipitation of Uranium(VI) with Calcite: XAFS, micro-XAS, and luminescence characterization. Geochimica et Cosmochimica Acta 65, 3491-3503.

Regenspurg, S., Peiffer, S., 2005. Arsenate and chromate incorporation in schwertmannite. Applied Geochemistry 20, 1226-1239.

Regenspurg, S., Schild, D., Schafer, T., Huber, F., Malmstrom, M.E., 2009. Removal of uranium(VI) from the aqueous phase by iron(II) minerals in presence of bicarbonate. Applied Geochemistry 24, 1617-1625.

Reguera, G., McCarthy, K.D., Mehta, T., Nicoll, J.S., Tuominen, M.T., Lovley, D.R., 2005. Extracellular electron transfer via microbial nanowires. Nature 435, 1098-1101.

Reimann, C., Matschullat, J., Birke, M., Salminen, R., 2009. Arsenic distribution in the environment: The effects of scale. Applied Geochemistry 24, 1147-1167.

Reimers, R.S., Krenkel, P.A., 1974. Kinetics of Mercury Adsorption and Desorption in Sediments. Journal (Water Pollution Control Federation) 46, 352-365.

Renshaw, J.C., Butchins, L.J.C., Livens, F.R., May, I., Charnock, J.M., Lloyd, J.R., 2005. Bioreduction of Uranium: Environmental Implications of a Pentavalent Intermediate. Environmental Science & Technology 39, 5657-5660.

Revsbech, N.P., Pedersen, O., Reichardt, W., Briones, A., 1999. Microsensor analysis of oxygen and pH in the rice rhizosphere under field and laboratory conditions. Biology and Fertility of Soils 29, 379-385.

Ribeiro, F.R., Fabris, J.D., Kostka, J.E., Komadel, P., Stucki, J.W., 2009. Comparisons of structural iron reduction in smectites by bacteria and dithionite: II. A variable-temperature Mössbauer spectroscopic study of Garfield nontronite. Pure Appl. Chem. 81, 1499-1509.

Richard, F.C., Bourg, A.C.M., 1991. Aqueous geochemistry of chromium: A review. Water Research 25, 807-816.

Roberts, L.C., Hug, S.J., Dittmar, J., Voegelin, A., Kretzschmar, R., Wehrli, B., Cirpka, O.A., Saha, G.C., Ashraf Ali, M., Badruzzaman, A.B.M., 2010. Arsenic release from paddy soils during monsoon flooding. Nature Geosci 3, 53-59.

Robertson, F.N., 1989. Arsenic in ground-water under oxidizing conditions, south-west United States. Environmental Geochemistry and Health 11, 171-185.

Rochette, E.A., Bostick, B.C., Li, G., Fendorf, S., 2000. Kinetics of Arsenate Reduction by Dissolved Sulfide. Environmental Science & Technology 34, 4714-4720.

Roman-Ross, G., Cuello, G.J., Turrillas, X., Fernandez-Martinez, A., Charlet, L., 2006. Arsenite sorption and co-precipitation with calcite. Chemical Geology 233, 328-336.

Rosso, K.M., Smith, D.M.A., Wang, Z., Ainsworth, C.C., Fredrickson, J.K., 2004. Self-Exchange Electron Transfer Kinetics and Reduction Potentials for Anthraquinone Disulfonate. The Journal of Physical Chemistry A 108, 3292-3303.

Saada, A., Breeze, D., Crouzet, C., Cornu, S., Baranger, P., 2003. Adsorption of arsenic (V) on kaolinite and on kaolinite-humic acid complexes: Role of humic acid nitrogen groups. Chemosphere 51, 757-763.

Sackett, D., Bedford, M.A., 1998. EPA method 6200 and field portable X-ray fluorescence, in: A presentation developed for the EPA Technology Innovation Office and On-Site In-Sights Workshops for innovative field characterization technologies.

Sadiq, M., 1997. Arsenic Chemistry in Soils: An Overview of Thermodynamic Predictions and Field Observations. Water, Air, & Soil Pollution 93, 117-136.

Salminen, R., Forum of the European Geological Surveys Directors.;Geologian tutkimuskeskus (Finland), 2005. Geochemical atlas of Europe. Geological Survey of Finland, Espoo.

Santi, C., Certini, G., D'Acqui, L.P., 2006. Direct Determination of Organic Carbon by Dry Combustion in Soils with Carbonates. Communications in Soil Science and Plant Analysis 37, 155-162.

Santini, J.M., Sly, L.I., Schnagl, R.D., Macy, J.M., 2000. A New Chemolithoautotrophic Arsenite-Oxidizing Bacterium Isolated from a Gold Mine: Phylogenetic, Physiological, and Preliminary Biochemical Studies. Appl. Environ. Microbiol. 66, 92-97.

Sarkar, D., ESSINGTON, M., MISRA, K., 1999. Adsorption of mercury(II) by variable charge surfaces of quartz and gibbsite. Soil Science Society of America journal 63.

Schindler, P., Kamber, H.R., 1968. Die Acidität von Silanolgruppen. Vorläufige Mitteillung. HCA 51, 1781-1786.

Schluter, K., 2000. Review: evaporation of mercury from soils. An integration and synthesis of current knowledge. Environmental Geology 39, 249-271.

Schroeder, D., 1999. An introduction to thermal physics. Addison Wesley, San Francisco CA.

Schroeder, D.C., Lee, G.F., 1975. Potential transformations of chromium in natural waters. Water, Air, & Soil Pollution 4, 355-365-365.

Schuster, E., 1991. The behavior of mercury in the soil with special emphasis on complexation and adsorption processes - A review of the literature. Water, Air, & Soil Pollution 56, 667-680.

Scott, D.T., McKnight, D.M., Blunt-Harris, E.L., Kolesar, S.E., 1999. Quinone Moieties Act as Electron Acceptors in the Reduction of Humic Substances by Humics-Reducing Microorganisms. Environmental Science & Technology 33, 372-372.

Scott, M.J., Morgan, J.J., 1995. Reactions at Oxide Surfaces. 1. Oxidation of As(III) by Synthetic Birnessite. Environmental Science & Technology 29, 1898-1905.

Scott, T.B., Allen, G.C., Heard, P.J., Randell, M.G., 2005. Reduction of U(VI) to U(IV) on the surface of magnetite. Geochimica et Cosmochimica Acta 69, 5639-5646.

Scribner, A.M., Kurtz, A.C., Chadwick, O.A., 2006. Germanium sequestration by soil: Targeting the roles of secondary clays and Fe-oxyhydroxides. Earth and Planetary Science Letters 243, 760-770.

Senesil, G.S., Baldassarre, G., Senesi, N., Radina, B., 1999. Trace element inputs into soils by anthropogenic activities and implications for human health. Chemosphere 39, 343-377.

Seyler, P., Martin, J.-M., 1991. Arsenic and selenium in a pristine river-estuarine system: the Krka (Yugoslavia). Marine Chemistry 34, 137-151.

Shackley, M., 2011. X-ray fluorescence spectrometry (XRF) in geoarchaeology. Springer,, New York :

Shi, X., Dalal, N.S., 1989. Chromium (V) and hydroxyl radical formation during the glutathione reductase-catalyzed reduction of chromium (VI). Biochemical and Biophysical Research Communications 163, 627-634.

Singer, P.C., Stumm, W., 1970. Acidic Mine Drainage: The Rate-Determining Step. Science 167, 1121 - 1123.

Smedley, P.L., Kinniburgh, D.G., 2002. A review of the source, behaviour and distribution of arsenic in natural waters. Applied Geochemistry 17, 517-568.

Smedley, P.L., Nicolli, H.B., Macdonald, D.M.J., Barros, A.J., Tullio, J.O., 2002. Hydrogeochemistry of arsenic and other inorganic constituents in groundwaters from La Pampa, Argentina. Applied Geochemistry 17, 259-284.

Smith, B. (Ed.), 2001. Depleted uranium: Sources, Exposure and Health Effects.

Smith, E., Naidu, R., Alston, A.M., 1998. Arsenic in the Soil Environment: A Review. Academic Press, pp. 149-195.

Solazzi, M.J., 1984. Disposable XRF sample cups and thin-film sample supports for x-ray fluorescence analysis. American Laboratory 16, 72-78.

Sposito, G., 2004. The surface chemistry of natural particles. Oxford University Press, Oxford ;;New York.

Sposito, G., 2008. The chemistry of soils, 2nd ed. Oxford University Press, Oxford ;;New York.

Straub, K., Benz, M., Schink, B., Widdel, F., 1996. Anaerobic, Nitrate-Dependent Microbial Oxidation of Ferrous Iron. Appl. Environ. Microbiol. 62, 1458-1460.

Straub, K.L., Schink, B., 2003. Evaluation of electron-shuttling compounds in microbial ferric iron reduction. FEMS Microbiology Letters 220, 229-233.

Struyk, Z., Sposito, G., 2001. Redox properties of standard humic acids. Geoderma 102, 329-346.

Stucki, J.W., 2011. A review of the effects of iron redox cycles on smectite properties. Comptes Rendus Geoscience 343, 199-209.

Stumm, W., Morgan, J.J., 1996. Aquatic Chemistry, 3rd ed. John Wiley & Sons, New York [etc.].

Sullivan, K.A., Aller, R.C., 1996. Diagenetic cycling of arsenic in Amazon shelf sediments. Geochimica et Cosmochimica Acta 60, 1465-1477.

Sun, X., Doner, H.E., 1998. Adsorption and Oxidation of Arsenite on Goethite. Soil Science 163.

Szecsody, J.E., Cantrell, K.J., Krupka, K.M., Resch, C.T., Williams, M.D., Fruchter, J.S., 1998. Uranium Mobility During In Situ Redox Manipulation of the 100 Areas of the Handford Site. PNNL-12048, Pacific Northwest National Laboratory, Richland WA.

Takeno, N., 2005. Atlas of Eh-pH diagrams. Geological Survey of Japan Open File Report.

Taneja, S.P., Jones, C.H.W., 1984. Mössbauer studies of iron-bearing minerals in coal and coal ash. Fuel 63, 695-701.

Tebo, B.M., Bargar, J.R., Clement, B.G., Dick, G.J., Murray, K.J., Parker, D., Verity, R., Webb, S.M., 2011. BIOGENIC MANGANESE OXIDES: Properties and Mechanisms of Formation. Annu. Rev. Earth Planet. Sci. 32, 287-328.

Thermo Scientific, 2011. Sample Analysis Via Energy Dispersive X-Ray Fluorescence (EDXRF) [WWW Document]. X Ray Fluorescence (XRF) Information. URL http://www.niton.com/portable-XRF-technology/how-xrf-works.aspx

Thinnappan, V., Merrifield, C.M., Islam, F.S., Polya, D.A., Wincott, P., Wogelius, R.A., 2008. A combined experimental study of vivianite and As (V) reactivity in the pH range 2-11. Applied Geochemistry 23, 3187-3204.

Thompson, A., Chadwick, O.A., Rancourt, D.G., Chorover, J., 2006. Iron-oxide crystallinity increases during soil redox oscillations. Geochimica et Cosmochimica Acta 70, 1710-1727.

Thompson, I.A., Huber, D.M., Guest, C.A., Schulze, D.G., 2005. Fungal manganese oxidation in a reduced soil. Environmental Microbiology 7, 1480-1487.

Tolcin, A.C., 2011. Zinc (2009 Minerals Yearbook). United States Geological Survey, Virginia, U.S.A.

Tournassat, C., Charlet, L., Bosbach, D., Manceau, A., 2002. Arsenic(III) Oxidation by Birnessite and Precipitation of Manganese(II) Arsenate. Environmental Science & Technology 36, 493-500.

Tufano, K.J., Fendorf, S., 2008. Confounding Impacts of Iron Reduction on Arsenic Retention. Environmental Science & Technology 42, 4777-4783.

Twidwell, L.G., Mehta, A.K., 1985. Disposal of arsenic bearing copper smelter flue dust. Nuclear and Chemical Waste Management 5, 297-303.

U.S. EPA, 1996. Method 3052 rev 0 -Microwave assisted acid digestion of siliceous and organically based matrices.

U.S. EPA Environmental Response Team, 2000. Soil Sampling (Standard Operating Procedures No. SOP 2012 Rev 0.0). U.S Environmental Protection Agency.

US-EPA, 1998. Field Portable X-ray Fluorescence Analyzer: Metorex X-MET 920-P and 940 (Environmental Technology Verification Report No. EPA/600/R-97/146). U.S. Environmental Protection Agency Office of Research and Development, Washington, DC, U.S.

Vandecasteele, C., Van den Broeck, K., Dutre, V., Cooreman, H., 1993. Applications of plasma source mass spectrometry II, in: Holland, G., Eaton, A. (Eds.), Environmental applications of ICP-MS. Royal Society of Chemistry, Cambridge.

Vandenberghe, R.E., De Grave, E., De Geyter, G., Landuydt, C., 1986. Characterization of goethite and hematite in a Tunisian soil profile by Mössbauer spectroscopy. Clays and Clay Minerals 34, 275-280.

Vanhaecke, F., Vanhoe, H., Dams, R., Vandecasteele, C., 1992. The use of internal standards in ICP-MS. Talanta 39, 737-742.

Vear, A., Curtis, C., 1981. A quantitative evaluation of pyrite weathering. Earth Surface Processes and Landforms 6, 191-198.

van Veen, W.L., Mulder, E.G., Deinema, M.H., 1978. The Sphaerotilus-Leptothrix group of bacteria. Microbiol. Rev 42, 329-356.

Veeramani, H., Alessi, D.S., Suvorova, E.I., Lezama-Pacheco, J.S., Stubbs, J.E., Sharp, J.O., Dippon, U., Kappler, A., Bargar, J.R., Bernier-Latmani, R., 2011. Products of abiotic U(VI) reduction by biogenic magnetite and vivianite. Geochimica et Cosmochimica Acta 75, 2512-2528.

Verhoeven, J.T.A., Setter, T.L., 2010. Agricultural use of wetlands: opportunities and limitations. Ann Bot 105, 155-163.

Violante, A., Pigna, M., 2002. Competitive Sorption of Arsenate and Phosphate on Different Clay Minerals and Soils. Soil Sci. Soc. Am. J. 66, 1788-1796.

Violante, A., Ricciardella, M., Del Gaudio, S., Pigna, M., 2006. Coprecipitation of Arsenate with Metal Oxides: Nature, Mineralogy, and Reactivity of Aluminum Precipitates. Environmental Science & Technology 40, 4961-4967.

Vitre, R. de, Nelson Belzile, Tessier, A., 1991. Speciation and Adsorption of Arsenic on Diagenetic Iron Oxyhydroxides. Limnology and Oceanography 36, 1480-1485.

Voegelin, A., Pfister, S., Scheinost, A.C., Marcus, M.A., Kretzschmar, R., 2005. Changes in Zinc Speciation in Field Soil after Contamination with Zinc Oxide. Environmental Science & Technology 39, 6616-6623.

Vorenhout, M., van der Geest, H.G., van Marum, D., Wattel, K., Eijsackers, H.J.P., 2004. Automated and Continuous Redox Potential Measurements in Soil. J. Environ. Qual. 33, 1562-1567.

Waite, T.D., Davis, J.A., Payne, T.E., Waychunas, G.A., Xu, N., 1994. Uranium(VI) adsorption to ferrihydrite: Application of a surface complexation model. Geochimica et Cosmochimica Acta 58, 5465-5478.

Walkley, A., 1947. A Critical Examination of a Rapid Method for Determination of Organic Carbon in Soils - Effect of Variations in Digestion Conditions and of Inorganic Soil Constituents. Soil Science 63, 251-257.

Wan, J., Tokunaga, T.K., Brodie, E., Wang, Z., Zheng, Z., Herman, D., Hazen, T.C., Firestone, M.K., Sutton, S.R., 2005. Reoxidation of Bioreduced Uranium under Reducing Conditions. Environmental Science & Technology 39, 6162-6169.

Wang, S., Mulligan, C., 2006a. Effect of natural organic matter on arsenic release from soils and sediments into groundwater. Environmental Geochemistry and Health 28, 197-214.

Wang, S., Mulligan, C.N., 2006b. Occurrence of arsenic contamination in Canada: Sources, behavior and distribution. Science of The Total Environment 366, 701-721.

Wang, Z., Wagnon, K.B., Ainsworth, C.C., Liu, C., Rosso, K.M., Frederickson, K.J., 2011. A spectroscopic study of the effect of ligand complexation on the reduction of uranium(VI) by anthraquinone-2,6-disulfonate (AH2DS). Radiochimica Acta 96, 599-605.

Wasson, S.J., Linak, W.P., Gullett, B.K., King, C.J., Touati, A., Huggins, F.E., Chen, Y., Shah, N., Huffman, G.P., 2005. Emissions of Chromium, Copper, Arsenic, and PCDDs/Fs from Open Burning of CCA-Treated Wood. Environmental Science & Technology 39, 8865-8876.

Webb, S., 2011. X-ray Utilities. Standford Synchrotron Radiation Lightsource.

Weber, F.-A., Hofacker, A.F., Voegelin, A., Kretzschmar, R., 2010. Temperature Dependence and Coupling of Iron and Arsenic Reduction and Release during Flooding of a Contaminated Soil. Environmental Science & Technology 44, 116-122.

Wei, T., 2010. Corrplot: Visualization of a correlation matrix.

Weidler, P.G., 1997. BET Sample Pretreatment of Synthetic Ferrihydrite and its Influence on the Determination of Surface Area and Porosity. Journal of Porous Materials 4, 165-169.

Wersin, P., Hochella Jr., M.F., Persson, P., Redden, G., Leckie, J.O., Harris, D.W., 1994. Interaction between aqueous uranium (VI) and sulfide minerals: Spectroscopic evidence for sorption and reduction. Geochimica et Cosmochimica Acta 58, 2829-2843.

Wheeler, B.D., Al-Farraj, M.M., Cook, R.E.D., 1985. Iron toxicity to plants in base-rich wetlands: Comparitive effects on the distribution and growth of Epilobium Hirsutum L. and Juncus Subnodulosus Schrank. New Phytologist 100, 653-669.

WHO IARC, 2004. Some Drinking-water Disinfectants and Contaminants, including Arsenic: Summary of Data Reported and Evaluation (No. Volume 84), IARC Monographs on the Evaluation of Carinogenic Risks to Humans. World Health Organisation International Agency for Research on Cancer.

Williams, P.N., Villada, A., Deacon, C., Raab, A., Figuerola, J., Green, A.J., Feldmann, J., Meharg, A.A., 2007. Greatly Enhanced Arsenic Shoot Assimilation in Rice Leads to Elevated Grain Levels Compared to Wheat and Barley. Environ. Sci. Technol. 41, 6854-6859.

Winkel, L., Berg, M., Amini, M., Hug, S.J., Annette Johnson, C., 2008. Predicting groundwater arsenic contamination in Southeast Asia from surface parameters. Nature Geosci 1, 536-542.

Wittbrodt, P.R., Palmer, C.D., 1997. Reduction of Cr(VI) by soil humic acids. European Journal of Soil Science 48, 151-162.

Wolfe, L.N., Macalady, D.L., 1992. New perspectives in aquatic redox chemistry: Abiotic transformations of pollutants in groundwater and sediments. Journal of Contaminant Hydrology 9, 17-34.

Wolthers, M., Charlet, L., van Der Weijden, C.H., van der Linde, P.R., Rickard, D., 2005. Arsenic mobility in the ambient sulfidic environment: Sorption of arsenic(V) and arsenic(III) onto disordered mackinawite. Geochimica et Cosmochimica Acta 69, 3483-3492.

World Coal Institute, 2010. Coal Facts: 2009 edition with 2008 data. World Coal Institute, London.

Xia, K., Skyllberg, U.L., Bleam, W.F., Bloom, P.R., Nater, E.A., Helmke, P.A., 1999. X-ray Absorption Spectroscopic Evidence for the Complexation of Hg(II) by Reduced Sulfur in Soil Humic Substances. Environmental Science & Technology 33, 257-261.

Xu, H., Allard, B., 1991. Effects of a fulvic acid on the speciation and mobility of mercury in aqueous solutions. Water, Air, & Soil Pollution 56, 709-717.

Young, I.M., Crawford, J.W., 2004. Interactions and Self-Organization in the Soil-Microbe Complex. Science 304, 1634-1637.

Zachara, J.M., Girvin, D.C., Schmidt, R.L., Resch, C.T., 1987. Chromate adsorption on amorphous iron oxyhydroxide in the presence of major groundwater ions. Environmental Science & Technology 21, 589-594.

Zhang, H., Selim, H., 2008. Reaction and Transport of Arsenic in Soils: Equilibrium and Kinetic Modeling, in: Advances in Agronomy. Elsevier, pp. 45-115.

Zhang, J., Lion, L.W., Nelson, Y.M., Shuler, M.L., Ghiorse, W.C., 2002. Kinetics of Mn(II) oxidation by Leptothrix discophora SS1. Geochimica et Cosmochimica Acta 66, 773-781.

Zhao, Y., Zhang, J., Huang, W., Wang, Z., Li, Y., Song, D., Zhao, F., Zheng, C., 2008. Arsenic emission during combustion of high arsenic coals from Southwestern Guizhou, China. Energy Conversion and Management 49, 615-624.

Zheng, Z., Wan, J., 2005. Release of contaminant U(VI) from soils. Radiochemica acta 93, 211-217.
Zhou, P., Gu, B., 2005. Extraction of Oxidized and Reduced Forms of Uranium from Contaminated Soils: Effects of Carbonate Concentration and pH. Environmental Science & Technology 39, 4435-4440.
Zhu, J., Pigna, M., Cozzolino, V., Caporale, A.G., Violante, A., 2011. Sorption of arsenite and arsenate on ferrihydrite: Effect of organic and inorganic ligands. Journal of Hazardous Materials 189, 564-571.
Zobrist, J., Dowdle, P.R., Davis, J.A., Oremland, R.S., 2000. Mobilization of Arsenite by Dissimilatory Reduction of Adsorbed Arsenate. Environmental Science & Technology 34, 4747-4753.
Zouboulis, A.I., Kydros, K.A., Matis, K.A., 1995. Removal of hexavalent chromium anions from solutions by pyrite fines. Water Research 29, 1755-1760.

Figures

Tables

Equations

Acknowledgements

During the preparation of this thesis, I have had the opportunity to spend time in three different institutions, The University of Grenoble, The University of Girona and The European Commission Joint Research Centre. In each of these institutions, I have been fortunate enough to meet people who have been generous to me with their time, knowledge and support. They have helped me with the innumerable challenges inherent both to living in new countries, and to multi-disciplinary research. Without this benefit, I am sure that it would not have been possible for me to complete this thesis and certainly this period of my life would have been a far less rich, rewarding and enjoyable experience. To these people I would like to say thank-you.

Funding: I am grateful for the financial support provided to me by both the French National Nuclear Waste Management Agency (ANDRA) and the AquaTRAIN Marie Curie Research Training Network.

Thesis directors/Supervisors: To Laurent Charlet and Gabriela Roman-Ross, who have always shared with me their creativity, knowledge and their enthusiasm for environmental research.

The AquaTRAIN Network: To the coordinator, work-package leaders and advisory panel, for their considered guidance, constructive criticism and inspiration during each of the AquaTRAIN workshops. To the researchers, whose friendship, formed from a multitude of shared experiences, has been an enormous support to me. In particular Lenny Winkel, Julia Leventon, Claudia Cascio, Geerke Floor, Enoma Omoregie and Raoul Marie Couture.

In Grenoble: To everyone (past and present) in the ISTerre Geochimie 4D group. Particularly Roland Hellmann (for, amongst other things, his formidable aggregate crushing and soil digging efforts in Macon), Fabrizio Bardelli, Florian Molton, Delphine Tisserand, Laura Leone and Cathy Pham. Also to Bruno and Martine Lanson from the mineralogy group who have frequently helped me in the laboratory and with XRD interpretation.

To all of my friends, particularly Dip, Michael, Johanna, Markus, Verena, Martin and Alexey for all of the outdoor climbing/hiking/cycling adventures and making Grenoble my home.

In Ispra : To everyone in the IES-Soil Action especially Luca Montanarella, Luis Lado Rodriguez, Frank Verheijen, Simon Jeffery and Hannes Isaak Reuter.

In Girona: To everyone in the Environmental and Analytical Chemistry group especially Eva Margui Grabulosa, Victor Matamoros Mercadal and Ester Cidoncha Castella.

Thesis Jury: To Eric Pili and David Polya for agreeing to review this manuscript and act as the external examiners during my thesis defence.

Family: To Peter Parsons, Barbara Parsons, Louise Parsons, Kristel Vidal and the rest of my family for their unwavering and unconditional love and support.

Curriculum Vitae

Date of Birth: 11th March 1985 Place of birth: Frimley, U.K.

Research interests

I aspire to further understand trace contaminant mobility in dynamic environmental systems by drawing upon a range of complementary disciplines including, geochemistry, hydrology, microbiology, spectroscopy, thermodynamic modelling and statistics. I believe that combining these inter-related disciplines over a range of scales, with novel field and laboratory studies, allows for a broad and practically applicable understanding of contaminant cycling in the environment. I am particularly interested in the behaviour of redox sensitive inorganic contaminants in low temperature three phase soil systems which are periodically subjected to both oxidising and reducing conditions.

Education

September 2007 – August 2011: Ph.D.

Université de Grenoble 1 - Joseph Fourier, studying for a doctoral degree in environmental geochemistry under the direction of Professor Laurent Charlet and Dr. Gabriela Roman-Ross in the Institut des Sciences de la Terre (ISTerre) as part of the EU-project AquaTRAIN. During this time I was also seconded for two, 6 month periods to the European Commission Joint Research Centre – Institute of Environment and Sustainability (EU-JRC-IES) in Ispra, Italy, and to the Analytical chemistry department of the University of Gerona, in Catalonia, Spain.

September 2003 – July 2007: MEarthSci

The University of Manchester, studying for an undergraduate research Masters in Earth Sciences with a speciality in Geomicrobiology.

I was awarded a first class master's degree with honours and received a special merit award for my final year thesis and the best in school award for my 3rd year project.

During my research project I worked as part of the Environmental Geochemistry and Geo-microbiology Group, under Professor Jon Lloyd. The title of my laboratory and field based project was "Isolating and characterising iron and sulphate reducing anaerobes from a 3000 year old acid rock drainage site. Acid mine drainage remediation potential of the community".

Publications related to this thesis

Quantitative use of FP-XRF for As analysis in Soils: Considerations for sample preparation and analytical validation. Chris Parsons, Eva Margui, Eric Pili, Geerke Floor and Gabriela Roman-Ross**.** In preparation. Target Journal: Journal of Hazardous Materials

Physicochemical Controls on Arsenic Distribution on the Saône Floodplain. Chris Parsons, Eric Pili, Gabriela Roman-Ross and Laurent Charlet. In preparation. Target Journal: European Journal of Soil Science

The Impact of Redox Cycling: Arsenic Attenuation in Contaminated Floodplain Soils. Chris Parsons, Raoul-Marie Couture, Enoma Omoregie, Fabrizio Bardelli, Jean-marc Greneche, Gabriela Roman-Ross and Laurent Charlet. In preparation. Target Journal: Nature Geoscience.

Redox cycling in clay rich barrier materials: Long term effects on contaminant mobility. Chris Parsons, Benoit Made and Laurent Charlet. In preparation. Target Journal: Chemosphere.

The geology, soil chemistry, climate, hydrology, land use and logistic considerations of key field sites within the AquaTRAIN network (2008). C. Parsons (coordinator). AquaTRAIN network deliverable for the European Commission.

Morphological constraints on the bioavailability of schwertmannite and its use in acidic enrichment cultures for Fe(III)- and sulphate-reducing bacteria. R.S. Cutting, C. Parsons, V.S. Coker, J.W. Fellowes, J. Martlew, C. Boothman, D.J. Vaughan and J.R. Lloyd. In preparation. Target journal: Geomicrobiology.

Oral Communications

Near surface redox oscillation within a clay rich calcareous substrate: Cumulative controls on contaminant mobility (Kd)
C Parsons. Bioprota 2011. International Workshop on the Functioning of the Geosphere-Biosphere Interface Zone. Session 3: Factors affecting the cycling of radionuclides and other trace pollutants within the GBIZ. September 6th to 8th 2011

The Effect of Flood-Induced Redox Oscillations on Arsenic Mobility in a Calcareous Fluvisol.
C. Parsons, R-M. Couture, E. Omoregie, F. Bardelli, J-M. Greneche, G. Roman-Ross and L. Charlet. *Goldschmidt 2011* Session 8c*: Biogeochemical Processes within Floodplain and Deltaic Sediments,* Prague. August 14th to 19th 2011

The Effect of Flood-Induced Redox Oscillations on Arsenic Mobility in a Calcareous Fluvisol.
C. Parsons, R-M. Couture, E. Omoregie, F. Bardelli, J-M. Greneche, G. Roman-Ross and L. Charlet. Symposium 6 of the 11th International Conference on the Biogeochemistry of Trace Elements (11th ICOBTE). July 3rd to 7th 2011.

Biogeochemical Controls on Arsenic Mobility in a Calcareous Fluvisol
C. Parsons. Seminar at the European synchrotron radiation facility (ESRF). Grenoble, France. October 11th 2010

Redox Controls on Arsenic Mobility in a Calcareous Fluvisol
C. Parsons, R-M. Couture, G. Roman-Ross, and L. Charlet. Geogenic Chemicals in Groundwaters and Soils, Orléans, France. July 8th and 9th 2010

Poster Presentations

Physical and Chemical Controls on Arsenic Distribution on the Saône Floodplain.
C. Parsons and L. Charlet. Geogenic Chemicals in Ground-waters and Soils, Orléans, France. July 8th and 9th 2010.

Modelling of Groundwater Arsenic Contamination in Nepal: Geostatistical Predictions of Risk Using Remote Sensing Images. C. Parsons, L. Rodriguez-Lado, H. Reuter, L Montanarella
Goldschmidt 2009: Session 15i Geogenic Chemicals. Davos, Switzerland. June 21st – 26th, 2009.

Other Skills/Responsibilities

I have a passion for mechanical and electronic engineering and am keen to continue to apply these skills in the laboratory.

Foreign languages: French (fluent), Spanish (conversational)

Sports: Swimming, running, cycling and mountaineering.

Other interests: Travel, music and aquaria systems.

I have held a full, clean, UK driving license since 2003.

Annex 1: Modelling of Groundwater Arsenic Contamination in Nepal: Geostatistical Predictions of Concentration Using Remote Sensing & Relief Data and the limitations of the Regression-Kriging Approach

This annex represents a short summary of work conducted while on secondment to the soil action group of the Institute of Environment and Sustainability at the European Commission Joint Research Centre under the supervision of Luis Lado Rodriguez in 2008. The work was conducted in collaboration with the Nepalese National Arsenic Steering Committee and the Nepalese Environment and Public Health Organization. The study attempted to use remote sensing data in conjunction with available aqueous arsenic concentration data from shallow tube wells to produce a predictive model capable of estimating the risk of high arsenic in areas of the Terai region of Nepal which have not yet been directly sampled.

Introduction

Since the initial detection of high groundwater arsenic concentrations in shallow aquifers of West Bengal in the early 1980's (2) a significant amount of academic of work has been conducted across South East Asia to understand, predict and remediate affected areas (12). It was only as recently as 1999 that this contamination was found to extend into shallow groundwater higher in the Ganges basin in Nepal when investigations were started by the Nepalese Department of Water Supply and Sewage (DWSS)(9).

The use of shallow groundwater (predominantly from tube wells) in the Terai region is extensive; Neku and Tandukar estimate domestic groundwater use (including potable water) by 90% of the Terai population (8) (approximately 12.9 million people). Despite the detection of high As concentrations and extensive use of untreated groundwater, vast highly populated areas remain un-sampled and no good predictive tool exists to determine which areas are likely to be at risk for high arsenic concentrations.

Regression kriging methodology

Due to scarce availability of data from depth this study attempts to produce a quantitative 2 dimensional model derived from freely available surface data following the generic framework for regression kriging proposed by Tom Hengl (3).

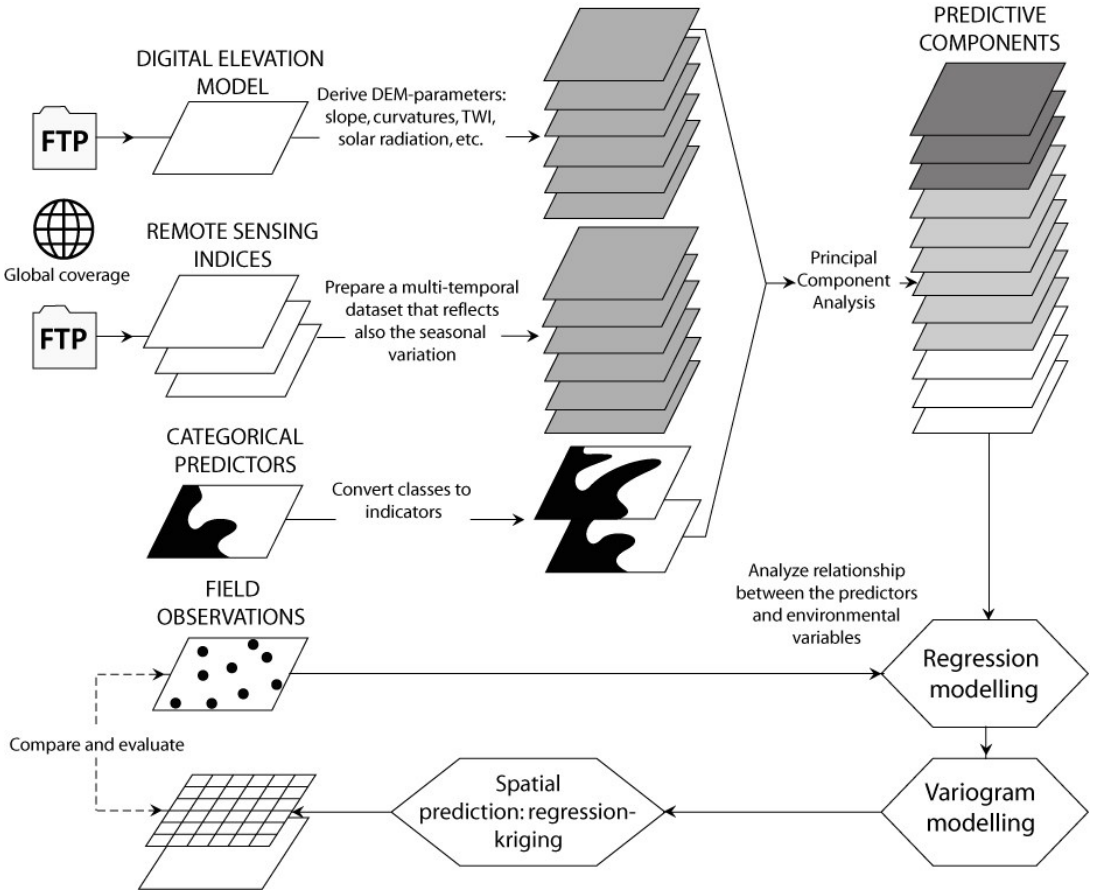

i. Generic conceptual framework for regression kriging proposed by Hengl (3)

Matheron first proposed in 1969 (6) that a variable at a certain location can be modelled as a sum of its deterministic and stochastic components (Equation i). In this study the deterministic component is modelled by multiple linear regression with auxiliary predictors, the residuals (or stochastic components) are modelled by kriging (see Figures ii and ii).

Equation i: $Z(s) = m(s) + \varepsilon'(s) + \varepsilon''$

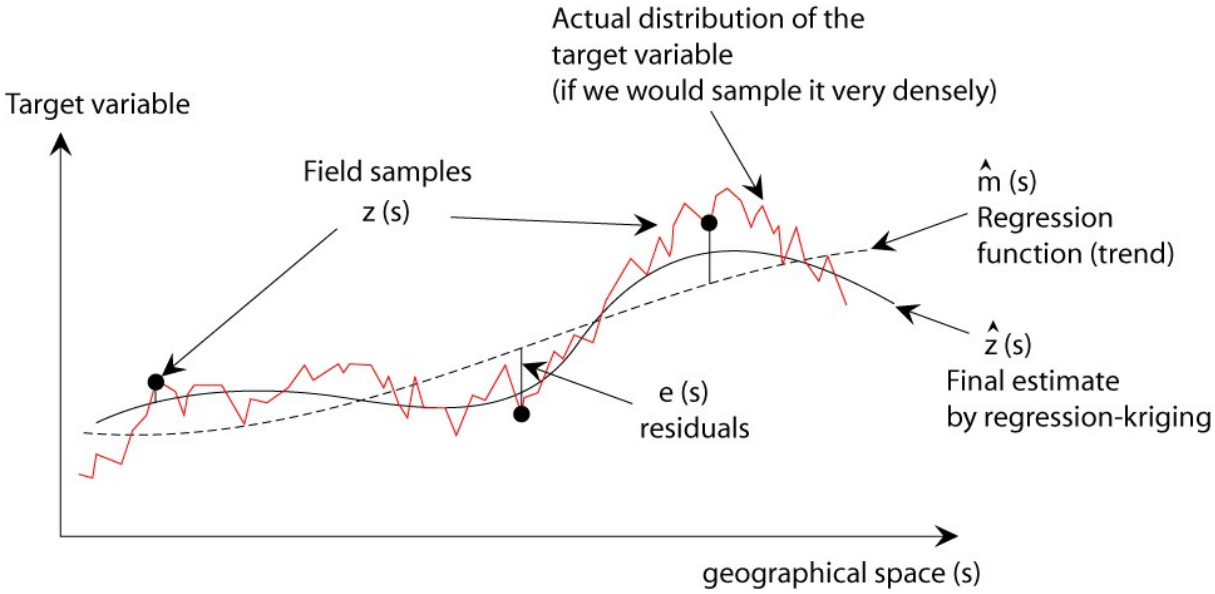

ii The concept of the regression kriging technique whereby a variable is modeled by a combination of linear regression (deterministic component) and kriging (stochastic component).

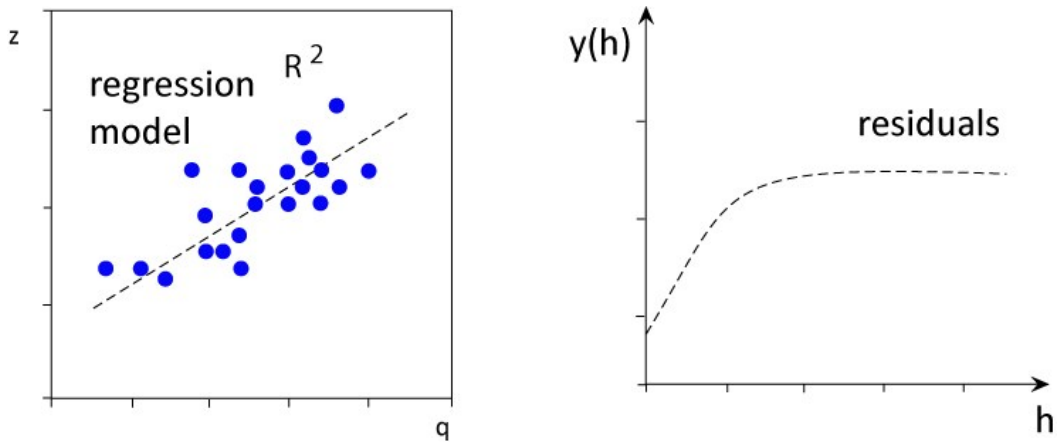

iii. Left: Multiple regression to model deterministic component. Right: Kriging to model deterministic component (relies on spatial autocorrelation of a variable shown by semi-variogram)

Sampling points: Data preparation

The groundwater database used to create and validate the presented model was provided by the Nepalese National Arsenic Steering Committee and the Nepalese Environment and Public Health Organization (11). The database is a compilation of measurements taken by 5 different organizations: the Department of Water Supply and Sewerage (DWSS), the Nepal Red Cross Society (NRCS), the Rural Water Supply and Sanitation Support Program (RWSSSP), Nepal Water for Health (NEWAH), the Rural Water Supply and Sanitation Fund Development Board (RWSSFDB)

From the 18,635 original data points a subset of 6,119 points was taken to exclude data which had not been geo-referenced, to remove uncertain As concentrations with values under the detection limit, duplicates and data from wells not within a depth range of 10-80m. The samples were

collected between 2000 and 2002 from wells installed between 1951 and 2002. Groundwater arsenic concentration ranges from 0-2,620ppb.

Auxiliary variables

Two classes of surficial auxiliary variables were used to produce this model.

1. Topographic variables including: Elevation, Slope, Flow length index, Topographic Convergence Index (TCI), Topographic Wetness Index (TWI), Sediment Transport Capacity (STC), Contour Curvature (CC), Slope Profile Curvature (SPC) and Total Curvature (TC) which were derived from a processed version of NASA SRTM 90m data (4) using AML scripts (10) and tools built into ArcGIS 9.2
2. Remote sensing Images: MODIS 16 day averaged Normalised Difference Vegetation Index (NDVI) images (250m).

These auxiliary variables (>30 raster data sets) were transformed into principal components to eliminate significant multicollinearity in the data. The regression model was built on the first 19 principal components. This choice increases computational efficiency in production of the linear and regression kriging models. Examples of auxiliary variables are given in Figures iv, v and vi)

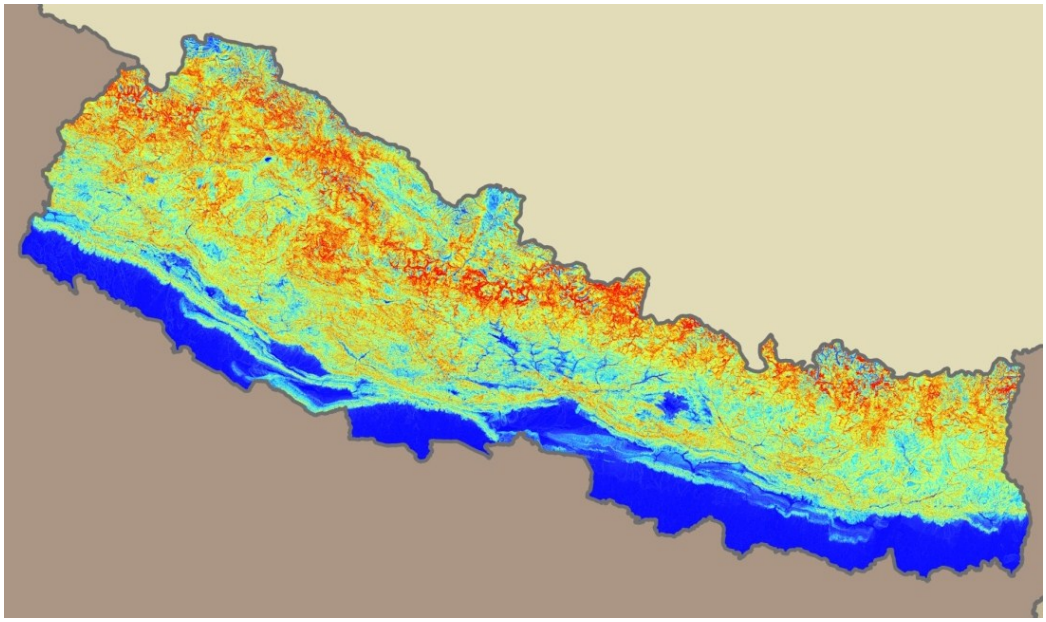

iv. Example of auxiliary variables 1: Terrain slope derived from the digital elevation model (blue = flat/0^{o} to red = steep/90^{o}).

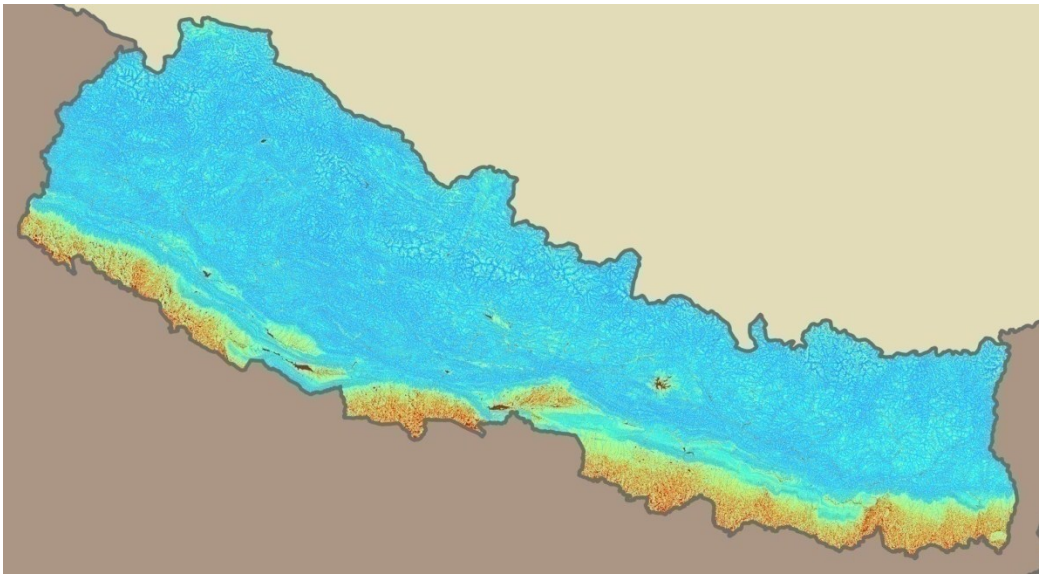

v. Example of auxiliary variables 2: Topographic wetness index derived from the digital elevation model (red = wet, blue = dry).

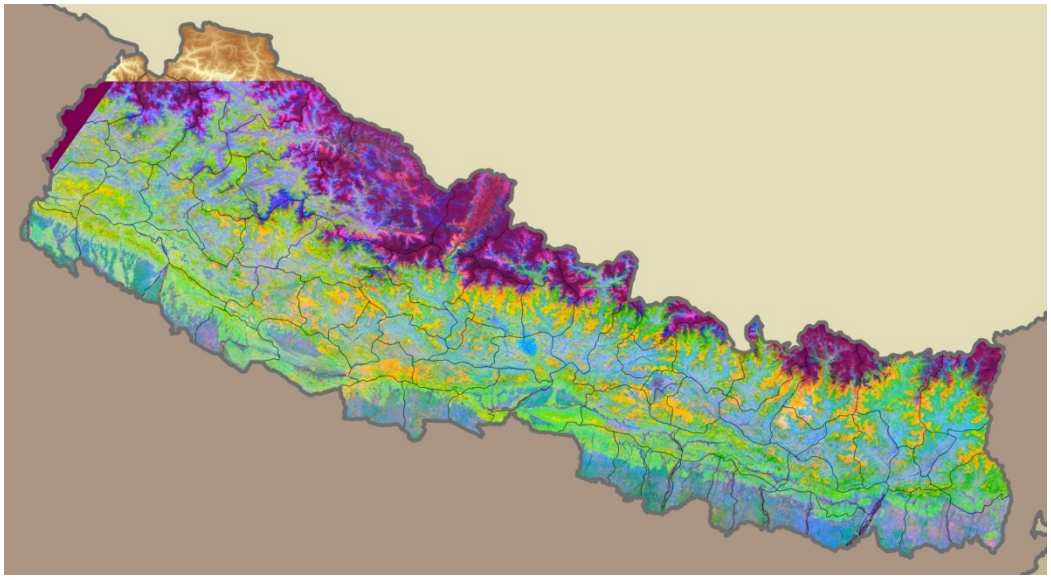

vi. Example of auxiliary variables 3: Composite (RGB) of principal components of normalized difference vegetation index data.

Results

Principal components of predictor raster data used to produce the linear model could only explain 12.69% of the variation found in the data (best correlated with flow length index, NDVI images and elevation). Therefore the kriging element of the final regression kriging model was given greater weight (trending towards situation C shown in viii). Arsenic concentration data was found to be spatially auto-correlated up to distance of approximately 10km with a strong directional weighting at 105/285^{o} which corresponds approximately to the orientation of the mountain front of the Himalaya e.g. perpendicular to erosional flux. Directional auto correlation is demonstrated in figure vii.

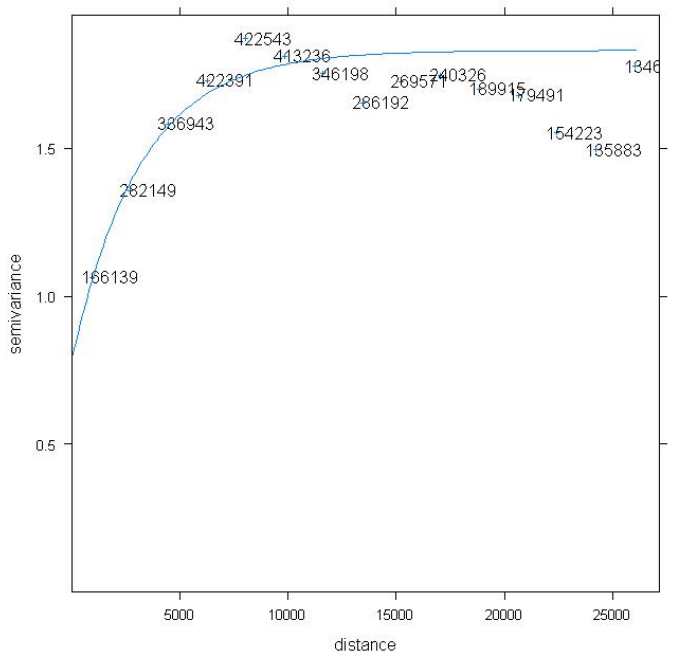

vii. Computed semivariogram showing directional spatial autocorrelation of As concentrations (105/285° weighting).

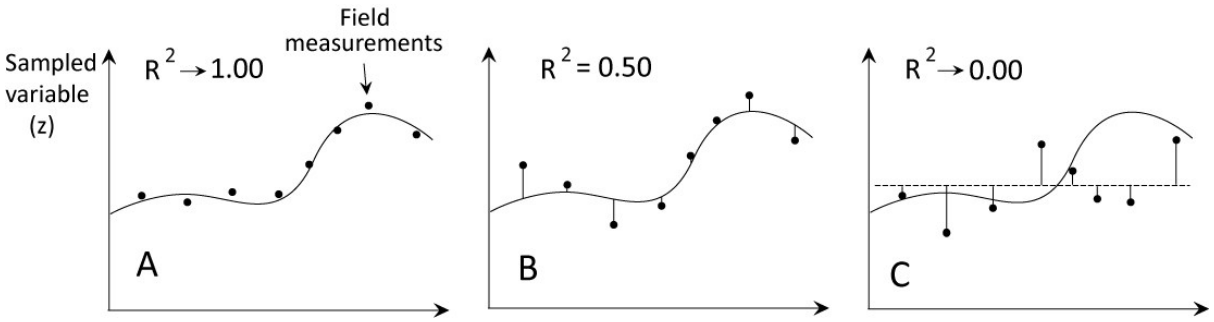

viii. A – Pure regression optimal – residuals ≈ 0. B – Combination of regression and kriging. C – Ordinary Kriging optimal.

The final model trends towards a classical ordinary kriging approach. This can be seen on the normalized error map of the final regression kriging model (Figure

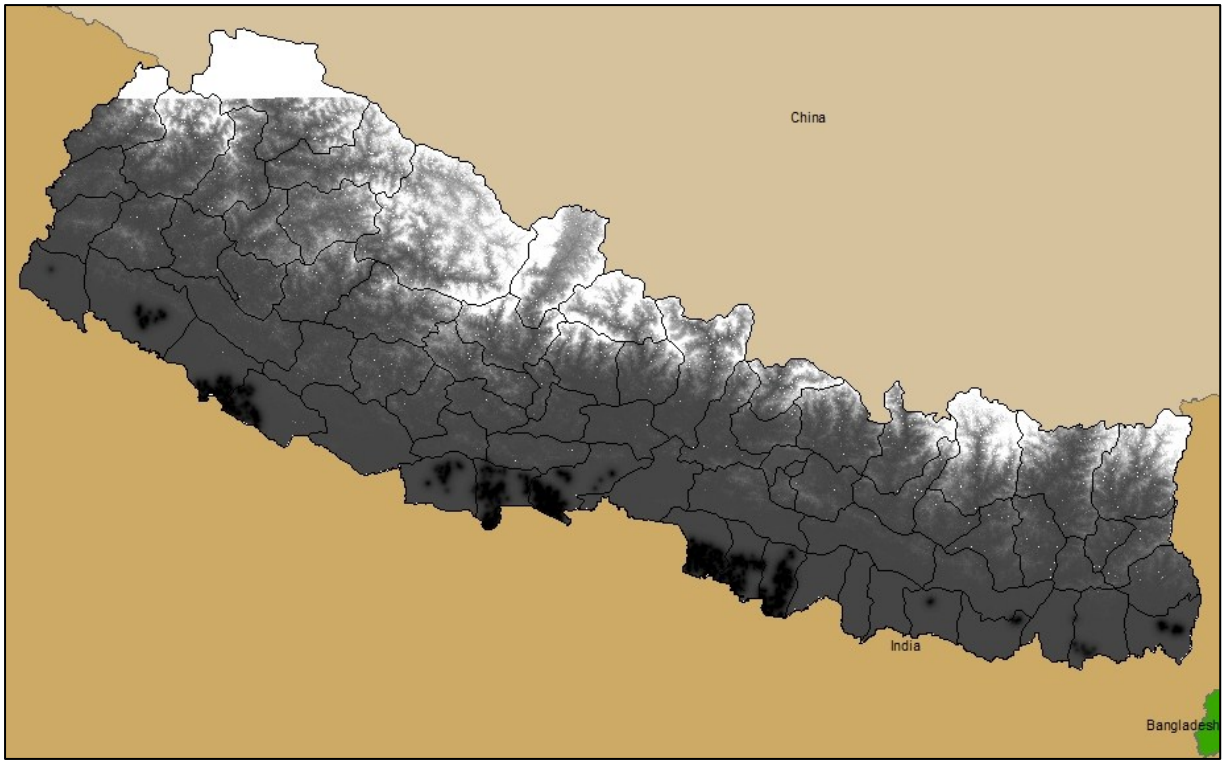

xii) - confidence is only high in the areas which were extensively sampled and deteriorates rapidly away from known points. Independent statistical validation of the final model was not performed.

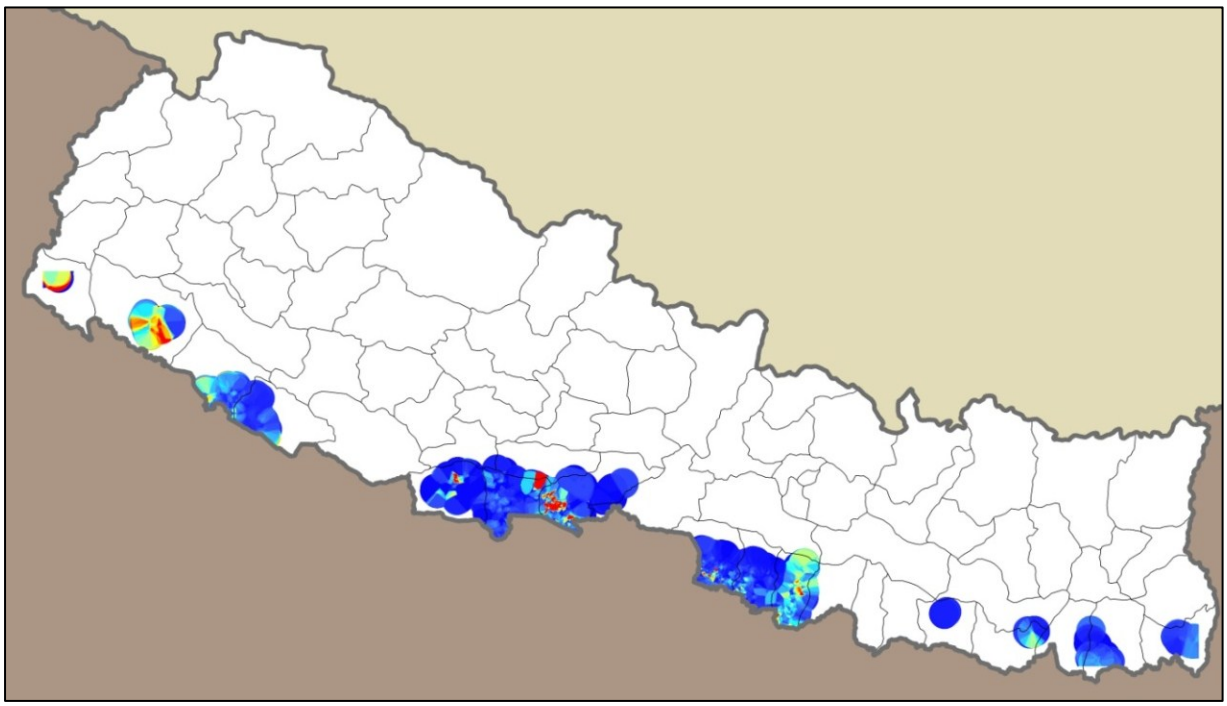

ix. Results of prediction using the ordinary kriging approach.

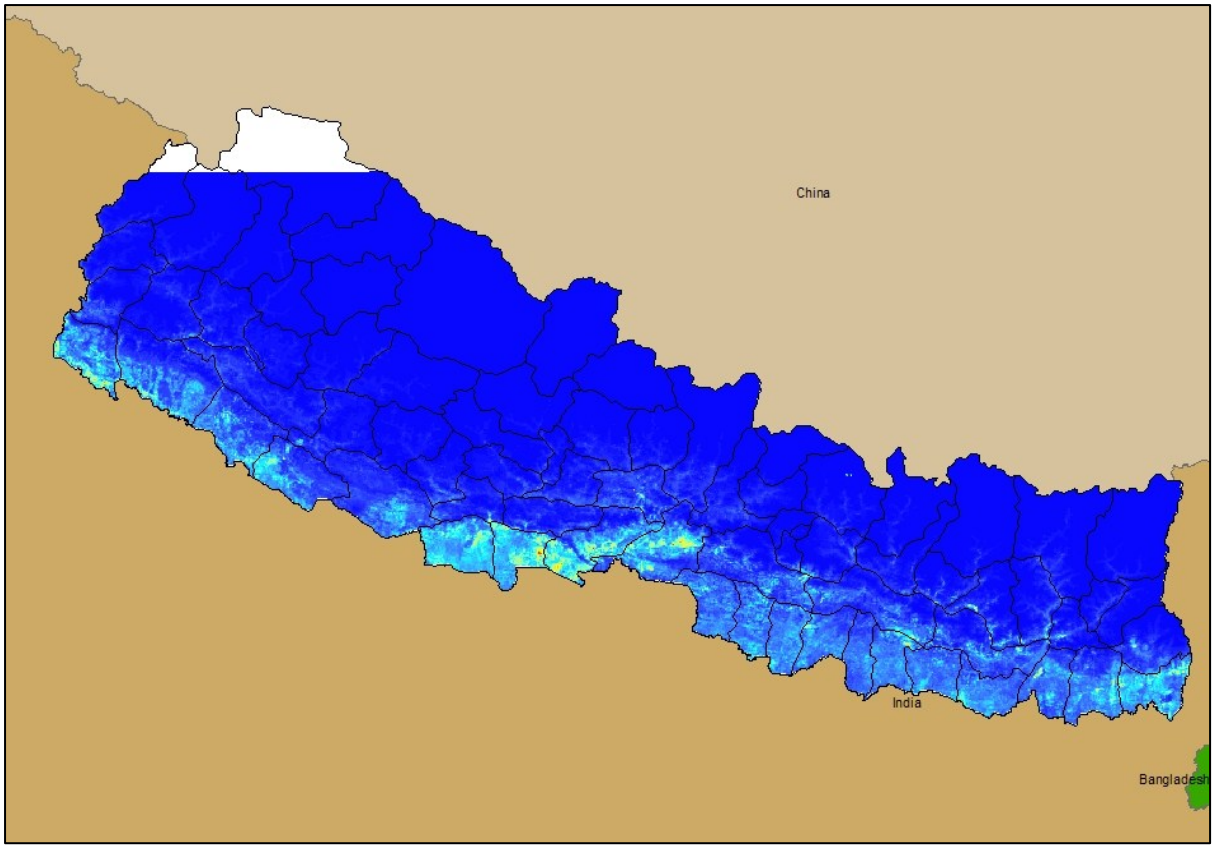

x. Results of the linear regression model (deterministic component). R^2 = 0.1267. Red = 310 ppb dark blue = 0 ppb.

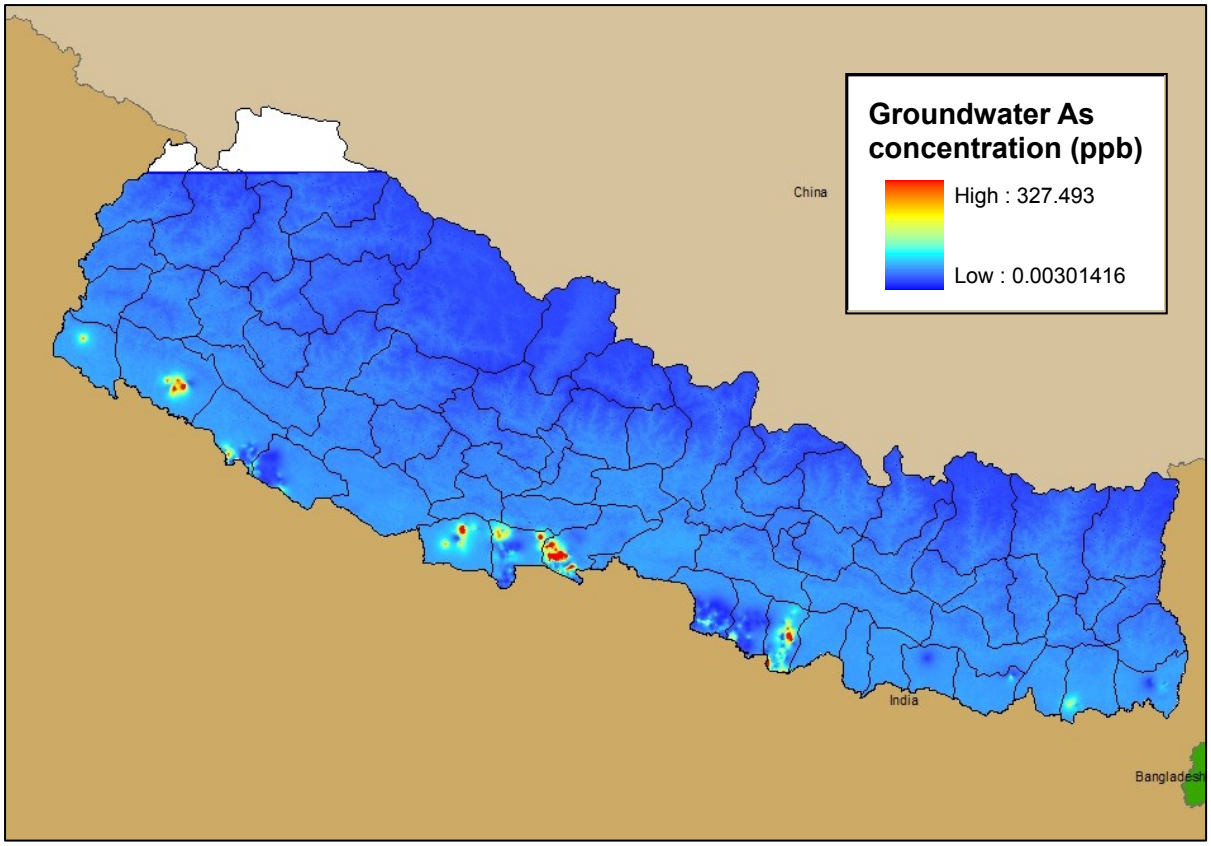

xi. Results of the combined regression-kriging model (deterministic and stochastic components). Red = 327 ppb dark blue = 0 ppb.

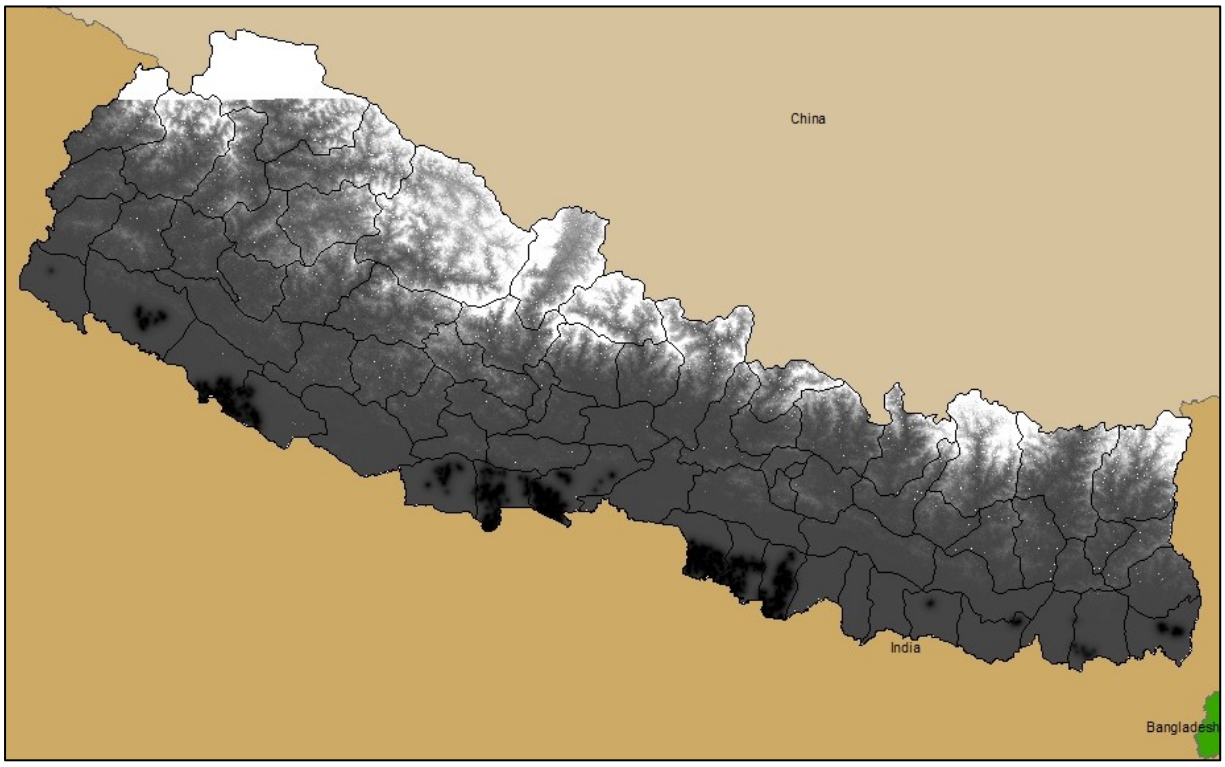

xii. Normalized error of regression kriging predictions (white = 1/high error, black = 0/low error).

Conclusions

Although the regression-kriging approach has been used with far greater success to predict groundwater arsenic concentrations in Cambodia and West Bengal (5,7) the proposed model does not provide a practically useful prediction of arsenic concentration in groundwater and does not significantly improve predictive power compared to classical techniques such as ordinary kriging. Validation of the methods was not performed due to the inability of the linear regression model to account for variability in the training data. The failing of the linear model indicates that arsenic variability is controlled by factors not captured in the selected auxiliary variables. It is thought that the lack of useful categorical predictors to form the linear model (soil and geological data) and the uneven distribution (clustering) of data are primarily responsible for the differences between this and previous studies.

Common between this and previous studies (5, 7) is the correlation between arsenic concentration in groundwater and flow length index, elevation and NDVI images, consistent with models of microbially mediated arsenic mobilisation from low lying, Holocene sediments (derived from the Himalaya) in reducing conditions (1).

References

(1) Charlet, L. & Polya, D.A. (2006), *Elements* **2**, 91–96.

(2) Garai, R. et al. (1984) *Journal of the Indian Medical Association,* 82**,** 34-35.

(3) Hengl, T. (2007). *A Practical Guide to Geostatistical Mapping of Environmental Variables.*

(4) Jarvis, A. et al. (2008). Hole-filled seamless SRTM data V4, International Centre for Tropical Agriculture (CIAT), available from http://srtm.csi.cgiar.org

(5) Lado, L. R. et al. (2008). *Applied Geochemistry,* 23, 3010-3018

(6) Matheron, G. (1969). *Vol. 1. Cahiers du Centre de Morphologie Mathematique*, Ecole des Mines de Paris, Fontainebleu

(7) Mondal, D. et al (2008). *Mineralogical Magazine*, February 1, 2008; 72(1): 461 – 465

(8) Neku, A. & Tandukar, N. (2003) in Boutron, C. & Ferrari, C. (Eds.) *Journal De Physique. IV : JP.* II ed. Grenoble.

(9) Pokhrel, D et al. (2009) *Environment International,* 35, 1, 157-161

(10) Reuter, H. I. (2005) Relief Analysis (Topo.aml) available from http://arcscripts.esri.com/details.asp?dbid=12974

(11) Shrestha, B. R. et al. (2004) *The State of Arsenic in Nepal - 2003.* Kathmandu, National Arsenic Steering Committee, Environment and Public Health Organization.

(12) Smedley, P. L. & Kinniburgh, D. G. (2002) *Applied Geochemistry,* 17**,** 517-568

We are grateful to the Nepalese National Arsenic Steering Committee and the Nepalese Environment and Public Health Organization.

Resumen: El arsénico es un metaloide tóxico y cancerígeno, ubicuo en la pedosfera y altamente sensible a las fluctuaciones de las condiciones redox del suelo, las cuales controlan tanto su toxicidad como su movilidad. La presente tesis doctoral tiene como objeto de estudio el ciclo biogeoquímico global del arsénico y examina la importancia de los aportes del arsénico antropogénicos y geogénicos al ciclo exógeno tomando en cuenta el uso creciente de recursos.

La contaminación con arsénico es generalmente difusa en las cuencas sedimentarias europeas. No obstante, las concentraciones en las aguas intersticiales del suelo pueden ser elevadas durante los periodos de saturación causados por el aumento de aguas subterráneas o inundaciones, cuyo incremento se prevé debido a los cambios climáticos. La espectrometría de fluorescencia de Rayos-X cuantitativa y sin estándar es utilizada para analizar el arsénico en suelos relativamente contaminados en la llanura aluvial del río Saône, mediante protocolos de preparación de muestras diseñados para mejorar la precisión analítica y la exactitud *in-situ* a bajas concentraciones de arsénico. La presencia de arsénico en estos suelos demuestra estar asociada a los (hidr)óxidos de hierro y de manganeso de tamaño de arcilla coloidal, los cuales experimentan una disolución reductora por acción microbiana durante las inundaciones, liberando así una importante concentración de arsénico en la fase acuosa. Si, posteriormente, el arsénico despedido no se elimina con el agua saliente, éste se vuelve a inmovilizar durante la oxidación del suelo y la re-precipitación de óxidos metálicos. Gracias a una combinación innovadora de análisis químicos por vía húmeda, ecología microbiana, espectroscopia, así como modelado termodinámico y cinético, demostramos que los ciclos de oxido-reducción secuenciales provocan una atenuación de arsénico acuoso durante condiciones de reducción debido al aumento de coprecipitacion y disminución de la actividad microbiana causada por el agotamiento de materia orgánica lábil. Se observan procesos de atenuación similares en caso de ausencia de actividad microbiana para Cr y As en arcillas piritas cuando son sometidos a oscilaciones de redox inducidas mediante la adición de sustancias húmicas reducidas. Es así como demostramos que los efectos acumulativos de ciclos sucesivos de redox son muy importantes para la movilidad contaminante en una variedad de ambientes.

Palabras clave: ciclos redox, arsénico, FP-XRF, pXRF, inundaciones, FeOOH, PHREEQC

Abstract: Arsenic is a toxic and carcinogenic metalloid, ubiquitous in the pedosphere and highly sensitive to fluctuations in soil redox conditions which dramatically influence both its toxicity and mobility. We review the global biogeochemical cycle of arsenic in light of increasing resource usage and re-evaluate the importance of anthropogenic and geogenic arsenic inputs to the exogenic cycle. Arsenic contamination is often diffuse in European sedimentary basins. Despite this, concentrations in soil pore-water may be high during periods of soil saturation caused by rising groundwater or surface flooding which is predicted to increase due to climatic change. Standardless quantitative X-ray fluorescence spectrometry is used to analyse for arsenic in moderately contaminated soils on the alluvial plain of the Saône River with sample preparation protocols designed to optimize analytical precision and accuracy in-situ at trace arsenic concentrations. Arsenic in these soils is shown to be associated with colloidal and clay sized iron and manganese (hydr)oxides which undergo microbially mediated reductive dissolution during flooding, releasing substantial arsenic to the aqueous phase. If released arsenic is not subsequently removed with receding flood water it is re-immobilized during soil oxidation and re-precipitation of metal oxides. We demonstrate through a novel combination of wet chemistry, microbial ecology, spectroscopy and thermodynamic and kinetic modelling that sequential reduction-oxidation cycles result in aqueous arsenic attenuation during reducing conditions due to increased co-precipitation and decreases in microbial activity due to depletion of labile organic matter. Similar attenuation processes are observed in the absence of microbial activity for Cr and As in pyrite-bearing clays when subjected to redox oscillations induced by addition of reduced humic substances. We demonstrate that the cumulative effects of successive redox cycling are therefore of great importance to contaminant mobility in a variety of environments.

Key words: Redox cycling, arsenic, FP-XRF, pXRF, flooding, FeOOH, PHREEQC

Résumé: L'arsenic est un metalloïde toxique et cancérigène. Ubiquiste dans la pedosphere, il est très sensible aux fluctuations des conditions redox du sol, ce qui influe significativement sa toxicité et mobilité. Nous étudions le cycle biogéochimique global de l'arsenic, en tenant compte de l'usage croissant des ressources, et passons en revue l'importance respective de l'arsenic geogénique et anthropogénique dans l'environnement. La contamination à l'arsenic est souvent diffuse dans les bassins sédimentaires de l'Europe. Cependant, des concentrations dans l'eau interstitielle du sol peuvent être élevées lors de périodes de saturation du sol causées par la monté des eaux souterraines ou les inondations, prévues d'augmenter dû aux changements climatiques. La spectrométrie de fluorescence X quantitative et sans standard a été utilisée pour analyser l'arsenic dans des sols relativement contaminés de la plaine alluviale de la Saône au moyen de protocoles de préparation d'échantillons conçus pour optimiser la précision d'analyse et l'exactitude *in situ* aux basses concentrations d'arsenic. L'arsenic dans ces sols est associe aux (hydr)oxydes du fer et de manganèse de la taille d'argile colloïdale. Ceux-ci subissent une dissolution réductrice par les microorganismes lors des inondations, libérant une importante concentration d'arsenic dans la phase aqueuse. Si, par la suite, l'arsenic dégagé n'est pas éliminé avec l'eau de crue évacuée, il est ré-immobilisé pendant l'oxydation du sol et la reprécipitation des oxydes métalliques. Grâce à une combinaison novatrice d'analyses chimiques par voie humide, d'écologie microbienne, de spectroscopie ainsi que de modélisation thermodynamique et cinétique, nous démontrons que les cycles d'oxydo-réduction séquentiels entraînent une atténuation d'arsenic aqueux dans des conditions réductrices dû à la coprécipitation croissante, et a une diminution de l'activité microbienne causée par l'appauvrissement en matière organique labile. Des processus d'atténuation similaires sont observés en l'absence d'activité microbienne pour Cr et As dans des argiles pyriteuses lorsque celles-ci sont exposés aux oscillations redox provoquées par l'ajout de substances humiques réduites. Ainsi, nous montrons que les effets cumulatifs de cycles redox successifs sont extrêmement importants pour la mobilité de divers contaminants dans l'environnement.

Mots clés: Cyclage redox, arsenic, FP-XRF, pXRF, inondations, FeOOH, PHREEQC.